THE DYNAMICS AND STABILITY OF FIXED BED CATALYTIC REACTORS

o-O-o

A thesis submitted for the degree of

Doctor of Philosophy

in

The University of Leeds

by

Colin Ivan Adderley, B.Sc. (Leeds)

under the direction of

C. McGreavy, B.Sc.(Leeds), M.Eng.,D.Eng.(Yale), C.Eng.,
M.I.Ch.E., F.B.C.S.

o-O-o

Department of Chemical Engineering,
Houldsworth School of Applied Science,
The University of Leeds,
LEEDS, LS2 9JT.

September 1973

ABSTRACT

Various aspects of the behaviour of fixed bed reactors supporting highly exothermic reactions, relevant to stable optimal design and control, have been studied using detailed mathematical models.

In order to establish the form of the simplest basic structure, two methods of describing radial heat transfer in two dimensional packed beds have been examined. It is shown that a lumped parameter single phase heat transfer model which implicitly incorporates the heterogeneous structure can account not only for the radial heat flux associated with both the fluid and solid phases but is also the more appropriate formulation since it allows the important reaction rate limitations due to intraparticle mass transfer to be properly estimated. Using this two dimensional, heterogeneous dynamic model of the reactor it has been possible to evaluate a simpler one dimensional formulation. It is shown that the latter gives an adequate description of the dynamic behaviour of the system, provided that the overall heat transfer coefficient between the fluid and the coolant is suitably defined, and may, therefore, be used for general studies of reactor performance.

Consideration has been given to the response of the reactor to sinusoidal perturbations of the inlet conditions. It has been found that at certain frequencies of oscillation temperature runaway may develop before a safe quasi-stationary state is reached. A detailed examination of this behaviour has shown that in addition to the non-linear effects the difference in the speeds of propagation of the concentration and temperature waves along the reactor as a result of the heterogeneity of the system is also very significant.

The effect of both cocurrent and countercurrent cooling of a single reactor tube has been examined. The behaviour for perturbations in coolant temperature is similar to that for inlet temperature and indicates potential difficulties in the design of control systems.

A mathematical model of a multitubular reactor with crossflow cooling has been developed and used to identify some of the problems which may arise in these systems. In

particular, considerable interaction between the individual reactor tubes occurs when significant conversion of the reactant takes place. This causes tubes in different parts of the bundle to exhibit different behaviour and with countercurrent cooling this may give rise to multiple steady states due to the feedback of heat within the system.

A technique has been developed for predicting regions of parametric sensitivity and temperature runaway in heterogeneous fixed bed reactors. The relationship between this form of instability and that due to multiple states of the catalyst pellet has been demonstrated. Application of this method to both the design and control of a reactor is discussed and it is shown that it provides an insight as to the behaviour of the system since it makes possible the establishment of a relationship between local and global reactor stability and the operating variables.

ACKNOWLEDGEMENTS

I am particularly indebted to my supervisor, Dr. C. McGreavy, for his constant encouragement and advice throughout the period of this research.

I would also like to thank Professor G. G. Haselden, for permitting me to carry out this work in the Department of Chemical Engineering, and the Science Research Council for financial support. I am also grateful to my friends and colleagues in the Department for their interest, in particular to H. Naim, Dr. M. A. Soliman and Dr. P. J. Heggs for their help and co-operation. Of the assistance that I have received from the members of staff, I would like to thank Mrs. J. Murray of the Houldsworth School Library and Mr. L. Bailey for his assistance with some of the computational problems. For so ably typing this manuscript, I owe thanks to Mrs. C. Heggs.

Last, and by no means least, I wish to thank my wife, Janet, for her patience and understanding during this work.

CONTENTS

LIST OF FIGURES

6.4 Magnitudes of deviations of the radial mean concentration and temperature profiles from the initial steady state during the response of the reactor to an inlet temperature perturbation of the form:
$T_0 = 0.03733 + 0.00056 \sin(2\pi \times 0.04 \times \tau)$.

6.5 Magnitudes of deviations of the radial mean concentration and temperature profiles from the initial steady state during the quasi-stationary state due to an inlet temperature perturbation of the form:
$T_0 = 0.03733 + 0.00056 \sin(2\pi \times 0.04 \times \tau)$.

6.6 Magnitudes of deviations of the radial mean concentration and temperature profiles from the initial steady state during the response of the reactor to an inlet temperature perturbation of the form:
$T_0 = 0.03733 + 0.00056 \sin(2\pi \times 0.02 \times \tau)$.

6.7 Radial mean temperature profiles during the response of the reactor to an inlet temperature perturbation of the form:
$T_0 = 0.03733 - 0.00056 \sin(2\pi \times 0.04 \times \tau)$.

6.8 Magnitudes of deviations of the radial mean concentration and temperature profiles from the initial steady state during the response of the reactor to an inlet temperature perturbation of the form:
$T_0 = 0.03733 - 0.00056 \sin(2\pi \times 0.04 \times \tau)$.

6.9 Radial mean temperature profiles during the response of the reactor to an inlet temperature perturbation of the form:
$T_0 = 0.03733 + 0.00112 \sin(2\pi \times 0.04 \times \tau)$.

6.10 Radial mean temperature profiles during the response of the reactor to an inlet temperature preturbation of the form:
$T_0 = 0.03733 - 0.00112 \sin(2\pi \times 0.04 \times \tau)$.

6.11(a) Steady state radial mean temperature profiles at the mean, maximum and minimum values of a sinusoidal inlet temperature perturbation of amplitude 0.00056 in the non-unique region.

6.11(b) Steady state reactor trajectories at the mean, maximum and minimum values of a sinusoidal inlet temperature perturbation of amplitude 0.00056 in the non-unique region.

6.12 Radial mean fluid temperature oscillations at various axial positions during the quasi-stationary state due to an inlet temperature perturbation of the form:
$T_0 = 0.03733 + 0.00056 \sin(2 \pi \times 0.04 \times \tau)$.

6.13 Radial mean fluid temperature oscillations at various axial positions during the quasi-stationary state due to an inlet temperature perturbation of the form:
$T_0 = 0.03733 + 0.00056 \sin(2 \pi \times 0.02 \times \tau)$.

6.14 Radial mean fluid temperature oscillations at various axial positions during the quasi-stationary state due to an inlet temperature perturbation of the form:
$T_0 = 0.03733 + 0.00056 \sin(2 \pi \times 0.02 \times \tau)$.

6.15 Comparison of quasi-stationary state fluid temperature oscillations at various axial positions due to positive and negative sinusoidal inlet temperature perturbations of the form:
$T_0 = 0.03621 \pm 0.00056 \sin(2 \pi \times 0.02 \times \tau)$.

6.16(a) Steady state radial mean temperature profiles at the mean, maximum and minimum values of a sinusoidal inlet concentration perturbation of amplitude 0.1.

6.16(b) Steady state reactor trajectories at the mean, maximum and minimum values of a sinusoidal inlet temperature perturbation of amplitude 0.1.

6.17 Magnitudes of deviations of the radial mean concentration and temperature profiles from the initial steady state during the response of the reactor to an inlet concentration perturbation of the form:
$C_{A0} = 1.0 + 0.1 \sin(2 \pi \times 0.02 \times \tau)$.

6.18 Magnitudes of deviations of the radial mean concentration and temperature profiles from the initial

LIST OF TABLES

.....

CHAPTER 1

INTRODUCTION

Whilst the basic principles of most unit operations were developed as many as forty or more years ago, it is only comparatively recently that systematic methods have been applied to the study of chemical processes in general and chemical reactor engineering in particular. The central feature of this approach has been the formulation and use of mathematical models in an attempt to simulate the chemical and physical processes which occur within these systems. The stimulus for this development has been provided by two factors. Firstly, economic pressures have brought about the need to design larger and more efficient plants and also to improve the efficiency of existing plants. This has meant that more reliable design methods have been required and more understanding of system performance has been needed in order that better control of these systems may be effected. The second factor has been the parallel development of low-cost high speed computers and improved numerical and mathematical techniques which have enabled engineers to tackle increasingly complex problems.

It has long been recognised that information obtained from pilot plant studies, although in many respects very useful, generally gives no real insight into the behaviour of a particular process. Without this understanding the wrong conclusions may often be drawn from a particular experiment or insufficient information may be obtained because the experimental measurements do not tell the whole story. This is particularly true of complex distributed parameter systems typified by the fixed bed catalytic reactor in which serious disturbances may occur with no immediately apparent effect on the measureable variables. Besides facilitating a deeper understanding of the behaviour of the system, mathematical modelling also has other more easily recognised advantages over an extensive program of experimentation. These are that it is relatively cheap and it permits the study of the system performance over a whole range of conditions in a comparatively short time.

Simulation may also be used to indicate undesirable or

dangerous modes of operation and so avoid damage to expensive equipment. In fixed bed reactors supporting highly exothermic reactions apparently safe perturbations of the system can cause very unsafe behaviour due to the complex way in which the physical and chemical processes occurring within the reactor interact and because of the very large amount of heat which is generated. This may result in damage to the reactor itself as well as the catalyst and can put the operating personnel at risk if any of the reactants or products are explosive. For these reasons extensive study of this and many other similar systems by simulation using a mathematical model offers considerable benefits.

This does not mean, however, that mathematical modelling removes the need for experimentation. On the contrary, this is always necessary especially to measure those parameters in the model which cannot be estimated by other means. Also since any mathematical model can only be regarded as an approximation of the physical and chemical processes within the system, its predictions must at some stage be checked against experimentally determined results. In this respect the role of the model is that of a tool to aid the experimentalist in the interpretation of his results and to predetermine undesirable operating conditions so that they may either be avoided or approached with care.

A further application of mathematical modelling is in the design and implementation of computer control schemes. An optimal control policy may be easily determined using suitable mathematical models of the system. Also in modern control strategies the control action must be rapidly determined from as few measurements as possible and to do this without violating the various system constraints is only possible by the use of a model which reliably predicts the system behaviour.

Because of its very complex behaviour, the fixed bed reactor is particularly well suited to mathematical modelling. As has been indicated above, the nature of the interactions between the various physical and chemical processes within the system cannot be easily understood and therefore may not be reliably predicted without simulation. Fixed bed reactors are widely used industrially for performing a variety of

chemical reactions. The application of interest in this thesis is that of carrying out strongly exothermic reactions between gaseous reactants on the active surface of catalyst pellets. Such reactions are typified by the partial air oxidation of hydrocarbons using a transition metal catalyst on a high temperature support. Because of the large amounts of heat generated and the exponential dependence of the reaction rate on temperature this class of reactions poses some very difficult problems both in the design of the reactor and in its subsequent control.

Much of the basic work in the identification of the important phenomena which occur in the packed bed reactor and the formulation of suitable mathematical models to describe this system has been carried out by Cresswell[13] and Thornton[12]. However, although considerable information exists on the steady state performance of a single reactor tube, no real attempt has been made to study either its dynamic behaviour or the effect of the external environment (i.e. the coolant) taking into account all the significant physical and chemical processes which occur within the reactor. Consideration of the effect of the cooling medium is particularly important in large industrial scale reactors which usually consist of many individual reaction units interactively connected by the flow of a coolant.

One of the aims of this work is to examine the pattern of dynamic behaviour of a single tube fixed bed reactor in which a strongly exothermic reaction takes place, principally in terms of the important thermal effects which may occur. This study is carried out in perfectly general terms using a simple reaction scheme and data which, although it refers to no particular process, is typical of that found with many reactions of industrial importance (e.g. the partial oxidation of hydrocarbons) and well illustrates the problems associated with these systems. Consideration is given to reactor instability, particularly that associated with parametric sensitivity, to determine under what conditions this phenomenon occurs and to examine its effect on reactor performance and control.

It is also intended to pay some attention to the development of a mathematical model of a multitubular reactor in

order to investigate the nature of the interaction of the individual reactor tubes. Because of the complexities of this system, this study necessarily takes the form of a preliminary investigation of steady state behaviour. Nevertheless it should still be possible to identify some of the important problems encountered in both the mathematical description and the operation of these systems.

By examination of the general pattern of behaviour of the fixed bed reactor in this manner, the essential characteristics of the system which must be taken into account in the design of a control strategy may be determined.

CHAPTER 2

PREVIOUS WORK AND DEVELOPMENT OF THE MODELS

2.1 Introduction

The interest in chemical reaction engineering has increased so rapidly in recent years that a voluminous amount of literature about reactor design and heterogeneous catalysis is now available. Amongst the useful textbooks dealing with the well-founded aspects of the subject are those by Aris,[1] Petersen,[2] Levenspiel,[3] Denbigh and Turner,[4] Thomas and Thomas,[5] Coulson and Richardson,[6] and Perlmutter.[7] Several "state of the art" reviews have also appeared, the notable recent ones being those by Froment,[8,9] Hlavacek[10] and Ray.[11] Thornton[12] has also given an excellent critical review.

Much of the recently published literature has tended to deal either with rather simple models of little practical application or else with complex models which are not pertinent to the reactor configurations of interest here. For example, stability analyses using quasi-homogeneous models and axial dispersion in adiabatic reactors have lately received considerable attention. Whilst such analyses have involved some elegant mathematical techniques and are indeed, in themselves, very interesting, the results can usually only be applied to certain specific systems and have little or no general application to industrial reactors. For this reason, it is not intended here to survey all the recent literature concerning catalysis and fixed bed reactors and in any case this would only tend to duplicate the efforts of the reviewers mentioned above. Instead, what is attempted in this chapter is to show how the basic reactor and catalyst pellet models used in this thesis have been developed and thereby set them in perspective. Some consideration is also given to the use of various models in the study of reactor stability.

2.2 The Catalyst Pellet

Consideration of the catalyst pellets in a packed bed reactor is necessary for two important reasons. The first reason, although perhaps obvious, is that the presence of the pellets significantly affects the flow distribution inside the reactor and therefore influences the dissipation of both

heat and mass. The second is that the catalyst pellets provide the surface on which the reaction takes place. Generally the pellets have an irregular porous structure so that the surface area available to the reacting gases may be very large. In order to reach the catalytic surface, however, the reactant gas molecules must overcome certain resistances to both mass and heat transport within the system. The effect of these resistances is generally to cause conditions within the catalyst pellets (i.e. reactant concentration and temperature) to differ from those in the surrounding gas phase and thereby inhibit, or enhance, the rate of reaction. Thiele[16] and Zieldowitsch[17] were the first to recognise and mathematically formulate the effect on the reaction rate due to reactant diffusion within the pores of the catalyst pellet. Their work on isothermal catalysts was extended by Wheeler[18] and Weisz and coworkers[19,20,21] mainly in an attempt to quantify the regions in which the reaction rate limitations due to pore diffusion were less than a specified amount. Wheeler[22] and Prater[23] demonstrated that when heat was generated by reaction throughout the catalyst pellet the heat transfer resistance provided by the pellet caused a temperature gradient which also affected the rate of reaction. Carberry[24] was the first to consider the finite rates of mass and heat transfer between the catalyst pellet and the surrounding gas phase and their effects on the reaction rate in a mathematical description of the catalyst pellet.

The transport resistances within the system are now generally identified[12,13] as:

(1) A mass transfer resistance within the catalyst pellet pores.
(2) A mass transfer resistance at the exterior pellet surface between it and the gas phase.
(3) A heat transfer resistance due to the structure of the pellet.
(4) A heat transfer resistance between the catalyst pellet and the surrounding gas.

All of these resistances affect the transport of heat and mass to and from the interior surface of the pellet and therefore influence the rate of reaction on that surface.

A general mathematical description of the catalyst pellet in the steady state which includes these four resistances,

as well as the reaction rate and heat generation rate expressions, results in a pair of non-linear, simultaneous, second order, ordinary differential equations describing the variation in reactant concentration and temperature with position inside the pellet. These equations are given in Appendix(1). The intraparticle heat and mass transfer resistances are described respectively by Fourier and Fickian type expressions and the interphase resistances form the boundary conditions of the resulting equations. Inevitably, to solve these equations a numerical method is necessary.[13] Within a mathematical model of the reactor, the object of solving the equations describing the catalyst pellet is not, however, to compute the concentration and temperature distribution within each pellet since this information is generally of little use by itself, even if it can be obtained accurately. What is required is an estimate of how the transport resistances affect the reaction rate and heat generation rate relative to the gas phase conditions which can be measured. That is to say, a knowledge of the effectiveness factor, η, is required so that the actual rate of reaction in each catalyst pellet may be expressed in terms of the gas phase conditions around the pellet. The effectiveness factor is defined as:

$$\eta = \frac{\text{Actual reaction rate at pellet conditions}}{\text{Reaction rate at fluid conditions.}}$$

Once known at each point in the bed, η may then be used in the equations describing the gas phase concentration and temperature throughout the bed to "correct" the reaction rate expression. Although the effectiveness factor is a very powerful concept, in non-isothermal reactors it varies with position in the bed since it is a function of concentration and temperature and this usually means that the pellet conditions must be computed at each point in order to evaluate it.

As mentioned above, solution of the general catalyst pellet model which includes a description of all the transport resistances is complex and tends, therefore, to be too time consuming to be included in a two dimensional or dynamic model of the reactor.[12] The relatively recent development of orthogonal collocation methods for solving differential equations indicates[14,26,27] that the use of the general pellet model for these purposes is at least feasible with a very powerful modern computer. However, the tendency in the past has been to attempt

to simplify the catalyst pellet model thereby making its solution on small inexpensive computers more tractable. Since computing costs are usually directly related to the size of the computer this is probably a more acceptable approach and the use of the sophisticated pellet model need only be employed in cases where the validity of approximate models is in doubt. Also, the approximate form may be used for a survey of feasible operating conditions which may subsequently be examined in more detail with the complex model.

Most published work appears to deal with systems in which either both interphase resistances (i.e. resistances (2) and (4)) or both intraphase resistances (i.e. resistances (1) and (3)) have been neglected without any attempt at justification. The intraphase resistances may, of course, be ignored without question when the catalyst pellets are non-porous and the reaction, therefore, only occurs at their exterior surface. If pore diffusion does occur, however, then its limiting effect on the rate of reaction can be substantial so that neglecting it will lead to completely wrong conclusions [12,35]. This point is demonstrated in the next chapter. The interphase mass transfer resistance is relatively small compared with the other transport resistances and can often be ignored without serious loss of accuracy.[25] The interphase heat transfer resistance, however, is quite large in most practical cases and it therefore has a significant effect on the pellet temperature.

Several methods of approximation have been proposed either to simplify the solution of the catalyst pellet equations or to enable direct computation of the effectiveness factor given the fluid conditions. Beek[29] expressed the reaction rate as a linear function of temperature and a somewhat similar technique was employed by Gunn.[32] These methods are of limited use since in most highly exothermic reactions the reaction rate is an extremely non-linear function of temperature. Rester and Aris[36] have shown how upper and lower bounds on the effectiveness factor may be predicted by variational techniques in the absence of both heat transport resistances. Their technique is potentially useful to the experimentalist who is interested in obtaining absolute values of the kinetic parameters for a particular reaction and it is applied to the case of a spatially non-constant internal mass transfer resistance

due to a non-uniform pore structure. Petersen[30,31,2] developed what is known as the asymptotic method of estimating effectiveness factors. This assumes that the reaction is confined to a thin layer of the catalyst under conditions of strong intraparticle mass transport resistance, and negligible interphase resistances. More recently Patterson and Cresswell[33] have used the similar concept of an effective reaction zone but including both the interphase and intraphase transport resistances to reduce the effectiveness factor calculation to the solution of a single algebraic equation. They have shown that for highly exothermic reactions, where the reactant is rapidly consumed before it can diffuse very far into the catalyst pellet, the approximation is very good. In some respects, however, this method lacks generality since it has only been developed for the steady state and the case of a single irreversible reaction. Similar criticisms can be made of the method of Jouven and Aris[34] by which effectiveness factors are estimated to within 5 and 10% accuracy using a best fitting interpolation formula.

Beek[29] noted that the principle factors affecting the reaction rate were the intraparticle mass transport resistance and the interphase heat transport resistance. The results of Hutchings and Carberry[25] showed that the ratio of the pellet Sherwood and Nusselt numbers is typically of the order of 1:1000 which therefore confirmed Beek's[29] observation. Computations performed by Cresswell[13] for a single irreversible reaction and later by Thornton[12] for a complex reaction scheme involving both consecutive and parallel reactions showed that in the case of gaseous reactants the pellet is essentially isothermal over the whole range of practical operating conditions and thermal conductivities. On the basis of these results Cresswell[13] developed the lumped parameter catalyst pellet model given in Appendix (1). In this model the catalyst pellet is assumed to be isothermal but at a temperature different from the surrounding gas due to the interphase heat transport resistance (i.e. the intraparticle heat transport resistance is neglected). In the case of first order reactions this assumption allows analytic solution of the equation describing mass transport to and within the catalyst particle and so the pellet model is reduced to a single non-linear algebraic equation in temperature. This allows very rapid

evaluation of the catalyst performance. Thornton[12] showed that the same simplification may be applied in the case of competing parallel and consecutive reactions as well as in the case of non-first order reactions with the use of a pseudo-first order rate expression. The use of pseudo-first order rate expressions in the isothermal pellet model has been studied in some detail by Rawlings.[37] Hlavacek and Kubicek[38,39] have further shown that the isothermal pellet model gives an accurate estimate of the steady state effectiveness factor over the whole industrially important range of parameters. They also proposed an algorithm to facilitate its solution in the case of non-first order or non-Arrhenius reaction rate expressions.

Several investigators [40,41,42,43,44] have experimentally studied the single catalyst particle in the steady state and demonstrated the existance of large temperature differences between the particle surface and the surrounding fluid. In particular, Irving and Butt[43] have shown that this interphase temperature rise is generally much greater than the intraparticle temperature rise. Hughes and Koh[44] measured steady and unsteady state temperature profiles within single pellets for the benzene hydrogenation reaction. They also found that the intraparticle temperature rise was quite small in comparison with the interphase rise and not sufficient by itself to affect the overall effectiveness factor to any large extent.

Only recently have single catalyst particles in the unsteady state received much attention, and most of this has been concerned with stability rather than an examination of the model structure. McGuire and Lapidus[45] used a dynamic model of the catalyst pellet which ignored the interphase transport resistances. This type of model has been shown to be inappropriate for the steady state description of exothermic reactions and it is, therefore, unsatisfactory in the unsteady state. Feick and Quon[46] examined three different dynamic models of the catalyst pellet in a study of the transient behaviour of a fixed bed reactor. These models were of increasing complexity; the first ignored all of the transport resistances, the second considered only the interphase resistances and the third took account of all the resistances. The results showed that the predicted transient behaviour of

made to establish the lack of importance of the heat transfer effects within the system. Also, because the system was designed to operate isothermally, the perturbations were applied to both the reactor inlet and the coolant so that the effect was distributed throughout the system. Perhaps the most important point about this work is that virtually all of the concentration disturbance occurred during the temperature perturbations and not subsequent to them and to infer from this that the concentration changes are "driving" the response is not possible. There is no evidence that this is the case with the highly exothermic reactions of interest here. Indeed, the experimental results of Kehoe and Butt[48] and Horak and Jiracek[49] show that the mass capacitance of the catalyst pellet is much less than the thermal capacitance so that the concentration changes within the pellet occur faster than the temperature changes. In these circumstances the concentration profiles within the pellets may be treated as if they pass through a series of pseudo-steady states which are determined by the changing temperature profiles.

By applying an analysis similar to that used in the steady state, Thornton[12] demonstrated that the catalyst pellet also remains essentially isothermal in the unsteady state. Although a slight intraparticle temperature gradient was evident at the beginning of the transient response the profile rapidly flattened indicating isothermality. The effectiveness factors predicted by both the fully distributed catalyst pellet model and the isothermal model were in excellent agreement throughout the transient response. This is not surprising since the magnitudes of the transport resistances inside and outside of the pellet are the same in both the steady and unsteady state. Kehoe and Butt[48] measured temperature profiles in catalyst particles subject to perturbations in the surrounding gas. They found that in certain cases the intraparticle temperature rise was significant and in pellets of relatively high thermal conductivity isothermality was obtained throughout the transient period. This is to be expected since, as they point out, the reaction approximated to the special case of zero order kinetics in most of their experiments, and Paterson and Cresswell[33] have shown that under these circumstances appreciable intraparticle temperature gradients can exist since the heat balance is independent of

the mass balance. Hughes and Koh[44] have demonstrated experimentally only a small intraparticle temperature rise during the transient response of a catalyst particle; most of this occurred near the surface and the bulk of the profile was flat. As mentioned above, these authors found that the interphase heat transfer resistance is far more important and during the transient response the intraparticle temperature gradient has very little effect on the effectiveness factor. In this respect the approximation of isothermality of the pellet is as good in the unsteady state as it is in the steady state.

Lumping the heat transfer resistance at the pellet surface and therefore treating the pellet as isothermal allows the mass transport equation to be solved analytically. As shown in Appendix (1), the dynamic model of the catalyst pellet then becomes a single first order, ordinary differential equation describing the change of pellet temperature with time. The advantages of this formulation are clearly evident; the model gives an accurate estimate of the reaction rate limitations imposed by the catalyst pellet and may be solved sufficiently rapidly to be included in a dynamic model of the reactor suitable for an extensive study of its unsteady state behaviour.

2.3 The Tubular Reactor

Having discussed the catalyst particles in isolation, attention is now directed at the mathematical description of their assembly in a reactor tube.

Broadly speaking, reactor models may be divided into two categories; quasi-homogeneous models in which no allowance is made for the difference between the fluid and pellet conditions (i.e. temperature and reactant concentration) and heterogeneous models where the reaction rate limitations due to the transport resistances in and around the catalyst pellets are explicitly described. In the heterogeneous models, these rate expressions are modified by an effectiveness factor which is obtained by solution of the catalyst pellet model. In the quasi-homogeneous models the presence of the catalyst pellets is acknowledged only by their effect on the mass and heat dispersion throughout the bed. For the reasons given

previously, it is often necessary to take account of the reaction rate limitations imposed by the catalyst pellets and several workers[8,12,13,46,53] have shown that with many highly exothermic reactions of industrial importance a heterogeneous model is essential to adequately describe the system.

The single tube reactor is essentially a length of pipe into which catalyst pellets are packed. In most cases with exothermic reactions this tube is immersed in some form of cooling medium. The reaction gases enter at one end and leave with the products at the other. There is, therefore, a bulk movement of gas in one direction. The processes of reaction and heat generation due to reaction cause temperature and concentration gradients along the tube parallel to this bulk movement of fluid and heat removal by the coolant through the walls of the tube causes temperature, and therefore concentration gradients, perpendicular to the bulk flow (i.e. radially). In some circumstances a diffusive heat and mass flux may also occur in the axial direction, parallel to the bulk flow. Although this diffusive axial flux has received considerable attention, especially from the point of view of determining reactor stability conditions, several investigators have shown [14,53,54] that for the flow velocities used in industrial practice axial dispersion of heat and mass has a negligible effect upon conversion when the bed length exceeds approximately one hundred catalyst particle diameters. Since this is usually the case, a description of axial heat and mass dispersion is not included in the reactor models used here.

To describe the spatial variations of temperature and reactant concentration within a reactor tube therefore requires a model which in some way accounts for both axial and radial gradients. In adiabatic reactors, which is not the case of interest here, there will, of course, be no need to consider radial gradients since heat is not removed or supplied through the tube walls.

Although the pellet distribution throughout the bed is random and the bed is discrete in nature, the problem of measuring transport coefficients and other bed properties, such as voidage, is best tackled by treating the bed as a continuum for the purposes of gas flow. This means that only average bed properties need be measured for use in the reactor model

and so reproducability of these values in other systems is then possible. The transport of heat and mass by the fluid in the bed may then be described in terms of differential equations making use of averaged or effective transport parameters. In some cases the local patterns of concentration and temperature may differ significantly from those obtained by the solution of differential equations and a better description may then be obtained by regarding the bed as a collection of individual void spaces containing catalyst pellets and connected to each other by small channels.[55] This type of finite-stage or mixing-cell model was first proposed by Deans and Lapidus[56] and has been used by several other workers [45,57]. In these models the interconnected void spaces are described as stirred tanks containing a catalyst particle. This type of formulation has certain mathematical advantages and has been exploited in fixed bed reactor optimisation studies [59]. Generally, however, the finite stage models lead to rather unrealistic discontinuous profiles, especially in the radial direction,[55] unless a large number of mixing cells is considered. In this case the computational effort required for solution of the model is greatly increased and as Feick[58] has shown it then corresponds to the finite difference representation of the differential equations used in the continuum model. For these reasons the reactor models used in this work are of the continuum type. The radial heat transport is described by a Fourier type expression using an effective radial thermal conductivity referred to the gas phase and the radial mass transport by a Fickian type expression using an effective radial diffusivity, in a manner analogous to that used in the catalyst pellet model. It has recently been suggested[60] that this formulation is inappropriate for the description of radial heat transport in the packed bed. Since this has very important implications on the reactor model structure and on the identification and subsequent description of the important physical processes, radial heat transport in packed beds and its description are examined in detail in the next chapter. Specifically it is shown that the continuum model which employs an effective radial thermal conductivity referred to the gas phase is, for several reasons, a more useful formulation of the heterogeneous reactor model.

It is worth examining some of the other assumptions implicit

in the formulation of reactor models. In all the models, axial symmetry of the concentration and temperature profiles is assumed. In single tube reactors this is usually the case since the coolant conditions do not vary around the tube circumference. In the larger industrial units where the coolant may flow perpendicular to the tube axes, the results of chapter 8 show that large temperature gradients may, under some circumstances, occur in the coolant flow direction. There will also, of course, be variations in the coolant velocity around the tubes. The difficulties of describing these variations are very great and to obtain an accurate description the temperatures and heat transfer coefficients around all the tubes would have to be measured or estimated. Even if sufficient data existed to estimate these variations to any degree of reliability the results would certainly not be reproducable in other systems or even in the same system.

Similar reasoning may be applied to conditions inside the tube so that it is generally assumed that within the bed every point on the surface of each catalyst particle is in contact with gas of uniform concentration and temperature and is also equally accessible for the purposes of heat and mass transport. This further implies that the rates of reaction and heat generation at each point in the bed may be calculated as if a catalyst particle is acting at that point.

For the purposes of the work described in this thesis the catalyst pellets are assumed spherical and of uniform size and activity. Other pellet shapes may be considered without much difficulty by defining an appropriate characteristic radius.[2] The effect of varying the pellet size throughout the bed, in an attempt to optimise the reactor performance, has been investigated by Naim[14] and Brusset et al.[93] Calderbank and coworkers[61] and Stewart and Sørensen[72] have modelled reactors in which the packing is diluted with inert spheres, and Shadman-Yazdi and Petersen[62] have considered the effect of varying the catalyst activity within individual pellets in order to obtain better yields in cases where the product can be consumed. Catalysts are usually subject to deactivation with time and more importantly with temperature; little is known, however, about the exact mechanism of catalyst deactivation except that a rapid increase in temperature will usually enhance it. In most studies of the dynamic behaviour of

reactors the perturbations last for a relatively short period compared with the time needed to cause significant deactivation. Over longer periods deactivation may need to be considered and studies have been made of long term performance where it is the principle factor.[59,70] When temperature runaway occurs deactivation can take place so that the kinetic model is no longer applicable. Since one of the purposes of reactor modelling is to identify regions of operation where such undesirable behaviour occurs, inclusion of catalyst deactivation effects in the models used here is not really necessary.

A common assumption employed in reactor modelling is that all of the physical and chemical parameters in the system are independent of position, concentration and temperature. Clearly this is not the case in practice, but usually the increase in computational effort required to solve a model which includes such variations (even when they are known) is not justified by the increase in accuracy which is obtained.[12] This is especially true in, for example, the case of heat transfer coefficients which can usually only be estimated to about 10% accuracy in any case. Perhaps the most doubtful of assumption is that of plug flow of the gas through the reactor which is related to the assumption of uniform bed voidage. The voidage of a packed bed is not uniform, being greatest near the tube wall;[63] since the gas will tend to take the path of least resistance through the bed, its velocity profile will therefore be deformed. This in turn will also cause a variation in the values of the mass and heat transport parameters. Thornton[12] has shown that the performance of a reactor can be significantly affected by small variations in even a uniform value of voidage. Valstar[55] found similar disagreement betweer the predictions of a reactor model which contained a velocity profile expression and one in which plug flow was assumed. More recently Stanek and Szekely[65] have suggested that significant gas flow maldistribution may occur not only due to local variations in bed voidage but also because of the variation in properties caused by the radial temperature gradients. These results appear to some extent to conflict with those of Hoiberg et al[64] who found that the steady state and transient response predicted by a plug flow model was no different from that predicted by a model which included an arbitrarily specified velocity profile with a large peak near the tube wall.

They concluded that in their system, at least, the radial heat and mass transfer occurred rapidly enough to counteract the effects of the higher local velocities. Clearly, then, more investigation of this problem is required. As Valstar[55] and Hoiberg et al[64] have shown, inclusion of a velocity profile in the reactor model is not difficult, however, the validity and applicability of both the model and its predictions is uncertain. The distribution of voidage within the bed, and therefore the form of the velocity profile, is very system dependent.[63] Since one of the aims of this work is to contribute towards a general picture of reactor behaviour, there seems to be little alternative to using the assumption of plug flow, at least until more is known about the fluid dynamics of packed beds.

As a result of these concepts and assumptions the reactor model becomes a set of simultaneous, non-linear partial differential equations describing the spatial variation of temperature and concentration within the bed. One equation consists of a heat balance over the reactor and the others are mass balances on each reactant. These equations are coupled with the catalyst pellet model and because of their high non-linearity a numerical method of solution is necessary.[13] Various numerical methods of increasing sophistication have been used; for example the alternating direction explicit method[46] and the recently developed orthogonal collocation procedures.[14,47,66,72] The most generally applicable method, however, is the Crank Nicolson finite difference representation of the differential equations. This is not only reliable and easy to program but is also the method against which the approximate solutions are checked.[14] In the solution of the reactor equations, at each point in the bed where the gas concentration and temperature are calculated the catalyst pellet model must also be solved to obtain the reaction rate and heat generation rate. This increases the computational effort considerably and can make the model quite unsuitable for a comprehensive study of reactor behaviour. (Note: In quasi-homogeneous models this is not necessary since the pellet conditions are assumed to be the same as those in the fluid and the solution is therefore greatly simplified). For this reason several methods have been developed to simplify the solution by reducing the number of pellet calculations which need

to be performed. Since it is the axial concentration and temperature profiles which are of principle interest, the obvious method is to eliminate the radial derivatives in the model. Simply to ignore the radial gradients is, however, inappropriate in many systems because the radial temperature profile especially significantly influences the reactor performance by determining the rate of heat removal from the bed.[12,64] The preferred approach, therefore, is to reduce the reactor model to a one dimensional form which incorporates some allowance for the effects of radial variations and from which it is possible to regenerate the radial profiles when these are required.

Turner[71] used a semi-empirical method of model reduction based on the use of pseudo-parameters to approximate the radial profiles and Naim[14] has recently extended this method to the unsteady state. Thornton[12] developed a one dimensional model based on the assumption of a parabolic radial temperature profile which results in a modified wall heat transfer coefficient. He showed that this formulation gives good agreement with the steady state predictions of the two dimensional model and proposed its application to the unsteady state. This model, which is described in Appendix (2), is particularly attractive for an extensive study of reactor performance because of the small amount of computational effort which it requires. It has, therefore, been evaluated in the dynamic form and used extensively in this thesis.

2.4 Stability

If very small changes in the inlet conditions of a reactor can cause very large changes to occur within the bed, then the reactor may be described as unstable in operation. Such instability may be due solely to parametric sensitivity, in which case removal of the disturbance will generally restore the original state, or to parametric sensitivity accompanied by the bed to exhibiting multiple states. In the latter case simply removing the disturbance will not always cause the reactor to return to its original state unless certain conditions are fulfilled.[12]

In either case, the consequences of the instability are similar; rapid reaction ignition or "blowout" may occur. Both of these phenomena are undesirable, more especially ignition since temperature runaway develops and this causes catalyst

deactivation and sintering, poor product selectivity and even damage to the coolant. A prior knowledge of the regions of potential instability is therefore desirable for the satisfactory and safe operation of the reactor.

The problem of instability in fixed bed reactors has been the subject of much of the recent literature and Ray[11] gives a good review of this work. Although, at an operational level instability is essentially a dynamic problem steady state information can be used to indicate regions of instability. For example, if for given inlet conditions a reactor may have two steady states then it may be possible with small perturbations, or even no perturbation at all, to cause it to switch rapidly from one to the other. If the parameter regions over which the two simultaneous steady states occur can be identified, then this behaviour may be avoided.

The catalyst pellets themselves may exhibit multiple steady states in which case the reactor will also show corresponding multiplicity. When the effects of axial heat and mass dispersion are included in the reactor model, examination of the equations shows that three steady state profiles are possible for identical feed conditions, even in quasi-homogeneous systems,[73] due to the backmixing of the fluid. Multiplicities of this kind have been well discussed by Perlmutter.[7] As Froment[9] has pointed out, however, the degree of fluid backmixing which has been found[74,75] to produce multiple steady states does not occur in industrial fixed bed reactors. Transport of heat from the reactor exit back to the entrance can occur external to the reactor due to either a recycle stream, in which case material is also transported backwards, or countercurrent cooling. Multiplicities caused by recycle have been studied both theoretically and experimentally,[76,77,78] the reactors of interest here, however, do not include a recycle stream. The occurrence of multiple steady states due to countercurrent cooling has been demonstrated experimentally by Luss and Medellin[117] with an unpacked, liquid phase single tube reactor; the possibility of this phenomenon with gaseous catalytic fixed bed reactors is examined in Chapters 7 and 8 of this thesis.

A large amount of the work reported in the literature concerns the development of stability criteria and the identification of regions of multiplicity for catalyst pellets without either the interphase or the intraparticle heat and mass transport

resistances. As was discussed in section 2 of this chapter, the only transport resistance which does not significantly affect the pellet performance over a wide range of parameters is the internal heat transfer resistance. Since, therefore, the stability criteria developed in the absence of interphase resistances cannot be extended to allow for them,[12] such criteria are of no practical use. Ray[11] has also shown that for a number of reactions the regions of multiplicity predicted for catalyst pellets with no interphase resistances are very unlikely to be attained in industrial reactors.

The stability criteria which have been proposed for catalyst pellets with no internal resistances[38,79] are a little more useful since they may, at least, be applied to non-porous particles and catalytic wires.

When all the transport resistances are included in the catalyst pellet model three steady states are possible for a given set of fluid conditions. Hatfield and Aris[80,81] have reported the possibility of five steady states, however this only seems to be possible outside the practical range of parameters (e.g. for low Sh/Nu ratios). In the case of three steady states of the catalyst pellet, the middle one is metastable. Cresswell[13,82] has derived necessary and sufficient conditions for multiplicity using a lumped parameter model of the catalyst pellet for single first order reactions. Thornton[12] and McGreavy and Thornton[83] have re-examined this problem and developed a method for predicting the region of multiple steady states of the pellet for both simple and complex reaction schemes. This method is particularly useful since the region of multiplicity may be plotted on a single phase diagram as a function of the fluid conditions for each reaction system. Reactor trajectories may be plotted on the same diagram thereby giving an immediate indication of potential instability and operating conditions. Essentially, the region of multiple steady states is characterised by an upper and lower bound of fluid temperature at a given fluid concentration. To attain the upper steady state the pellet must be perturbed across the upper bound and subsequent movement to the lower steady state is only possible by crossing the lower bound. In this way, the catalyst pellet exhibits hysteresis in the region of multiple steady states and does not actually attain the middle, metastable state. This behaviour has been demonstrated experimentally with a single catalyst

pellet, in which the ethylene hydrogenation reaction occurred, by Furusawa and Kunii[84] and Ray[11] reports that similar behaviour has been observed by Horak and Jiracek.[49] Thornton[12] and McGreavy and Soliman[85] have also investigated the dynamic behaviour of single catalyst particles in the region of multiplicity and the latter were able to determine the amplitude and frequency of fluid perturbations which cause the pellet to remain in the upper state.

The phenomenon of parametric sensitivity outside of the region of multiplicity has received little attention: the analyses which have been performed have been concerned only with quasi-homogeneous systems.[67,68,69] Thornton's[12] results indicate that parametric sensitivity near regions of multiplicity is likely to be a more serious problem than the multiplicity itself. This point is examined in Chapter 4 of this thesis.

2.5 Concluding Remarks

In contrast to the considerable effort devoted to simplifying the reactor models some investigators have formulated more complex models. For example, catalyst pellets in non-uniform concentration and temperature fields have been studied from the point of view of stability;[86,87,88] other workers have considered the existence of asymmetric intraparticle profiles in catalyst slabs and pellets in a symmetric environment[89,90,91] and an interesting paper by Luss[92] shows that severe heating of individual active sites may occur whilst the catalyst support remains relatively cool. Experimental verification of these models, and results, is virtually impossible and their use, at present, in viable reactor models is out of the question.

By and large, the problem of the formulation of tractable models which sufficiently describe the reactor seems to have been overcome. This has been due mainly to the identification of the important physical and chemical processes which occur in these highly complex systems. Much work on simplified or very specific systems has been done but still very little information is available on the general behaviour of industrially orientated systems. Now that most of the mathematical tools are available such a study is possible.

CHAPTER 3

HEAT TRANSFER IN PACKED BEDS

3.1 Introduction

The rate of reaction, and therefore the rate of heat generation for exothermic reactions is extremely dependent on temperature, usually in a non-linear manner. It is, therefore, essential that a mathematical model of a packed bed reactor should contain an adequate description of the heat transfer processes occurring within the bed. Not to do so, at the design stage, could lead to either a very conservative design or disastrous situations during operation of the reactor caused by, for example, temperature runaway. However, which heat transfer processes to include in the model and how to describe them must be decided. Consideration of these factors is not only relevant to the basic structure of the reactor models used in this thesis but also raises some fundamental questions concerning the whole philosphy of system modelling.

In the synthesis of any system model, the first requirement is to establish the criteria which must be met by the model. For the extremely complex system represented by the fixed bed reactor this is of considerable importance since to attempt to describe all chemical and physical processes occurring within the bed would clearly lead to an intractable model. To avoid this, the following factors must be considered:

1. In what context will the model be used?
2. What level of detail and complexity are needed to provide a quantitative description of performance for use in a criterion function?
3. Can measurements be made of the parameters which appear in the model?

Clearly, if certain effects are found to be unimportant over a particular parameter range, then their inclusion in a model intended for use in that range unnecessarily complicates the model and wastes computation time. Also there is little point in studying a system model which contains parameters

that cannot be measured or estimated since no reliability can be attached to its predictions.

Implicitly, in the approach adopted here, an attempt is made to identify the basic structural features, developing the model in terms of the physical or chemical processes considered to be rate limiting. In so doing it is necessary to use only average values for the bed. For example, it is not feasible to consider variations due to the shape of the particles, or the change in some coefficients around the pellets, since these could not be measured and could certainly not be predicted in other situations. Nor is it likely to be feasible to consider anything other than average bed properties, even though there will, in fact, be local variations. Moreover, there is the question concerning coefficients which are obtained from simple experimental measurements and their use in more complex situations. In a reacting system with heat generation it may be inappropriate to use the same effective heat transfer coefficients as obtained from a non-reacting system.

In a non-isothermal, non-adiabatic reactor heat, and mass, transfer may occur both axially and radially. (Here it should be noted that the axial transport referred to is not that due to the bulk movement of the reacting gases, but rather that due to dispersion processes). Reactor models which include a description of axial heat transfer have received considerable attention since they predict the possibility of more than one steady state occurring within the bed.[73] Clearly when synthesising models for use in the conditions under which this phenomenon may occur then it is essential that the mechanism of axial heat transfer is included. However, Carberry and Wendel[53] have shown that axial heat dispersion has no effect on the reactor profiles when the bed depth exceeds 50 particle diameters. More recently, Karenth and Hughes[54] and Naim[15] have confirmed this result. Moreover it has been shown[74,9] that for highly exothermic partial oxidation reactions the parameter range over which axial heat transfer is important lies considerably outside that used in practice in industrial units. The length of industrial fixed beds removes the need for reactor models to include axial diffusion and the risks involved with multiple steady states

due to this phenomenon, except perhaps for very shallow beds.[74] The reactor models developed and studied in this thesis are intended for use with industrial units and so with regard to points (1) and (2) above, axial mixing effects are not included in their formulation.

Radial heat transfer in non-adiabatic packed beds is a far more important process since this is the means by which the bed exchanges heat with its surroundings. Recently the method of describing radial heat transfer in a mathematical model of the packed bed reactor has become a point of conjecture.[60,94] Specifically the point at issue has been that radial heat transport due to the presence of the solid phase must be accounted for by a two phase heat transfer model[60] since it may not be adequately described by the single phase model[95] which makes use of effective heat transport coefficients. This is not, in fact, the case; as will be shown later in this chapter, although the contribution to radial heat transfer due to the presence of the solid may need to be considered, it can be taken care of in the existing lumped parameter models[95] if the effective radial thermal conductivity is properly defined. Moreover, the advantage of the single phase model over the two phase description is that it can automatically account for what is perhaps the most significant phenomenon, namely mass transfer limitations in the solid. It will be shown that all the features predicted by the complex two phase model are reproduced using the simpler representation.

3.2 The Mechanisms of Radial Heat Transfer

The separate conductivities of the solid and fluid have been the subject of considerable study, although, regrettably, most of the work appears to have been confined to the examination of packed bed heat exchangers. The solid conductivity has been investigated by Kunii and Smith[96] in the absence of forced convection and reaction, and by Krupiczka[97] at low temperatures, to avoid radiation effects, and by Wakao and Kato[98] who considered only solid-solid contact and radiation. Other workers[28,99,100] have studied flow and radial dispersion in packed beds in order to quantify the effect of radial fluid flow on the conductivity. Singer and Wilhelm[101] were the first to study the contributions of each phase to a single overall effective conductivity, and much work on this problem

has followed.[102,103,104,105,96] The more important mechanisms of radial heat transfer have been shown to be:[101,103]

(a) Thermal conduction through the solid.
(b) Thermal conduction through the contact surfaces of two adjacent particles of packing.
(c) Radiation between the surfaces of two particles.
(d) Thermal conduction through the gas film around the contact surfaces of two particles.
(e) Radiation between neighbouring gas pockets (in the voids between particles).
(f) Molecular thermal conduction of the gas.
(g) Heat transfer by lateral mixing of the gas.

Both in evaluating experimental values and in using them for design calculations, it should be remembered that the effective coefficients are strictly only defined when the area and temperature profiles are specified so that the heat flux can be determined. In particular, the areas for transfer of some of the fluxes are not the same. It is common practice to refer them to a common area and this must necessarily redefine the effective coefficient. It is essential to make sure which coefficient is used. Where heat flux through the solid is considered to be by conduction, the point contact area severely limits the net flux, and when the coefficient is re-expressed in terms of the mean cross-sectional area of the pellet, the numerical value is correspondingly very much smaller than the intrinsic value. Many values quoted in the literature are often obscure on this point and can be misleading.

Mechanisms (a) to (d) have usually been taken to contribute to the effective conductivity of the solid[101,103] and mechanisms (e) to (g) contribute to the gas conductivity. To ascertain their relative importance, it is convenient to discuss each separately, although, in some cases, the mechanisms are related.

(a) Thermal Conduction through the solid

Most workers,[60,101,102,103] when assessing the contribution of this mechanism to the radial transfer of heat have assumed that heat is conducted through the pellet from the hotter

surface, nearer the centre of the bed, to the cooler one nearest the tube wall, parallel to the direction of heat flow in the gas, i.e. they have assumed the temperature gradient, within the pellet, in the radial direction to be smooth. This assumption is best illustrated by the expressions used by De Wasch and Froment[60] and Argo and Smith[102] for the effective radial conductivity of the solid. No account has been taken of the effect of heat generation within the particle, on this assumption since most of the theory has been developed for packed bed heat exchangers. When a gaseous reactant diffuses into a catalyst particle, it is adsorbed at various sites, where it reacts. In the case of an exothermic reaction, this causes heat generation throughout the particle which is therefore at a higher temperature than the surrounding gas. In these circumstances, assuming a uniform external fluid field, the heat flow within the particle would be radially outwards from its centre. Even in the case of a non-uniform external field,[88] the temperature within the particle will be higher than that at the surface. Only when severe external gradients exist will the heat flow, with chemical reaction inside the catalyst particle, be parallel to the heat flow in the external fluid. Usually, in packed bed reactors, such severe external gradients will only occur in a narrow region near the tube wall.

(b) Thermal conduction through the contact surfaces of two adjacent particles of packing.

Heat conduction through contact points depends upon the conductivity of the solid and upon the contact areas between particles. Surface coating of the particles, if any, will also contribute. Little is known about contact conductivity, although if the particles are forced together the contact resistance will certainly be less than if the bed is loosely packed. Singer and Wilhelm[101] found that for high conductivity packing materials, such as metals, differences in contact conductivities contribute little to the effective conductivity of the solid, and with low conductivity materials, such as those used for catalyst supports, conduction through contact is of negligible importance.

Even if it were possible to measure the contact conductivities accurately enough, there still remains the problem

of determining the area of contact between adjacent particles of packing. This is the reason why gas fillet conduction has usually been lumped with contact conduction. The area of contact will clearly depend on the shape of the packing surface. Wakao and Kato[98] have found that when the inter-particular radiation is significant then the effective conductivity of the packing is insensitive to the contact area. In the case of spherically shaped catalyst particles, only point contact between particles is possible. With cylindrical packing it is possible that some flat end surfaces will be in contact, but mostly there will be only point or line contact between particles. Clearly then, in either case, the contact area between particles will be extremely small, making the amount of conduction through the solid by contact negligible when compared with the other mechanisms, for example, turbulent mixing in the gas.

(c) Radiation between the surfaces of two adjacent particles

Radiative heat transfer does not become important until a temperature of approximately 600 K is reached. Even then, although the emissivity of a catalyst particle is close to unity, because of its irregular surface, the amount of radiation from particle to particle is small compared with the radial heat flux due to the other modes of radial heat transfer.

(d) Thermal conduction through the gas film around the contact surface of two particles

The assumptions made by most workers[100,101,102] have been that there is a linear radial temperature gradient through the solid, and that around the point of contact of two solid particles there exists a stagnant fillet of gas at a temperature intermediate between that of the two particles. It was then assumed that heat is conducted through this fillet from the hotter to the cooler particle. The problem encountered has been to determine a suitable "average thickness" of the gas fillet. Yagi and Kunii[103] have used the data of previous workers, for non-reacting systems, to obtain a correlation for this thickness, assuming that it is independent of Reynolds number. Clearly, this will give rise to error since at high Reynolds numbers the gas fillet will be smaller than at low values. This is relevant to the point raised earlier regarding the use of average values for the bed coefficients and the feasibility

of measuring them.

No data exists for reacting systems. In estimating the effect of this mode of heat transfer, similar arguments to those used above apply. Because of the effect of reaction, the radial temperature gradient is not a smooth function and the temperatures of two adjacent solid surfaces will probably be higher than that of the gas film between them. Both surfaces will, therefore, be discharging heat to the fillet.

It appears then that this mode of heat transfer through the solid will contribute little, if any, to the total radial effect.

(e) Radiation between neighbouring gas pockets in the voids between particles.

The same reasoning used for radiation between adjacent particles applies here. The radiation between neighbouring gas pockets will be less than that between adjacent particles since they are at a higher temperature than the gas in reacting systems. In any event, this contribution to radial heat transfer will be negligible compared with that due to eddy diffusion of the gas.

(f) Molecular thermal conduction of the gas

If the Reynolds number based on a particle diameter exceeds approximately 40, as is the case in industrial units, then molecular thermal conduction in the gas is negligible compared with radial heat transfer by lateral mixing.[106]

(g) Heat transfer by turbulent mixing

This is by far the most significant contributor to radial heat transfer in packed bed reactors. It is perhaps the most studied and best understood mechanism. Lateral mixing of the gas controls the radial heat flux in the bed.[103]

Having examined the seven possible modes of radial heat transfer, their contributions to an effective radial conductivity, or to separate effective conductivities for each phase, may be discussed.

3.3 Composite Effective Thermal Conductivities

Using the reasoning put forward above, the solid conductivity may be expected to be small compared with that of a gas in a reacting system. The gas conductivity will almost be

solely dependent on turbulent lateral mixing. Indeed, the solid adds little to the value of the effective overall thermal conductivity referred to the gas phase. The actual heat flux through the solid can be expected to be extremely small, and it is rather the effects due to the presence of the solid which increase the radial heat transfer. For example, radiation from particle to particle. Other far more important factors contribute much more to the radial heat flux. This would appear to be supported by the results of the extensive study by Singer and Wilhelm[101] who found that for most ceramic packings the radial thermal conductivity of the solid is negligible compared with that of the gas.

The two phase heat transfer model, however, attempts to sum up these various thermal transport processes which occur due to the presence of the solid and describes them as a radial heat flux within the solid as if it were a continuous phase. This is not only an apparently false interpretation of the physical situation but it also gives rise to several problems. In order to solve the equations which constitute the model, the parameters must be measurable or at least capable of being accurately estimated. The separate effective conductivities of the solid and the gas in packed bed reactors cannot be reliably measured. Moreover, the same problem arises with the heat transfer coefficients at the tube wall; separate values of these are required for the solid and the gas if a two phase description of radial heat transfer is used. The experimental results for heat transfer parameters are usually correlated as a single effective overall radial thermal conductivity and a single effective overall wall heat transfer coefficient without distinguishing between the solid and the fluid[104,107] since these are the only values which can be simply measured. McKeon[107] has found that because of the necessity of obtaining average bed values of the heat transfer parameters, for use in a mathematical model of the bed, it is difficult to accurately predict even lumped values of these parameters. Splitting these measured overall values into separate solid and fluid values would, therefore, probably introduce further errors since the equations governing the two separate conductivities arise from mostly conceptual rather than practical considerations. Any errors introduced in this way are further compounded in estimating the solid to wall and gas to wall heat transfer co-

efficients. Yagi and Kunii[108] have proposed an equation for the solid to wall value but, as De Wasch and Froment[60] point out, it contains a parameter for which no data is available. De Wasch and Froment[60] circumvented this problem by assuming that at the tube wall the gas and solid temperatures are equal. This enabled them to split the measured value of the overall effective wall heat transfer coefficient into separate solid and gas values by comparing the two fluxes at the wall. However, the validity of the values obtained in this way depends on the validity of the calculated values of effective conductivity, which, as pointed out above, are subject to some uncertainty. Perhaps the greatest deficiency of the two phase approach is that it fails to recognise the importance of diffusion in the solid. In the two phase heat transfer model the solid, as well as the gas, is treated as a continuum which fills the whole volume of the reactor tube, for the purposes of heat transfer due to the presence of the solid. In order to maintain consistency in the model, mass diffusion within the solid must be described in the same way. However, unlike heat transport, mass transport within the solid is essentially a local phenomenon; within the solid there is not a radial mass flux from the centre of the reactor to the tube wall, and so to describe one in this manner is not very meaningful. In quasi-homogeneous systems this is not a problem since diffusion of mass within the solid is not a rate limiting process. In heterogeneous systems, however, it is necessary to be able to calculate the effectiveness factor, which is a measure of the reaction rate limitation caused by diffusion, as the calculation proceeds to obtain accurate results. The importance of this is illustrated by figure 3.1.This shows axial profiles of radial mean temperature predicted by the reactor model both with and without an effectiveness factor calculation. As can be seen, assuming an effectiveness factor of unity leads to temperature runaway, whereas accounting for internal solid mass transfer predicts a perfectly safe profile since the effectiveness factor is much less than unity. With the two phase heat transfer model the effectiveness factor must be specified a priori for a logically consistent representation and this is usually only possible when the system is known to be quasi-homogeneous, in which case it is unity.

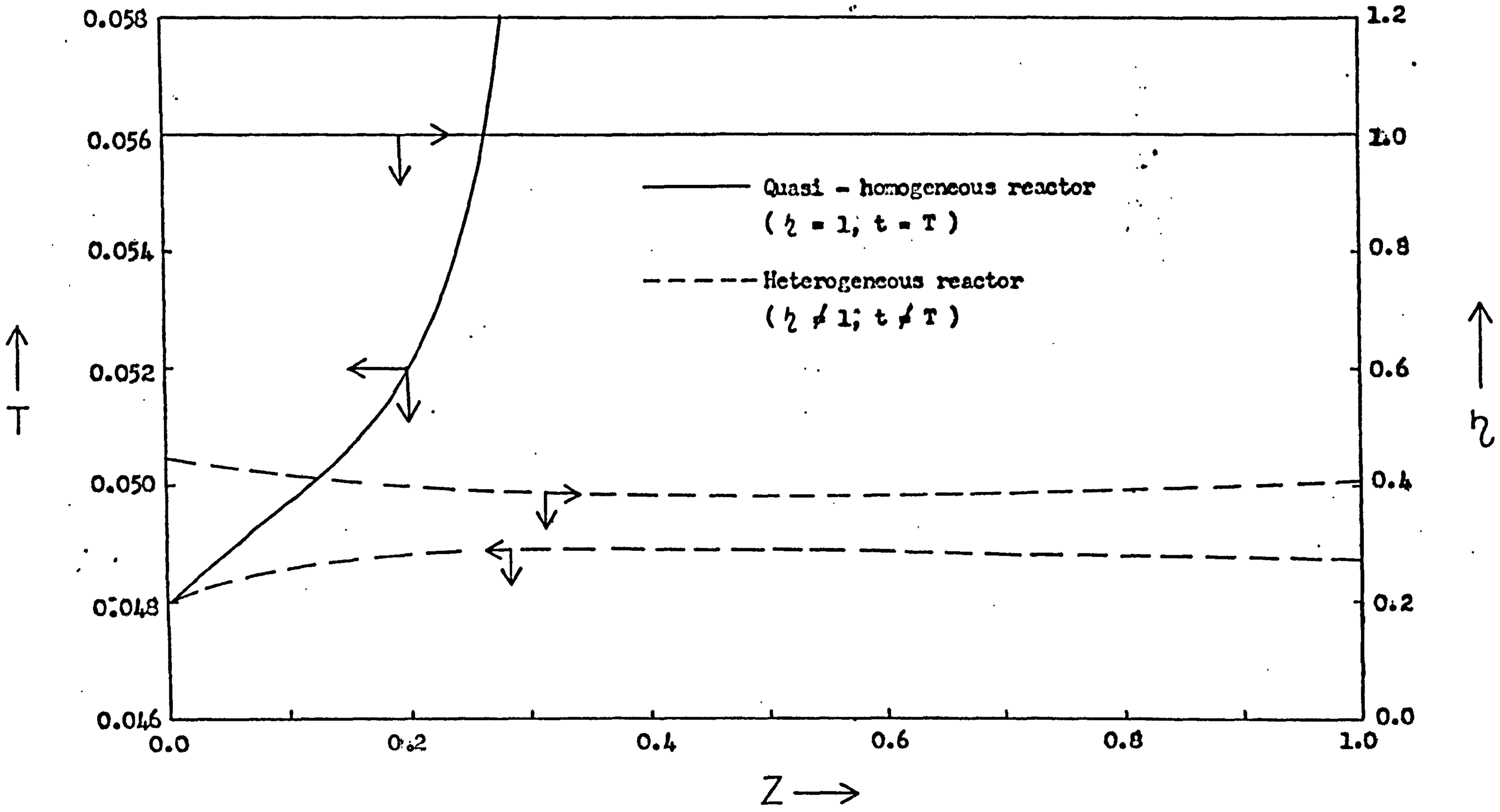

Figure 3.1 Axial profiles of radial mean temperature and effectiveness factor predicted by model I for quasi - homogeneous and heterogeneous systems. (Data as given in Table 3.1)

Furthermore the use of the model in transient studies must also be considered. It is difficult to see how the capacitance of the catalyst pellets may be described in the two phase approach since again this is a local solid property.

The use of a single overall effective thermal conductivity, as measured, in the heat transfer model is therefore a better approach, particularly in heterogeneous systems and this would appear to be supported by the results of Olbrich.[94]

3.4 The Lumped Parameter Model for Radial Heat Transfer

The equations of the single phase (lumped parameter) and two phase models are given in dimensionless form below, for a simple $A \rightarrow B$ reaction scheme. In both models the form of the fluid field equations is essentially the same. The difference lies in the manner in which heat transfer due to the presence of the solid is described and the ease with which local intraparticle concentration gradients can be accounted for.

Model I (single phase)

Fluid

$$\frac{\partial^2 C_A}{\partial r^2} + \frac{1}{r}\frac{\partial C_A}{\partial r} - S_1\frac{\partial C_A}{\partial z} - S_2 \zeta R' = 0 \qquad (3.1)$$

$$\frac{\partial^2 T}{\partial r^2} + \frac{1}{r}\frac{\partial T}{\partial r} - S_3\frac{\partial T}{\partial z} + S_4(t - T) = 0 \qquad (3.2)$$

with boundary conditions:

$$\left.\begin{aligned} C_A &= C_{AO} \\ T &= T_0 \end{aligned}\right\} \quad \text{at } z = 0,\ 0 \leqslant r < 1$$

$$\frac{\partial C_A}{\partial r} = \frac{\partial T}{\partial r} = 0, \text{at } r = 0,\ 0 < z \leqslant 1$$

$$\left.\begin{aligned} \frac{\partial C_A}{\partial r} &= 0 \\ \frac{\partial T}{\partial r} &= Nu_w(T_c - T) \end{aligned}\right\} \quad \text{at } r = 1,\ 0 < z \leqslant 1$$

Solid

$$S_5(C_A - C_{pAs}) = \zeta R' \qquad (3.3)$$

$$S_6(C_A - C_{pAs}) - t + T = 0 \qquad (3.4)$$

where:

$$S_1 = \frac{R^2 u_s}{LD_{fA}} \qquad S_2 = \frac{R^2(1 - e)}{D_{fA}}$$

$$S_3 = \frac{R^2 u_s \rho c_p}{LK_{fs}} \qquad S_4 = \frac{3R^2 h(1-e)}{bK_{fs}}$$

$$S_5 = \frac{3k_{gA}}{b} \qquad S_6 = \frac{(-\Delta H)C_0 R_g k_{gA}}{hE}$$

$$Nu_w = \frac{RU}{K_{fs}}$$

Model II (two phase)

Fluid

$$\frac{\partial^2 C_A}{\partial r^2} + \frac{1}{r}\frac{\partial C_A}{\partial r} - F_1 \frac{\partial C_A}{\partial z} - F_2 \zeta R' = 0 \qquad (3.5)$$

$$\frac{\partial^2 T}{\partial r^2} + \frac{1}{r}\frac{\partial T}{\partial r} - F_3 \frac{\partial T}{\partial z} + F_4(t - T) = 0 \qquad (3.6)$$

with boundary conditions:

$$\left.\begin{aligned} C_A &= C_{AO} \\ T &= T_O \end{aligned}\right\} \quad \text{at } z = 0,\ 0 \leqslant r < 1$$

$$\frac{\partial C_A}{\partial r} = \frac{\partial T}{\partial r} = 0 \quad \text{at } r = 0,\ 0 < z \leqslant 1$$

$$\left.\begin{aligned} \frac{\partial C_A}{\partial r} &= 0 \\ \frac{\partial T}{\partial r} &= Nu_w^f(T_c - T) \end{aligned}\right\} \quad \text{at } r = 1,\ 0 < z \leqslant 1$$

Solid

$$F_5(C_A - C_{pAs}) = \zeta R' \qquad (3.7)$$

$$\frac{\partial^2 t}{\partial r^2} + \frac{1}{r}\frac{\partial t}{\partial r} - F_6(t - T) + F_7 \zeta R' = 0 \qquad (3.8)$$

with boundary conditions:

$$\frac{\partial t}{\partial r} = 0 \quad \text{at } r = 0,\ 0 < z \leqslant 1$$

$$\frac{\partial t}{\partial r} = Nu_w^s(T_c - t) \quad \text{at } r = 1,\ 0 < z \leqslant 1$$

where:

$$F_1 = S_1 \qquad F_2 = S_2$$

$$F_3 = \frac{R^2 u_s \rho c_p}{Lk_f} \qquad F_4 = \frac{3R^2 h_c(1-e)}{k_f b}$$

$$F_5 = S_5 \qquad F_6 = \frac{3R^2 h_c(1-e)}{k_s b}$$

$$F_7 = \frac{R^2(1-e)(-\Delta H)R_g C_0}{k_s E}$$

$$Nu_w^f = \frac{RU_f}{k_f} \qquad Nu_w^s = \frac{RU_s}{k_s}$$

The finite difference form of the two dimensional reactor equations is given in Appendix (3). Solution may be accomplished by a marching technique proceeding from the reactor inlet to the outlet.

In order to be able to compare the two models, the data of De Wasch and Froment,[60] which is given in Table 3.1, has been used. For this data, the reaction rate is expressed in terms of the solid conditions for a first order, irreversible reaction with Arrhenius kinetics. Thus in equations (3.1), (3.3), (3.5), (3.7) and (3.8), R' is given by:

$$R' = A_0 \exp(-1/t) C_{pAs}$$

In both models the temperatures have been made dimensionless with respect to the activation energy and the gas constant.

Model I employs the isothermal pellet model discussed in the previous chapter. Thus the concentration of the reactant at the catalyst pellet surface, C_{pAs}, may be expressed as a function of the solid temperature, t, by solving the equation describing diffusion within the solid (see Appendix (1)), and so the effectiveness factor, η, may be evaluated at each point in the bed during the calculation. It can be seen from equations (3.5) to (3.8) that, as has been mentioned above, this is not possible in Model II, since the solid is described as a continuum by equation (3.8). Consequently, the effectiveness factor must be predicted, or specified, in some manner before the calculation begins. Indeed, De Wasch and Froment[60] specified $\eta = 1$ so that only a surface reaction was considered. Except where stated, this simplification has been retained here for both reactor models so that they may be compared for the same system.

In Model II, the two parallel heat transfer paths are described explicitly, the one in the solid and the other in the fluid. Model I, on the other hand, accounts for the radial heat transfer which occurs due to the presence of the solid by means of the effective overall radial thermal conductivity

TABLE 3.1 Data used in Chapter 3 for comparison of the heat transfer models.

A_o	2.72×10^9	sec^{-1}	S_1	0.521
b	0.15	cm	S_2	0.134
c_p	0.237	cal gm^{-1} K^{-1}	S_3	0.262
D_{fA}	7.23	cm^2 sec^{-1}	S_4	105.5
e	0.38		S_5	300.0
E	27.0×10^3	cal $gmole^{-1}$	S_6	57.5×10^{-4}
h_c	5.15×10^{-3}	cal cm^{-2} sec^{-1} K^{-1}	Nu_w	2.3
h_p	4.33×10^{-3}	cal cm^{-2} sec^{-1} K^{-1}		
h_r	0.537×10^{-3}	cal cm^{-2} sec^{-1} K^{-1}	F_1	0.521
K_{fs}	1.84×10^{-3}	cal cm^{-1} sec^{-1} K^{-1}	F_2	0.134
k_f	1.12×10^{-3}	cal cm^{-1} sec^{-1} K^{-1}	F_3	0.4303
k_{gA}	15.0	cm sec^{-1}	F_4	89.1
k_g'	1.039×10^{-4}	cal cm^{-1} sec^{-1} K^{-1}	F_5	300.0
k_p	2.6×10^{-3}	cal cm^{-1} sec^{-1} K^{-1}	F_6	138.6
k_r	0.32×10^{-3}	cal cm^{-1} sec^{-1} K^{-1}	F_7	51.7×10^{-4}
k_s	0.72×10^{-3}	cal cm^{-1} sec^{-1} K^{-1}	Nu_w^f	2.3
K_p	2.78×10^{-3}	cal cm^{-1} sec^{-1} K^{-1}	Nu_w^s	2.3
L	100.0	cm		
P	1.0			
R	1.25	cm		
u_s	241	cm sec^{-1}		
$(-\Delta H)$	307×10^3	cal $gmole^{-1}$		
U_f	2.06×10^{-3}	cal cm^{-2} sec^{-1} K^{-1}		
U_s	1.33×10^{-3}	cal cm^{-2} sec^{-1} K^{-1}		
U	3.39×10^{-3}	cal cm^{-2} sec^{-1} K^{-1}		
ϱ	0.54×10^{-3}	gm cm^{-3}	ζ	1.0
C_o	1.7×10^{-7}	gmole cm^{-3}	C_{Ao}	1.0
T_o', T_c'	643	K	T_o, T_c	0.04733

referred to the gas, the effective gas-to-wall heat transfer coefficient and the solid-to-gas heat transfer coefficient. It is important, therefore, that when significant radial heat transfer due to the presence of the solid occurs the appropriate values of these parameters are used. The overall effective thermal conductivity and gas-to-wall heat transfer coefficient present no problems since as measured experimentally they automatically include the effects of the solid. The pellet-to-gas heat transfer coefficient, however, is somewhat different since the measured value is generally only the convective value. In model I, a heat balance on each pellet is required in order to compute the pellet temperature at each point in the bed. The heat removal from each pellet is described solely by the surface heat transfer coefficient, h. Since the total heat removal from each pellet must be accounted for in this balance it is, therefore, necessary to include interparticular radiatior and conduction, when these are significant, in the parameter h, as well as convection, since these are all processes by which heat is removed from each pellet. Clearly this is not necessary in model II since interparticular radiation and conduction are accounted for in the effective conductivity of the solid and so the value of h is only that due to convection, h_c.

When radial heat transfer due to the presence of the solid is significant, an estimate of the effective surface heat transfer coefficient, which includes the heat loss from each pellet due to interparticular radiation and conduction, for use in model I may be obtained in the following manner.

Let the effective surface heat transfer coefficient, h, be the sum of the coefficients for convection and radiation and contact between the particles. Thus:

$$h = h_c + h_p + h_r \qquad (3.9)$$

The convective coefficient, h_c, may be evaluated in the usual way, for example by the Handley and Heggs[109] correlation. The radiation and point contact coefficients, h_r and h_p, may be deduced as follows. Consider two adjacent spherical particles of packing. The heat transferred from particle 1 to particle 2 is:

$$\text{by radiation} = k_r \frac{\pi d_p^2}{4 d_p} (t_1 - t_2)$$

and by contact = $k_p \frac{\pi d_p^2}{4d_p} (t_1 - t_2)$

where the area for heat transfer is the projected cross-sectional area of the pellets and the thermal conductivities, k_r and k_p, are defined accordingly. The temperatures t_1 and t_2 are the surface temperatures of pellets 1 and 2 respectively and are assumed to be uniform. Now, if this heat is transferred to the gas by means of the surface heat transfer coefficients, h_r and h_p, then heat transferred from the surface of pellet 1 to the gas is:

by radiation = $h_r \frac{\pi d_p^2}{2} (t_1 - T)$

and by contact = $h_p \frac{\pi d_p^2}{2} (t_1 - T)$

Therefore we may write:

$$h_r (t_1 - T) = \frac{k_r}{2\bar{d}_p} (t_1 - t_2)$$

and

$$h_p (t_1 - T) = \frac{k_p}{2\bar{d}_p} (t_1 - t_2)$$

If it is further assumed that $t_2 = T$ then

$$h_r = \frac{k_r}{2\bar{d}_p} \quad \text{and} \quad h_p = \frac{k_p}{2\bar{d}_p} \tag{3.10}$$

Clearly particle 2 will not be at the same temperature as the gas surrounding particle 1. However, in most cases the difference will not be too large and the assumption is reasonable.

Here, it is worth noting that Argo and Smith[102] proposed expressions for h_r and h_p, in a similar type of analysis, which are inconsistent since h_r is given as:

$$h_r = \frac{2k_r}{d_p} + \frac{k_r h}{K_p}$$

so that if $k_r > K_p$ then $h_r > h$ which is not possible since

$$h = h_c + h_p + h_r$$

In equation (3.10) Damkoehler's[110] simplified expression for radiation may be used to obtain k_r, viz:

$$k_r = 4d_p P/(2 - P) \times 1.234 \times 10^{-4} \times T^3/100^4 \times \varepsilon_2/(\varepsilon_2 + \varepsilon_3)$$

k_p may be obtained in a manner similar to that used by Beveridge and Haughey,[111] viz:

$$k_p = \frac{K_p}{\phi} \varepsilon_3/(\varepsilon_2 + \varepsilon_3) + \frac{k'_g}{\phi} \varepsilon_2/(\varepsilon_2 + \varepsilon_3)$$

with the appropriate area corrections.

Thus k_p and k_r obtained from these expressions may be substituted into equations (3.10) to give h_p and h_r. These values are then used together with the appropriate value of h_c in equation (3.9) to give the effective heat transfer coefficient, h.

Using the data given in Table 3.1 and the above equations to compute h, model I was solved for the same conditions as model II. Figure 3.2 shows how close the agreement is between the predicted axial profiles of the centre-line temperatures and the radial mean temperatures of both models when the value of h used in model I is evaluated in this way. This agreement is confirmed by the typical radial temperature profiles shown in figure 3.3. For practical purposes the difference is indistinguishable.

Also shown in figure 3.2 are the axial profiles of radial mean temperature and centre-line temperature predicted by model I when the effectiveness factor is not unity but is computed as the calculation proceeds. It can be seen that in this case the predicted temperature profiles are considerably different from those when $\zeta = 1$, and this serves to further emphasise the importance of being able to calculate the reaction rate limitations due to intraparticle mass transfer as the computation proceeds.

Figure 3.4 shows axial profiles of radial mean temperature predicted by both models when the value of h used in both of them is that due only to convection. As can be seen the difference in the profiles predicted by the two models is not great, the maximum value being approximately 0.0004 in dimensionless form, which corresponds to 5.5K for the activation energy given in Table 3.1. Model I predicts a slightly higher temperature than model II since in this case the effects of interparticle radiation and conduction have not been included in h. Thus the pellets are slightly hotter and so the rate of reaction and therefore the rate of heat generation is greater than that predicted by model II. Hence, it is important to incorporate all significant mechanisms and this is achieved by identifying the general structure of the system as reflected in the com-

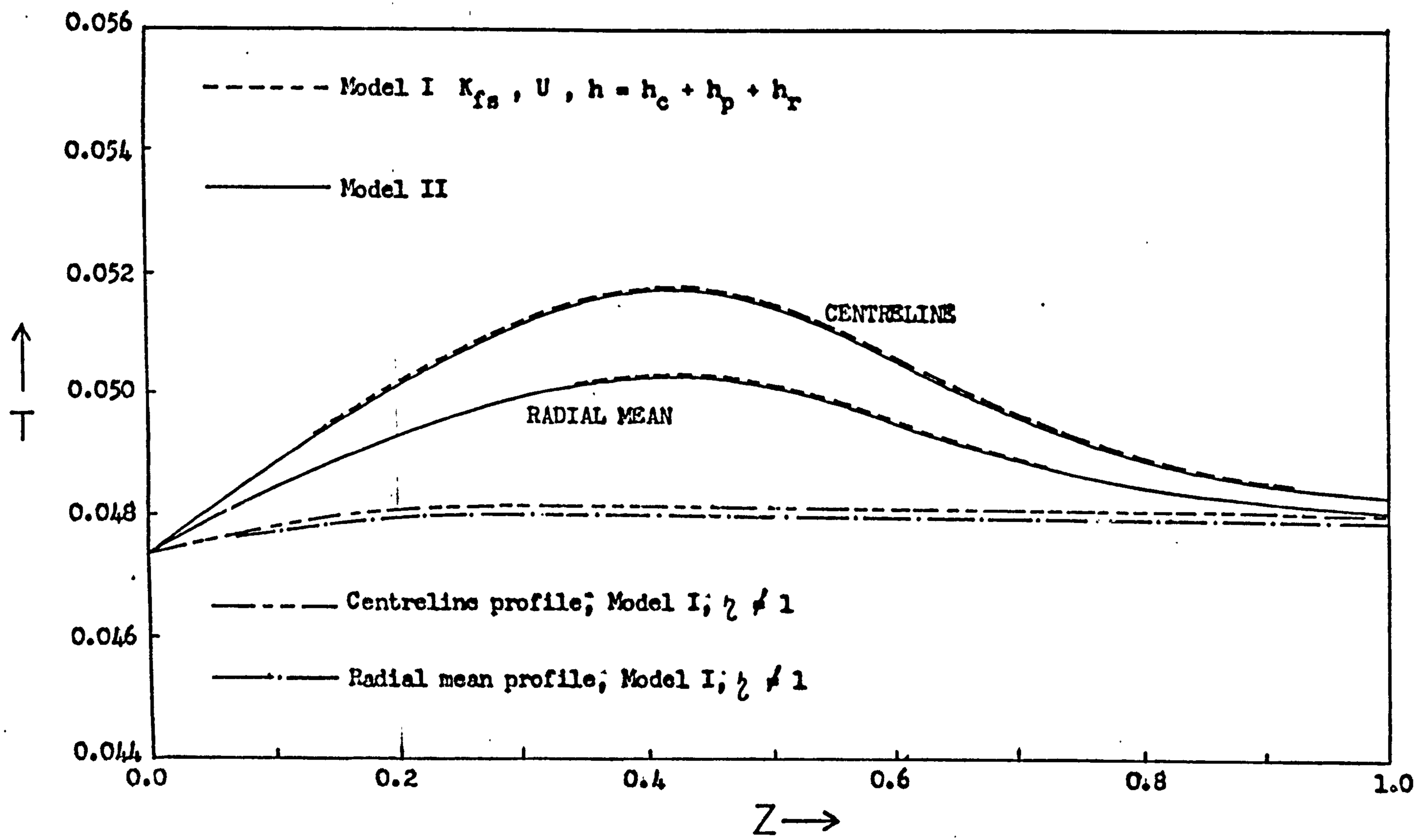

Figure 3.2 Axial temperature profiles predicted by Models I and II: (Data as given in Table 3.1)

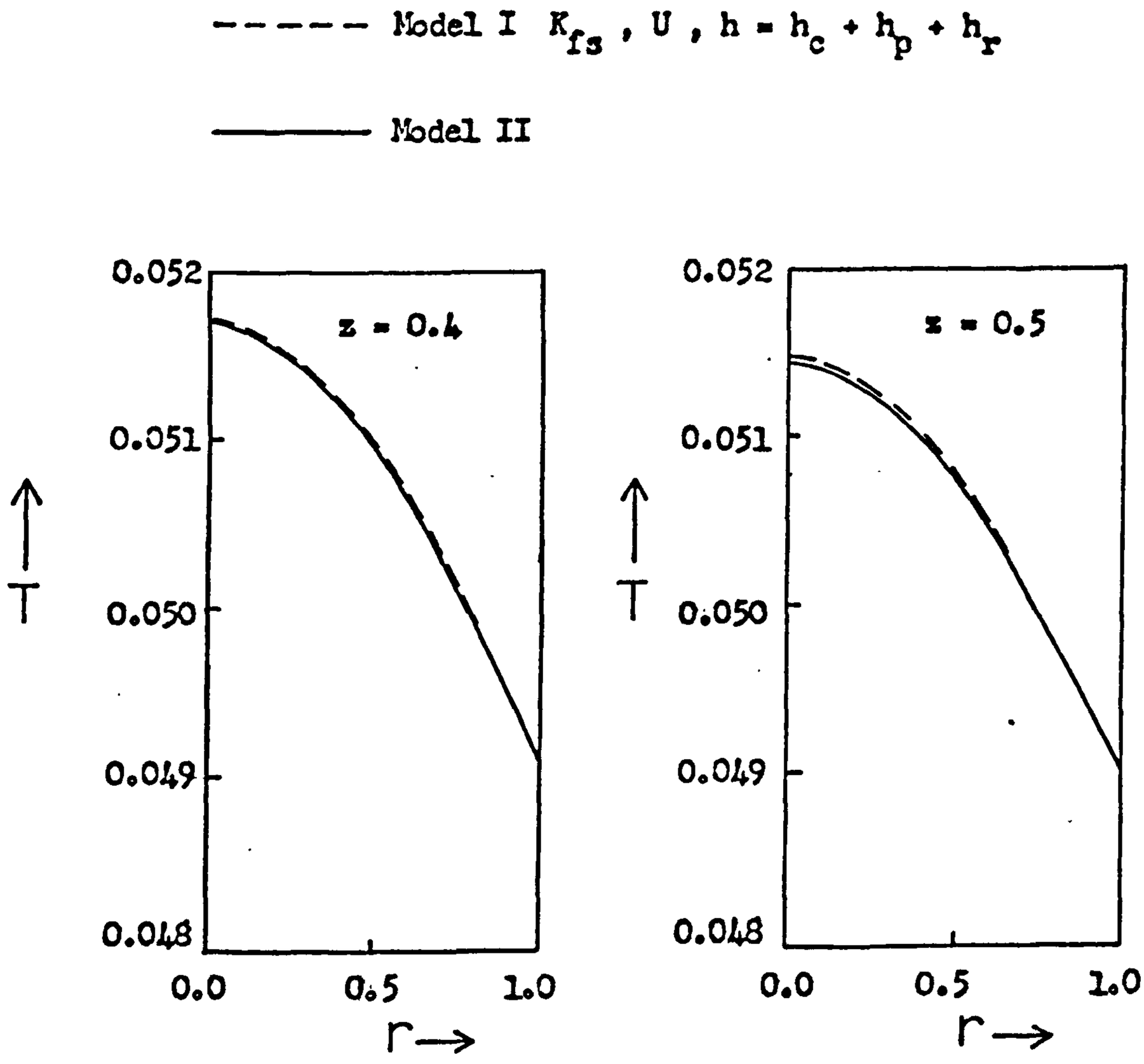

Figure 3.3 Radial temperature profiles predicted by Models I and II at two axial positions. (Data as given in Table 3.1)

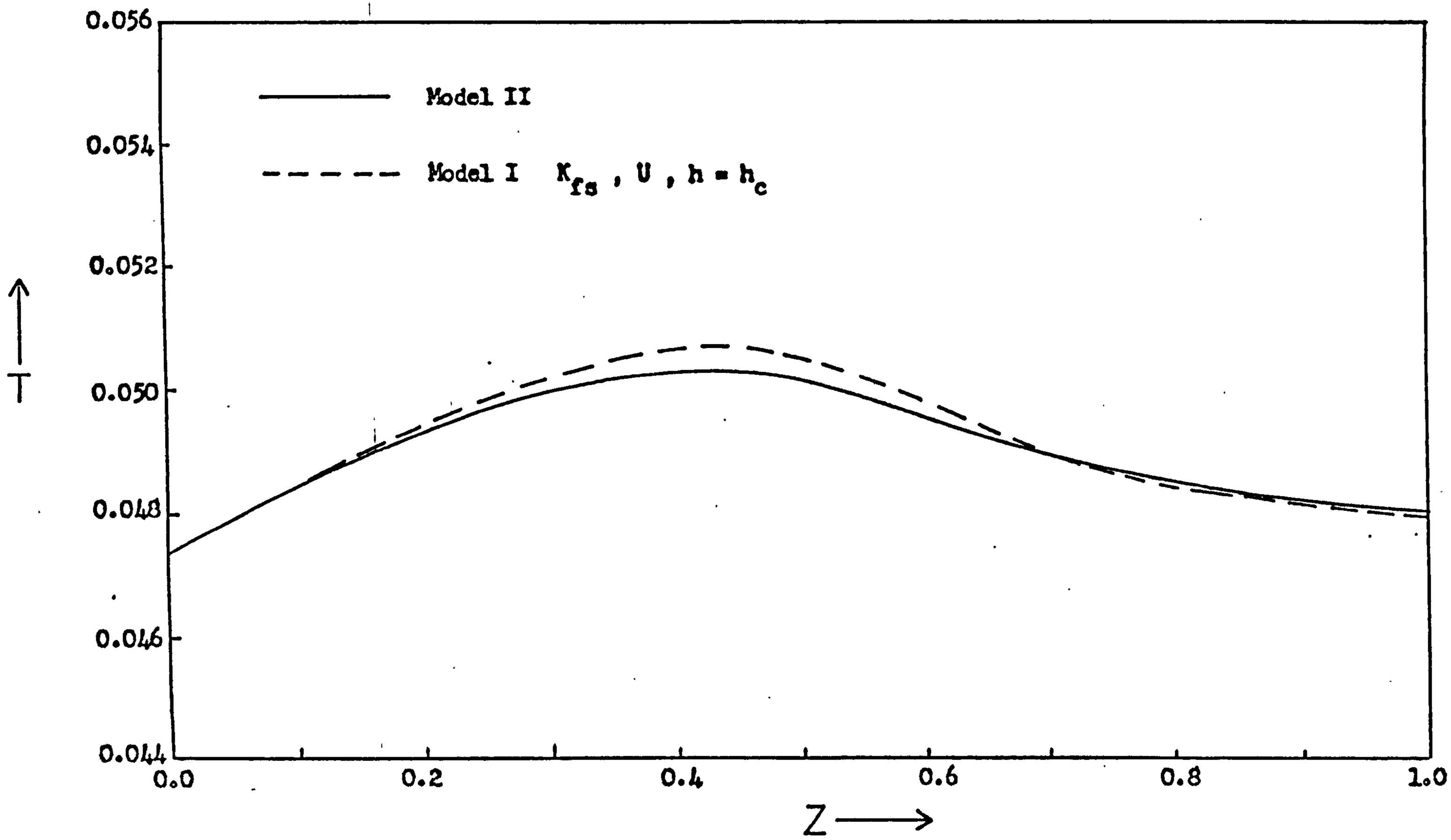

Figure 3.4 Axial profiles of radial mean temperature predicted by Models I and II using the convective value of the pellet surface heat transfer coefficient. (Data as given in Table 3.1)

posite representation of the overall coefficient.

3.5 Concluding Remarks

Axial diffusion of heat in industrial sized fixed bed catalytic reactors is far less important than radial heat transfer. The general problem of representing radial heat transfer in these reactors has been discussed and in particular the importance of the radial heat flux due to the presence of the solid has been examined. Two models of packed bed reactors which describe this heat flux in different ways have been compared. One model explicitly accounts for heat transfer due to the solid using separate effective radial thermal conductivities and wall heat transfer coefficients for the gas and solid whilst the other makes use of lumped values of these parameters referred to the gas phase. It has been shown that even when the radial heat flux due to the presence of the solid is significant the latter model automatically includes all the effects of the more complex representation provided that the appropriate expression for the solid-to-gas surface heat transfer coefficient is used. When radial heat transfer due to the presence of the solid is important then this parameter should contain an allowance for the heat lost from each particle due to radiation to and contact with adjacent particles as well as the usual solid to gas losses. A method of estimating this parameter has been proposed.

The particular advantage of the single phase heat transfer model is that it offers the possibility of accounting for mass transfer effects within the solid, which, under certain circumstances, are of considerable importance, by enabling the computation of an effectiveness factor as the calculation proceeds. This cannot be consistently incorporated into the two phase model because the solid is described for heat transfer purposes as a continuum. Since the diffusion equations in the solid should be formulated in the same way as the solid heat balance, this would mean describing mass transfer within the solid as a radial flux within the bed, whereas it is a purely local phenomenon. Consequently the mass transfer limitations within the solid must be estimated before the calculation begins in the two phase model and the effectiveness factor must be specified. This is not usually possible except in the case of isothermal process or a quasi-homogeneous system where no diffusion with-

in the solid occurs and so the effectiveness factor is unity. In truly heterogeneous systems where heat effects are significant this is clearly an unsatisfactory approach and so the single phase heat transfer model is far more useful.

CHAPTER 4

PARAMETRIC SENSITIVITY AND TEMPERATURE RUNAWAY

4.1 Introduction

Despite the appreciable effort that has been expended on analysing the stability of fixed bed catalytic reactors, it has mainly been directed at one particular aspect of the problem, namely that associated with multiple steady state solutions. No really definitive discussion has been given which in particular takes account of the heterogeneity of the system and the relation between catalyst particle and reactor stability. Much of the work reported on quasi-homogeneous systems is inappropriate[68,67,69] since the distinction between solid and fluid properties has been ignored. An adequate representation of highly exothermic reactions demands the use of a heterogeneous model, and in particular, Thornton[12] has shown that temperature runaway may occur within a catalyst pellet without the surrounding fluid conditions apparently reflecting such changes.

It is important to appreciate that potential problems of control may arise from a number of different sources, of which the possibility of multiple steady state solutionsof the catalyst particle is but one. In particular, difficulties can arise from operating in regions which exhibit parametric sensitivity. Here, small changes in the control variables can cause very large changes in some of the process state variables, equivalent to temperature runaway. An example of this is shown in figure 4.1 where steady state axial profiles of radial mean temperature are plotted at two coolant temperatures differing by the equivalent of only 5 K. At the slightly higher coolant temperature, temperature runaway has clearly occurred, and yet the reactor trajectory is outside of the region of multiple steady states.

Thornton[12] has shown that it is probable that parametric sensitivity causes instability when a packed bed reactor is subject to perturbations in the inlet conditions. If very small changes in the inlet conditions of a reactor can cause very large changes further down the bed, then the reactor may be described as unstable in operation. Such instability may be due solely to parametric sensitivity or to a combination of parametric sen-

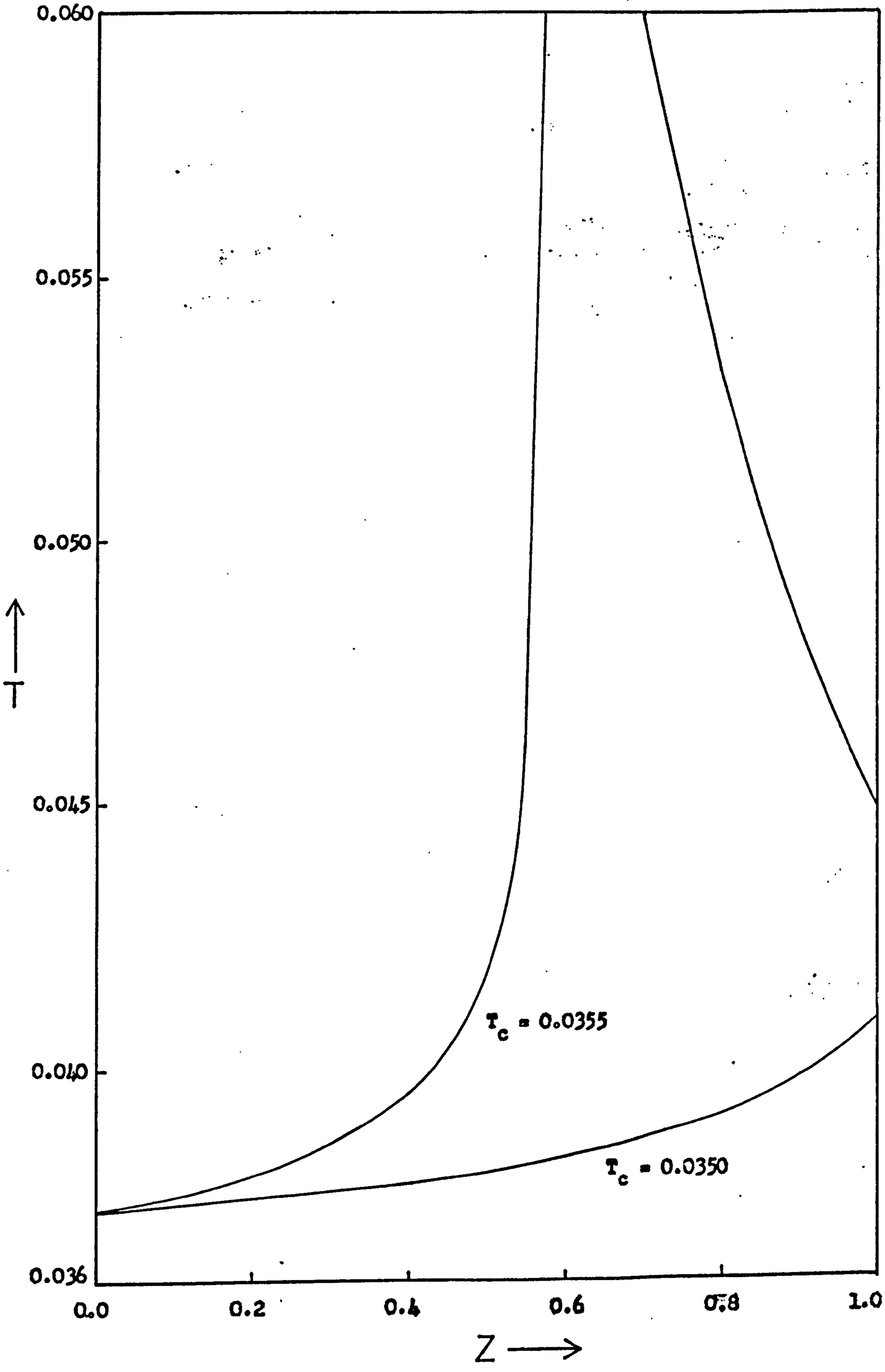

Figure 4.1 Axial profiles of radial mean temperature at two values of coolant temperature in the region of parametric sensitivity. (B_0 = 7.67 x 10^{-5}, other data as given in Table 5.1)

sitivity and the bed to exhibiting multiple states. In either case the consequences are much the same, namely a tendency for undesirable temperatures to develop which can result in deterioration of the catalyst.

The analysis described here deals with establishing criteria for limits of reactor stability arising from the region of parametric sensitivity as a consequence of the heterogeneity of the system, and methods of employing these criteria in reactor design or control studies are also discussed. Although developed for a single first order A → B reaction scheme, the method can easily be extended to more complex cases as is shown in Appendix (4).

4.2 Calculation of the Limits of the Runaway Region

Using the isothermal pellet assumption, for the single first order A → B reaction, the heat balance on the catalyst pellet reduces to:

$$t = T + BSh_A(r - g)/(sg + r) \qquad (4.1)$$

where

$$r = \theta \exp(-1/2t)$$
$$g = \tanh(r)$$
$$s = Sh_A/2 - 1$$

Equation (4.1) may be solved for t by any of the normal root finding techniques. Figure 4.2 shows a plot of fluid temperature (T) versus pellet temperature (t) for three sets of reaction parameters. From figure 4.2 it can be seen that increasing B, the thermal load factor, at constant Sh_A and θ leads to multiple solutions of equation (4.1) as shown by curve (3). McGreavy and Thornton[112] defined this non-unique region in terms of the pellet temperature and the thermal load factor by setting the derivative $\frac{dT}{dt} = 0$. This made it possible to plot the non-unique region for any pair of values of Sh_A and θ on a T vs. B phase diagram. Although this analysis is adequate for defining the region of multiple solutions of the catalyst pellet model, it does not identify the regions where the catalyst temperature is very sensitive to its surrounding fluid conditions. Curve (2) in figure 4.2, for example, shows a region, XY, where the pellet temperature is very sensitive to small changes in the fluid temperature but multiplicity of solutions does not occur. Yet, clearly, temperature runaway will occur under such conditions.

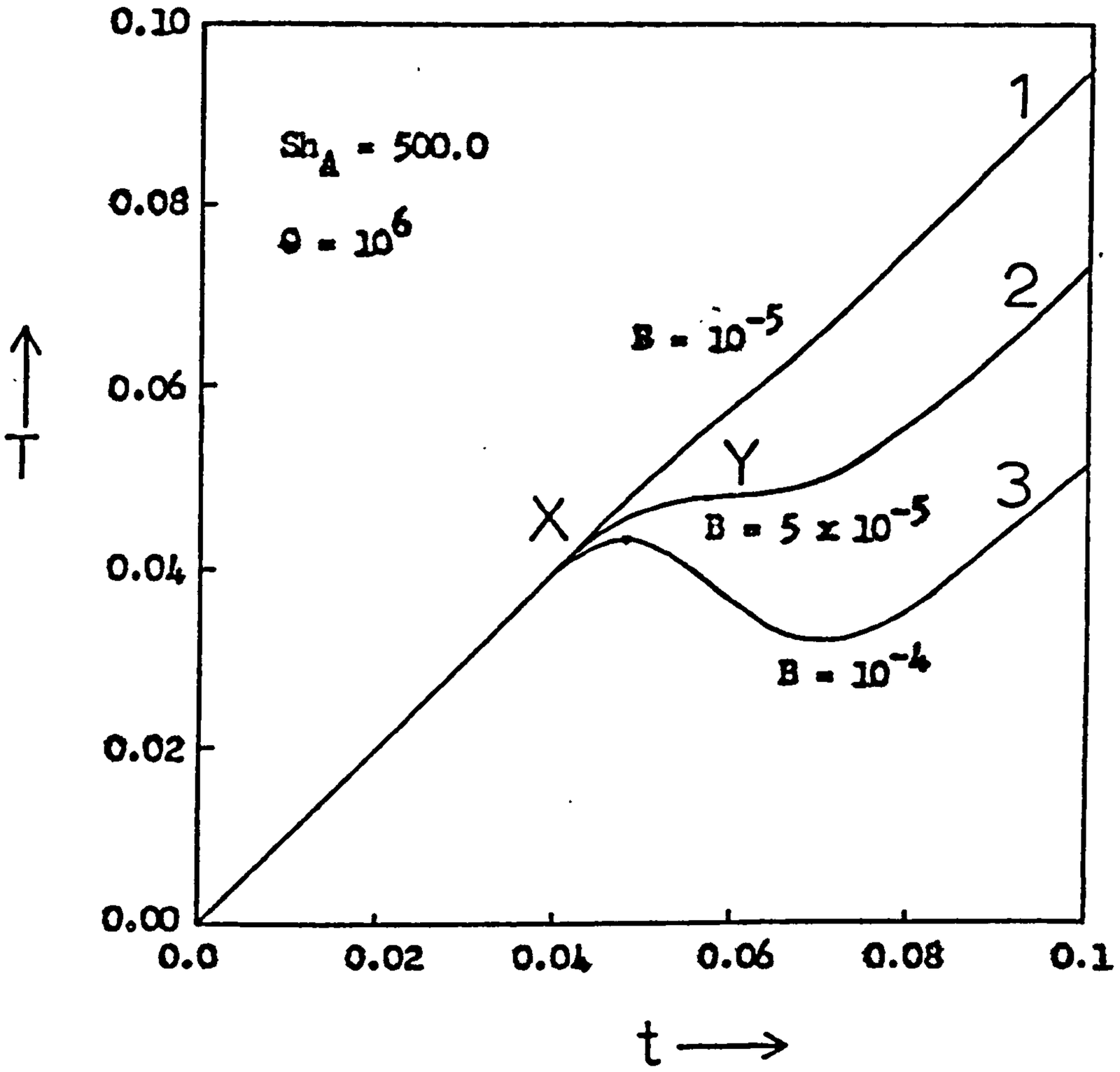

Figure 4.2 The relationship between T and t obtained by solving the catalyst pellet model for typical values of the parameters.

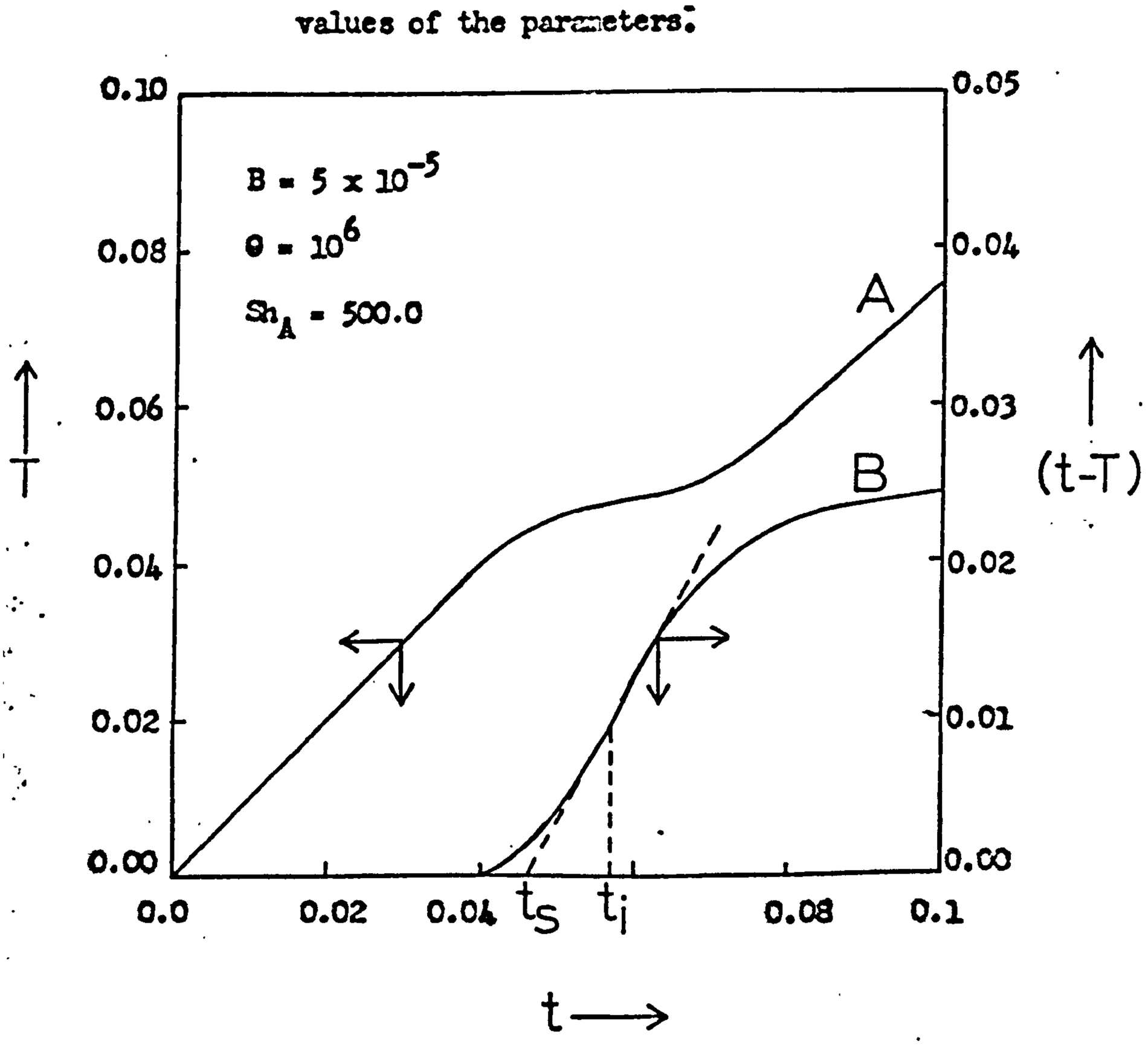

Figure 4.3 The relationship between T, t, and (t - T) for typical parmeter values.

Here it should be noted that the isothermal catalyst pellet model, employed in this analysis, displays only a single trifurcation point; i.e. only a single region of the type XY on curve (2) of figure 4.2, whereas other investigators[33] have demonstrated the existence of two such regions when using a fully distributed model of the catalyst pellet model in special cases such as with zero order reactions. One region, at low values of Thiele Modulus, is due to intraparticle thermal resistance and is consequently not identified by the isothermal pellet model, whilst the other region, occurring at higher values of Thiele Modulus corresponds to that identified by the isothermal pellet model, due to interphase thermal resistance. Clearly, if conditions are met where the intraparticle thermal resistance is significant then the isothermal pellet model is not applicable and so a different analysis of parametric sensitivity is necessary.

Curve (A) of figure 4.3 corresponds to curve (2) of figure 4.2. Curve (B) of figure 4.3 is a plot of the difference between the pellet and fluid temperatures, $(t - T)$ against the pellet temperature. As would be expected curve (B) shows that this interphase temperature difference becomes significant when the pellet temperature becomes very sensitive to the fluid temperature. This is precisely at the point when temperature runaway occurs.

To quantify the limits of this runaway region, i.e. the domain of pellet temperature sensitivity, there are three immediately obvious methods. Firstly, a single pellet temperature might be defined as the "safest" maximum pellet temperature for which temperature runaway may be avoided. This method is, however, not very useful since a good deal of computation would be necessary to make sure that this arbitrarily defined catalyst temperature applied for all sets of operating conditions. Secondly, a limit might be defined by setting the derivative $\frac{dT}{dt}$ equal to some arbitrary value, say α; or thirdly adopting a modification of the latter by setting $\frac{d(t - T)}{dt}$ equal to some value, γ. Although all of these methods are attractive since they involve the minimum of analysis they present the problem of determining satisfactory values for α and γ. Moreover, both of these gradients depend on B, Sh_A and θ, so that numerical investigation would again be necessary to determine safe, but not too conservative, values for all ranges of parameters.

Perhaps the main advantage of these methods is that the definition of temperature runaway is left entirely to the investigator, or designer, in his choice of values of α and γ. However, all of these approaches are unsatisfactory because of their lack of generality. A better approach to the problem is one in which the sensitive, or runaway, region may be determined from the properties of the system and not by arbitrarily defined numerical values of temperature or temperature gradients.

A general method whereby the significant change of gradient of the (t - T) vs. t curve could be adequately predicted is needed. Examination of the (t - T) vs. t curves for a range of parameters show that these curves have a point of inflexion which lies beyond the point at which the gradient becomes significant. A tangent to this curve through the point of inflexion crosses the pellet temperature axis at the value of t at which the interphase temperature difference, (t - T), begins to increase in importance, i.e. at the beginning of the runaway region (see broken line in figure 4.3). It can now be considered how the temperature runaway limit defined in this way may be determined non-graphically.

Let the pellet temperature at the point of inflexion of the (t - T) vs. t curve be t_i. The value of t_i can be determined by setting the derivative, $d^2(t - T)/dt^2$, equal to zero.

From equation (1):

$$\frac{d(t - T)}{dt} = \frac{BSh_A^2 r(rg^2 - r + g)}{4t^2(sg + r)^2} \qquad (4.2)$$

hence:

$$\frac{d^2(t - T)}{dt^2} = \frac{BSh_A^2}{4(sg + r)^4 t^4} \times$$

$$\left\{\tfrac{1}{2}(sg + r)^2 r(r(1 - g^2)(2rg - 1) + g) - r(rg^2 - r + g)(r(sg + r)(s(1 - g^2) + 1) + 2t(sg + r)^2)\right\} \qquad (4.3)$$

setting this equal to zero and rearranging gives:

$$t_i = \frac{r_i(1 - g_i^2)(2r_i g_i - 1) + g_i}{4(g_i - r_i(1 - g_i^2))} - \frac{r_i(s(1 - g_i^2) + 1)}{2(sg_i + r_i)} \qquad (4.4)$$

where

$$r_i = \theta \exp(-1/2t_i) \quad \text{and} \quad g_i = \tanh(r_i)$$

Hence t_i is a function of Sh_A and θ only but not B. i.e. for any pair of values of Sh_A and θ, t_i is constant for all B.

Equation (4.4) may be solved for t_i by any of the usual root finding techniques, although the Reguli Falsi method is perhaps preferable since it does not require the somewhat tedious evaluation of the derivative of equation (4.4). The disadvantage of this method of solution is that an initial search must be made to find two suitable starting values. However, since Sh_A and θ are usually constant in any given system, equation (4.4) has only to be solved once for any system and so a rapid method of solution is not essential.

The gradient of the $(t - T)$ vs. t curve at the point of inflexion, t_i, is given by setting $t = t_i$ in equation (4.2). Thus, the point on the pellet temperature axis where the tangent through the point of inflexion meets this axis, t_s, is given by:

$$BSh_A \frac{(r_i - g_i)}{(sg_i + r_i)(t_i - t_s)} = BSh_A^2 \frac{r_i(r_i g_i^2 - r_i + g_i)}{4t_i^2(sg_i + r_i)^2} \qquad (4.5)$$

Rearrangement of equation (5) gives:

$$t_s = t_i - \frac{4t_i^2(r_i - g_i)(sg_i + r_i)}{Sh_A r_i(r_i g_i^2 - r_i + g_i)} \qquad (4.6)$$

Equation (4.6) shows that t_s is also a function of only Sh_A and θ.

Therefore, t_s is the pellet temperature at the limit of the runaway region. For a given pair of values of Sh_A and θ, t_i may be calculated from equation (4.4) and then used to find t_s from equation (4.6). This value of t_s may be substituted into the pellet heat balance equation, (4.1), to find pairs of values of the fluid temperature, T, and dimensionless thermal load factor, B, which may be plotted on a T vs. B phase diagram. Figure 4.4 shows such a plot. Note that equation (4.1) gives a straight line for T vs. B since t_s is constant for all T and B, however the B scale in figure (4.4) is logarithmic and so a curve is obtained. Points above the line on this diagram are in the runaway region and points below it are in the "safe" region.

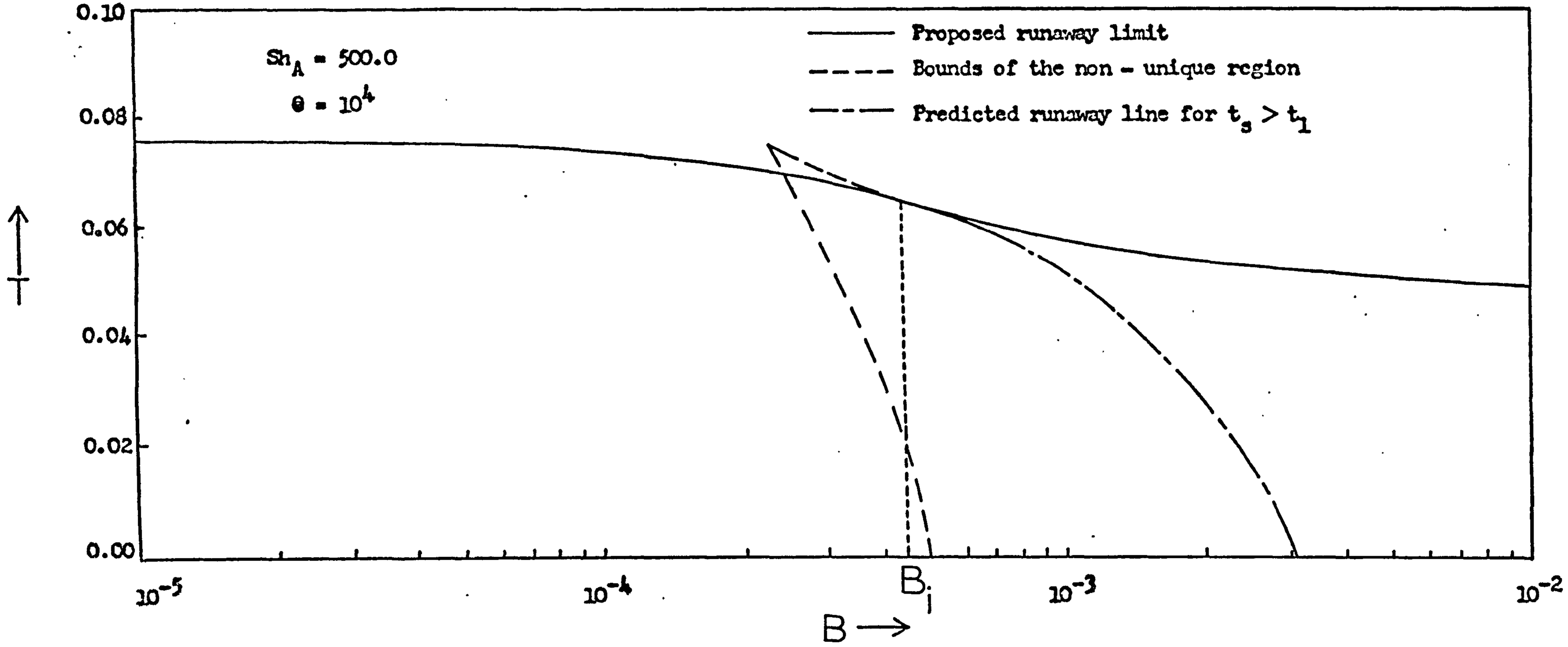

Figure 4.4 The runaway limit on the T vs B phase diagram for a typical set of parameters.

TABLE 4.1 The influence of B on the interphase temperature difference.

$Sh_A = 500$, $\theta = 10^4$, $t_s = 0.07599$			
B	T	t - T	(t-T)/T%
10^{-5}	0.07575	0.00024	0.32
3×10^{-5}	0.07526	0.00073	0.97
5×10^{-5}	0.07477	0.00122	1.63
7×10^{-5}	0.07428	0.00171	2.80
10^{-4}	0.07354	0.00245	3.33
2×10^{-4}	0.07109	0.00490	6.89
4×10^{-4}	0.06619	0.00980	14.80
5×10^{-4}	0.06374	0.01225	19.22
10^{-3}	0.05149	0.02450	47.58

TABLE 4.2 Data of Van Welsenaere and Froment[68] used for the comparison with the quasi-homogeneous runaway criterion.

G_2	0.0254
G_3	0.697
G_4	92.25
B_o	0.274×10^{-5}
θ	1.01×10^5
Nu_w	2.67
Sh_A	621.4
Nu	13.15
T(inlet)	0.0518
T_c	0.0518

4.3 Evaluation and Refinement of the Method

Table 4.1 shows the effect of increasing B on the difference in temperature between fluid and catalyst, for typical values of Sh_A and θ .

As can be seen, the predicted runaway limit is excellent for medium and low values of B. As B becomes less than 10^{-5}, the gradient at the point of inflexion of the (t - T) vs. t curve decreases and so t_s tends to become what may be considered a conservative, although no less valid, limit of runaway. At low values of B, temperature runaway tends to be less of a problem since this represents a low thermal load factor. From figure 4.2 it can be seen that as B decreases, then the region XY tends to decrease so that, for the parameter values used in this figure, it might be assumed that for $B \leqslant 10^{-5}$ parametric sensitivity does not exist. Indeed in terms of the dimensionless temperatures used in this study, t is not apparently very sensitive to T for $B \leqslant 10^{-5}$. However, the temperatures t and T have been made dimensionless with respect to the activation energy of the reaction, E, and so a small value of (t -T) may represent a significant temperature difference at a high temperature level depending on the magnitude of E. Even as B tends to zero so that t and T become equal then although t_s does not mark the onset of parametric sensitivity, it is useful since it sets a value for temperature runaway derived consistently with that when parametric sensitivity occurs. It should be noted that the practical range of B is approximately 10^{-5} to 5×10^{-2}.

When, at the higher values of B, the runaway line moves into the non-unique region, the meaning of the limit and its interaction with non-uniqueness needs to be examined in detail. In the cusp of the non-unique region, on the T vs. B phase diagram, t_1^*, the pellet temperature at the upper bound of the non-unique region, is greater than the runaway pellet temperature, t_s. This situation is shown schematically in figure 4.5, where t_{s1} corresponds to a value of t_s in the cusp of the non-unique region. In this case, the line SP then represents the interphase temperature difference, (t - T). As B increases, t_1^* decreases and approaches t_s until $t_s = t_1^*$. At this point, the temperature difference (t - T) is represented by the line WX of figure 4.5, and on the T vs. B diagram the runaway line is tangential to the upper bound of the non-unique region (see

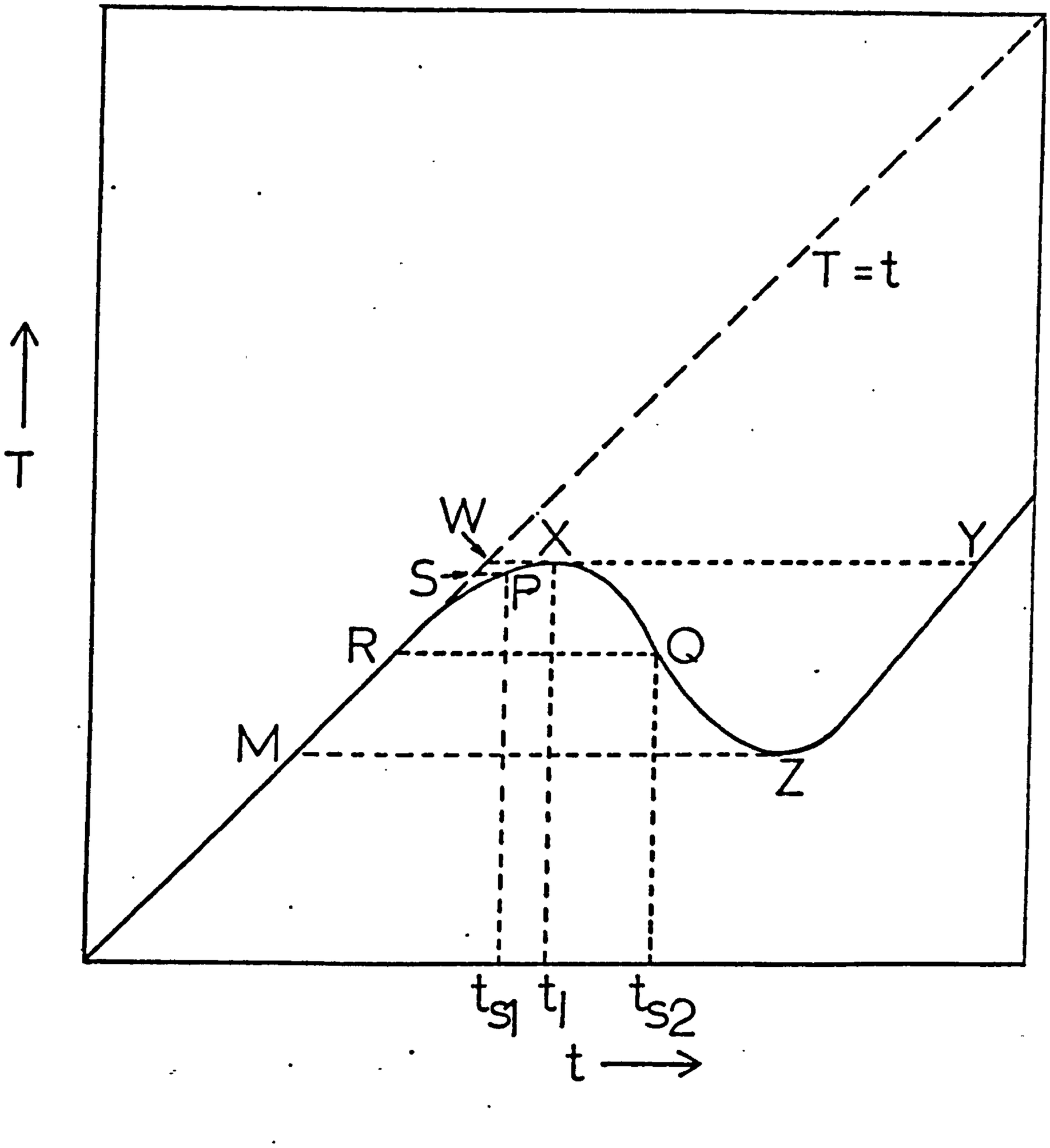

Figure 4.5 Schematic diagram showing the behaviour of t_g in the non - unique region.

figure 4.4). A further increase in B, from this point, causes t_s to become greater than t_1^*. This is represented by t_{s2} in figure 4.5. Here the interphase temperature difference is large —— line RQ of figure 4.5. However, the point Q represents an unattainable state in the non-unique region; as the fluid temperature around the pellet, T, increases the pellet temperature gradually rises until it reaches t_1^* and then it 'jumps' from point X of figure 4.5 to point Y. Similarly, when T is decreasing, the pellet follows the curve YZ and then 'jumps' from point Z to point M. Thus the curve XZ is never followed. (This behaviour is described in detail in reference 112). For this reason, $t_s > t_1^*$ has no meaning since in this case t_s lies on the curve XZ. For the parameters used in Table 4.1, the runaway line is tangential to the upper bound of the non-unique region at $B = 4.7 \times 10^{-4}$ and $T = 0.06472$. In Table 4.1, therefore, $B = 5 \times 10^{-4}$ and 10^{-3} correspond to $t_s > t_1^*$, and so that value of $(t - T)$ appears large and is, in fact, equivalent to the line RQ of figure 4.5. Thus, referring to figure 4.4, the runaway line to the right of $B = B_i$, where the line is tangential to the upper bound of the non-unique region has no significance, and from this point for increasing B the upper bound of the non-unique region is the runaway limit.

Figures 4.6 and 4.7 show the effect on the runaway line of varying the parameters θ and Sh_A respectively. The broken lines in these figures are the loci of the points at which the runaway lines are tangential to the upper bound of the non-unique region. As may be seen, increasing θ at constant Sh_A causes this point of tangency to move to the right of the T vs. B diagram, i.e. the value of B at the tangent point increases. Increasing Sh_A at constant θ causes this point to move in the opposite direction so that as Sh_A tends to infinity the proposed runaway line becomes less useful over the realistic range of B, and the upper bound of the non-unique region at $Sh_A = \infty$ becomes an adequate limit to the runaway region over this range of B. This is particularly true at high values of θ where when $Sh_A = \infty$ the point of coincidence of the two lines is less than $B = 10^{-5}$?

It is interesting to note that in the cusp of the multiple solutions region of the T vs. B diagram, the runaway line is at lower temperatures than the upper bound of the non-unique

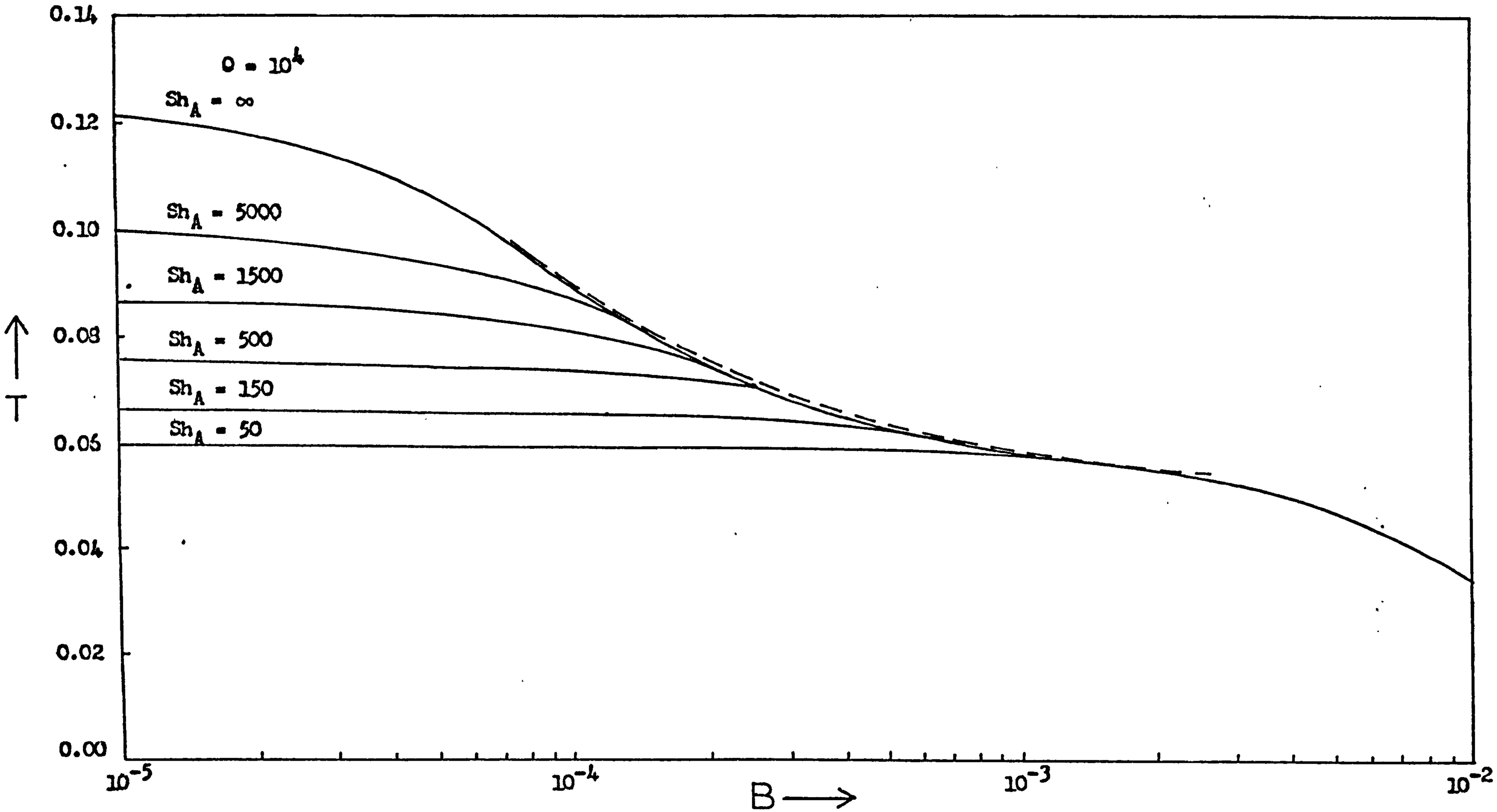

Figure 4.6 The effect of Sh_A on the runaway limit for $\theta = 10^4$

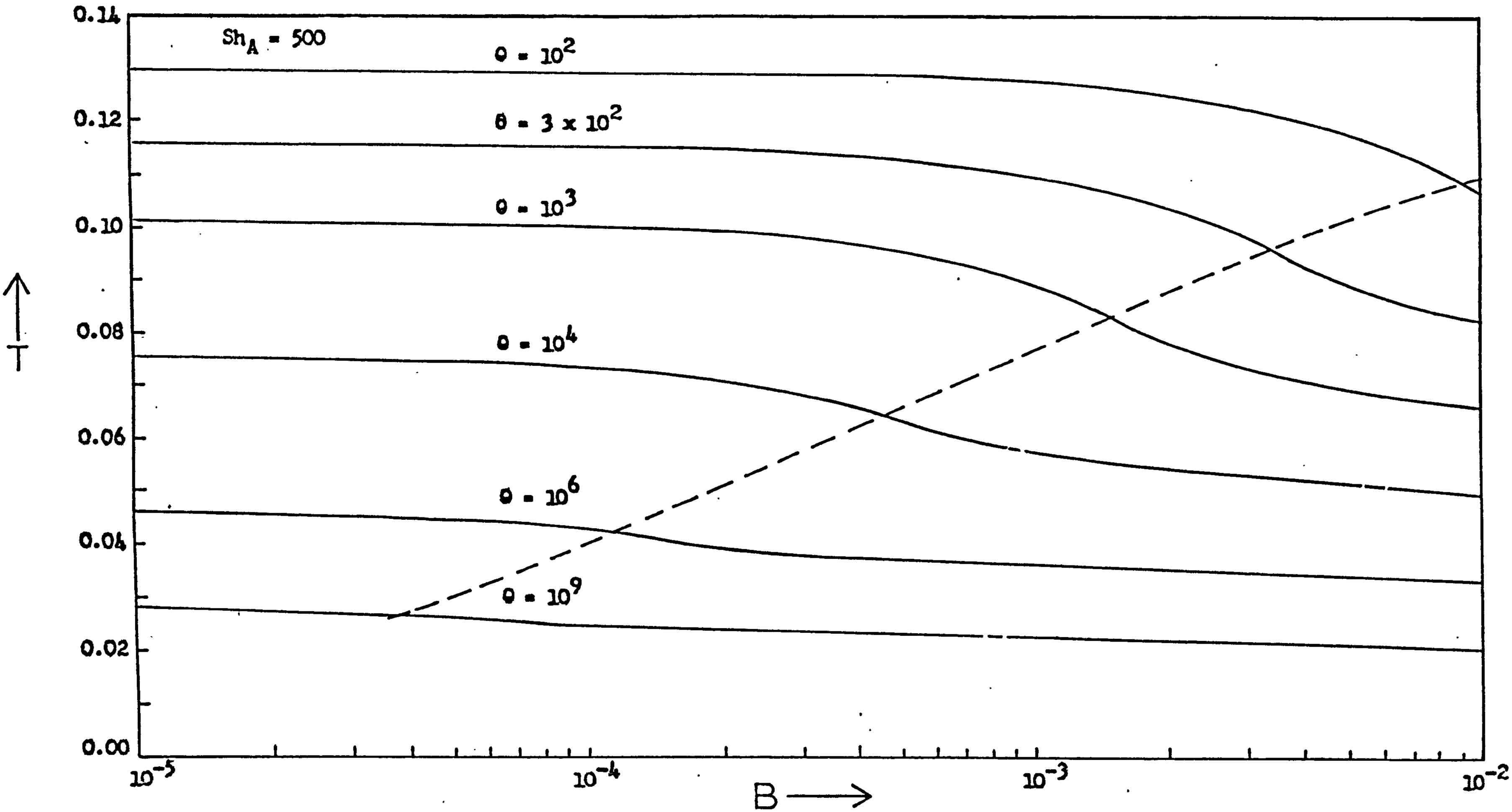

Figure 4.7 The effect of θ on the runaway limit for Sh_A = 500

region. This clearly shows that in this region parametric sensitivity causes the transition to the upper steady state and the runaway line is therefore a more important limit than the upper bound of the non-unique region in this area.

4.4 The Use of the Method in the Design and Control of a Reactor

A plot of the fluid temperature, T, against the dimensionless thermal load factor, B, which is directly proportional to the reactant concentration is characteristic of a set of operating conditions and on such a graph the runaway limit, together with the region of multiple solutions, can be drawn for a given system, as shown in figure 4.4. By solving the equations describing the heterogeneous reactor it is possible to plot longitudinal trajectories for particular radial positions on the same chart. If any of these curves cross the runaway line then temperature runaway has occurred at some point in the bed and the reactor may be described as unstable. Even if a particular trajectory only just crosses the runaway line but does not go very far past it then this indicates potential instability and therefore problems of control since the trajectory passes into a region of parametric sensitivity and high temperatures may develop during any perturbations from this state. Indeed, it is in indicating trajectories of this nature that the runaway criterion is particularly useful since although high fluid temperatures are not apparent, the potential instability of the state is easily observed.

Some typical trajectories of radial mean conditions are plotted in figure 4.8 showing the influence of the coolant temperature in relation to the runaway limit at two values of inlet concentration. The data used in these simulations is given in Table 5.1. Figure 4.9 shows longitudinal trajectories at various radial positions with a coolant temperature of 0.03742 and inlet concentration 1.0. It is apparent from this graph that it may often be necessary to use the axial temperature rather than the radial mean values when attempting to choose operating conditions which avoid temperature runaway.

The preceding analysis has given a criterion for temperature runaway in heterogeneous reactors which is based on the intrinsic properties of the system. It is useful to ex-

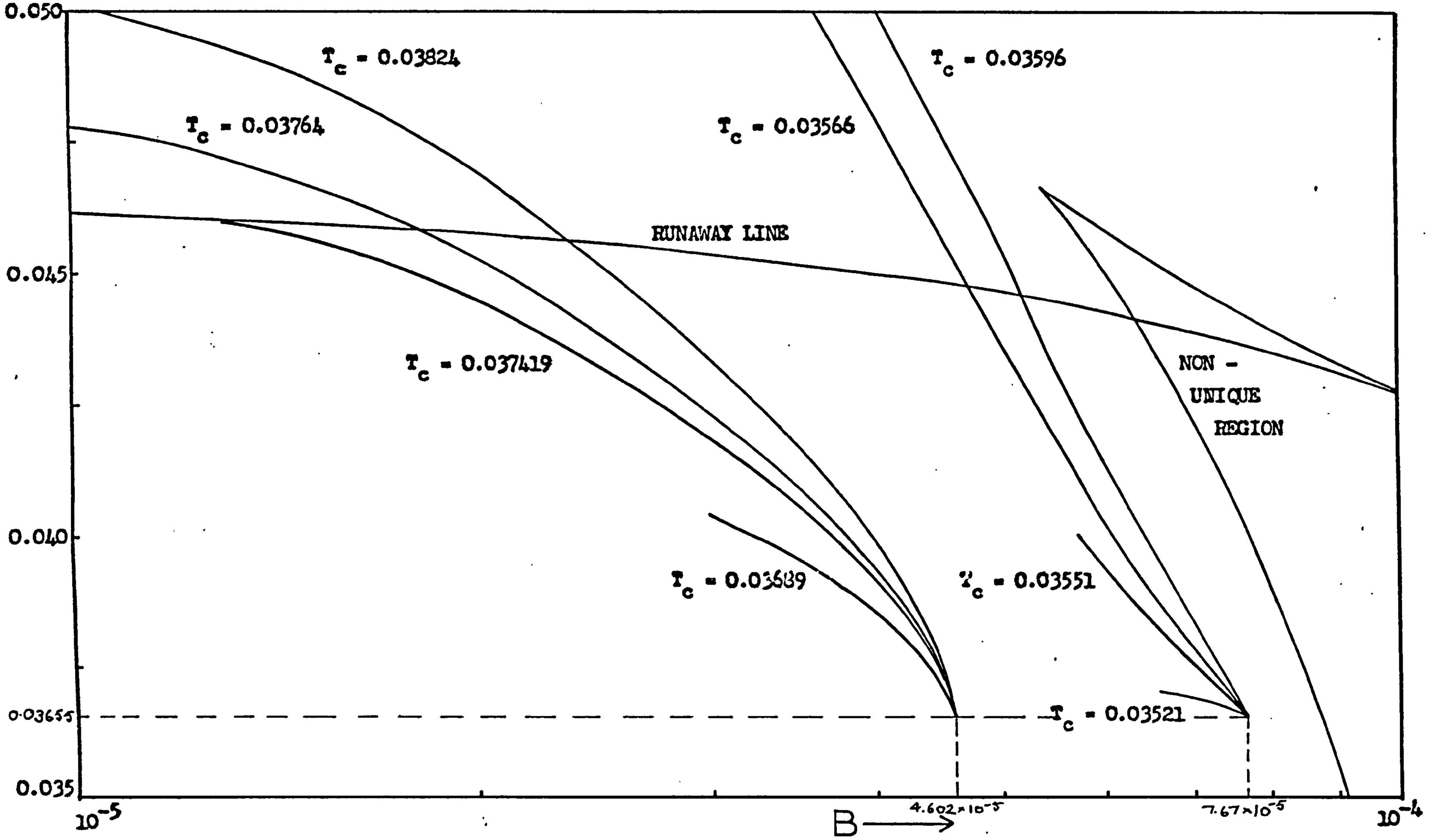

Figure 4.8 The effect of the coolant temperature on the reactor trajectories at two sets of inlet conditions. (Data as given in Table 5.1)

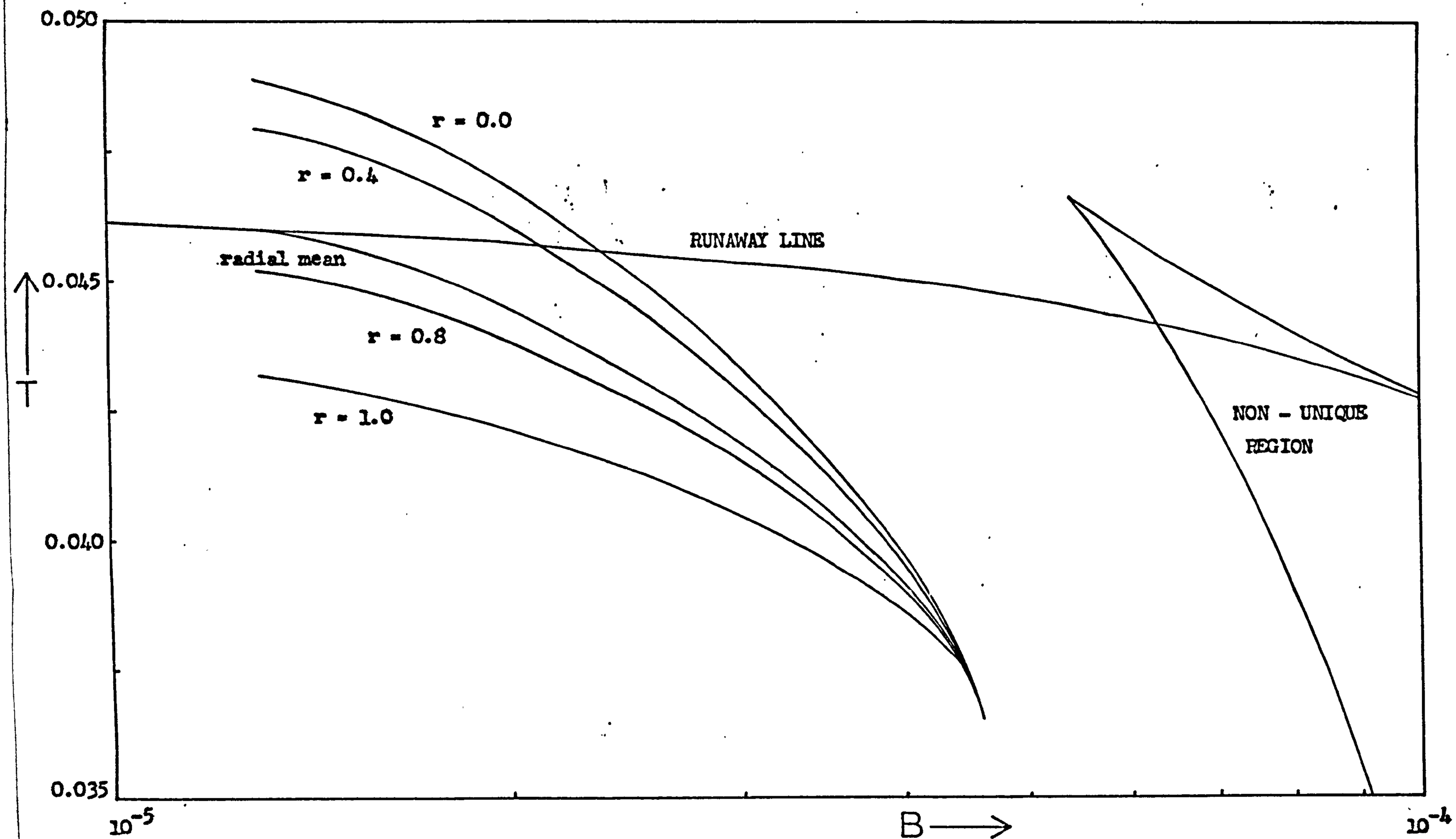

Figure 4.9 Reactor trajectories at various radial positions. ($B_p = 4.602 \times 10^{-5}$, $T_o = 0.036554$; $T_c = 0.03742$, other data as given in Table 5.1)

amine how this criterion might be effectively used firstly in the design and subsequently in the control of such systems.

Generally, the reactor designer is confronted with a fixed set of parameters and he must make the best design within the degrees of freedom left available to him. The fixed conditions are the reaction rate parameters and thermodynamic properties, the type of catalyst to be used and the maximum allowable pressure drop across the bed. Thus the degrees of freedom which are left are the inlet conditions, including the coolant temperature and the dimensions of the reactor tube. However, total freedom in the choice of values for these parameters is never the case. For the class of problems specifically considered in this thesis the choice of gas flow rate is confined to a very narrow range; the upper constraint being that which produces the maximum allowable pressure drop, which is, of course, related to the tube and catalyst particle dimensions and the lower constraint is determined by the minimum allowable gas to tube wall heat transfer coefficient and gas to pellet mass transfer coefficient. Generally, since heat removal from the bed to the coolant is the most important process the design will be based on the maximum available gas flow rate. In most situations the tube diameter is determined primarily by the related factors of cost and availability, the most commonly used values being either 1" or 0.75", and is, therefore, not a true design variable. Thus, in general, for a given system most parameters are fixed at the outset, or at best confined to very narrow limits, and only the inlet conditions and the tube length, below a certain maximum, remain as freely manipulable design variables. Values of these parameters must then be chosen which give an economically satisfactory safe design, avoiding temperature runaway or regions of instability.

In the discussion which follows attention is mainly confined to the case of equal coolant and gas inlet temperatures since this is the situation usually encountered in practice. In any case it probably represents the worst case for exothermic reactions since with these reactions heat removal is the greatest problem and so it would not be realistic to use a coolant temperature higher than the gas inlet value. Nevertheless, the analysis could easily be extended to the case of

differing coolant and inlet temperatures and even adiabatic operation, so this does not represent a limitation on the development.

Rigorous determination of critical reactor operating conditions, i.e. conditions which cause the reactor trajectory on the T vs. B phase diagram to reach the runaway line but not cross it, obviously requires numerical integration of the reactor equations. It is useful, therefore, to limit the amount of computation which needs to be performed by determining the range of operating conditions which have to be considered, and yet still give a feel for the relationship between the significant variables.

Clearly, a trivial, but necessarily stated upper limit to the inlet temperature of the gas at any inlet concentration is provided by the runaway line on the T vs. B diagram. However, the lower limit of the inlet temperature, and also the coolant temperature, often depends on the length of the reactor as well as the inlet concentration, although a value may be determined as is shown later. For any given inlet and coolant temperature the range of inlet concentration which need be considered is easily determined. This range is more conveniently expressed in terms of the inlet value of the thermal load factor, B_i, which is directly proportional to reactant concentration.

The upper limit on B_i is based on the assumption that the designer will wish to avoid reactor operation in the non-unique as well as the runaway region. This is usually the case, due to the inherent problems of reactor control when operating in this region. Consider the point where the runaway line crosses the lower bound of the non-unique region on the T vs. B diagram. If the adiabatic trajectory through this point meets the line $T = T_0$ at a value of B outside of the non-unique region, then this value of B represents the maximum permissable inlet value to avoid operation in the non-unique region under adiabatic conditions. This is generally the case since the slope of the adiabatic trajectory is usually much greater than that of the lower bound of the non-unique region. If this value of B lies inside the non-unique region, then the maximum value of B_i is given by the value of B where the line $T = T_0$ crosses the lower bound of the non-

unique region. Let the value of B in either case be B_{iu}. Since reactor trajectories on the T vs. B diagram start with an adiabatic slope for $T_0 = T_c$ and then bend under this line due to heat exchange between the bed and the coolant, then B_{iu} represents an approximate upper limit on B_i to avoid the non-unique region under non-adiabatic conditions. Clearly it will be less than the actual upper limit for non-adiabatic operation, but because of this it guarantees that if temperature runaway is avoided then, for $B_i < B_{iu}$, operation in the non-unique region is also avoided. It is, therefore, the best obtainable upper limit on B_i at any inlet temperature without extensive computation. B_{iu} may be easily determined either graphically or computationally using the equations for the non-unique region and the runaway line.

The lower limit on B_i, B_{il}, which need be considered is also easily determined. For the one dimensional heterogeneous reactor model described in Appendix (2) the equations are:

$$\frac{dC_A}{dz} = - G_2 \zeta k_1 C_A \qquad (4.7)$$

$$\text{and} \quad \frac{dT}{dz} = G_4(t - T) - \frac{2Nu^*_w}{G_3}(T - T_c) \qquad (4.8)$$

where $t = T + BSh_A(r - g)/(sg + r)$

$$k_1 = \theta^2 \exp(-1/T)$$

and $$\zeta = 1.5Sh_A(r - g)/k_1(sg + r)$$

From equations (4.7) and (4.8) the gradient of the reactor trajectory on the T vs. B diagram is given by:

$$\frac{dT}{dB} = - \frac{G_4(t - T)}{G_2 \zeta k_1 B} + \frac{2Nu^*_w(T - T_c)}{G_2 G_3 \zeta k_1 B} \qquad (4.9)$$

When the reactor trajectory passes through a maximum, $\frac{dT}{dB} = 0$. (A maximum in the phase trajectory corresponds to a maximum in the axial temperature profile). Hence the locus of this maximum on the T vs. B diagram is given by:

$$- \frac{G_4(t_m - T_m)}{G_2 \zeta k_1 B_m} + \frac{2Nu^*_w(T_m - T_c)}{G_2 G_3 \zeta k_1 B_m} = 0$$

which on rearrangement becomes:

$$G_4(t_m - T_m) = \frac{2Nu^*_w}{G_3}(T_m - T_c) \qquad (4.10)$$

The subscript m denotes the value at the maximum. The

pellet temperature, t_m, is given by equation (4.1):

$$t_m = T_m + B_m Sh_A (r_m - g_m)/(sg_m + r_m)$$

The only operating variable in equation (4.10) is the coolant temperature, T_c. The loci given by equation (4.10) on the T vs. B diagram are shown in figure 4.10 for various values of T_c. Thus for a given value of coolant temperature the locus of the maximum of the reactor trajectories may be plotted. It is interesting to note that one of the criterion for temperature runaway given by Van Welsenaere and Froment[68] for quasi-homogeneous reactors is based on the fact that the locus of the reactor trajectory maxima passes through a maximum and appears to have been derived empirically by cbservation of computed reactor trajectories. Examination of the equations of the quasi-homogeneous system has shown that there is, in fact, a fundamental reason why this criterion applies for that system and this is demonstrated in Appendix (5). As is demonstrated later in this chapter, however, the results for quasi-homogeneous systems cannot be applied to a heterogeneous reactor because of their conservatism. The actual position of the maximum on this locus depends on the inlet reactant concentration and temperature when $T_0 \neq T_c$. A critical trajectory will be one where the maximum occurs at the runaway line, that is the locus of the maximum given by equation (4.10) which crosses the runaway line, since increasing the value of B_i from the critical value will cause the maximum of the trajectory to occur above the runaway line; decreasing B_i will ensure that the maximum occurs below this line. At the maximum of the critical trajectory, coordinates (B_{cr}, T_{cr}) on the T vs. B diagram, the pellet temperature is given by t_s. Thus substituting $t_m = t_s$ in equation (4.10) and solving this equation simultaneously with the pellet equation gives the maximum of the critical trajectory for any value of T_c.

The slope of the adiabatic line on the phase diagram is given by:

$$\frac{dT}{dB} = -\frac{G_4}{1.5G_2} \qquad (4.11)$$

Therefore the value of B_i, B_{il}, for the adiabatic line through the maximum of the critical trajectory is given by:

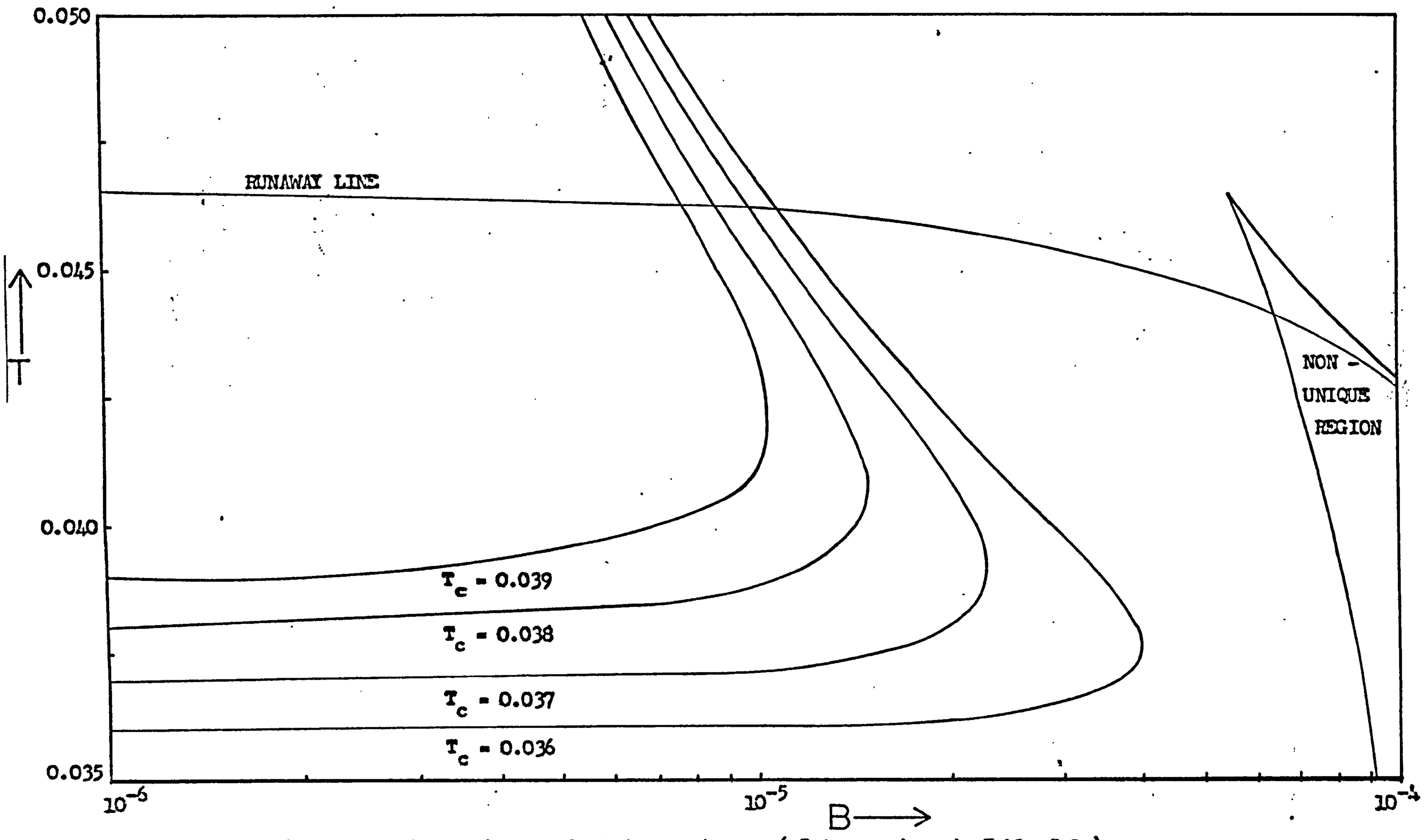

Figure 4.10 Maxima curves for various coolant temperatures. (Data as given in Table 5.1)

$$B_{il} = B_{cr} + 1.5G_2(T_{cr} - T_0)/G_4 \qquad (4.12)$$

Since reactor trajectories on the T vs. B diagram start with an adiabatic slope for $T_0 = T_c$ and then bend under the adiabatic line, B_{il} is the minimum value of B_i which need be considered for a given inlet and coolant temperature. For $B_i < B_{il}$ at $T_0 = T_c$ the maximum temperature in the reactor will always occur below the runaway line. This lower limit on B_i tends to be slightly conservative, the actual value being a little larger. However, it represents the best estimate which may be obtained. A method of extrapolation proposed by other workers[68] for quasi-homogeneous reactors cannot be used to obtain a less conservative estimate in the heterogeneous case because of the difference of the shape of the reactor trajectories in this case. Nevertheless, B_{il} represents a very useful limit since safe operation for $B_i < B_{il}$, at a given coolant and inlet temperature, can be guaranteed. At low values of inlet and coolant temperature the situation which is illustrated schematically in figure 4.11 may arise. Clearly, the value of B_{il} determined by the above method, as shown in this figure, will be very conservative in such situations. A better estimate of B_{il} may be obtained by drawing the adiabatic trajectory through the maximum value of B on the curve giving the locus of the trajectory maxima, i.e. through the point marked X in figure 4.11. Computationally this requires finding the coordinates of point X on the T vs. B diagram. From equation (4.10) and the pellet equation the locus of the trajectory maxima may be expressed as:

$$B_m = 2Nu_w^*(T_m - T_c)(sg_m + r_m)/G_3G_4Sh_A(r_m - g_m) \qquad (4.13)$$

The point X may then be found by differentiating equation (4.13) with respect to T_m and setting this derivative equal to zero. Let the coordinates of the point X, evaluated in this way be (B_a, T_a). If B_{il} determined from the adiabatic line through the point where the locus of the trajectory maxima crosses the runaway line, as described above, is less than B_a then the situation illustrated in figure 4.11 will arise. In this case a better estimate of B_{il} may then be obtained by replacing B_{cr} and T_{cr} in equation (4.12) by B_a and T_a.

From figure 4.10 it can be seen that as T_c is decreased, the point marked X in figure 4.11 approaches the non-unique

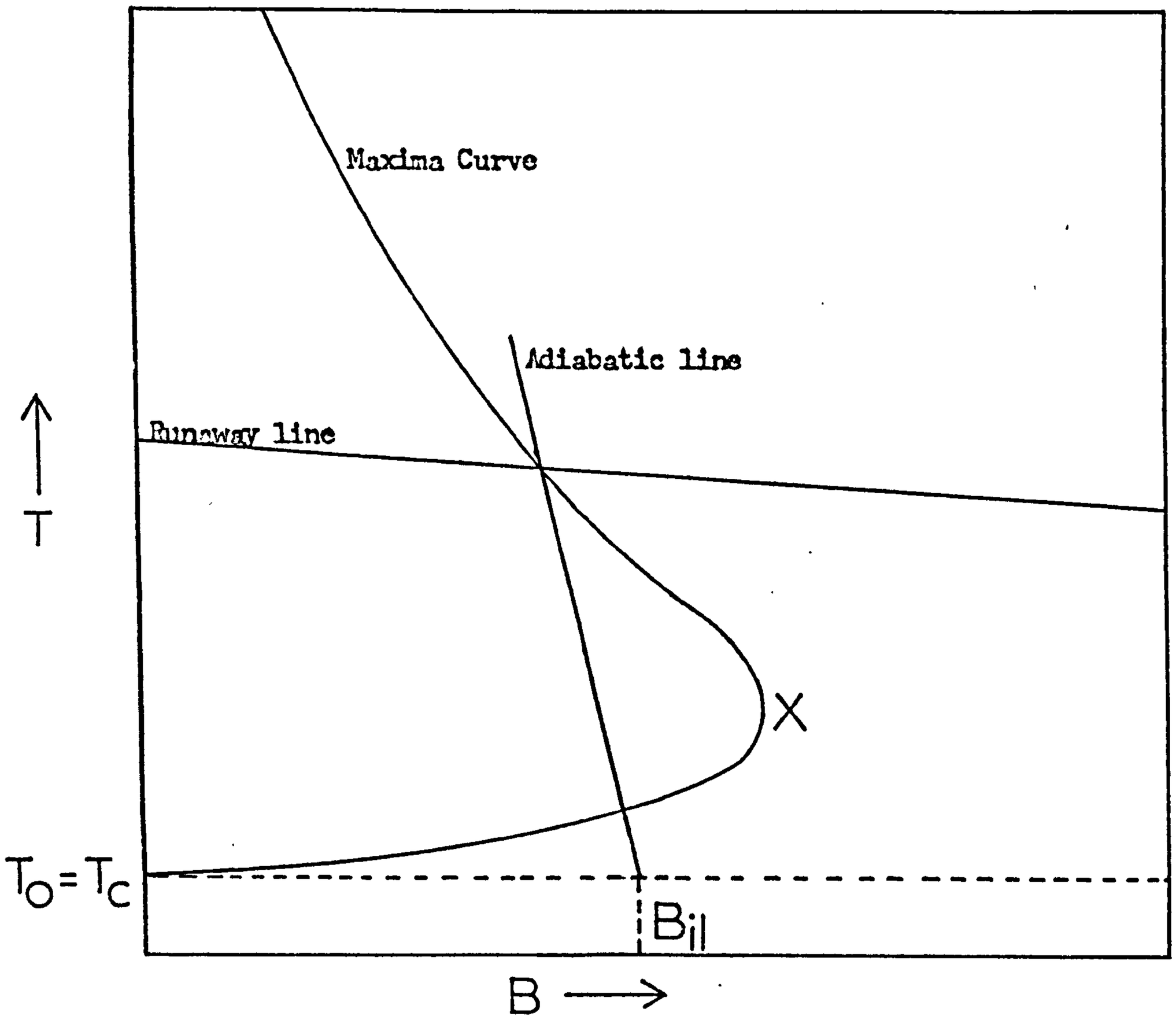

Figure 4.11 Schematic diagram showing the location of B_{il} on the T vs B phase diagram.

region as does the point at which the locus of the trajectory maxima crosses the runaway line. This may be used to calculate the theoretical minimum coolant and inlet temperature which need be considered for any system if operation in the non-unique region is to be avoided. B_{iu} is the maximum value of B_i which avoids operation in the non-unique region at a given coolant and inlet temperature as discussed previously. Thus the minimum value of inlet temperature for $T_0 = T_c$ is that at which B_{il} determined from equation (4.12) is greater than or equal to B_{iu} if B_{il} is greater than B_a, or that at which B_a is greater than or equal to B_{iu} if B_{il} (from equation (4.12)) is less than B_a. This minimum value of T_0, for $T_0 = T_c$, is fairly easily found by computation although graphically the task may be somewhat arduous. It must be remembered that this minimum value of T_0 applies only for $T_0 = T_c$ and for operation outside of the non-unique region. For any value of T_0 less than that determined in this way safe operation is guaranteed for $B_i < B_{iu}$. In most cases this value of T_0 results in virtually no reaction occurring within the bed because of the very low initial rates. However, its evaluation is useful in cases where no information exists on the sort of temperature which must be used for a particular system. When this is the case, it precludes the necessity of trial and error integration of the reactor equations to find a minimum working value. Consequently, for any inlet and coolant temperature the range of inlet concentration, or thermal load factor, which will produce temperature runaway depending on the length of the reactor may be rapidly determined. Here it should be noted that for a given inlet and coolant temperature, the range of inlet concentration described by B_{il} and B_{iu}, for any system, is a working range. Temperature runaway may occur at any value of B_i within this range and the remaining parameter which determines this is the reactor length. The calculation of this range is simply a means of saving unnecessary work in, for example, the solution of the bed equations. The upper limit on B, B_{iu}, is somewhat different in nature from the lower limit, B_{il}. At a given inlet and coolant temperature with the inlet value of B less than B_{iu} the steady state reactor trajectory will not pass through the non-unique region provided that the length of the reactor is such that it does not cross the runaway line. The lower limit on the inlet value of B, B_{il}, is, however, a global

limit for the given inlet and coolant temperature. For all inlet values of B less than B_{il} at the inlet and coolant temperature for which B_{il} is determined, the reactor trajectory will never cross the runaway line whatever the length of the reactor. This could, of course, be used as an upper limit on the value of B_i so that safe operation is always guaranteed for any reactor length. However, this tends to lead to rather conservative reactor designs due to the low rates of reaction at low values of B_i and very long reactors would be necessary to achieve a given conversion. In some circumstances using B_{il} as an upper limit may be acceptable particularly when the pressure drops in the bed and therefore the length of the reactor is not a serious constraint or when there is very great uncertainty in, for example, the heat transfer parameters.

Figure 4.12 shows schematically the limits on B_i and their relation to other regions on the T vs. B phase diagram.

Once the range of B_i has been determined at a chosen inlet and coolant temperature what remains to be done is to find some value of B_i within that range for which temperature runaway will not occur for a particular reactor length. If the reactor length is chosen first then trial and error solution of the bed equations is necessary to find a suitable value of B_i at each value of the inlet and coolant temperatures. Like all trial and error processes this can be a wasteful and time consuming process. Also this method would fail to give a total picture of the situation since information about only a single reactor length is obtained. A better approach is to integrate the bed equations for various values of B_i in the range B_{il} to B_{iu} for different values of inlet and coolant temperature and determine the critical length of the reactor in each case. This is not a particularly time consuming process with a one dimensional model of the reactor, especially since the runaway line in the form of the pellet temperature at runaway, t_s, can be used to stop the integration at each value of B_i as soon as the reactor trajectory reaches the runaway limit. Furthermore the range of coolant temperatures which need be considered may often be limited by the nature of the cooling medium; for highly exothermic reactions a molten salt coolant is usually employed and so the minimum coolant temperature is determined by the viscosity decrease with temperature. This can result in a minimum value greater than that determined by the previously

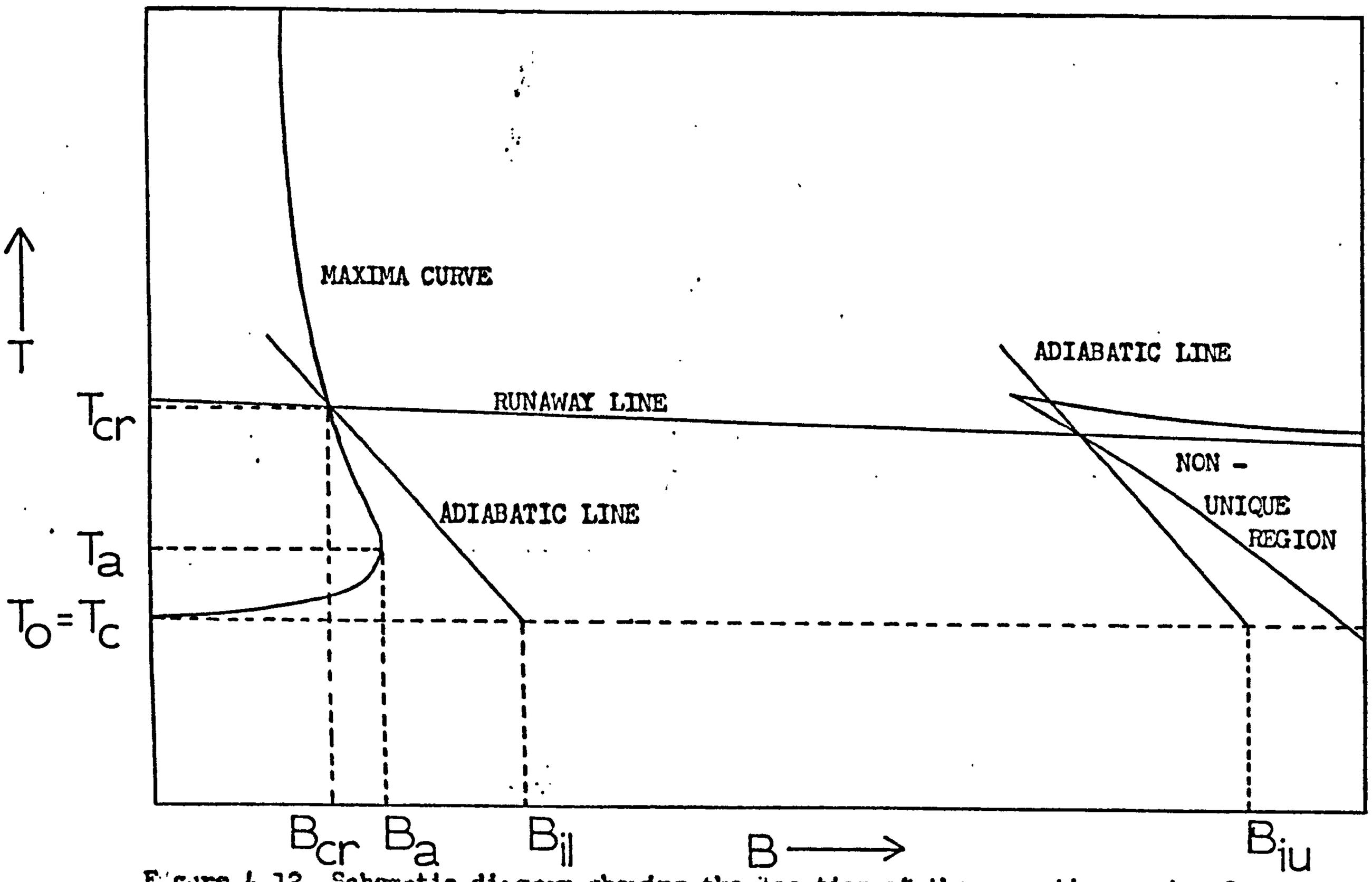

Figure 4.12 Schematic diagram showing the location of the operating region for a particular coolant and inlet temperature.

described method. The upper limit on the coolant temperature may be less than that described by the runaway line, for $T_0 = T_c$, since above a certain temperature charring and decomposition of the salt or exacerbation of its corrosion rate on the reactor tube may occur.

The length of the reactor determined at each set of inlet conditions is then the critical or maximum value for which temperature runaway can be avoided in the steady state at those conditions. By this method, charts of critical length versus inlet concentration, or thermal load factor, at various inlet and coolant temperatures, may be drawn for the system. Figure 4.13 shows such a chart for the data given in Table 5.1. The critical length in figure 4.13 is expressed as a dimensionless value for convenience, although this is not essential and actual length could be used. Figures 4.14 and 4.15 show how the parameters θ , N_{uw} and Sh_A respectively affect these charts. Usually only one chart is required for a particular system since these parameters are constant for previously stated reasons. The advantage of this approach is that the chart conveys at a glance the critical inlet conditions for any reactor length or conversely the critical length for any inlet conditions, and so the task of the designer is considerably simplified. A scale of pressure drop could also be added to the charts and during their preparation similar graphs of reactor outlet conditions, or reactant conversion at various lengths could also be drawn.

Perhaps the greatest advantage of this approach to the design problem is the information which these charts give concerning the control of the reactor and the way this may be used in the design of control systems. For example, using figure 4.13, graphs of the form of figure 4.16 can be constructed. This figure shows a plot of critical inlet temperature against critical inlet thermal load factor as a function of reactor length. Thus, for a particular reactor length, this graph shows how, if one of the inlet conditions is varied, the other should be adjusted to prevent temperature runaway occurring in the new steady state. This information has to be related to the dynamic changes but can be very easily included in a computer control algorithm for a particular reactor. When a reactor is operating in the steady state at critical or subcritical conditions and a perturbation of one of the inlet

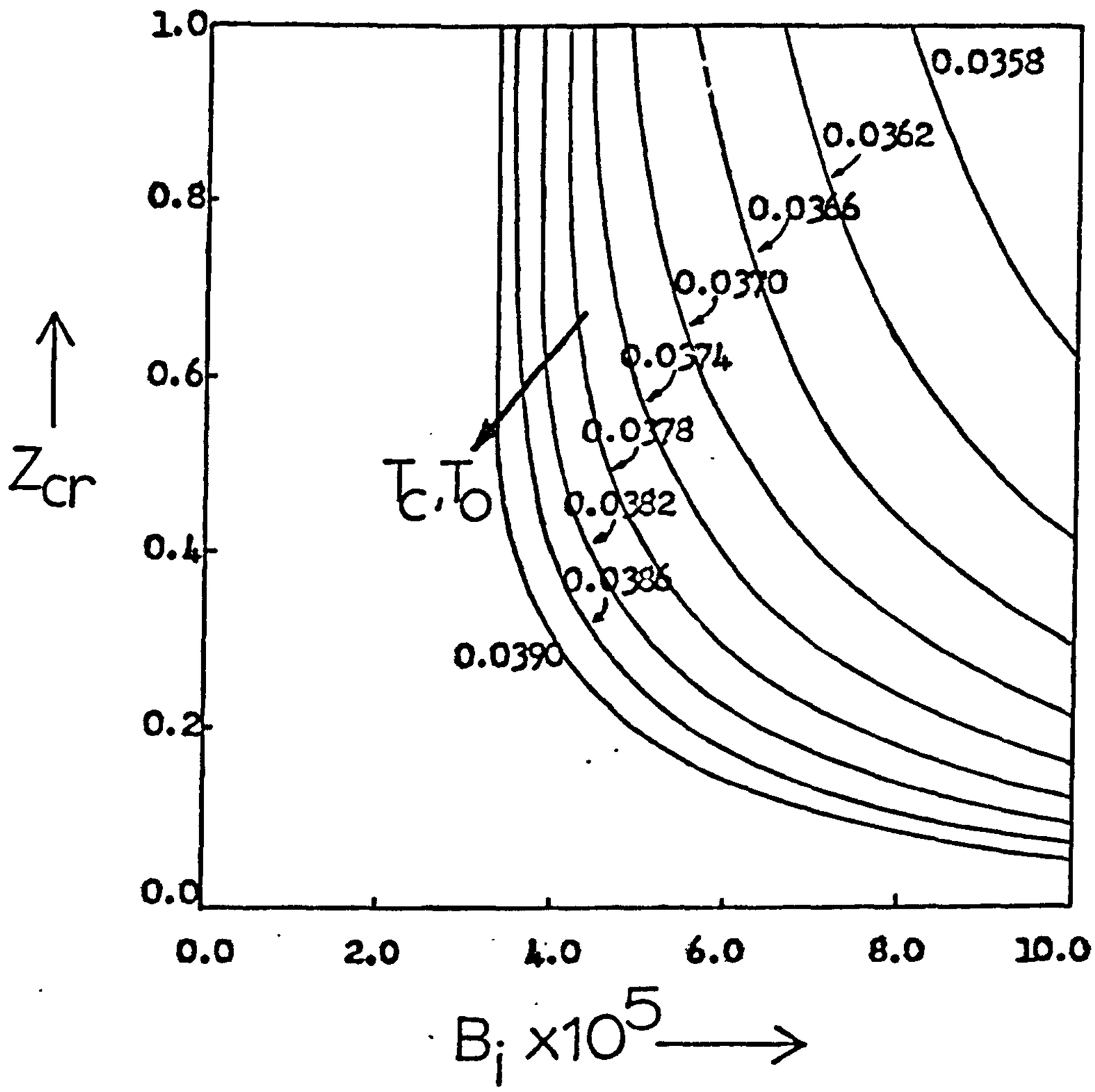

Figure 4.13 The effect of the inlet conditions on the maximum reactor length to avoid temperature runaway. (Data as given in Table 5.1)

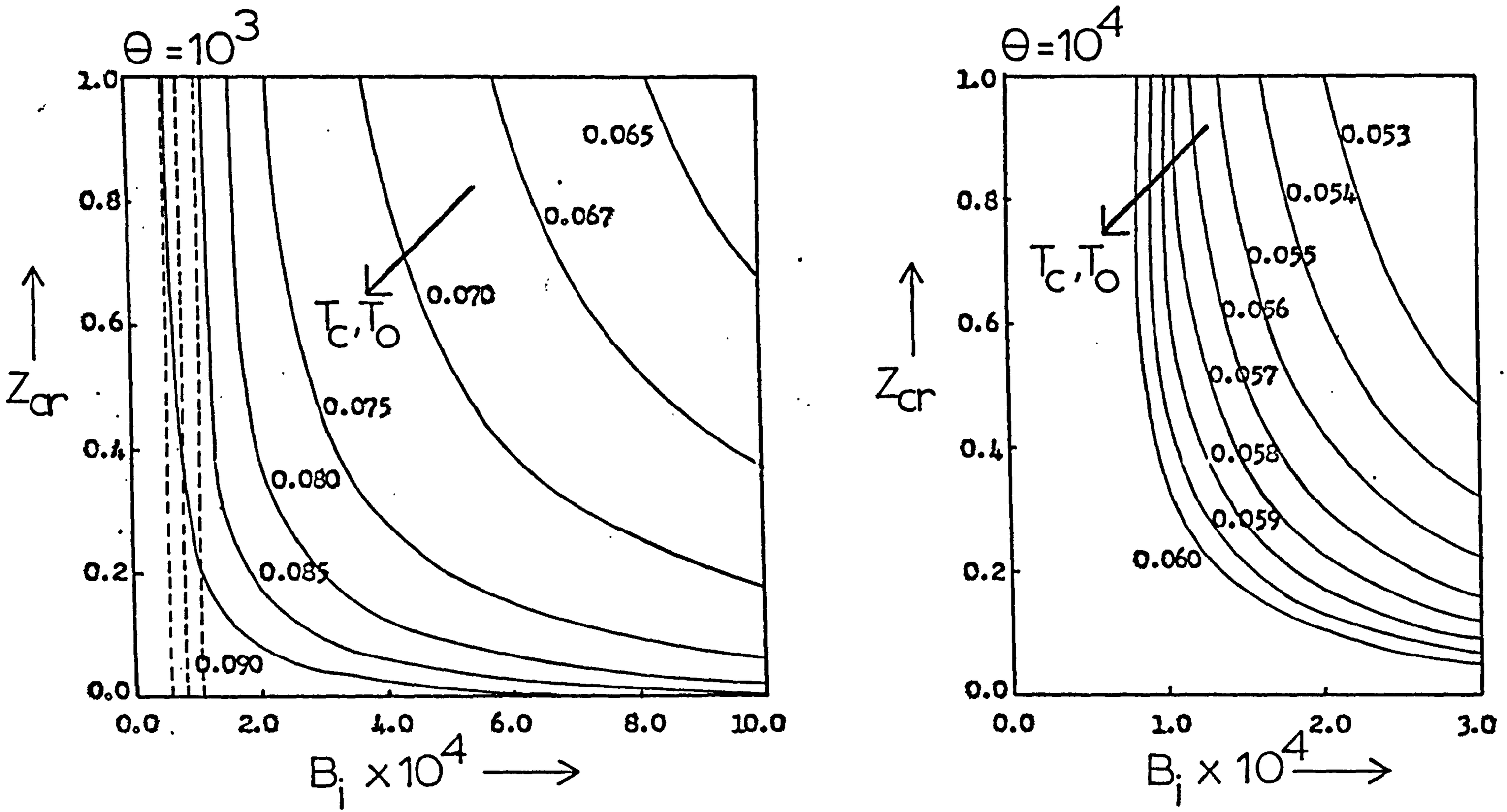

Figure 4.14 The effect of Θ on the inlet conditions and the maximum reactor length to avoid temperature runaway. (Data as given in Table 5.1)

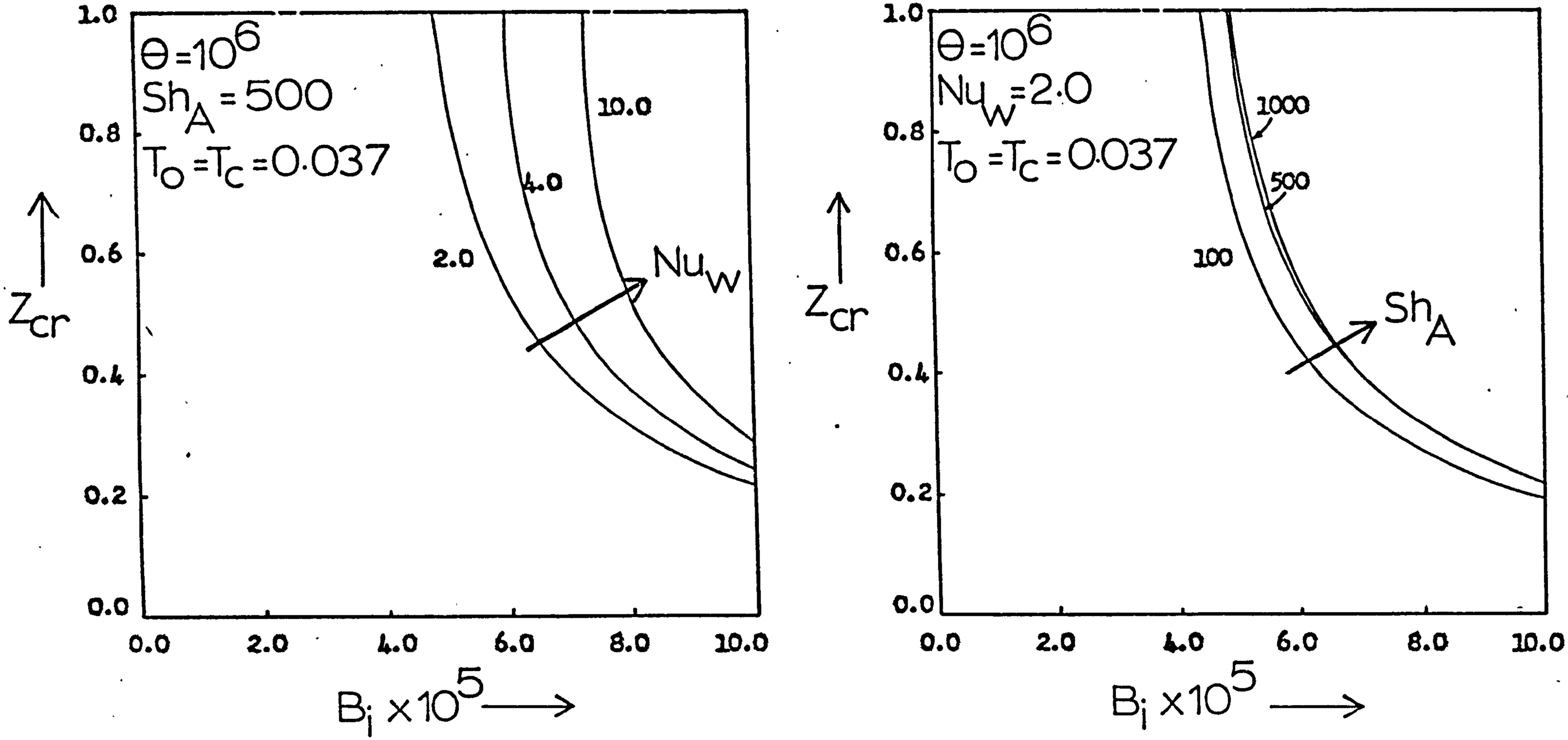

Figure 4.15 The effect of Nu_w and Sh_A on the z_{cr} vs B_i curves at a particular coolant and inlet temperature. (Data as given in Table 5.1)

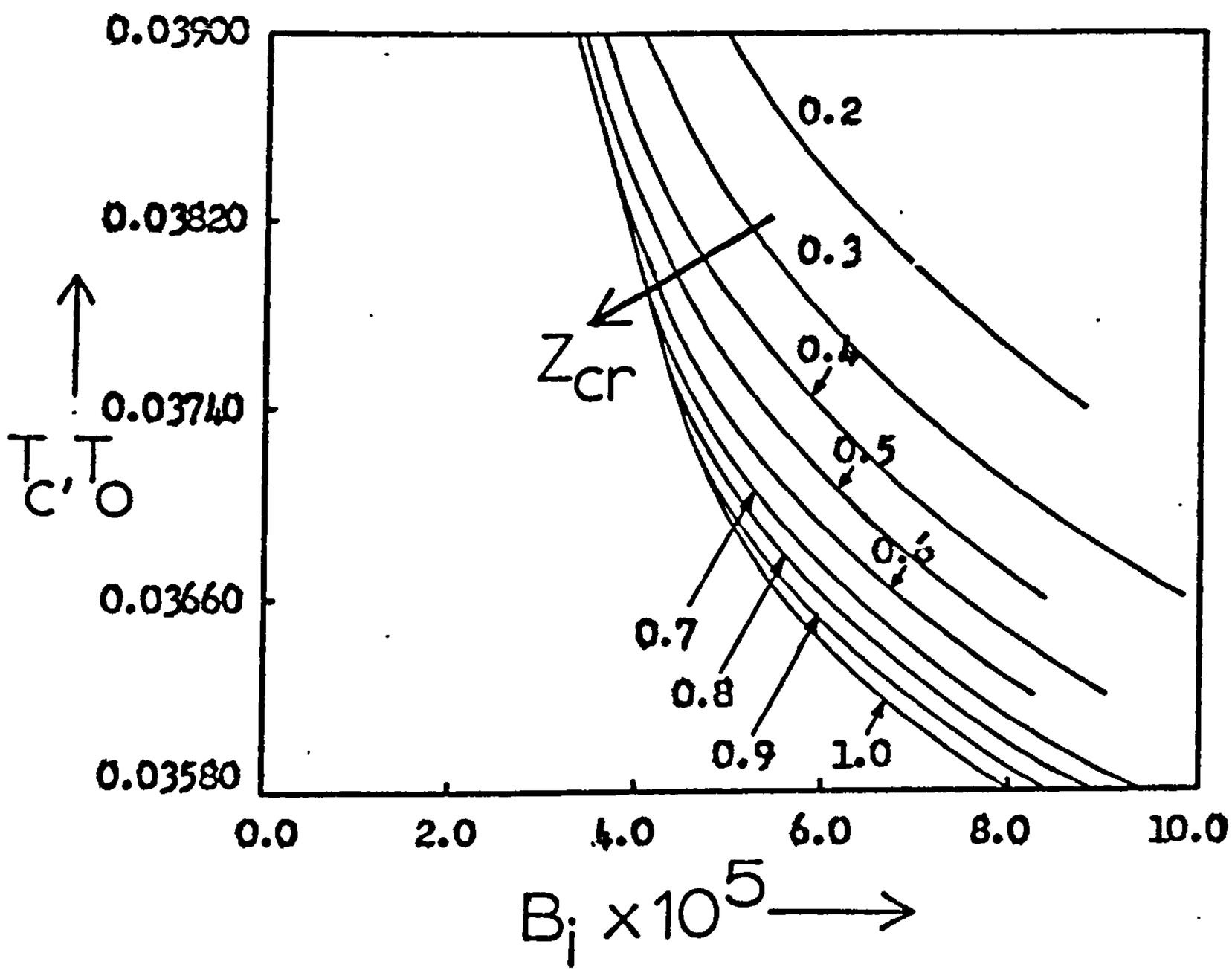

Figure 4.16 Inlet conditions to avoid temperature runaway for various reactor lengths.
(Data as given in Table 5.1)

variables occurs, then such a control algorithm indicates the adjustment in the other inlet conditions to compensate for this perturbation. However, it is essential that this adjustment does not lead to temperature runaway in the new steady state and so some form of check or constraint on the control action is required. One method of providing this check is to integrate the bed equations at the new values of the inlet conditions. Unfortunately, this would be a lengthy process for a control algorithm and undesirable behaviour could occur before the control action takes place, especially when the reactor is operating close to the critical conditions. What is required, therefore, is a much more rapid check on the proposed control action, and this can be provided by graphs of the form of figure 4.16. For a particular reactor length, the plot of critical inlet temperature against critical inlet thermal load factor, or concentration, can be fitted to a simple algebraic function. For example, the line for the reactor length corresponding to $z = 1.0$ in figure 4.16 can be fitted to a function of the form:

$$T_0 = P\exp(-B_i)(1 + B_i)/B_i^2 + Q \qquad (4.14)$$

where P and Q are constants which can be determined by a simple regression analysis. Clearly, since the curves of figure 4.16 form a family, a similar relationship between T_0 and B_i may be used for other reactor lengths by appropriate adjustment of P and Q. This functional relationship between the critical inlet conditions for the reactor may be included in the control algorithm. Thus, once the new values of the inlet variables have been selected by the controller, equation (4.14) may be used to check extremely rapidly whether or not they will lead to a safe operating state. For example, if at the new value of inlet concentration the value of T_0 computed by equation (4.14) is less than the selected value of inlet temperature then the new steady state will lead to temperature runaway and so a smaller value of inlet temperature is required.

This procedure will clearly be much quicker than any attempt at solving the bed equations and by providing more insight into the general behaviour will, therefore, lead to far better and more effective reactor control. Also since the global stability of the reactor is essentially expressed by equation (4.14) as a function of the inlet conditions, it may

not be essential to monitor the conditions in other parts of the reactor although this will depend on the tightness of the control and the type of perturbations which are likely to occur.

4.5 Comparison with Previous Methods

Only two criteria have been proposed previously for temperature runaway, by Barkelew[67] and Van Welsenaere and Froment.[68] Both of these criteria lead to the same result although the latter is simpler to use. However, as mentioned previously these criteria only apply to quasi-homogeneous systems.

It is, perhaps, instructive to compare the runaway criterion proposed in section 4.3 of this chapter with that of Van Welsenaere and Froment.[68] Although it is suggested by these authors that their method applies to fixed bed reactors in general, it was, in fact, developed on the basis of a one dimensional quasi-homogeneous model. In this the effectiveness factor is taken as unity and therefore the reaction rate limitation by the solid catalyst is ignored. In the heterogeneous case where the solid and fluid conditions differ, the effectiveness factor must be calculated at each point in the bed, especially in the region of temperature runaway, and is usually quite different from unity.

For Van Welsenaere and Froment's data, given in Table 4.2, their criterion gives an upper limit of dimensionless concentration to avoid temperature runaway as 2.035. It should be noted that this represents the maximum concentration which can be used to avoid runaway with any reactor length and, therefore, must be expected to be conservative. Figure 4.17 shows the axial temperature profiles predicted by both the quasi-homogeneous and heterogeneous models using this criteria, and figure 4.18 shows the corresponding trajectories on the T vs. B phase diagram.

Clearly, whilst Van Welsenaere and Froment's criteria are very good for quasi-homogeneous systems they are not useful in the heterogeneous case since they then give far too conservative limits on the inlet conditions. Also if the reactor conditions are such that effectiveness factors greater than unity occur, then the criteria for the quasi-homogeneous system would not give safe operating conditions.

Obviously, the runaway criteria for a quasi-homogeneous

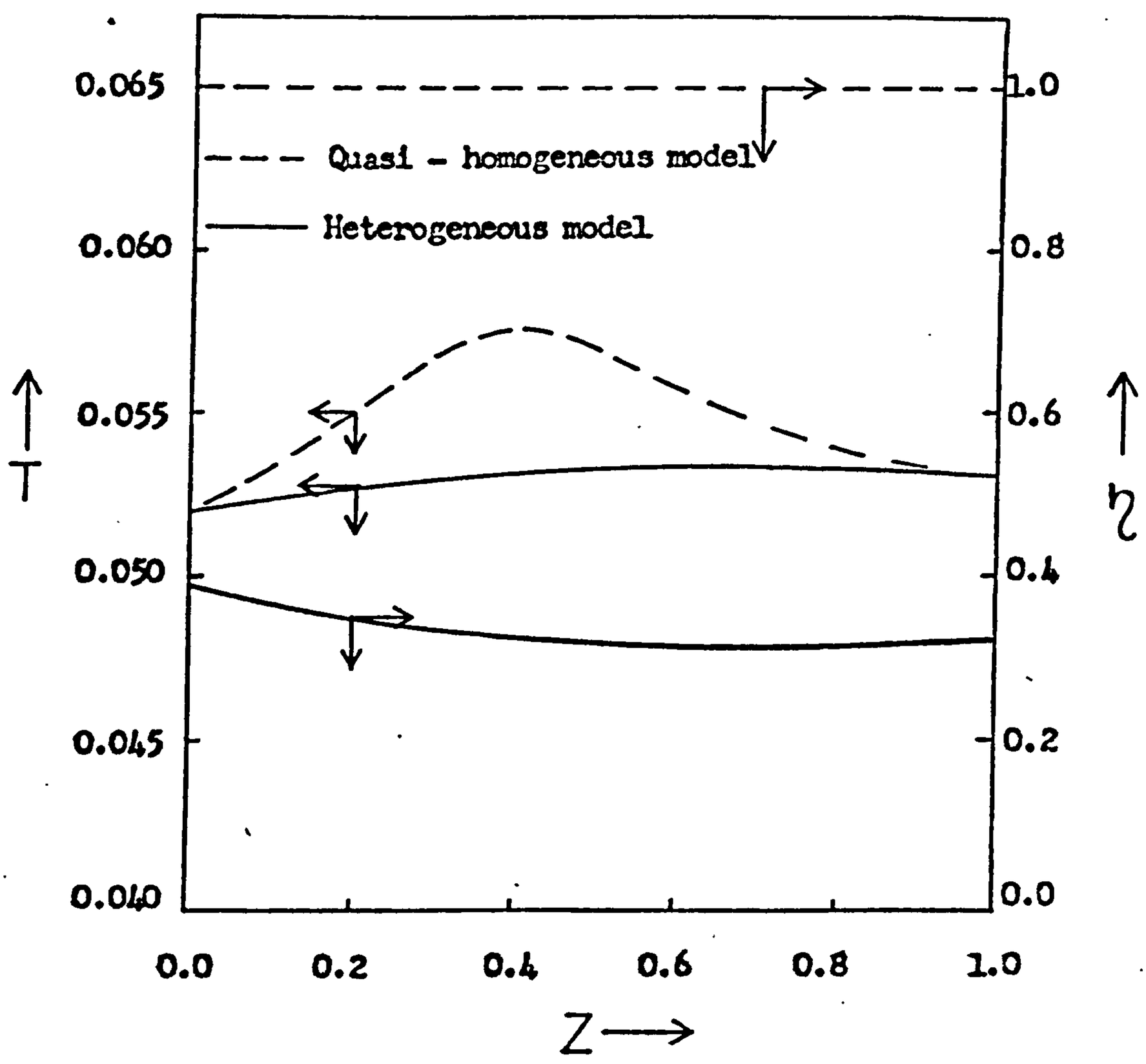

Figure 4.17 Axial profiles of radial mean temperature and effectiveness factor obtained using the runaway criterion of Van Welsenaere and Froment. (Data as given in Table 4.2; C_o = 2.035)

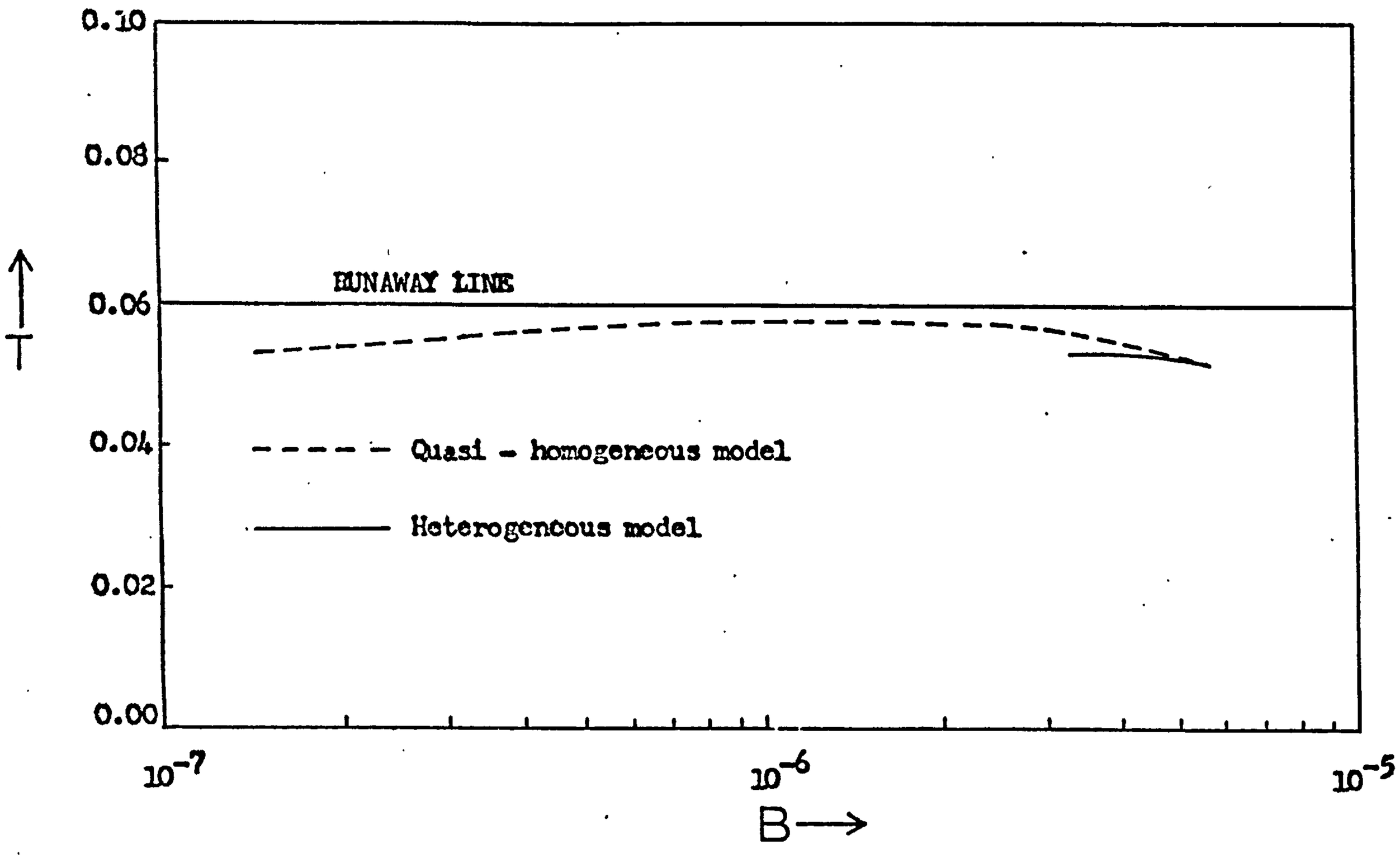

Figure 4.18 Reactor trajectories obtained using the runaway criterion of Van Welsenaere and Froment. (Data as given in Table 4.2, C_o = 2.035)

system cannot be expected to apply in the heterogeneous case. The source of the parametric sensitivity which leads to temperature runaway is different in each system. In the quasi-homogeneous case it is due to the exponential term in the reaction rate expression, whilst in the heterogeneous case it is due to the heterogeneity of the system and the way in which rate terms interact inside the pellet.

6. Concluding Remarks

A method of identifying regions of temperature runaway in fixed bed catalytic reactors has been proposed, which is not dependent on arbitrarily defined numerical values of temperature but which is determined from the intrinsic properties of heterogeneous systems. The relationship between instabilities which arise as a consequence of parametric sensitivity and those which are due to multiple steady states has also been examined.

The way in which this method may be used in the design and control of reactors has also been discussed. It has been shown how simple charts giving information about the inlet conditions and reactor dimensions which lead to critical situations may be constructed in order to facilitate a full evaluation of the various reactor operating conditions. These charts may also be used in the development and implementation of computer control strategies for the reactor. The method suggested for this can also be applied when other system constraints exist; for example, a maximum reactor outlet temperature, even when these constraints do not coincide with the runaway criterion. However, because of the instability which arises due to parametric sensitivity it is unlikely that reactor operation will be desired above the runaway limit.

Although the proposed criterion for temperature runaway has been developed for the steady state operation of the reactor, it may be used to give an insight into the dynamic behaviour since it identifies qualitatively a region of parametric sensitivity in state variable space. Its use in analysing the dynamic effects of fixed bed reactors is demonstrated in subsequent chapters..

CHAPTER 5

THE DYNAMIC MODEL OF THE REACTOR

5.1 Introduction

Whilst digital simulation has provided a very powerful tool in the study of chemical reactors, because of the considerable computational effort required attention has been mostly confined to an examination of the steady state behaviour. As pointed out in chapter 2, most investigators have tried to overcome this problem by formulating simple models which neglect certain phenomena associated with either the fluid or solid phases. The application of these models is, therefore, limited to specific systems, at least until their use in more complex situations has been justified.

The most comprehensive dynamic models of the fixed bed reactor which have been reported in the literature are those of Feick and Quon[46] and Stewart and Sørensen.[72] Both of these formulations employ fully distributed models of the catalyst pellet and describe axial as well as radial diffusion within the reactor. In the former case, the computation time required to solve the model was so great that no more than an extremely limited study of the reactor behaviour could be performed. This was mainly due to the effort required to solve the catalyst pellet model. Stewart and Sørensen[72] appear to have overcome this problem to a certain extent by using an orthogonal collocation method to solve the system equations. However, since they were mainly concerned with the mathematical aspects of the solution, no attempt was made to study the reactor behaviour in any detail.

The essential requirements of any system model are that it should provide an adequate description of the system with the minimum of computational effort. This is especially true for a dynamic model of the fixed bed reactor where usually the equivalent of a steady state solution must be generated very many times in order to describe the reactor behaviour over a period of time. It is essential, therefore, that such a model contains a description of only the important physical and chemical processes within the system..

The factor which most affects the computational load in a

heterogeneous reactor model is the level of complexity adopted in the formulation of the catalyst pellet model. As has been discussed in chapter 2, the lumped thermal resistance model of the catalyst pellet (Appendix (1)) has been shown to give an accurate estimate of the pellet performance over a wide range of parameters and also requires relatively little computational effort for solution. It is, therefore, very suitable for inclusion in a dynamic model of the reactor.

A reduction in the dimensionality of the reactor model will also reduce the computational load. However, as with any approximate method of solution, the predictions of a one dimensional model must be compared with those of a two dimensional formulation in order to establish the validity and, therefore, the usefulness of the model. Once this has been done, the simpler model may then be used more efficiently to study the effects of various factors on the reactor performance.

In chapter 3 the suitability of two methods of describing radial heat transfer in packed bed reactors was examined. It was shown that the single phase approach was the more appropriate since it allowed a consistent description of the important reaction rate limiting effects within the catalyst pellets. In this chapter, this approach is adopted in the formulation of a two dimensional dynamic model of the reactor which is used to evaluate a simpler one dimensional model. Also, in order to establish what are the important dynamic elements in the reactor, consideration is given to the inclusion of a description of the reactor tube wall in the reactor model. Since this has a finite thermal capacitance the conditions under which it may significantly affect the dynamic behaviour of the reactor are examined with the use of the one dimensional model.

5.2 The Two Dimensional Dynamic Model

5.2.1 Formulation and Solution of the Equations

The reaction scheme considered is the simple, first-order, irreversible A $\longrightarrow$ B reaction with Arrhenius kinetics.

Attention is confined to a long cylindrical reactor tube packed with spherical catalyst pellets, with the outside of the tube surrounded by a coolant at a constant temperature. The fluid stream is assumed to pass through the bed in plug flow and the bed is sufficiently long that the effects of axial

dispersion may be neglected.

The equations representing the heat and mass balances on the reactor may be written in dimensionless form as follows:

$$\frac{\partial^2 C_A}{\partial r^2} + \frac{1}{r}\frac{\partial C_A}{\partial r} - G_1\frac{\partial C_A}{\partial z} - G_1 G_2 \zeta k_1 C_A = G_5\frac{\partial C_A}{\partial \tau} \qquad (5.1)$$

$$\frac{\partial^2 T}{\partial r^2} + \frac{1}{r}\frac{\partial T}{\partial r} - G_3\frac{\partial T}{\partial z} + G_3 G_4 (t - T) = G_6\frac{\partial T}{\partial \tau} \qquad (5.2)$$

with boundary conditions:

$$\frac{\partial C_A}{\partial r} = \frac{\partial T}{\partial r} = 0 \qquad \text{at } r = 0,\ z > 0,\ \tau \geqslant 0$$

$$\frac{\partial C_A}{\partial r} = 0$$

$$\text{at } r = 1,\ z > 0,\ \tau \geqslant 0$$

$$\frac{\partial T}{\partial r} = Nu_w(T_c - T)$$

and initial conditions:

$$C_A = C_A(r,\tau),\quad T = T_0(r,\tau) \qquad \text{at } z = 0,\ \tau \geqslant 0,\ 0<r<1$$

$$C_A = C_A(r,z),\quad T = T_0(r,z) \qquad \text{at } \tau = 0,\ z \geqslant 0,\ 0<r<1$$

where:

$$G_1 = \frac{R^2 u}{LD_{fA}} \qquad G_2 = \frac{(1 - e)LD_{pA}}{b^2 ue}$$

$$G_3 = \frac{R^2 u \rho c_p}{K_f L} \qquad G_4 = \frac{3hL(1 - e)}{bu \rho c_p e}$$

$$G_5 = \frac{(\sout{Le/u})}{} G_1 * \frac{L}{u} \qquad G_6 = \frac{(\sout{G_5})}{} G_3 * \frac{L}{u}$$

$$Nu_w = RU/K_f e \qquad k_1 = \theta^2 \exp(-1/T)$$

Equations (5.1) and (5.2) are coupled with the dynamic model of the catalyst pellet given in Appendix (1) through the variables ζ and t.

Solution of the equations may be accomplished by a marching technique starting at the reactor entrance and working through to the exit at each time step, using the finite difference formulation described in Appendix (3). At each radial node the unknowns are C_A, T, t and ζ at the axial and time node under consideration, and the solution may be obtained as follows:

(1) Assume radial profiles of C_A and T at the first axial position where they are unknown for the current time position.

(2) Using the assumed values of C_A and T from step (1) solve the catalyst pellet model over the time step to give values of t and ζ at each radial node at the current time.

(3) Calculate the radial profiles of C_A and T at the current time using the values of t and η obtained from step (2) and compare them with the profiles assumed in step (1). If agreement is satisfactory, continue to step (4), otherwise repeat from step (2).

(4) Repeat from step (1) while $z \leqslant 1$ (i.e. until the reactor exit is reached).

(5) Repeat the whole computation for the next position in time and continue for as long as necessary.

The initial steady state conditions are conveniently defined by setting the time derivatives in equations (5.1) and (5.2) equal to zero and solving the equations using the finite difference approximation given in Appendix (3).

5.2.2 Reduction of the Model to Pseudo-Steady State Form

Values of the system parameters used in the simulations are given in Table 5.1. When programmed in Fortran on an IBM 1130 computer with floating point hardware, solution of the model represented by equations (5.1) and (5.2) was found to require between twenty and thirty minutes per time step. The time required for solution over each time interval is a function of the number of nodes in the finite difference representation of the spatial coordinates. For the data given in Table 5.1, the number of nodes required for a convergent solution within each time interval is of the order of 20 in the radial direction and 200 in the axial direction. A reduction in these values leads to a saving in computation time in two ways; namely a direct saving in the amount of calculation to be carried out, since the number of solutions of the catalyst pellet model is reduced, and a further saving in backing storage access time. Generally, on small computers, the use of backing storage for

TABLE 5.1 Data used in Chapters 5, 6, and 7.

A_0	8.29×10^{10}	sec^{-1}	θ	1.0×10^{6}
E	26.6×10^{3}	cal $gmole^{-1}$	B_o	4.602×10^{-5}
$(-\Delta H)$	300×10^{3}	cal $gmole^{-1}$	Sh_A	500.0
D_{pA}	3.66×10^{-3}	cm^2 sec^{-1}	Nu	1.0
k_{gA}	4.36	cm sec^{-1}	G_1	0.84
h	1.20×10^{-3}	cal cm^{-2} sec^{-1} K^{-1}	G_2	0.0949
b	0.21	cm	G_3	0.84
L	125	cm	G_4	76.85
u	164	cm sec^{-1}	G_5	0.84 secs
R, R_1	2.1	cm	G_6	0.84 secs
R_2	2.5	cm	Nu_w	2.0
U	6.7×10^{-4}	cal cm^{-2} sec^{-1} K^{-1}	Nu_w^*	1.33
e	0.4		K_T	1.55 secs
c_p	0.25	cal gm^{-1} K^{-1}	K_w	1300 secs
$\varrho^* c_p^*$	0.0177	cal cm^{-3} K^{-1}		
$\varrho_w c_{pw}$	1.0	cal cm^{-3} K^{-1}		
K_p	$5.04 * 10^{-4}$	cal cm^{-1} sec^{-1} K^{-1}		
T_o'	500	K	T_o	0.03733
T_c'	500	K	T_c	0.03733
C_o	2.84×10^{-7}	gmole cm^{-3}	C_{Ao}	1.0

Chapter 5 only

$h_f : h_c$ 1 : 1	Nu_{wf}	4.0	Nu_{wo}	4.0	Nu_{wf}^*	2.0
$h_f : h_c$ 1 : 4	Nu_{wf}	2.5	Nu_{wo}	10.0	Nu_{wf}^*	1.6
$h_f : h_c$ 1 : 10	Nu_{wf}	2.2	Nu_{wo}	22.0	Nu_{wf}^*	1.42

Chapter 6 only

$(-\Delta H)$	500×10^{3}	cal $gmole^{-1}$	B_o	7.67×10^{-5}
Unique region :				
T_o'	500	K	T_o	0.03733
T_c'	465	K	T_c	0.03500
			C_{Ao}	1.0

TABLE 5.1 (Continued)

Non - unique region :				
T_o'	482	K	T_o	0.03621
T_c'	465	K	T_c	0.03500
			C_{Ao}	1.304
Chapter 7 only				
u_c'	8	cm sec^{-1}	G_{cc}	577
M_c	427.3	gm sec^{-1}	K_c	15.6 secs
c_{pc}	0.373	cal gm^{-1} K^{-1}		

this type of calculation is essential because of the large amount of information which must be retained between successive spatial and time increments. Against any reduction in computation time caused by using larger spatial increments must be weighed the reduction in accuracy and numerical stability which is likely to occur. These problems have been discussed in detail by Cresswell[13] and Thornton.[12] In general, with highly non-linear systems of equations of this type it is essential that the truncation errors are kept to a minimum, and this is achieved by using a fine grid. Clearly, more sophisticated numerical techniques may be used to circumvent this problem.[12,15] The finite difference scheme used here is both simple to program and accurate and may be used as the basis for checking the solutions obtained by the more approximate methods.

Since the spatial increments used in the solution of equations (5.1) and (5.2) must be fairly small, one way of attempting to decrease the time required for solution is to use as large a time increment as possible. However, with $G_5 = G_6 = 0.84$ it has been found that to obtain a converged solution when step changes occur in the reactor inlet conditions, a time interval of the order of 0.01 seconds is required. Clearly, with time steps of this size the use of the model is severely limited. As Thornton[12] has pointed out, the thermal capacity of the catalyst pellets is much greater than the capacity of the surrounding fluid to absorb heat and mass and therefore the transient response of the reactor will be slow compared with the residence time. This means that the dynamic behaviour of the fluid may be approximated to a series of pseudo-steady states. Figure 5.1 shows the effect of applying this approximation, by setting $G_5 = G_6 = 0$, on the computed response of the reactor to a step decrease in inlet temperature. The model incorporating the fluid capacitances predicts a slightly slower response due to these capacitances, but the differences between the profiles is negligible compared with the magnitudes of the changes which are occurring and considering the severity of the conditions. Treating the fluid as being at a pseudo-steady state allows the use of a time interval of one to two seconds to obtain a converged solution, and so clearly the reduction in computational effort required to follow the whole response is considerable. One further advantage of

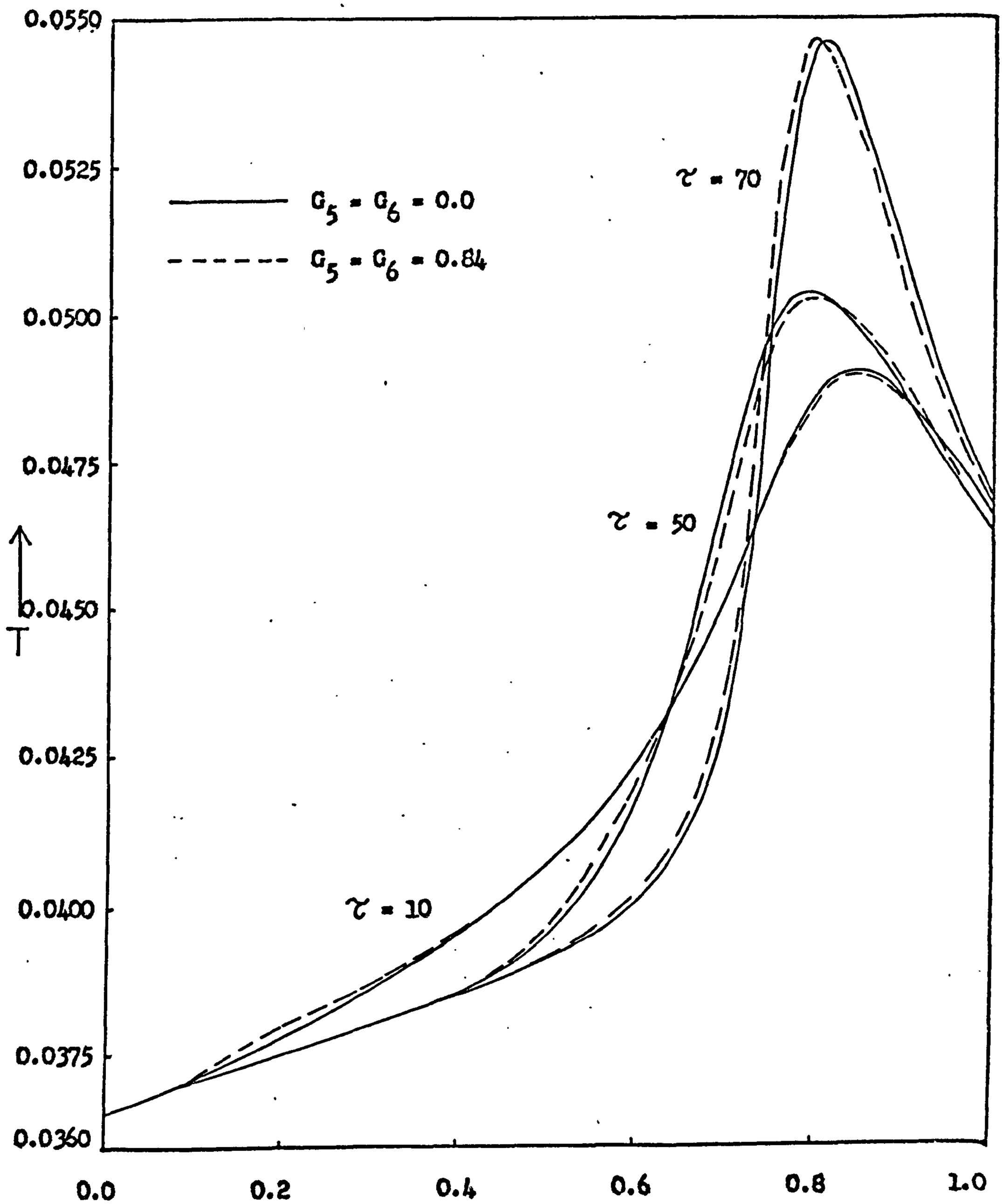

Figure 5.1 The effect of the parameters G_5 and G_6 on the axial profiles of radial mean temperature in the reactor following a step decrease of 0.00075 in the dimensionless inlet temperature. Data as given in Table 5.1. For the given E this change represents approximately 10 K.

the pseudo-steady state formulation is that the solution over each time interval requires approximately half as much computation time as the model incorporating the fluid capacitances. This is due to a reduction in both the amount of computation and the backing storage access time, since less information has to be retained between successive time steps. Clearly, this saving will not be so great on a large computer where the use of backing storage is not necessary.

5.2.3 Comparison with the One Dimensional Model

Before comparing the transient responses of the reactor predicted by the one and two dimensional models it is first necessary to examine the limitations of the one dimensional formulation in the steady state. This is especially true if, as is usually the case, the steady state version of the models are used to give initial conditions for the dynamic model since any discrepancies between them in the steady state will also appear in the unsteady state.

In a simple one dimensional model the state variables (concentration and temperature) are assumed constant across the tube radius and the parameters have the same values as those used in the two dimensional model. Unless the heat removal through the tube wall is very small, for example in near adiabatic reactors or in reactors where the fluid temperature is not very different from the coolant temperature along the whole length of the tube, so that the radial temperature profiles are very flat, then the predictions of such a model will significantly differ from those of a two dimensional model of the same system. In most cases, and especially in the region of the hot spot, the radial temperature profile will be far from flat due to the radial removal of heat. Thornton[12] observed that the radial temperature profile is essentially parabolic in shape and this enabled him to express the fluid temperature at any point across the tube radius in terms of its radial mean value. Also, the wall heat transfer coefficient expressed as the wall Nusselt number may be modified so that at each axial position in the bed, the heat removal by the coolant may be expressed in terms of the radial mean temperature, T, rather than the value at the tube wall, $T|_{r=1}$. Thus the modified wall Nusselt number, Nu_w^*, is defined by:

$$Nu_w^*(T - T_c) = Nu_w(T|_{r=1} - T_c).$$

Assuming a parabolic form for the radial temperature profile enables Nu_w^* to be expressed in terms of Nu_w only. Thus

$$Nu_w^* = 4Nu_w/(4 + Nu_w)$$

It can be seen from this that $Nu_w^* < Nu_w$ so that the greater temperature driving force for heat removal, $(T - T_c)$, is compensated. Using this corrected wall Nusselt number allows the formulation of a one dimensional model in terms of the radial mean state variables and reaction rate terms. A problem arises, however, in the evaluation of these reaction rate terms. Specifically, since the kinetic rate expressions are highly non-linear functions of temperature, the reaction rate evaluated at the mean conditions is less than the true mean value. Thus within the main reaction zone of the reactor where the radial variations of temperature and concentration are more pronounced, the one dimensional model predicts lower temperatures than the two dimensional model. For most conditions this means simply that the temperature at the hot spot is not so great, although as McGreavy and Adderley[113] have demonstrated, if the steady state exhibits temperature runaway then the one dimensional model can predict a hot spot further down the bed than the two dimensional model. Clearly, although in the steady state the quantitative features of the temperature profile are still to some extent retained, this may result in incorrect prediction of the transient response of the reactor.

In the one dimensional model since the radial temperature profile is assumed parabolic it may be generated once the radial mean temperature is known. No similar generation of the radial concentration and effectiveness factor profiles is possible, however, and so to evaluate the radial mean reaction rate at each axial position necessitates that these remain constant, at their mean values, across the tube radius. When the mean reaction rate is evaluated in this way it will obviously be overestimated since both the concentration and effectiveness factor decrease across the tube radius towards the centre, especially in the region of the hot spot. Consequently, the axial temperature profiles predicted in this way by the one dimensional model will be higher than those obtained from the two dimensional model.

Thornton[12] showed that agreement can be obtained between

the steady state axial profiles of radial mean concentration and temperature by appropriate choice of the wall Nusselt number for the one dimensional model. This entails calculating the axial profile of radial mean temperature using the two dimensional model and then trying successive values of the wall Nusselt number in the one dimensional model until a good fit is obtained. The result of this trial and error approach is shown in figure 5.2. It can be seen that using a value of $Nu_w = 1.75$ in the one dimensional model gives good agreement between the two models for the data given in Table 5.1. Equally good agreement is also obtained between the axial profiles of radial mean concentration using this value of the wall Nusselt number.

Figure 5.3 shows steady state radial temperature profiles predicted by both the two dimensional model (solid line) and the one dimensional model (broken line) with $Nu_w = 1.75$. In the region of the hot spot the profiles generated by the one dimensional model are flatter than those obtained from the two dimensional model so that although the mean values agree very well there is a discrepancy at, for example, the tube axis ($r = 0$). The extent of this difference in centre-line temperatures along the reactor is shown in figure 5.4 and it can be seen that the one dimensional model underestimates the centre-line temperature especially in the region of the hot spot despite the agreement between the radial mean values. For the purposes of reactor control it is probably more important to accurately predict the centre-line temperature in the reactor since this is where temperature runaway is first likely to occur. For the purposes of obtaining a general picture of the dynamic behaviour of the reactor the mean values of the state variables in the radial direction are sufficient.

Figure 5.5 shows axial profiles of radial mean temperature predicted by both the one and two dimensional models in response to a step decrease in the reactor inlet temperature. As can be seen, the agreement between the two models is excellent. The one dimensional model agrees with the two dimensional formulation not only qualitatively but almost quantitatively as well. As might be expected when the temperature profiles are in such close agreement the concentration profiles are also very similar. The agreement between the radial temperature profiles predicted by both models is not quite so good, particularly in

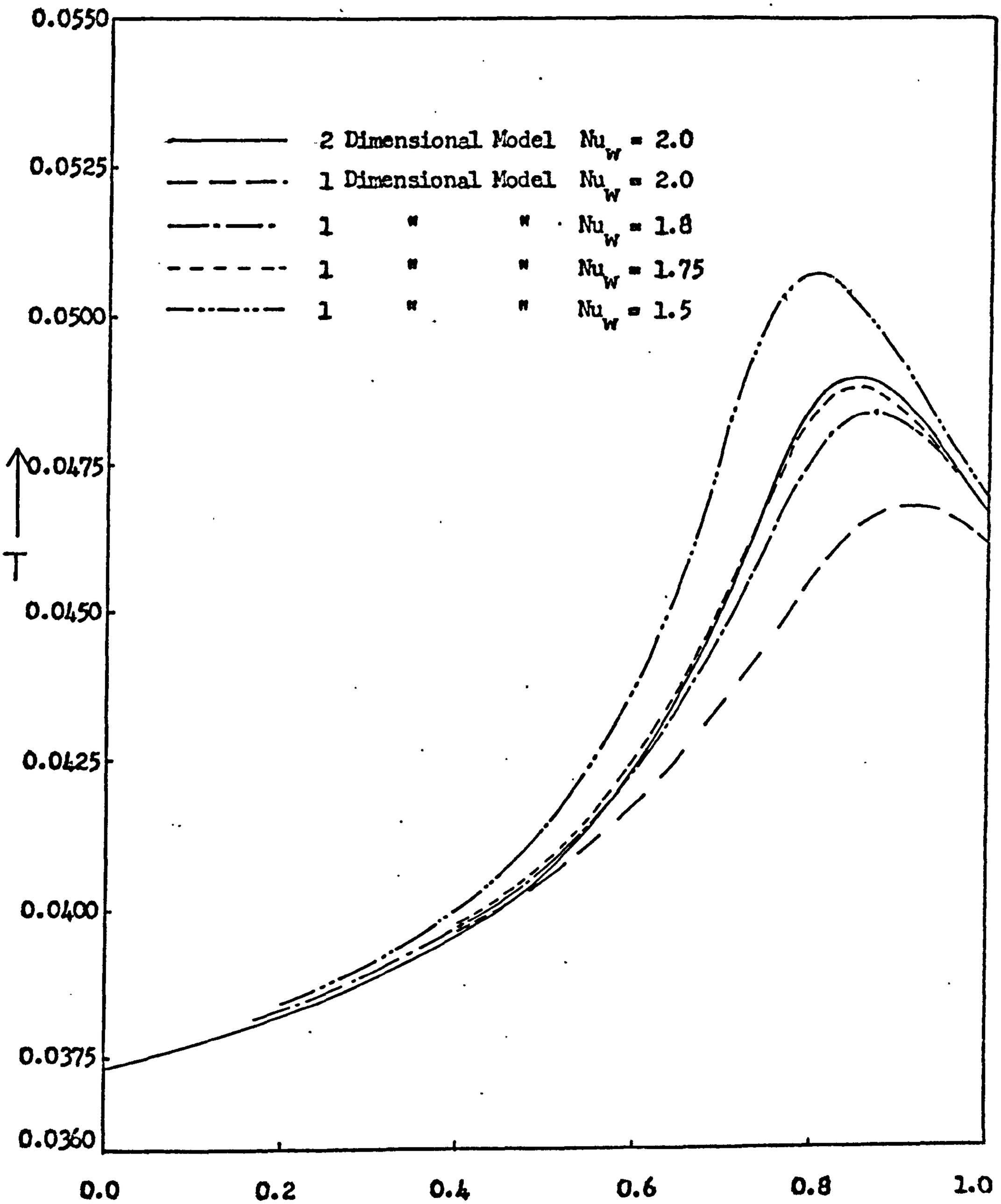

Figure 5.2 Comparison of the steady state profiles of radial mean temperature predicted by the two dimensional model and the one dimensional model using various values of the wall Nusselt number. (Data as given in Table 5.1)

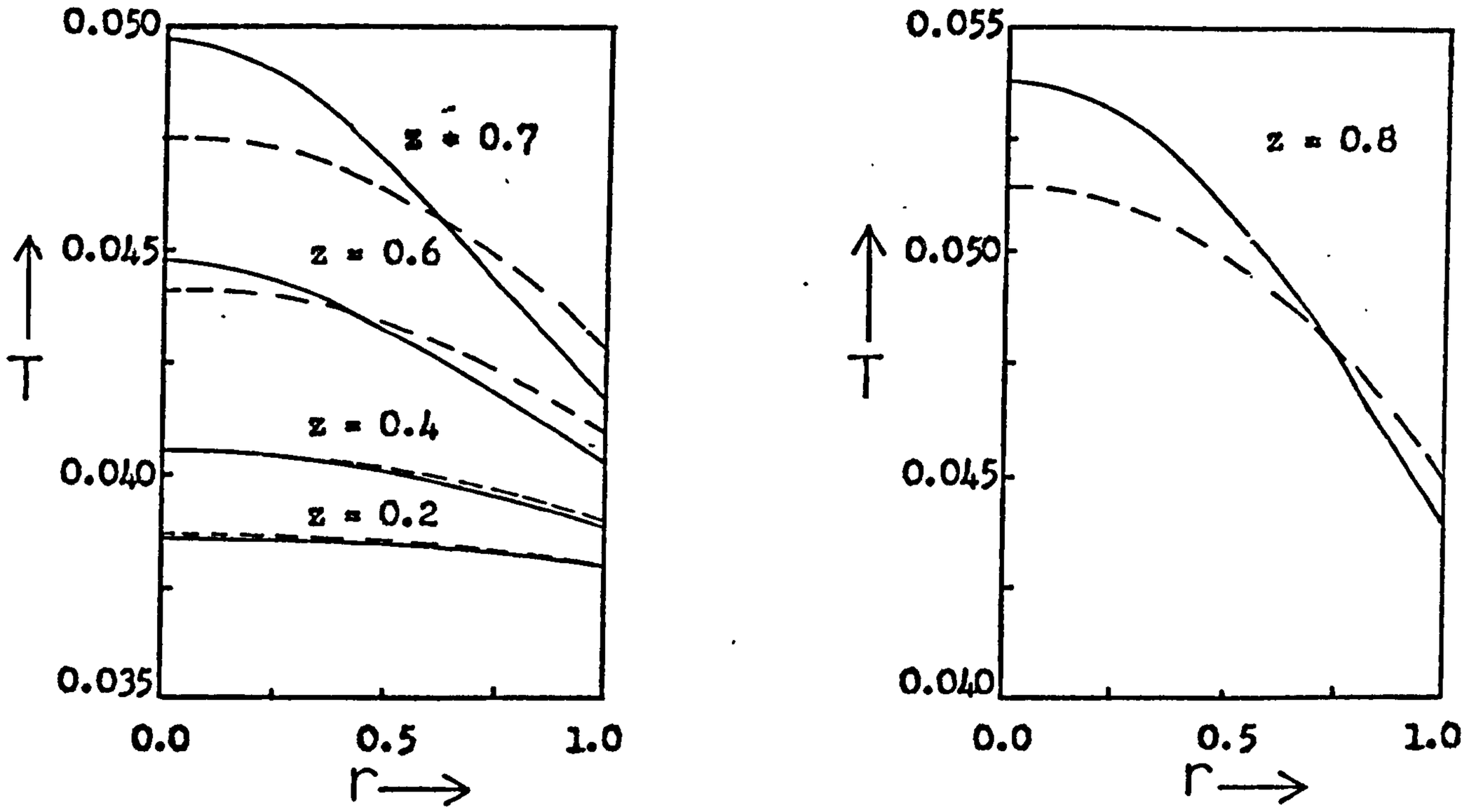

Figure 5.3 Comparison of steady state radial temperature profiles predicted by the two dimensional model with $Nu_w = 2.0$ (solid line) and the one dimensional model with $Nu_w = 1.75$ (broken line). (Data as given in Table 5.1)

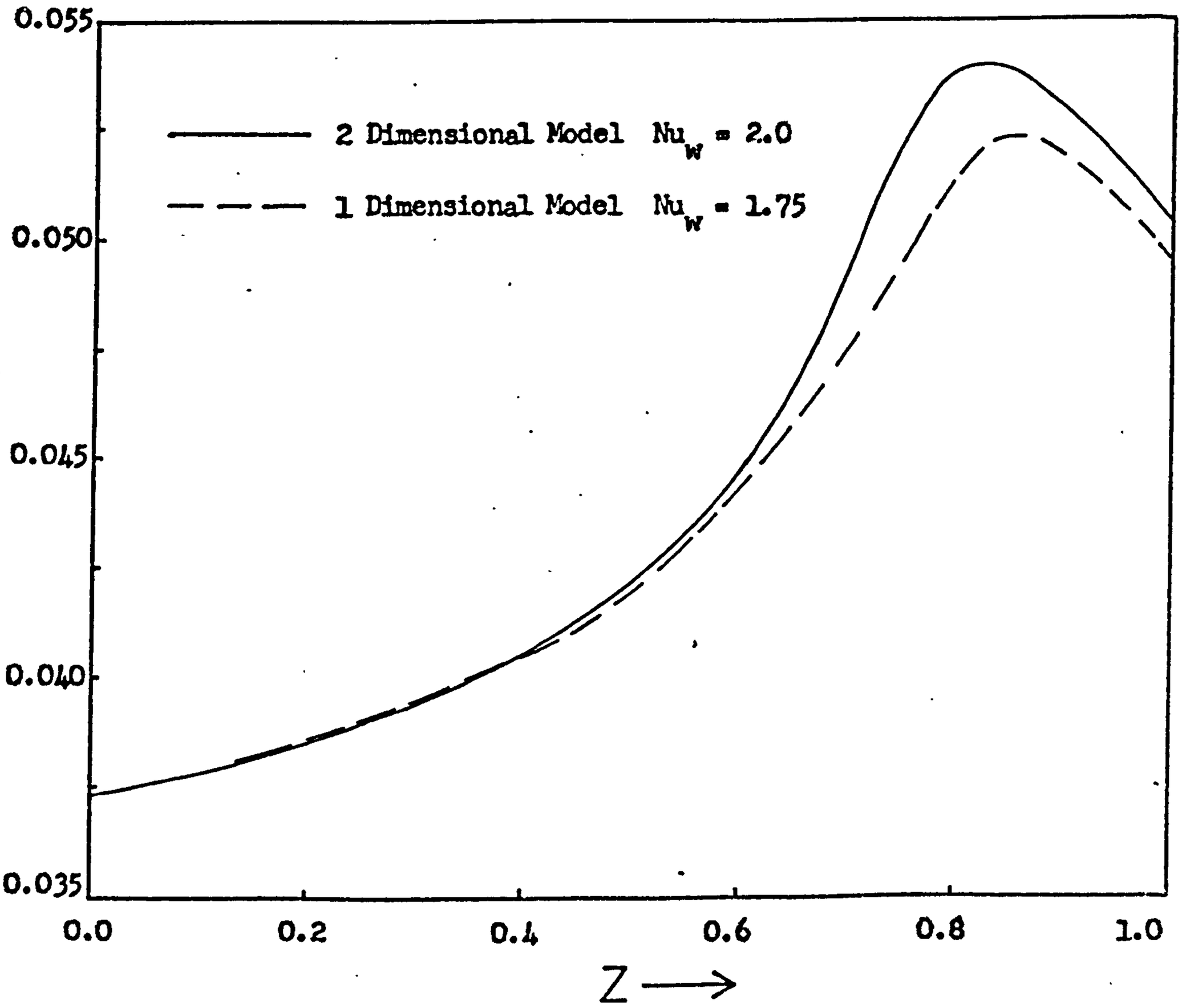

Figure 5.4 Comparison of steady state centreline (r = 0) temperature profiles predicted by the one and two dimensional models. (Data as given in Table 5.1)

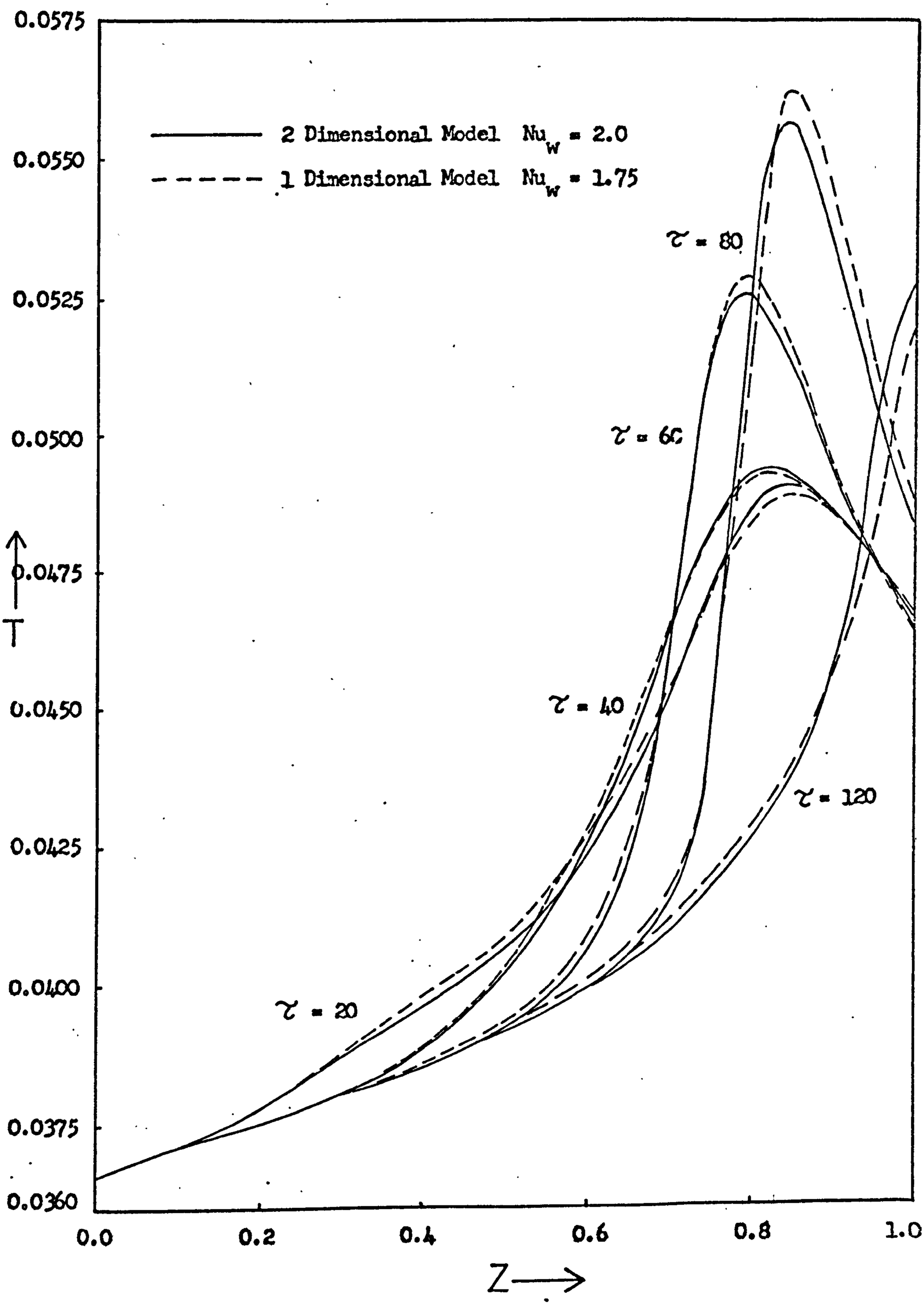

Figure 5.5 Comparison of axial profiles of radial mean temperature predicted by the one and two dimensional models following a step decrease of 0.00075 in the dimensionless inlet temperature. (Data as given in Table 5.1)

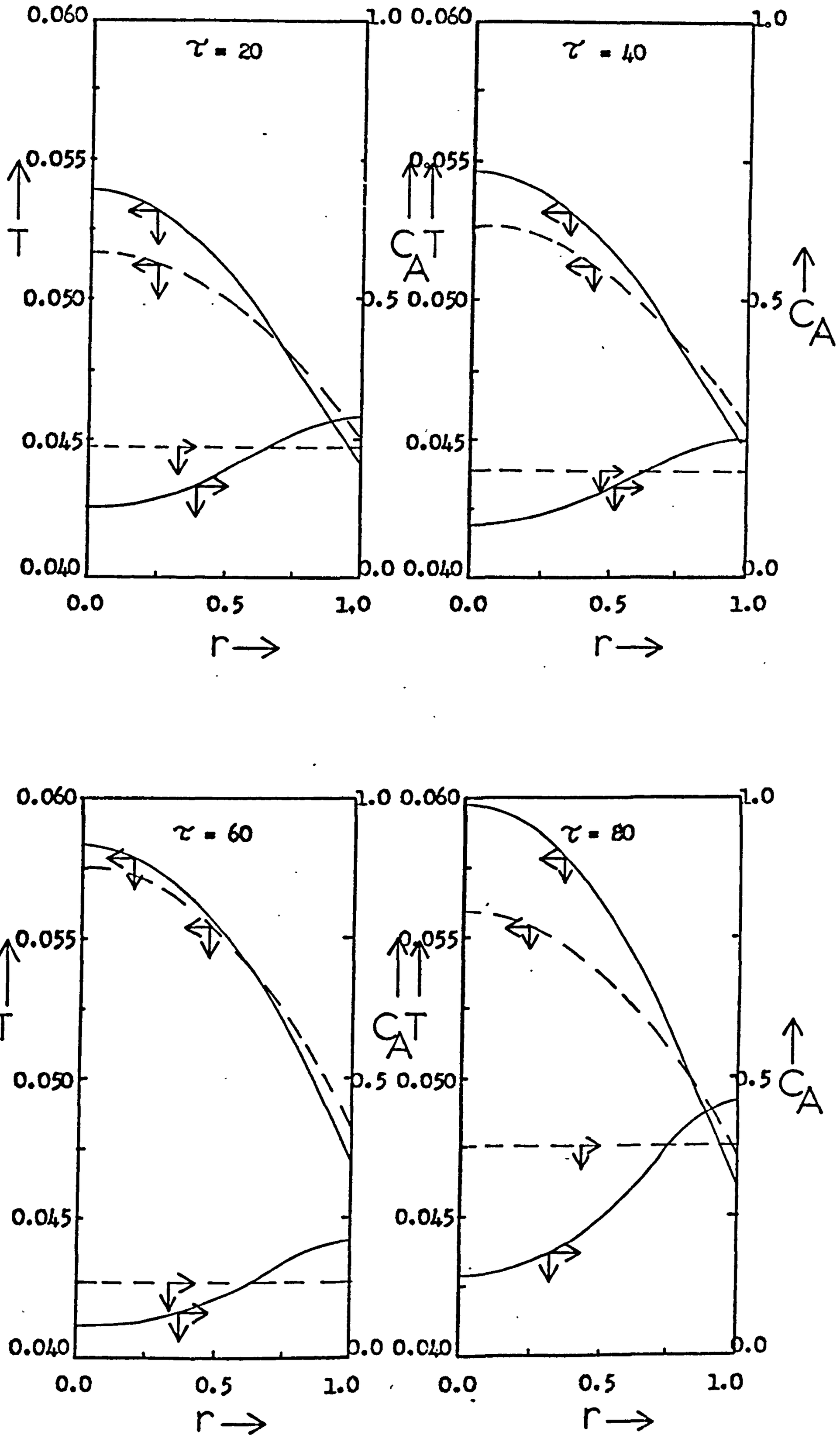

Figure 5.6 Comparison of radial concentration and temperature profiles at z = 0.8 predicted by the one dimensional model with $Nu_w = 1.75$ (broken line) and the two dimensional model (solid line) following a step decrease of 0.00075 in the dimensionless inlet temperature.

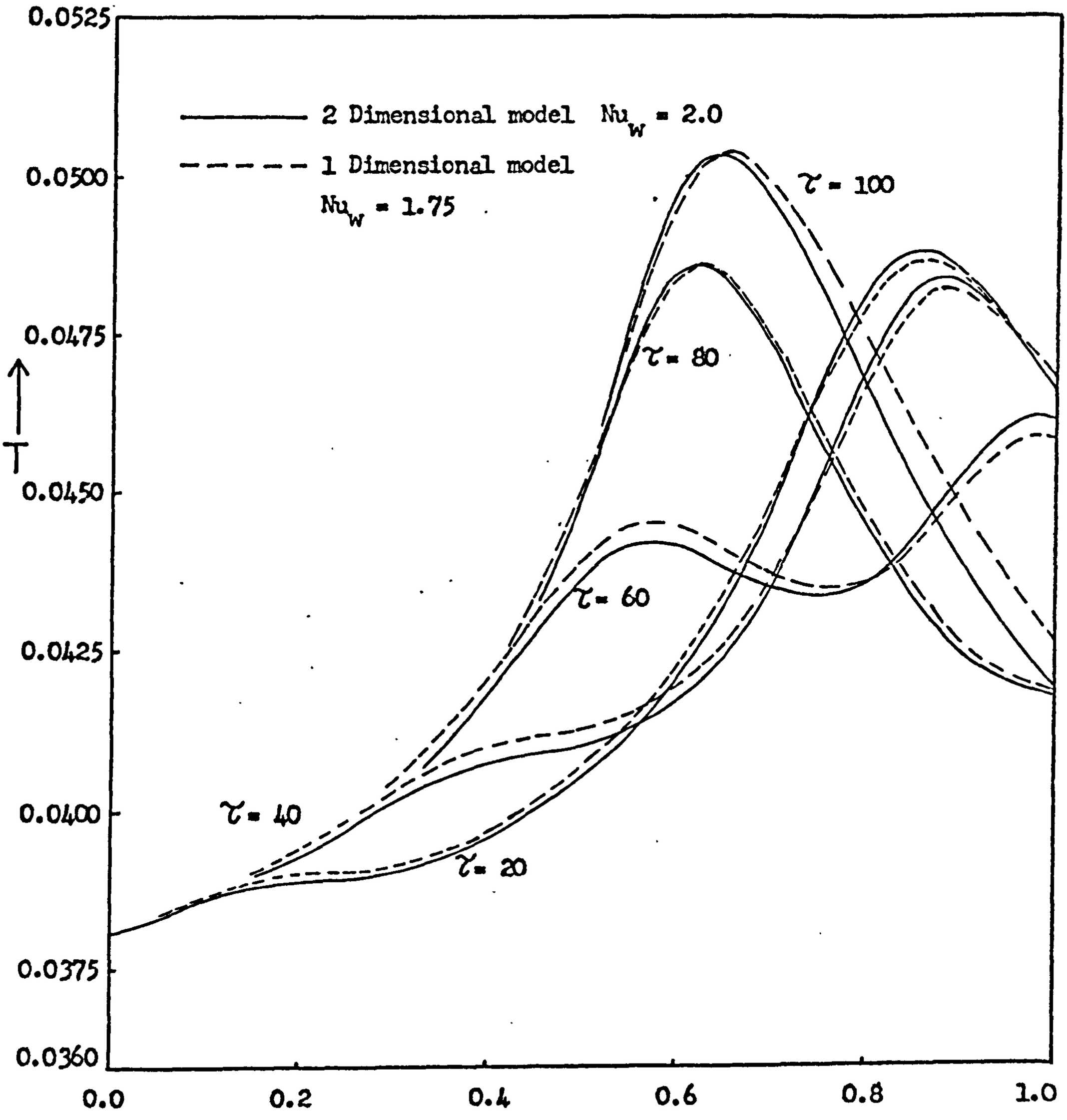

Figure 5.7 Comparison of radial mean temperature profiles predicted by the one and two dimensional models following a step increase of 0.00075 in the dimensionless inlet temperature. (Data as given in Table 5.1)

the region of the hot spot and this might be anticipated from the results of the steady state comparison. Radial profiles of both temperature and concentration at $z = 0.8$, which is approximately the position of the initial steady state temperature peak, are shown at various times during the response in figure 5.6. The centre-line temperature predicted by the parabolic profile from the one dimensional model is lower than that predicted by the two dimensional model in each case. The general forms of the two profiles are, nevertheless, similar. There is, of course, no similarity in the radial concentration profiles predicted by the two models since no allowance for a radially varying concentration is made in the one dimensional model, although the mean values are in close agreement throughout the response.

Axial profiles of radial mean temperature predicted by both models in response to a step increase in inlet temperature are shown in figure 5.7. Again, the agreement between the two models is very good. The slightly faster formation of the new hot spot predicted by the one dimensional model is due to the fact that it tends to underestimate the rate of increase of the centre-line temperature. As this new temperature peak forms, the two dimensional model shows that most of the change first occurs at the hotter regions near the centre of the tube and so the radial mean temperature does not increase quite as fast as the one dimensional model suggests. Nevertheless, the extent of the discrepancy between the mean profiles predicted by both models is very small and is never more than one per cent.

The agreement between the two models when ramp changes in inlet temperature and step and ramp changes in concentration occur has been found to be as good as that for the very severe perturbations shown here. This suggests that the one dimensional model is eminently suitable for carrying out an extensive study of the reactor dynamics. Such circumstances are indeed fortunate since the use of the two dimensional model would be out of the question because of its large computational demands.

5.3 The Effect of the Tube Wall

5.3.1 Formulation and Solution of the Equations

The transient response of the reactor appears to be mainly determined by the transfer of heat at finite rates between the

stationary thermal capacitances; that is to say, between the fluid and the catalyst pellets. In the previous studies the coolant has been assumed to be at a constant temperature which is unaffected by the transfer of heat from the tubeside fluid. Even when this is the case, the tube wall which has a finite thermal capacitance is interposed between the coolant and the tubeside fluid and so its effect, if any, on the dynamic behaviour of the reactor needs to be examined. Having established the suitability of the one dimensional dynamic model for describing the unsteady state behaviour of the reactor, it may, therefore, be used at least for a qualitative study of this effect.

Assuming that there is no conduction of heat in the tube wall and that the coolant is at a constant temperature along its outside, at each point along the reactor a heat balance on the tube wall gives:

(a) in the steady state:

$$h_f(T'\big|_{y = R_1} - T'_w) = h_c(T'_w - T'_c) \qquad (5.3)$$

where the wall to coolant heat transfer coefficient, h_c, is based on the inside area of the tube.

and

(b) in the unsteady state:

$$\rho_w c_{pw}(R_2^2 - R_1^2)/2R_1 \frac{dT'_w}{d\tau} = h_f(T'\big|_{y = R_1} - T'_w) + h_c(T'_c - T'_w) \qquad (5.4)$$

with the initial condition $T'_w = T'_{w0}$ at $\tau = 0$.

If in the reactor model (Appendix (2)) T_c is replaced by T_w and the wall Nusselt number is defined in terms of the fluid to wall heat transfer coefficient, h_f, then $Nu_{wf} = R_1 h_f / K_f e$.

The effective wall Nusselt number is then defined by:

$$Nu^*_{wf}(T - T_w) = Nu_{wf}(T\big|_{r = 1} - T_c)$$

For a parabolic radial temperature profile in the reactor, Nu^*_{wf} is given[12] by:

$$Nu^*_{wf} = 4Nu_{wf}/(4 + Nu_{wf})$$

Rearranging equations (5.3) and (5.4) and expressing them in dimensionless form gives:

$$Nu_{wf}^{*}(T - T_w) = Nu_{wO}(T_w - T_c) \qquad (5.5)$$

and

$$K_w dT_w/d\tau = Nu_{wf}^{*}(T - T_w) + Nu_{wO}(T_c - T_w) \qquad (5.6)$$

with initial condition:

$$T_w = T_{wO} \quad \text{at} \quad \tau = 0$$

where

$$Nu_{wO} = R_1 h_c/K_f e \text{ and } K_w = \varrho_w c_{pw}(R_2^2 - R_1^2)/2K_f e$$

Both equations now contain the radial mean temperature of the reactor, T, which is used in the one dimensional model. Equation (5.5) which gives the temperature of the tube wall at each axial position in the steady state may be used to obtain the initial condition for equation (5.6). It should be noted, however, that the presence of the tube wall does not affect the steady state of the reactor.

In the unsteady state, equation (5.6) must be solved simultaneously with the reactor and pellet equations at each axial position. This may be conveniently accomplished using the Runge-Kutta-Merson Alogrithm used for the solution of the catalyst pellet equation. The method of solution of the whole set of equations is then very similar to that described in Appendix (2) for the reactor with no wall capacitance; each time the catalyst pellet equation is solved so is equation (5.6) to give T_w.

5.3.2 Discussion of the Results

In order to obtain an indication of the effect of the tube wall without extensive simulation of all types of response, only step changes in reactor inlet temperature have been simulated. As mentioned previously, this represents the most severe disturbance to which the reactor is likely to be subjected and in general most other perturbations can be expressed in terms of a series of step changes.

Any effect which the tube wall capacitance is likely to have on the transient response of the reactor will depend on both its value and the relative rates of heat transfer to and from it, that is on the material of the tube and its thickness and on the ratio of the inside and outside heat transfer coefficients. In general in industrial reactors the tubes are made from mild or stainless steel and their thickness is un-

likely to exceed approximately 0.4 cm. This value of tube thickness and the properties of stainless steel have been used in this study since these give an upper limit on the tube wall capacitance and therefore represent a worst case. Three values of the ratio of the inside and outside heat transfer coefficients have been used with a constant value of the overall coefficient between the tubeside fluid and the coolant so that the initial steady state of the reactor is the same in each case. These values of $h_f:h_c$ are 1:1, 1:4 and 1:10. In industrial reactors most control can be exercised over the value of the outside coefficient, h_c, and with highly exothermic reactions where the maximum amount of heat removal is necessary, it is usually arranged that h_c is much greater than h_f so that the ratio of 1:10 represents the realistic situation.[114] The data used for the simulations is given in Table 5.1.

Figures 5.8, 5.9 and 5.10 show axial profiles of radial mean temperature at three times during the response of the reactor to a step decrease in inlet temperature for each of the $h_f:h_c$ ratios. It can be seen that only when the wall to coolant heat transfer coefficient is less than ten times the value of the inside wall to fluid coefficient does the presence of the tube wall have any significant effect on the response of the reactor. Even at the $h_f:h_c$ ratio of 1:4 the effect is not great. As might be expected, the tube wall capacitance tends to slow down the response of the reactor. In the case of equal inside and outside heat transfer coefficients this causes the initial steady state temperature peak to increase and move out of the bed more slowly when a step decrease in the inlet temperature occurs. This is due to the slower cooling which occurs at the front of the bed, which, therefore, slows the increase in reactant concentration reaching the hot spot. The slower cooling of the front end of the bed occurs because the tube wall is able to heat up. As the $h_f:h_c$ ratio increases then the rate at which heat is removed from the tube wall to the coolant, relative to the rate at which it reaches the wall from the fluid, increases. Thus, at low values of the $h_f:h_c$ ratio, although heat is transferred to the wall at a greater rate it is removed at much slower rate and so this effect tends to slow the overall rate of cooling of the bed. Thus, when cooling is occurring within the bed it is heat transfer between

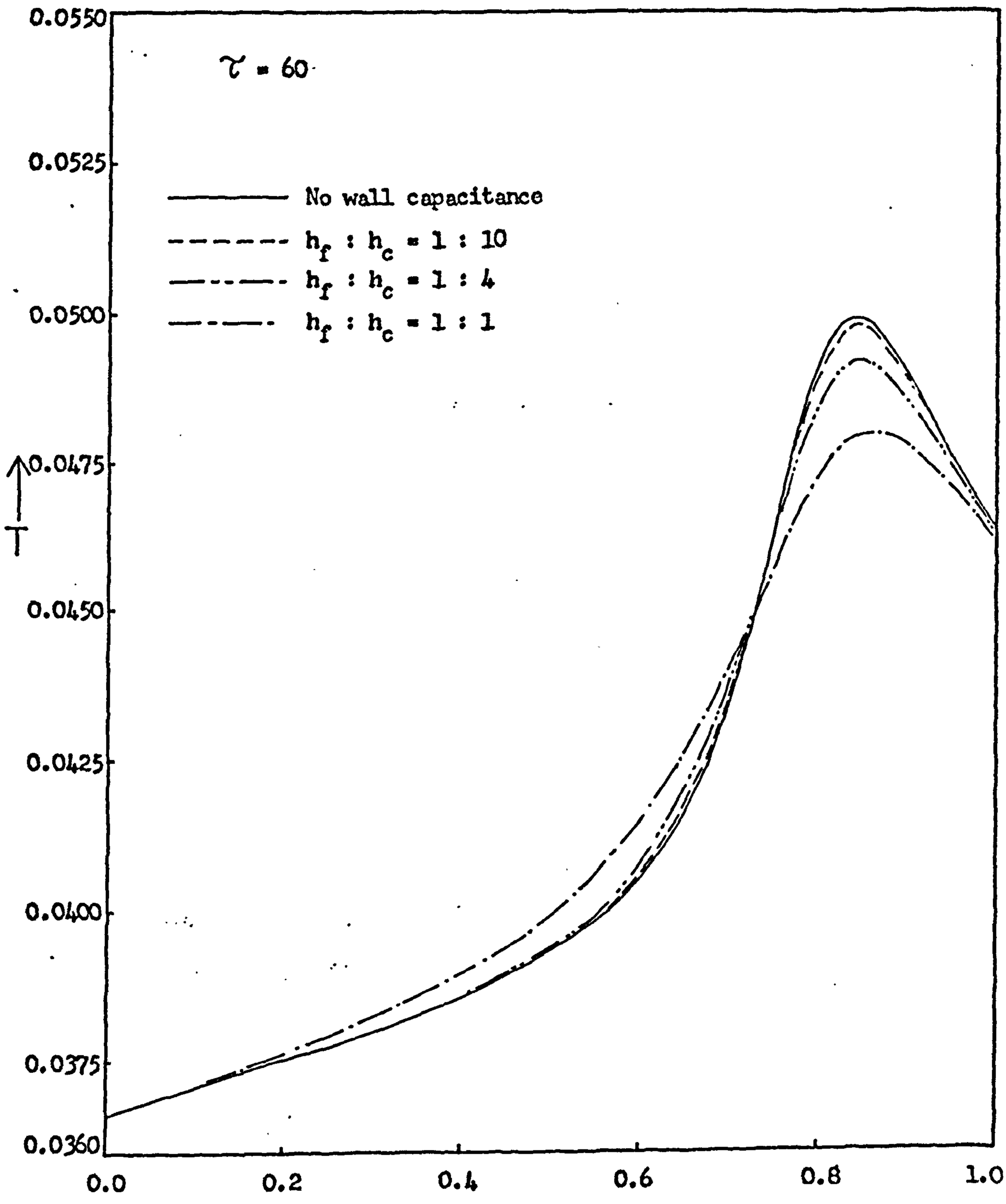

Figure 5.8 The effect of the ratio $h_f : h_c$ on the axial profiles of radial mean temperature 60 seconds after a step decrease of 0.00075 in the dimensionless inlet temperature. (Data as given in Table 5.1)

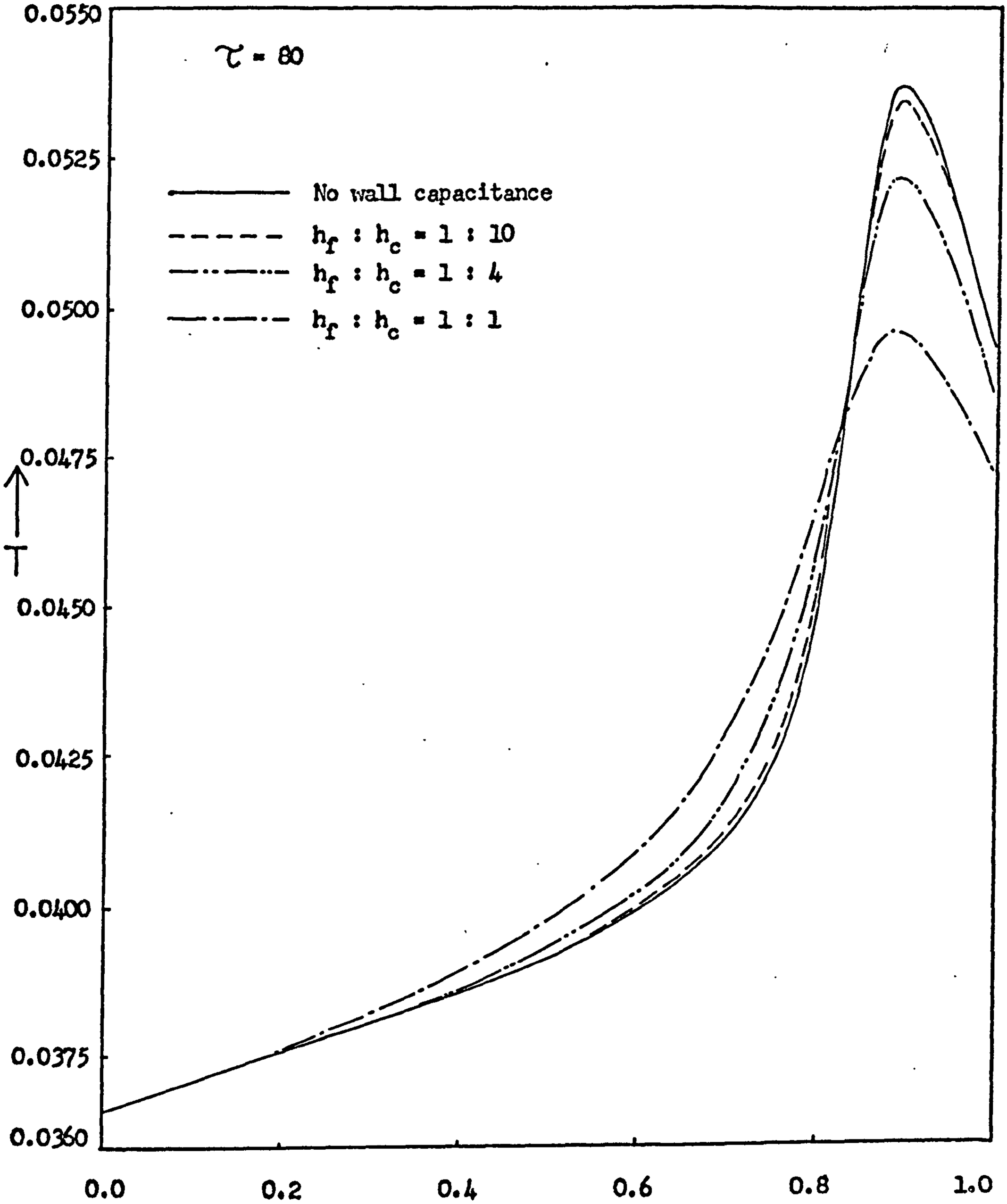

Figure 5.9 The effect of the ratio $h_f : h_c$ on the axial profiles of radial mean temperature 80 seconds after a step decrease of 0.00075 in the dimensionless inlet temperature. (Data as given in Table 5.1)

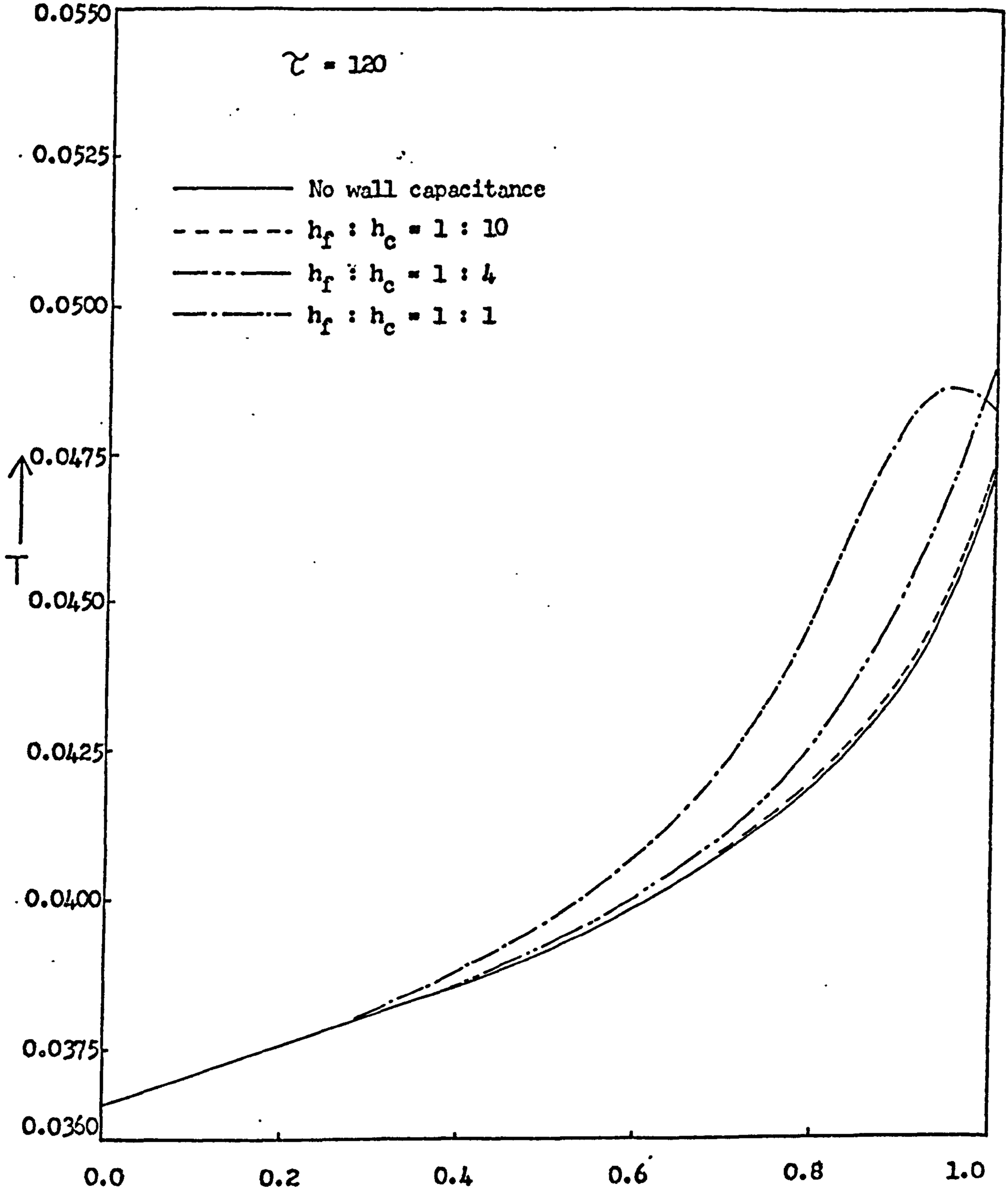

Figure 5.10 The effect of the ratio $h_f : h_c$ on the axial profiles of radial mean temperature 120 seconds after a step decrease of 0.00075 in the dimensionless inlet temperature. (Data as given in Table 5.1)

the wall and the coolant which is important; the higher this rate of heat transfer, then the less effect the tube wall has on the overall reactor response.

Figures 5.11, 5.12 and 5.13 show axial profiles of mean temperature at various times following a step increase in reactor inlet temperature for the three $h_f:h_c$ ratios. Again, the effect of the tube wall is only significant for $h_f:h_c <$ 1:10. At the front of the bed, heating occurs when the inlet temperature is increased and this is due both to the higher temperature of the gases entering the bed and the increase in the rate of reaction and, therefore, heat generation caused by this higher temperature. The effect of the tube wall is still to slow the response of the reactor and is again greatest at the lower values of $h_f:h_c$. In this case, however, it is due to the relative rates of heat transfer from the fluid to the tube wall. Heat is transferred from the fluid to the tube wall more easily at the lower values of $h_f:h_c$ and so the wall heats up more. However, this heating of the tube wall has less effect on the rate of heat generation within the reactor than that due to the higher temperatures caused by a lower rate of heat removal to the wall. Consequently, the rate of heating at the front of the bed is slower for the lower values of $h_f:h_c$. This, in turn, slows the decrease in concentration reaching the initial steady state temperature peak which, therefore, decays more slowly. The slower decay of this peak is also caused by a slower rate of heat removal to the coolant at the low $h_f:h_c$ ratios in the same way that slower cooling of the front of the bed occurs in response to a step decrease in inlet temperature.

In general, the higher the ratio of the inside to outside heat transfer coefficients the less the tube wall is heated and so it has less effect on the transient response of the reactor. For cases where the wall to coolant heat transfer coefficient is more than ten times greater than the inside fluid to wall value the effect of the tube wall on the dynamic behaviour is negligible. It should be noted that a similar conclusion was reached when the inside coefficient was held constant and the outside value increased, although these results, which are not shown here, are not strictly comparable since the initial and final steady states are necessarily different for each value of the outside coefficient.

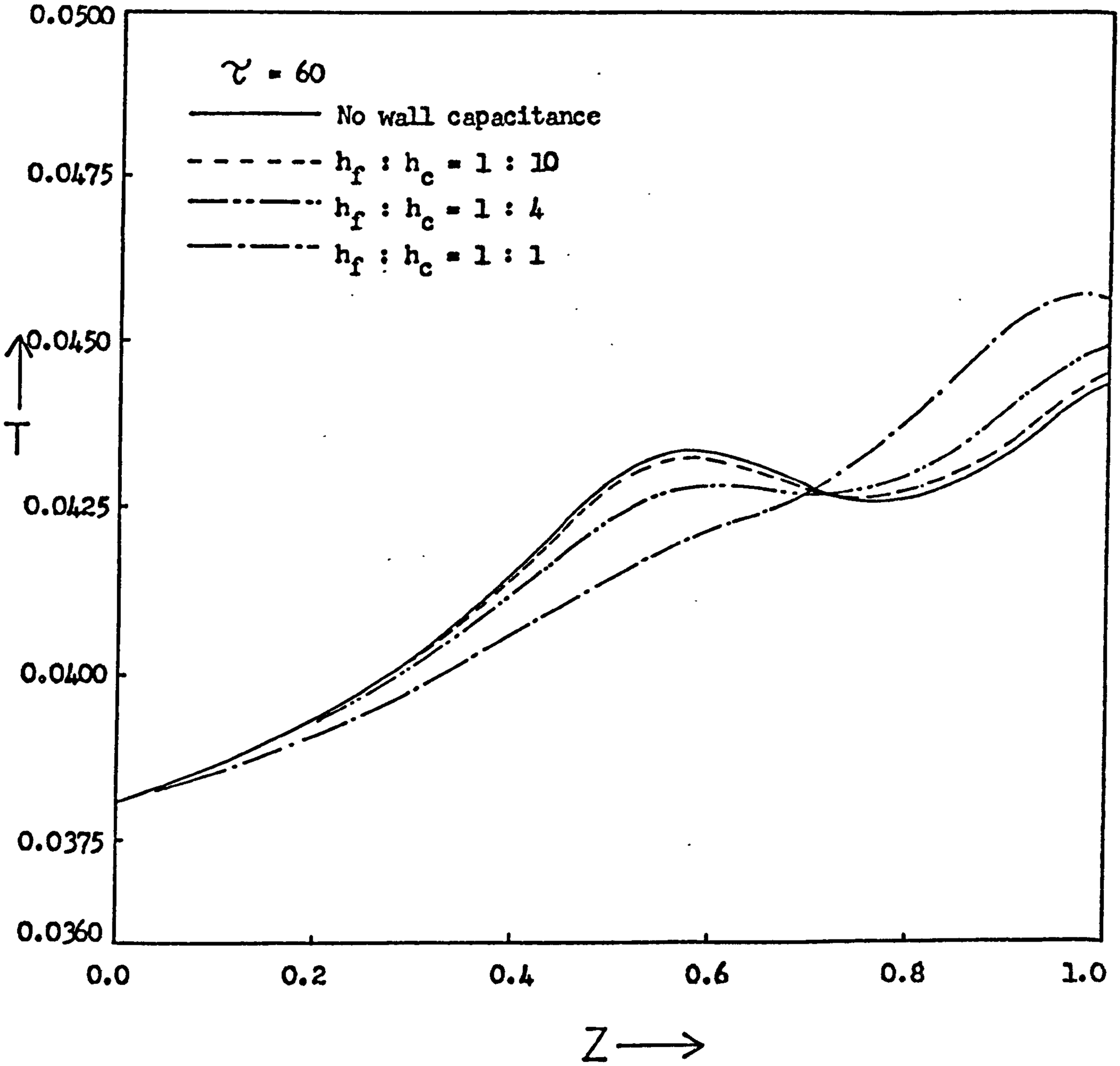

Figure 5.11 The effect of the ratio $h_f : h_c$ on the axial profiles of radial mean temperature 60 seconds after a step increase of 0.00075 in the dimensionless inlet temperature. (Data as given in Table 5.1)

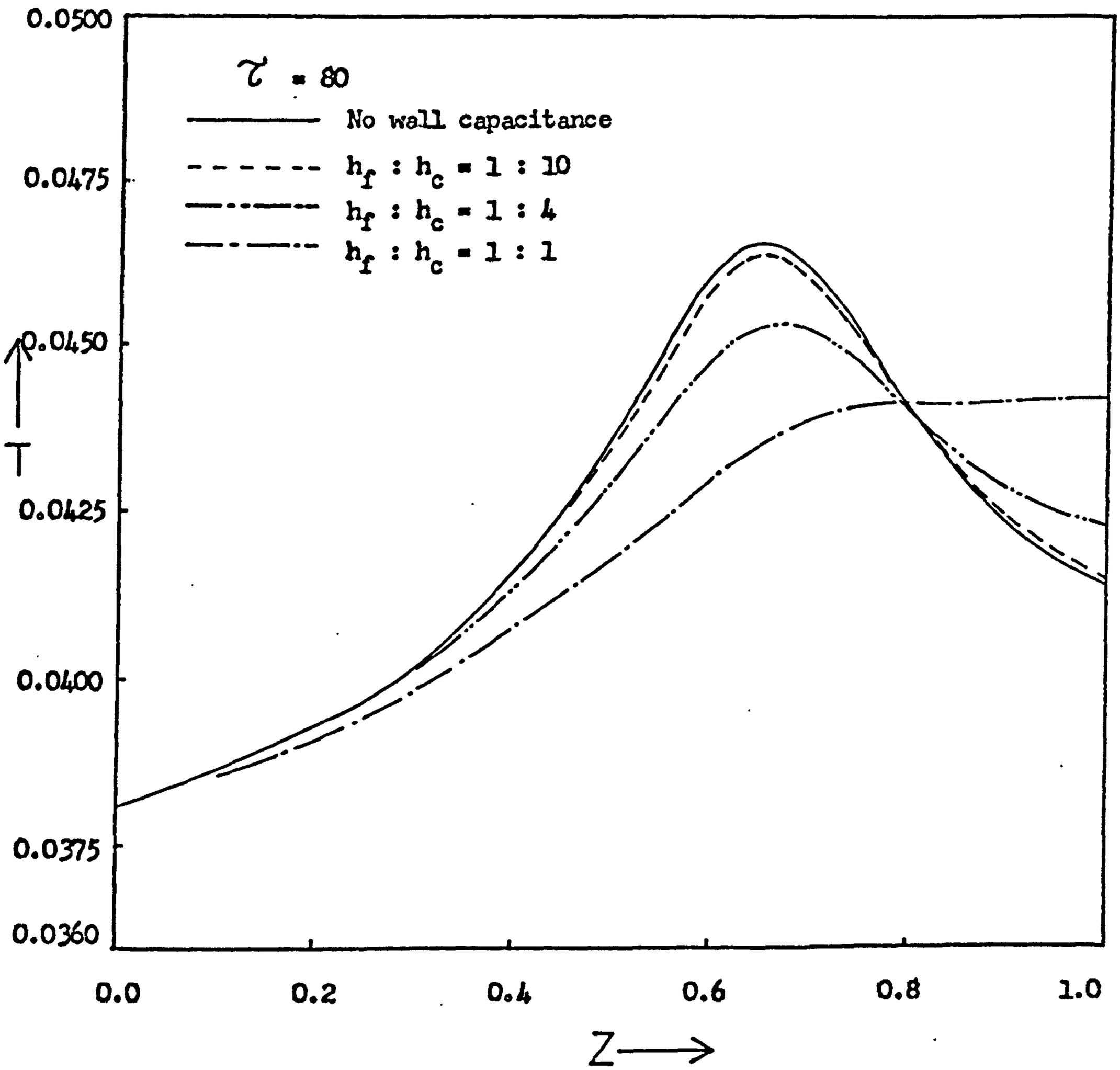

Figure 5.12 The effect of the ratio $h_f : h_c$ on the axial profiles of radial mean temperature 80 seconds after a step increase of 0.00075 in the dimensionless inlet temperature. (Data as given in Table 5.1)

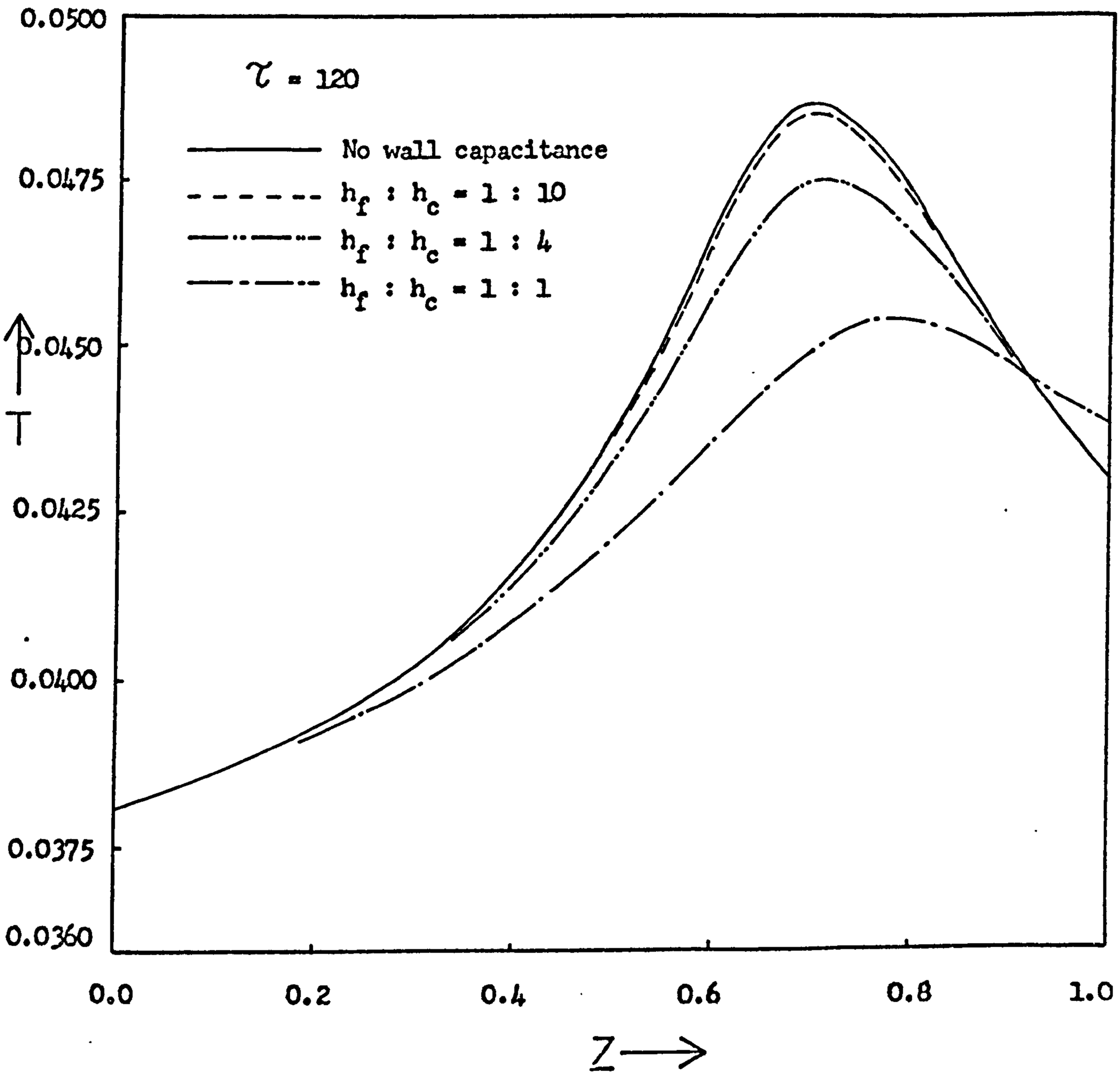

Figure 5.13 The effect of the ratio $h_f : h_c$ on the axial profiles of radial mean temperature 120 seconds after a step increase of 0.00075 in the dimensionless inlet temperature. (Data as given in Table 5.1)

Axial conduction within the tube wall is also justifiably neglected in the realistic case of a large outside wall to coolant heat transfer coefficient since little heating of the tube wall occurs and it remains essentially isothermal due to the high rate of heat removal to the coolant. Even at the lower values of this coefficient when heating of the wall does occur the results indicate that the radial heat flux towards the coolant would tend to be much larger than that possible axially within the tube wall so that the latter may be neglected in this case. This is largely due to the much smaller area for heat transfer associated with the axial flux and also because although heating of the wall above the coolant temperature does occur the gradients within it are not particularly large.

5.4 Concluding Remarks

A two dimensional dynamic model of the fixed bed reactor has been formulated and used to evaluate a simpler one dimensional model. It has been shown that with appropriate correction of the wall heat transfer coefficient the simple model gives an accurate qualitative description of the transient response of the reactor, although, as might be anticipated from the results of steady state studies,[12] it tends to predict somewhat flatter radial temperature profiles than are obtained from the two dimensional model. The axial profiles of the radial mean state variables are, however, in good agreement with those predicted by the two dimensional model throughout the transient response. Because it predicts flatter radial temperature profiles, the one dimensional model tends to underestimate the centre-line temperature in the reactor. This might, at first, be thought to be due to overestimation of the rate of heat removal through the tube wall. However, the temperature at the axis of the reactor, predicted by the one dimensional model, is rather insensitive to the value of the wall heat transfer coefficient and this suggests that the problem is mainly due to underestimation of the reaction rate at the higher temperatures. Since the reaction rate is a highly non-linear function of temperature the radial temperature profile becomes distorted near the centre of the tube at the higher temperature levels and, therefore, does not retain the parabolic form which is assumed for it in the one dimensional model. Turner[71] has developed a method for compensating for this distortion in the steady state by applying a radial correction to the reaction

rate expression in the one dimensional model. He has also shown that correction of the wall heat transfer coefficient without prior reference to the steady state solution of a two dimensional model is possible. The application of these methods to the unsteady state problem is currently under development[15] and it appears that it is possible to apply them successfully in this case also.

At present, however, the one dimensional model examined in this chapter appears suitable for an extensive study of the general pattern of the dynamic behaviour of the reactor since it can give good agreement both quantitatively and qualitatively with the more complex two dimensional model in terms of the mean values of the radial profiles. The two dimensional model is wholly unsuitable for this purpose because of its large computational load, whereas the one dimensional model requires approximately only one fifteenth of the computation time. The preferred approach is, therefore, to use the one dimensional model for a general study of reactor performance and then subsequently, if necessary, to investigate particular aspects of behaviour using the two dimensional model.

In order to establish whether a description of the reactor tube wall is necessary in a dynamic model of the reactor, its effect on the transient response has been studied using the one dimensional model. It has been found that the importance of the tube wall is determined by the relative magnitudes of the heat transfer coefficients on its inside and outside. Specifically, if the outside, coolant to wall, heat transfer coefficient is an order of magnitude, or more, greater than the inside, wall to fluid, value, then the effect of the tube wall capacitance on the system is negligible. In industrial fixed bed reactors supporting highly exothermic reactions where the outside heat transfer coefficient is commonly ten to twenty times greater than the inside value,[114] the tube wall does not represent a significant dynamic element in the system and, therefore, need not be included in the reactor model.

CHAPTER 6

THE RESPONSE OF THE REACTOR TO SINUSOIDAL PERTURBATION OF THE INLET CONDITIONS

6.1 Introduction

Temperature and concentration disturbances propagate through fixed bed catalytic reactors in a wavelike manner. Whilst a knowledge of the interactions between such travelling waves is essential to the design of an adequate control system for the reactor, there appears to have been only limited investigation of such phenomena.

Foss and his co-workers have studied the effect of sinusoidal perturbations of the inlet concentration and temperature on both a homogeneous liquid system[115] and a heterogeneous gaseous system.[64,116] In the liquid system the reactor tube was packed with inert glass spheres which acted merely as a heat sink causing a time delay. In the gaseous reactors, attention was confined to the development of a suitable linearised model of the system and study of the quasi-stationary state. Denis and Kabel[51, 128] have investigated the propagation of both saw-tooth and square waves in an heterogeneous reactor where the rate of adsorption of the reactant on to the catalyst surface is assumed to be the significant dynamic effect. Hansen[129] has considered oscillatory inlet conditions on an adiabatic fixed bed reactor. However, he too has mainly confined his attention to the applicability of the model and the quasi-stationary state behaviour. None of these workers appear to have considered the problems of stability which may occur as a consequence of oscillatory inlet conditions of such reactors.

McGreavy and Thornton[83] have studied the response of a single catalyst particle to oscillations in both the temperature and concentration of the fluid surrounding it. They showed that it was possible for a particle to pass transiently into a region which, in the steady state, would correspond to temperature runaway, and then return to the initial steady state. McGreavy and Soliman[85] have recently given a criterion which relates the permissible amplitude and frequency of the oscillations which will cause a catalyst pellet to behave in this way.

Both of these studies, however, concerned single catalyst pellets in the region of multiple solutions. A brief examination of the response of a whole bed to oscillating inlet conditions, with reference to stability, has been reported by McGreavy and Adderley.[113] They were able to draw only general conclusions from the results, however, because the initial state from which the reactor was perturbed exhibited temperature runaway.

This chapter concerns the extension of the single pellet studies to the investigation of the behaviour of a fixed bed reactor undergoing sinusoidal perturbations of the inlet temperature and concentration. The high non-linearity of the system makes conventional frequency response analysis inappropriate.

The reaction scheme considered is the simple, irreversible, first order A⟶B reaction with Arrhenius kinetics. The reactor model used is one dimensional, with an assumed parabolic temperature profile, as described in Appendix (2). This is coupled with the isothermal catalyst pellet model given in Appendix (1). For the reasons given in chapter 5 the mass and heat capacitances of the fluid and the heat capacitance of the tube wall are neglected in the reactor model, and in the catalyst pellet model, only the heat capacitance of the pellet is considered. The data used for the simulations is given in Table 5.1.

Since temperature runaway may occur as a consequence of either parametric sensitivity or multiple solutions, two initial steady states have been considered. One of these lies entirely in the region of unique solutions with the inlet conditions adjusted so that temperature runaway occurs solely as a consequence of parametric sensitivity, and the other has been chosen so that it lies entirely in the region of multiple solutions.

The form of the inlet perturbations applied to the reactor is:

$$f_i(\tau) = f_{0i} + A \sin(2\pi\omega\tau)$$

where:

$f_i(\tau)$ = value of inlet variable at time τ

f_{0i} = value of inlet variable at time zero

A = Amplitude of the oscillation

ω = frequency of the oscillation

The sign of A can have a profound effect on the response of the reactor since it determines the initial direction of the perturbation. For this reason, both positive and negative sinusoidal oscillations have been studied.

The response of the reactor to sinusoidal inlet conditions has been divided into two distinct stages; the initial transient, which occurs as the first cycle of the perturbation passes through the bed, and the quasi-stationary state which occurs after the initial transient has died away and in which the reactor merely oscillates about a fixed mean. The length of the initial transient is determined by the heat capacitance of the pellets since this regulates the speed of the temperature waves through the bed.

Because of the complex nature of the phenomena which occur during sinusoidal perturbations of the inlet variables, some typical responses have been described in detail to illustrate the important, general features of the behaviour.

6.2 Temperature Forcing

6.2.1 The Unique Region

Figure 6.1a shows the axial profiles of radial mean temperature of the initial steady state and also of the steady state which would occur at the maximum and minimum values of a sinusoidal inlet temperature oscillation of amplitude 0.00056. (This represents approximately 7.5 K for the activation energy given in Table 5.1). The phase trajectories of these three states are shown in figure 6.1b. All three lie entirely in the region of unique solutions and in the steady state at the maximum of the oscillation temperature runaway occurs, the reactor trajectory crossing the runaway line on the phase diagram.

At the amplitude of 0.00056 the initial transient gives rise to temperature runaway for all frequencies below approximately 0.125 Hz. Only at frequencies below approximately 0.0345 Hz is this temperature runaway condition maintained in the quasi-stationary state; at frequencies above this value the safe low temperature region is regained by the bed and the quasi-stationary state is confined there, the reactor trajectories of the quasi-stationary state remaining entirely below the

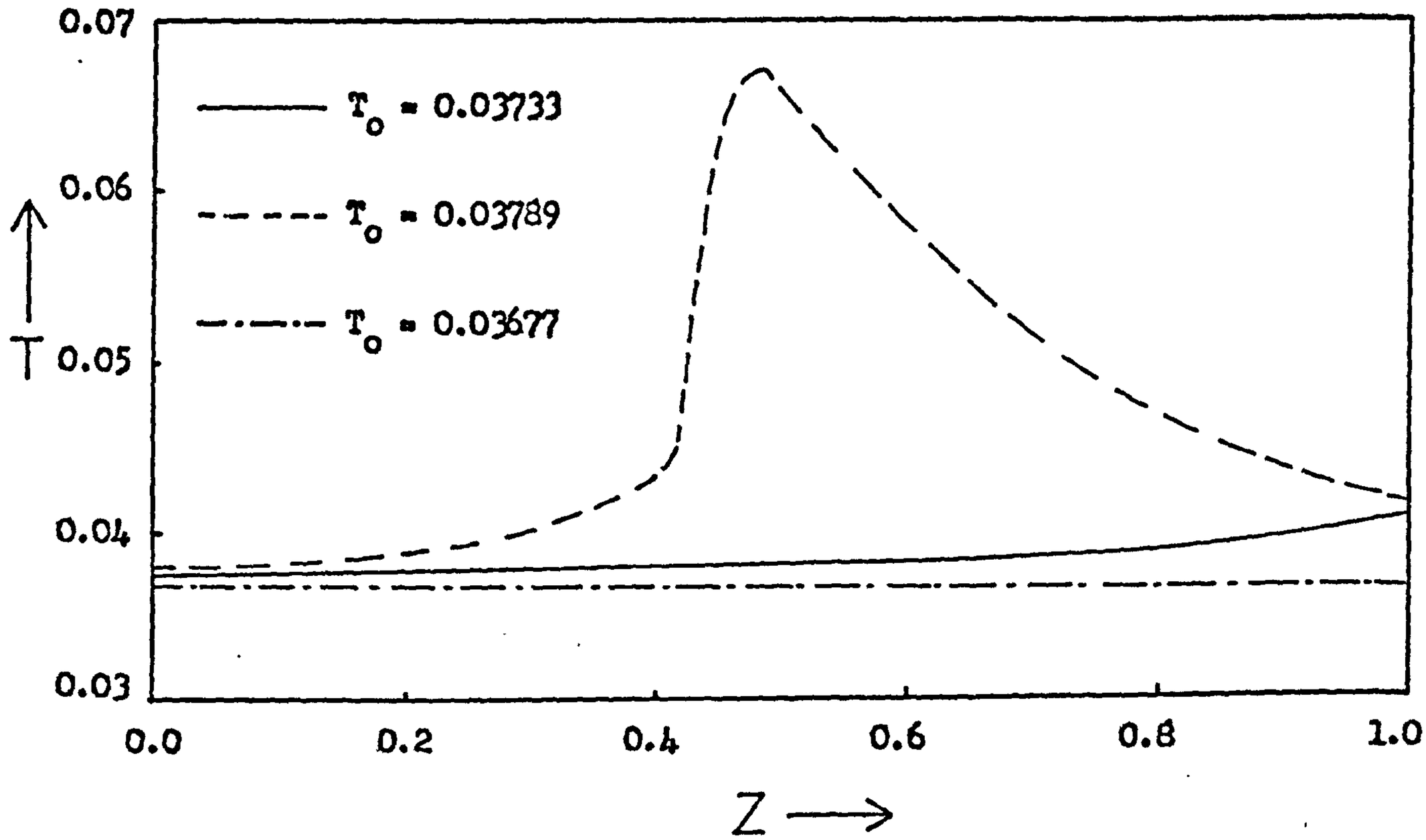

Figure 6.1(a) Steady state axial profiles of radial mean temperature at the mean, maximum and minimum values of a sinusoidal perturbation of dimensionless inlet temperature of amplitude 0.00056. (Data as given in Table 5.1)

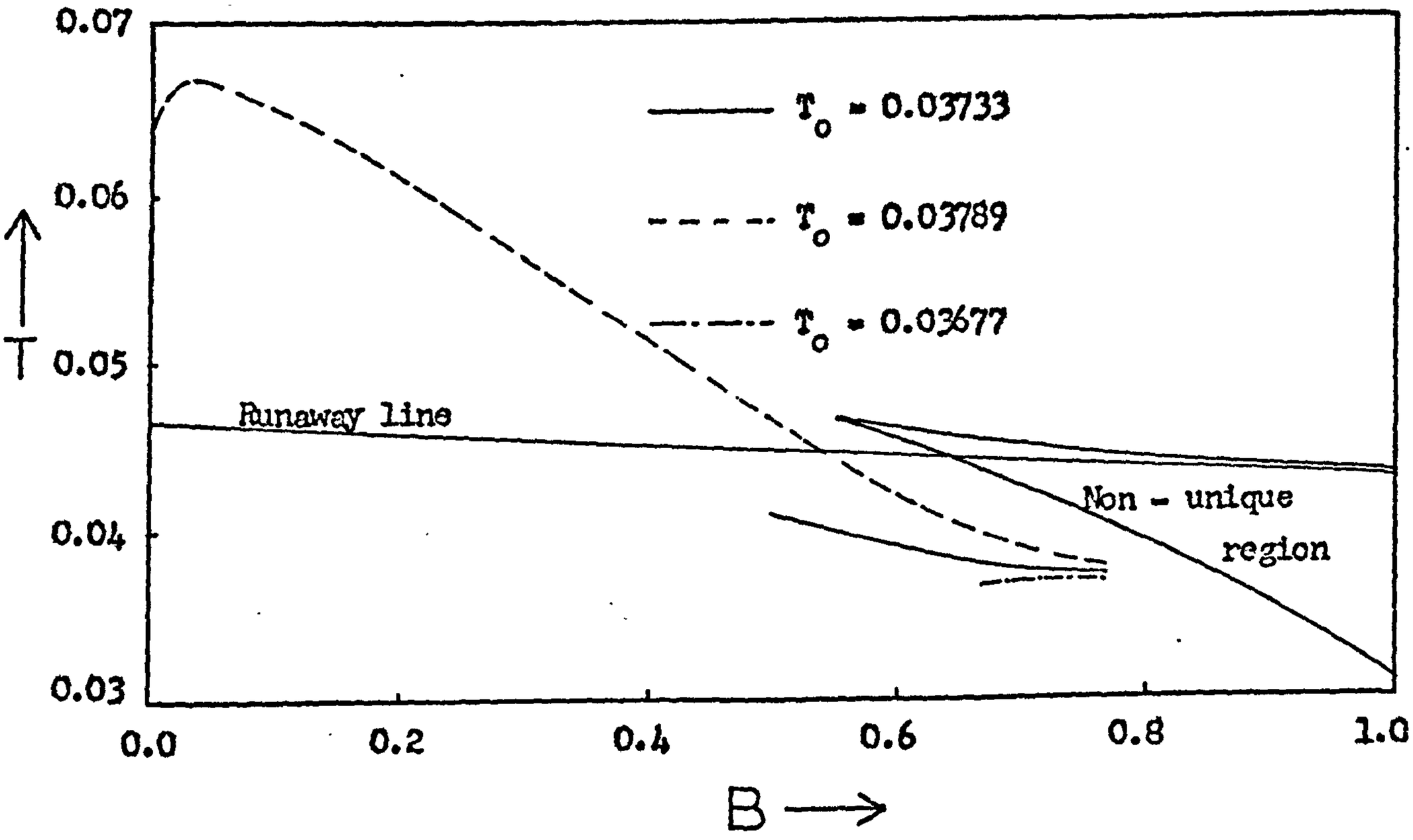

Figure 6.1(b) Steady state reactor trajectories at the mean, maximum and minimum values of a sinusoidal perturbation of dimensionless inlet temperature of amplitude 0.00056. (Data as given in Table 5.1)

runaway line on the phase diagram.

At the same amplitude but with a negative sine wave, the behaviour is somewhat different. At no frequency does the bed pass transiently into the region of temperature runaway. Below a frequency of approximately 0.0345 Hz temperature runaway occurs in the initial transient and is maintained in the quasi-stationary state, however, above this frequency temperature runaway does not occur at all.

Increasing the amplitude of the inlet temperature oscillation causes these "threshold" frequencies to increase. For example, with an inlet temperature amplitude of +0.00112 temperature runaway does not occur above a frequency of approximately 0.2 Hz, and below 0.067 Hz temperature runaway is maintained in the quasi-stationary state. Conversely, decreasing the amplitude of the inlet temperature oscillation brings about a decrease in the value of these frequencies until the amplitude of the oscillation is such that temperature runaway does not occur at all. This happens when the steady state which would occur at the maximum of the inlet oscillation does not exhibit temperature runaway.

In order to understand this behaviour the initial transient response of the reactor must be examined in detail. This has been accomplished by studying axial profiles of the magnitudes of deviations of the concentration and temperature from the initial steady state. These deviations are defined by:

$M_f = (f(\tau) - f_0)/f_0$ where:

$f(\tau)$ = value of concentration or temperature at point z and time τ.

f_0 = value of concentration or temperature at point z and time zero.

Thus the initial steady state of the reactor is represented by the abscissa ($M_f = 0$) when axial profiles of M_f are plotted.

6.2.1(a) Positive Sine Waves

Consider first the inlet temperature amplitude of 0.00056 at a frequency of 0.04 Hz. Since the sine wave is positive, the inlet temperature initially rises and at this frequency temperature runaway occurs before the bed settles down to a quasi-stationary state entirely in the low temperature region

(below the runaway line on the phase diagram). This is illustrated by the axial profiles of radial mean temperature shown in figures 6.2 and 6.3. A runaway temperature peak is at first induced near the exit of the bed (figure 6.2) which settles down to a quasi-stationary state in the low temperature region (figure 6.3) when this peak has passed out of the bed. Figure 6.4 shows axial profiles of the magnitudes of the deviations, of the radial mean concentration and temperature, from the initial steady state at various times during the initial transient. The quasi-stationary state profiles of these deviations are shown in figure 6.5.

The effect of the initial cycle of the inlet temperature is shown in figures 6.4a to 6.4e. The initially rising inlet temperature causes the temperature in the latter half of the bed to fall, at first, below the steady state value. This is the so-called "wrong-way" transient which has been observed both experimentally and theoretically by several workers during step changes in the inlet temperature (e.g. references 64 and 12). The increased inlet temperature causes a higher rate of reaction near the entrance to the bed which causes greater consumption of the reactant in this region. Consequently, less reactant is available further down the bed and so the rate of heat generation there falls off. Figures 6.4a and 6.4b clearly show that the decrease in reactant concentration throughout the bed is felt immediately whereas the temperature in most of the bed does not change for some time. This is due to the thermal capacitance of the catalyst pellets. In the absence of appreciable reactant adsorption at the catalyst surface, as is the case here, the mass capacitance of the pellets is negligible and so the concentration wave tends to travel at the velocity of the fluid which is, of course, much greater than the velocity of the temperature wave.

After one cycle of the inlet temperature, the initial temperature crest has advanced into the bed followed by a trough. Due to this temperature trough the reaction rate falls off at the bed entrance and so induces a concentration crest. Thus, for a while, increased concentration is reaching the leading temperature crest and so more reaction takes place there preventing the attenuation of this crest which would occur due to the heat removal processes (figures 6.4d and 6.4e). The rapidly

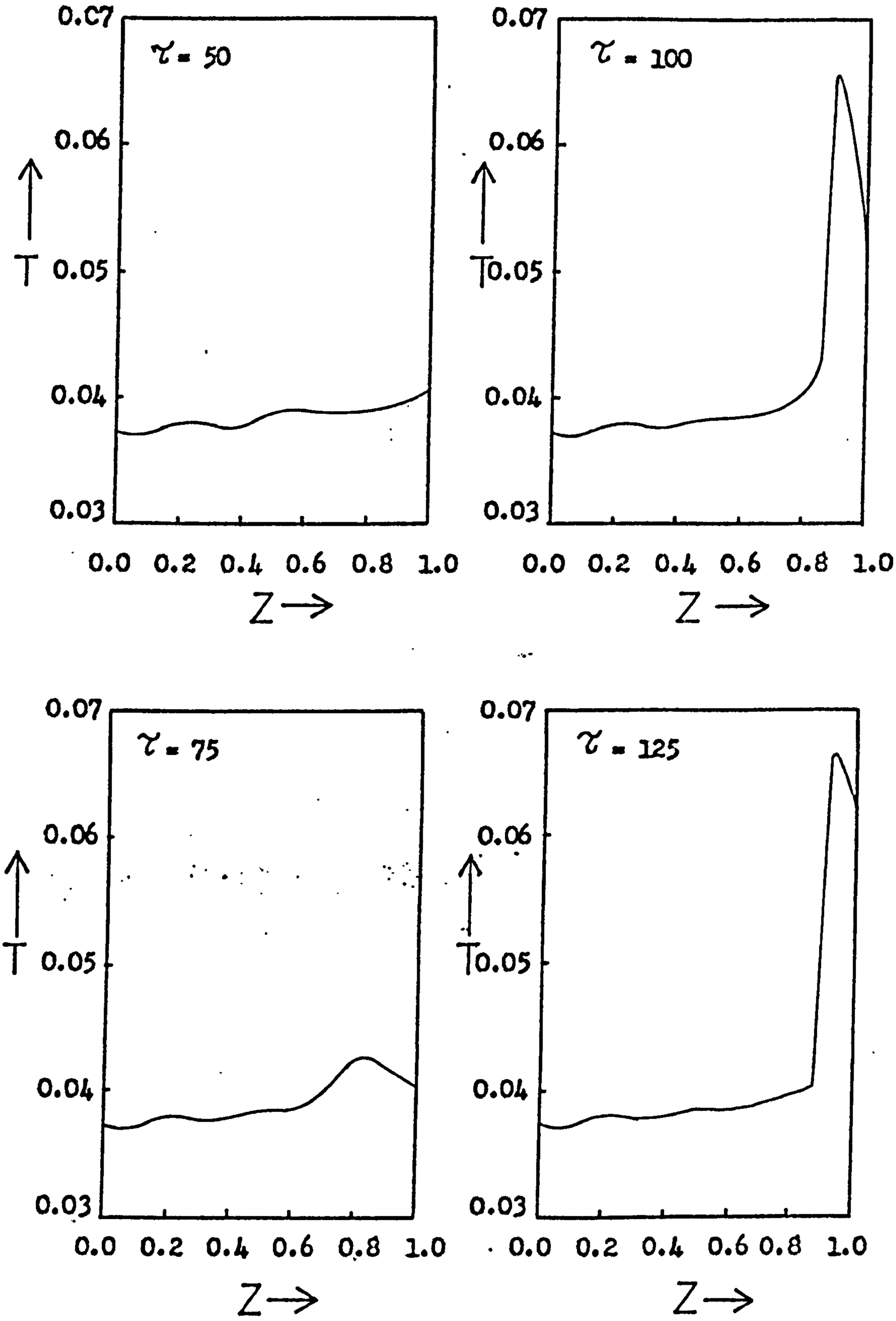

Figure 6.2 Axial profiles of radial mean temperature during the initial response of the reactor to a dimensionless inlet temperature perturbation of the form : $T_o = 0.03733 + 0.00056\ \mathrm{Sin}(2\pi \times 0.04 \times \tau)$. (Data as given in Table 5.1)

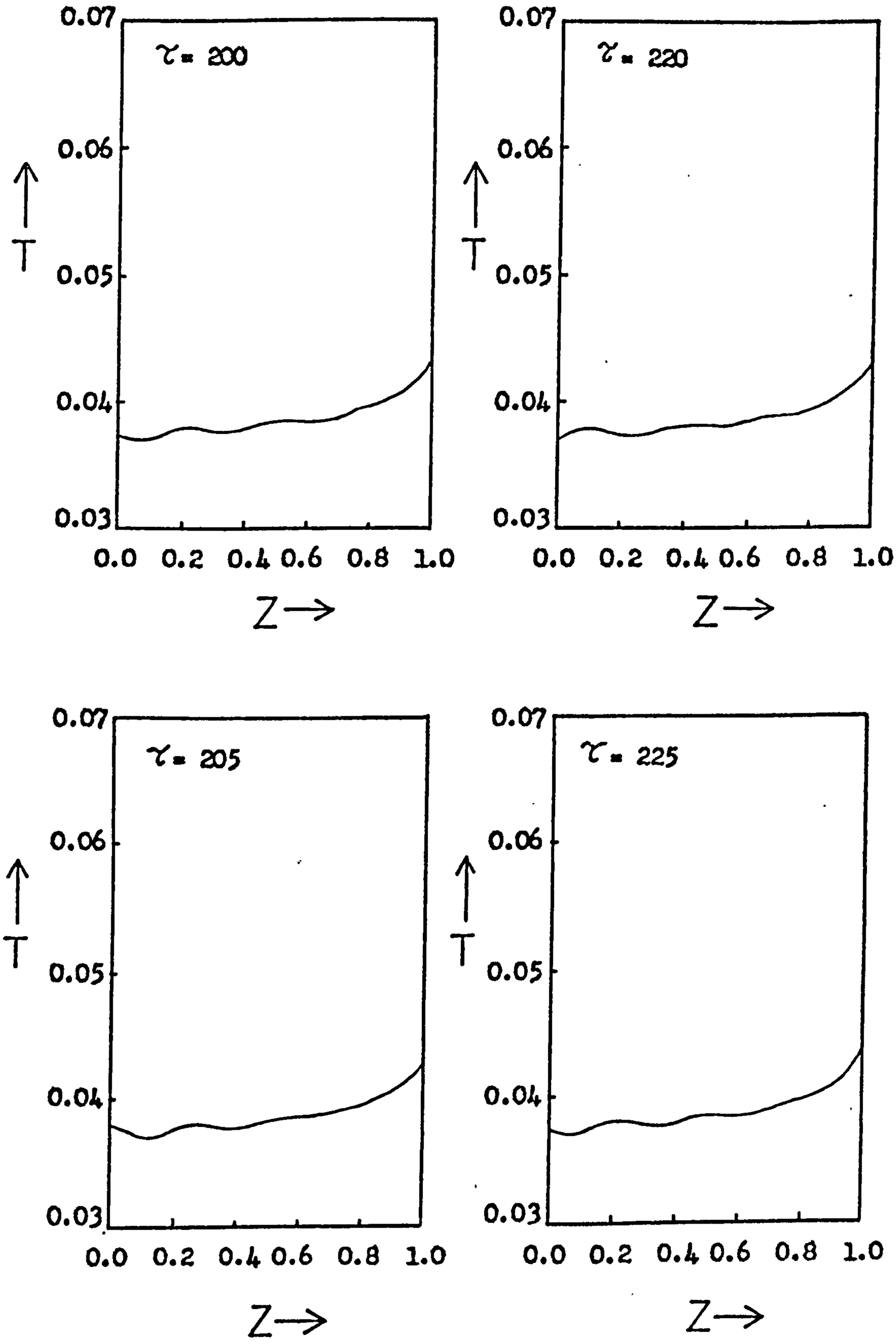

Figure 6.3 Axial profiles of radial mean temperature during the quasi - stationary state due to a dimensionless inlet perturbation of the form : $T_o = 0.03733 + 0.00056\ \mathrm{Sin}(2\pi \times 0.04 \times \tau)$. (Data as given in Table 5.1)

Text cut off in original

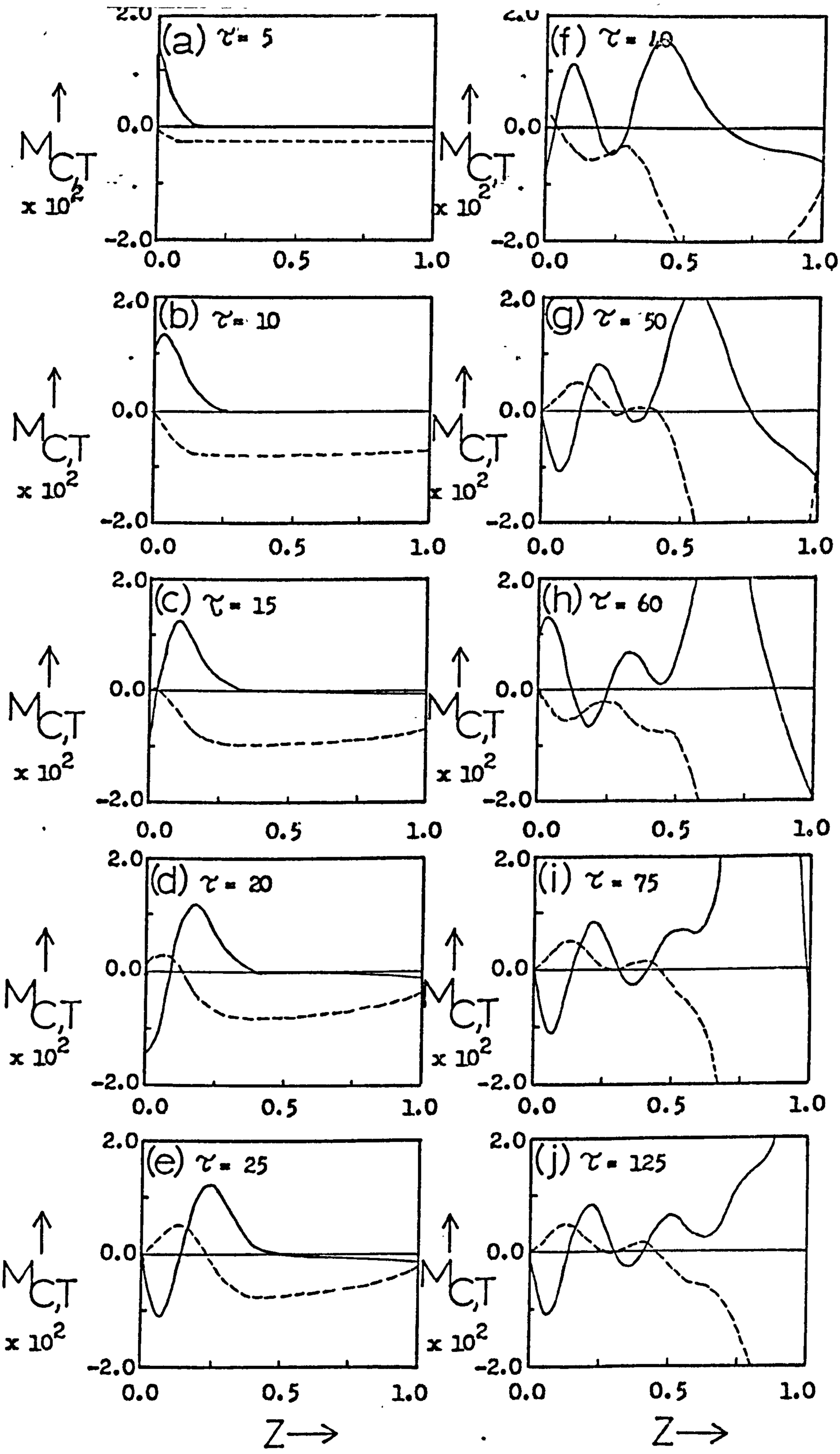

Figure 6.4 Axial profiles of magnitudes of deviations of the radial mean concentration (broken line) and temperature (solid line) from the initial steady state during the response of the reactor to a dimensionless inlet temperature perturbation of the form : $T_o = 0.03733 + 0.00056\ \mathrm{Sin}(2\pi \times 0.04 \times \tau)$. (Data as given in Table 5.1)

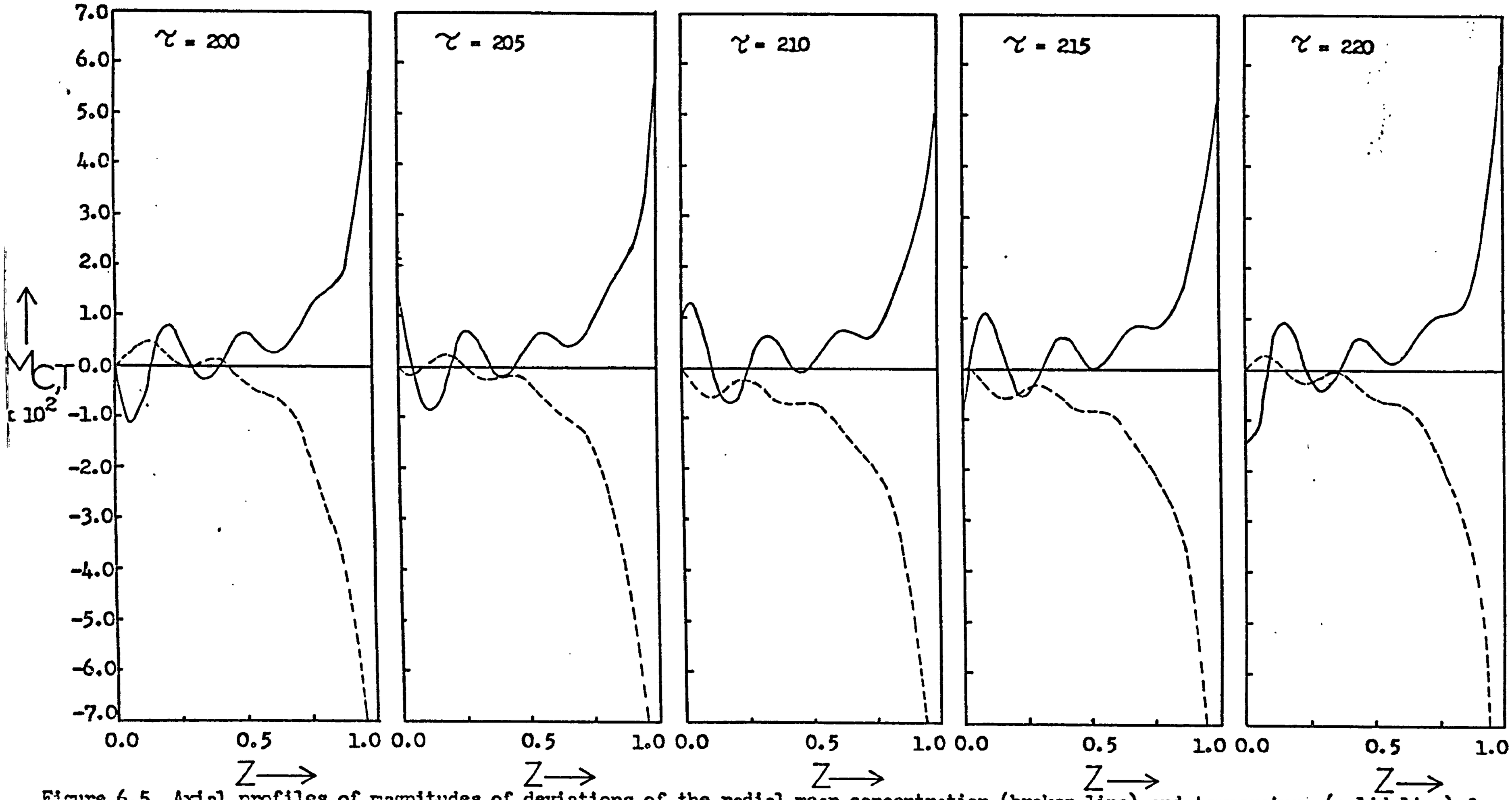

Figure 6.5 Axial profiles of magnitudes of deviations of the radial mean concentration (broken line) and temperature (solid line) from the initial steady state during the quasi - stationary state due to a dimensionless inlet temperature perturbation of the form : $T_o = 0.03733 + 0.00056\ \mathrm{Sin}(2\pi \times 0.04 \times \tau)$. (Data as given in Table 5.1)

moving fluid carries material of lower reactant concentration through the slowly advancing temperature crest into the regions in front of it. It does not, however, carry heat with it because of its very low thermal capacity. Thus, in front of the temperature wave, the concentration and, therefore, the rate of heat generation falls off lowering the temperature there even further.

During the second cycle of the inlet temperature, the magnitude of the deviation from the steady state of the leading temperature crest is increased whilst that of the subsequent crest decreases. These two effects are related. The second temperature trough induces an increase in concentration throughout the bed which might be expected to amplify both temperature crests in the bed. This does not happen, however, because of the effect of the thermal capacitance of the catalyst pellets. The induced wave of increased concentration passes through the second temperature crest before its reaction rate begins to change. By this time a third temperature crest has entered the bed (figure 6.4h) inducing a concentration decrease which attenuates the second crest. The higher temperature of the leading crest is met by an increase in concentration of reactant which causes even more heat generation. Amplification of the leading, but not of subsequent temperature crests, occurs because when the leading temperature crest passes down the first half of the bed it is heating the pellets from their steady state temperature whereas when subsequent temperature crests move along this region they are heating pellets from below the steady state temperature because of the passage of temperature troughs into the bed. Since the reaction rate, and therefore the heat generation rate, increase non-linearly with temperature the leading temperature crest, therefore, reaches much higher temperatures than subsequent ones. The heat capacitance of the pellets prevents them cooling quickly and so prevents the reaction rate changing rapidly. This effect is more damaging at high temperatures since it causes the catalyst pellets to remain hot during an induced decrease in concentration so that rapid reaction ensues when the concentration increases again.

Temperature runaway is, therefore, prevented from occurring in the quasi-stationary state because of the relative velocities

of the temperature and concentration waves. This is such that temperature crests are unable to interact constructively with the concentration crests at any point in the bed. The thermal capacitance of the catalyst pellets slows down the temperature waves so that, at any point in the bed, before a pellet is heated to a temperature high enough to cause runaway, it is met by a decrease in concentration which faces the temperature in the other direction. In other words, the frequency of the inlet temperature oscillation prevents any point in the bed remaining at a high temperature and concentration sufficiently long enough to cause runaway to develop. The quasi-stationary state is discussed further in section 6.2.3 of this chapter.

Decreasing the frequency to, say, 0.02 Hz at the inlet temperature amplitude of 0.00056 gives rise to an initial transient qualitatively similar to that described above. The important differences are, however, that the magnitudes of the deviations from the initial steady state are greater, and also that the temperature runaway occurring near the exit of the bed during the initial transient persists in the quasi-stationary state (figures 6.6a to 6.6j). The leading temperature crest develops runaway for reasons similar to those described above for a higher frequency. At this low inlet temperature frequency, the induced concentration increases exist long enough to allow sufficient heat generation to take place to heat the catalyst particles to higher temperatures. The thermal capacitance of the pellets then prevents them from cooling very much when the concentration falls and so they remain hot enough to cause rapid reaction when the concentration rises again. For this reason the temperature near the end of the bed is unable to fall below the runaway region, as is the case at the higher frequencies, and so the quasi-stationary state exhibits temperature runaway.

When the frequency is increased above 0.125 Hz with an inlet temperature amplitude of 0.00056 temperature runaway occurs neither during the initial transient response nor in the quasi-stationary state. In the light of the previous comments, the reason for this is quite clear. The leading temperature crest, and also the subsequent ones, is prevented from rising to a high temperature and approaching the parametrically

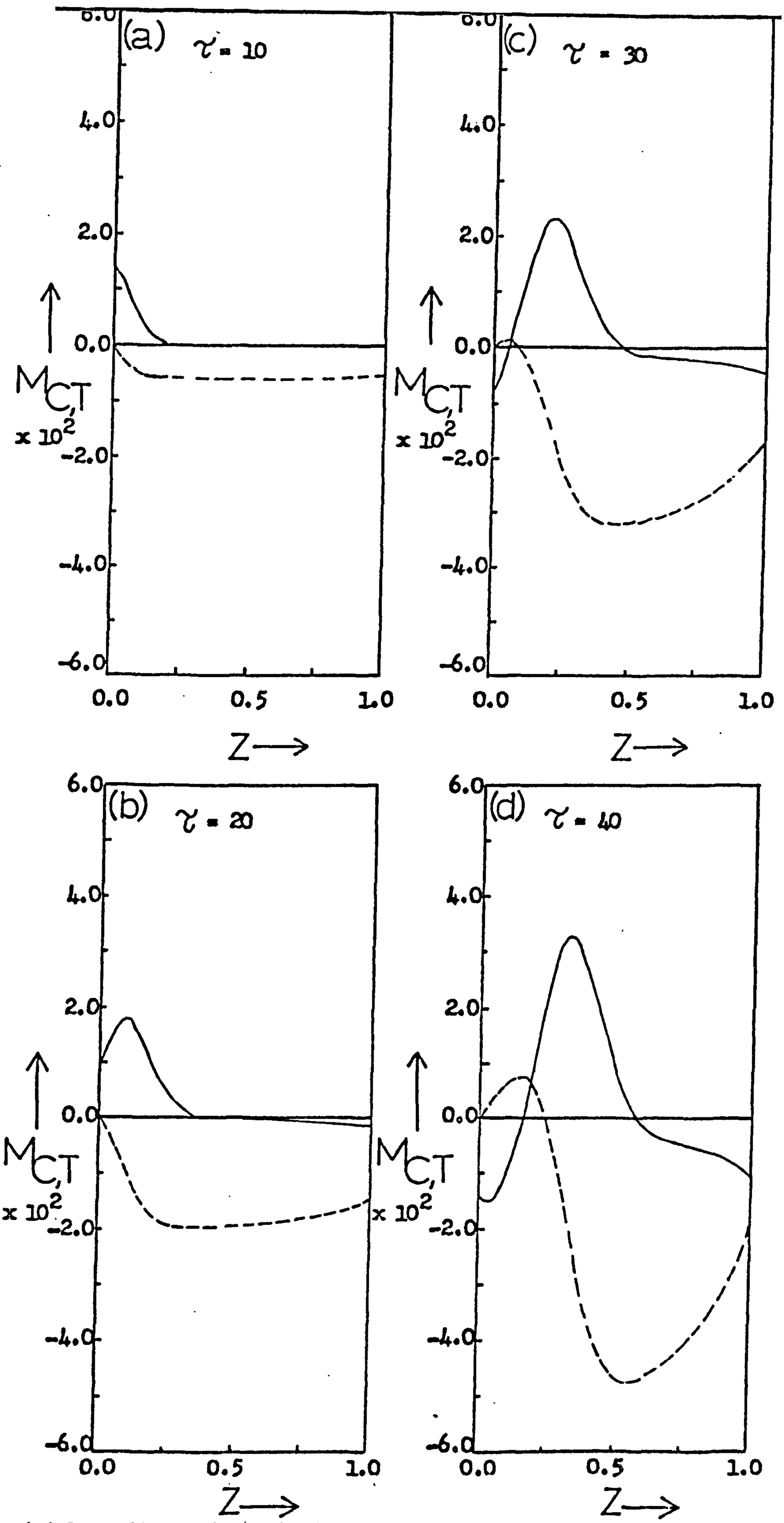

Figure 6.6 Axial profiles of magnitudes of deviations of the radial mean concentration (broken line) and temperature (solid line) from the initial steady state during the response of the reactor to a dimensionless inlet temperature perturbation of the form : $T_0 = 0.03733 + 0.00056 \sin(2\pi \times 0.02 \times \tau)$. (Data as given in Table 5.1)

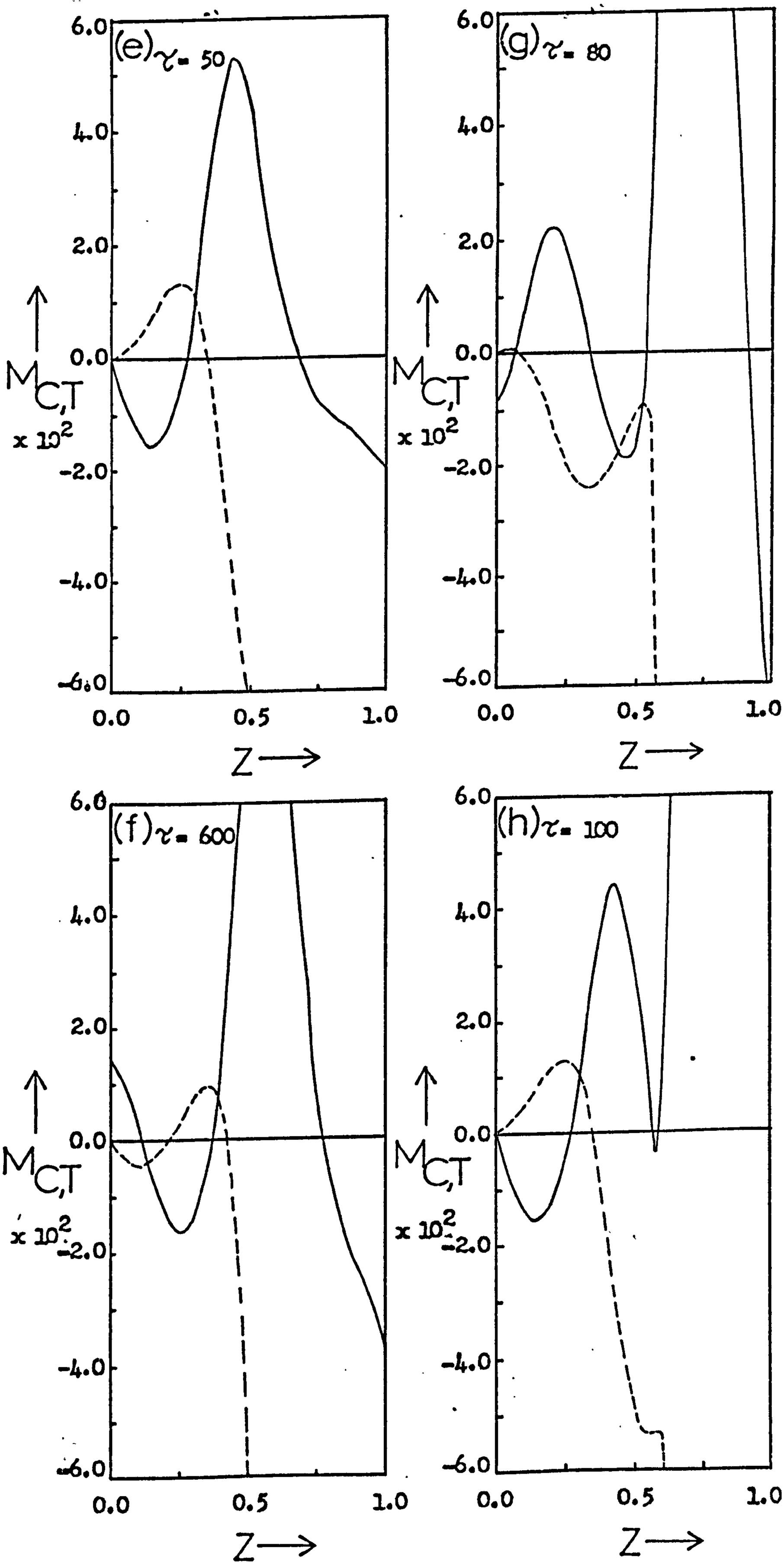

Figure 6.6 (Continued)

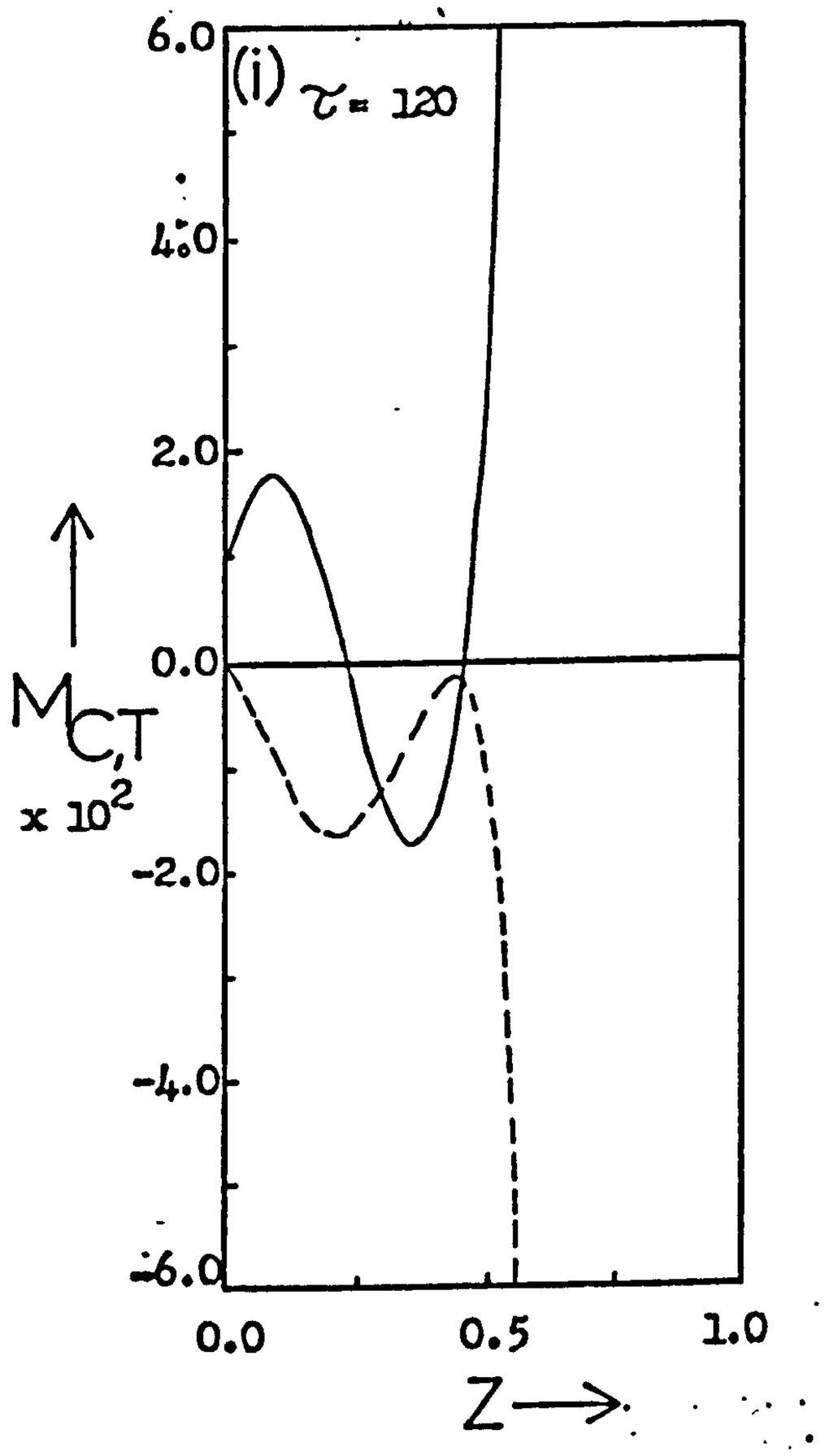

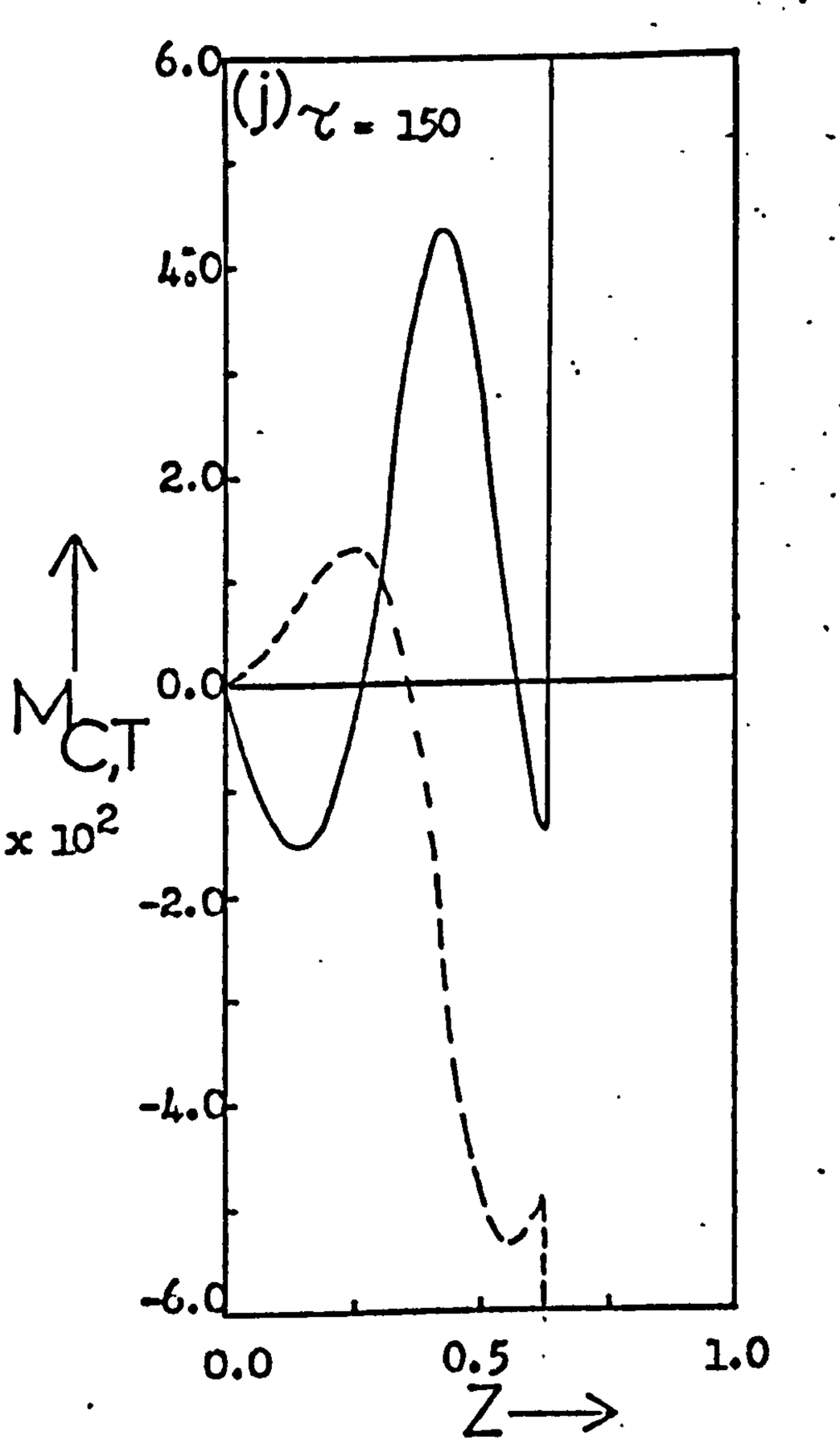

Figure 6.6 (Continued)

sensitive region near the runaway line on the phase diagram. This is because the induced concentration increases do not remain in the bed long enough to cause the increase in reaction rate necessary to overcome both the thermal capacitance effect of the pellets and the heat removal processes. This reduces the amplitude of the oscillations throughout the bed, both in the initial transient and the quasi-stationary state.

6.2.1 (b) Negative Sine Waves

When the inlet temperature sine wave is negative so that the inlet temperature initially decreases, the behaviour of the initial transient is somewhat different from that found with a positive amplitude, in the unique region.

At, for example, an inlet temperature amplitude of 0.00056 and a frequency of 0.04 Hz the reactor moves to a low temperature quasi-stationary state without passing transiently into the temperature runaway region, as is the case with a positive sine wave of amplitude 0.00056 at this frequency.

Figure 6.7 shows axial profiles of radial mean temperature at various times for an inlet temperature amplitude of 0.00056 and frequency of 0.04 Hz. Axial profiles of radial mean concentration and temperature deviations from the initial steady state are shown at various times during this perturbation in figure 6.8. The initial "wrong-way" transient is again evident (figures 6.8a to 6.8e), but since the inlet temperature is at first decreasing the whole bed is initially subject to an increase in concentration of reactant causing the temperature in the latter regions to increase. The first temperature trough into the bed at first decreases in depth (i.e. temperature increases) since it encounters the higher than steady state reactant concentration. As the first temperature crest enters the bed behind this trough it induces a fall in concentration throughout the bed. This causes the reaction rate to drop and so the temperature rise in the rest of the bed is arrested. The temperature does not fall immediately, however, because of the thermal capacitance of the pellets. During the next cycle of the inlet temperature (figures 6.8f and 6.8g) the leading trough advances down the bed increasing in amplitude (i.e. temperature decreasing). This is despite the entrance into the bed of a second temperature trough which induces an increase in reactant concentration. The reason for this is that the

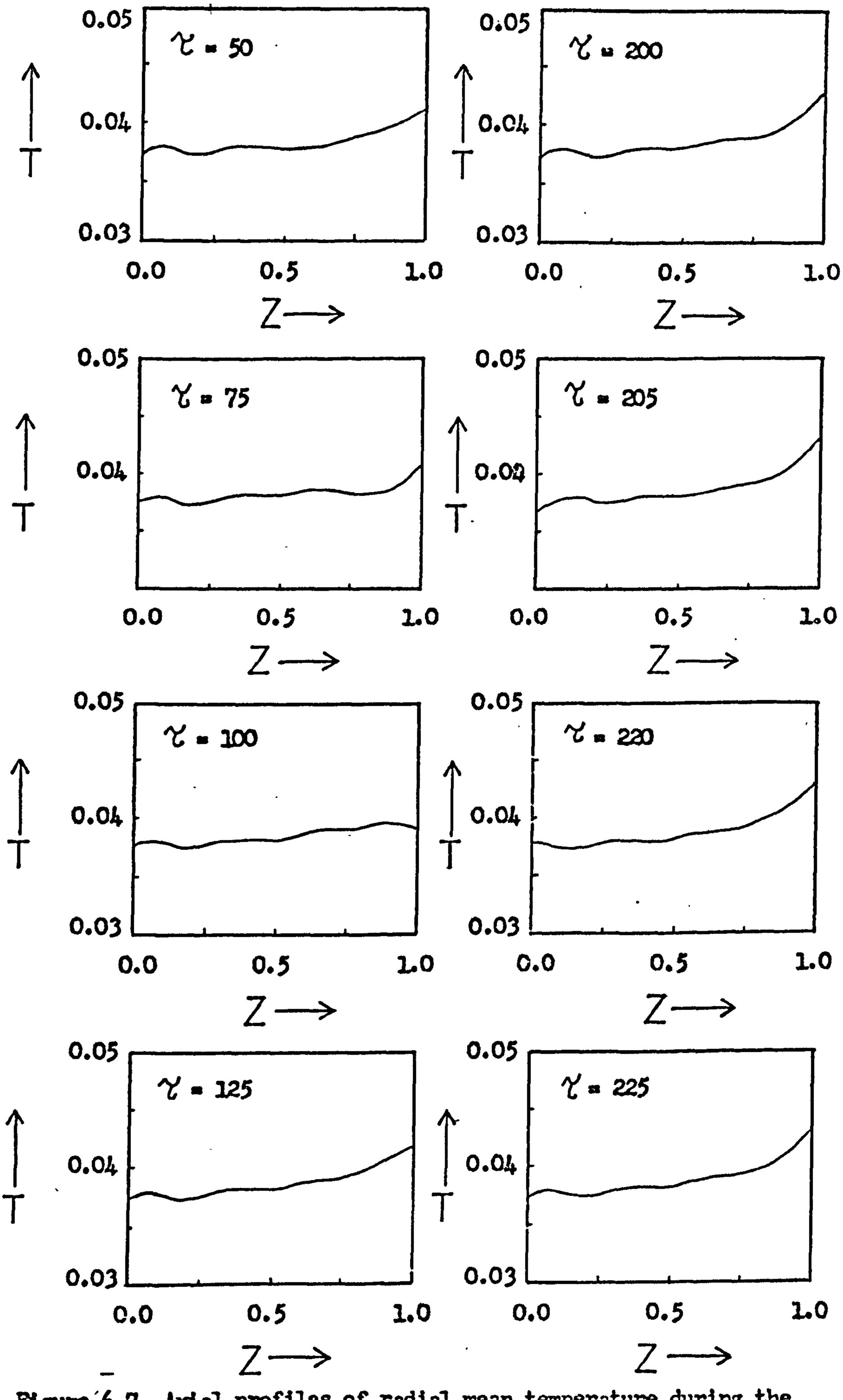

Figure 6.7 Axial profiles of radial mean temperature during the response of the reactor to a dimensionless inlet temperature perturbation of the form : $T_o = 0.03733 - 0.00056 \sin(2\pi \times 0.04 \times \tau)$. (Data as given in Table 5.1)

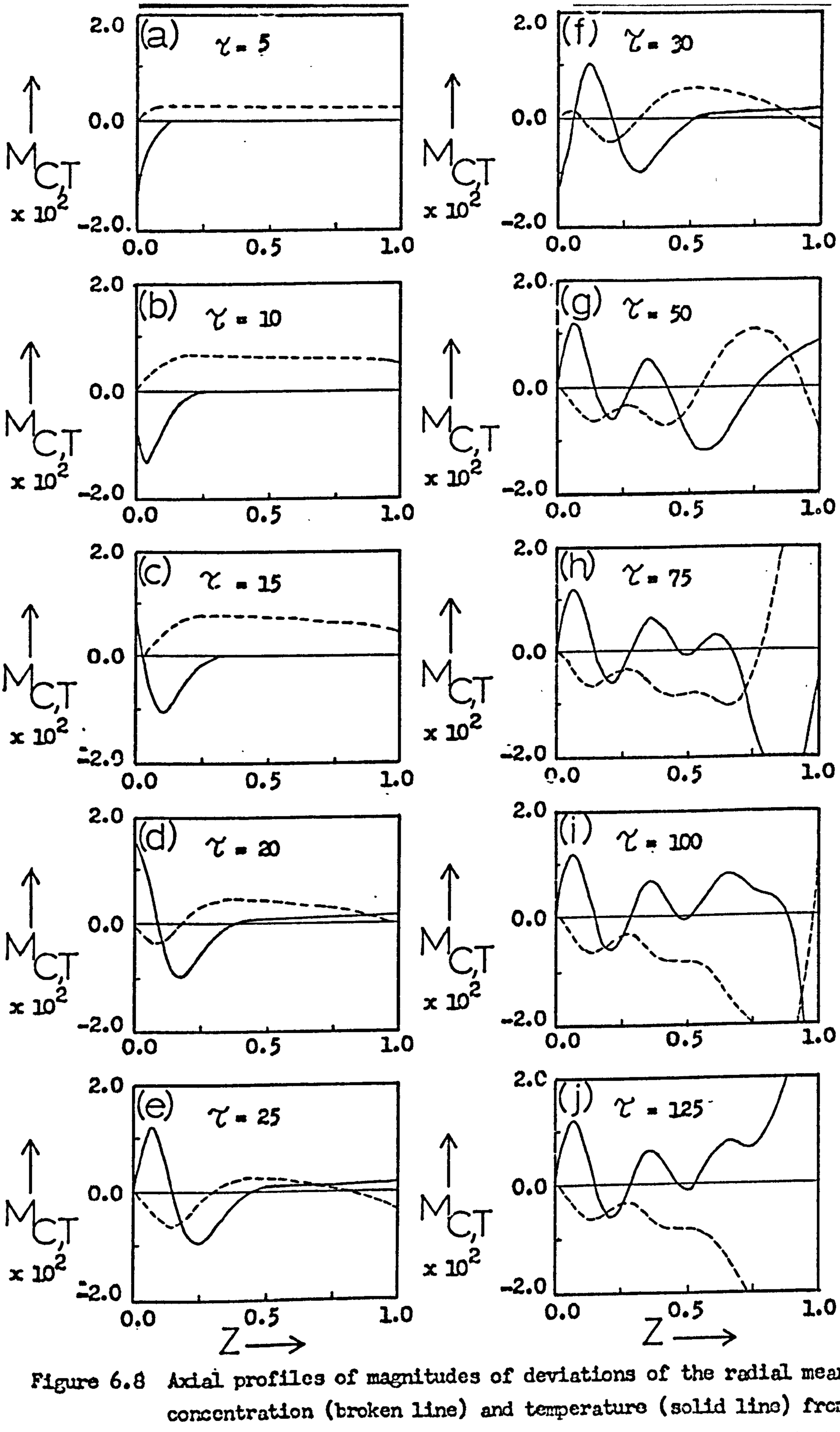

Figure 6.8 Axial profiles of magnitudes of deviations of the radial mean concentration (broken line) and temperature (solid line) from the initial steady state during the response to a dimensionless inlet temperature perturbation of the form : $T_o = 0.03733 - 0.00056 \sin(2\pi \times 0.04 \times \tau)$. (Data as given in Table 5.1)

temperature at the base of the leading trough is so much lower than the steady state value that even though it receives a concentration of reactant higher than the steady state value it is not high enough (due to the previous temperature crest where some has been consumed) nor does it remain long enough (due to the frequency of the inlet perturbation) to cause sufficient heat generation to overcome both the heat removal process and the thermal capacitance effect of the catalyst pellets and so cause the temperature to rise. This effect is repeated as the trough moves further down the bed and so it increases in depth. During this time the regions of the bed behind the leading temperature trough settle down to quasi-stationary state oscillations and the whole bed maintains this state when the leading trough leaves it. The temperature crests in the quasi-stationary state do not run away at this frequency, for the same reasons as those given for a positive sine wave at this amplitude and frequency, namely that the frequency of the forcing temperature oscillation does not allow the induced concentration increases to remain long enough for the reaction rate to overcome the heat removal and thermal capacitance effects.

When the frequency of the inlet temperature oscillation is decreased below 0.0345 Hz for an amplitude of 0.00056 the quasi-stationary state exhibits temperature runaway. Although the leading temperature trough moves through the bed increasing in depth, the subsequent temperature crests which enter the bed are amplified and run away. This is for exactly the same reasons which cause temperature runaway in the quasi-stationary state with a positive inlet temperature sine wave. Because of the frequency of the forcing temperature oscillation, the induced concentration increases persist long enough to interact constructively with the temperature crests.

6.2.1 (c) <u>The Effect of the Amplitude</u>

Changing the amplitude of the inlet temperature oscillations in the unique region merely causes a shift in position of the previously described 'threshold' frequencies for each type of behaviour. At higher values of the inlet temperature amplitude, temperature runaway, either temporarily in the initial transient or permanently in the quasi-stationary state, occurs at higher frequencies. Lowering the amplitude means that these 'threshold' frequencies are raised. This is because of the

way in which temperature runaway is propagated. In order that the temperature at any point in the bed can rise to a high value, the rate of heat generation at that point must be sufficient to overcome both the heat removal by the coolant and the thermal capacitance effect of the pellets. This may be accomplished either by a point in the bed receiving very large concentration increases for a short time or smaller concentration increases for a long time. When the amplitude of the forcing temperature perturbation is increased then the induced concentration increases are larger and so the time for which they must remain to cause temperature runaway is less, and so a higher frequency will cause temperature runaway.

At high inlet temperature amplitudes the differences in the propagation of temperature runaway, when it occurs in the quasi-stationary state for both positive and negative sine waves, is more obvious. Figures 6.9 and 6.10 show, as an example, axial profiles of radial mean temperature at various times during the initial transient for an inlet temperature frequency of 0.04 Hz and amplitude of 0.00112 for positive and negative sine waves respectively. Not only does the initial transient last longer with the positive sine wave, but temperature runaway is initiated at a point nearer the bed entrance. With the negative sine wave, runaway is not caused by the leading temperature trough, for previously given reasons, but by the crest which enters the bed during the second half-cycle. Because of the large amount of cooling caused by the leading trough as it passes down the bed, this temperature crest is not amplified sufficiently to enter the runaway region until it reaches the end of the bed. When the inlet temperature sine wave is positive a temperature crest enters the bed during the first half-cycle and it is this crest which causes runaway. The cooling effect in the latter regions of the bed caused by the 'wrong-way' transient is not as great as that caused by the leading trough which occurs with the negative sine wave. Consequently temperature runaway starts earlier in the bed. This leading runaway temperature crest moves very slowly because it consumes reactant at such a rate that very little reaches the part of the bed in front of it. Thus, here, the bed heats up more slowly and the hot spot moves to its quasi-stationary state position near the end of the bed more slowly.

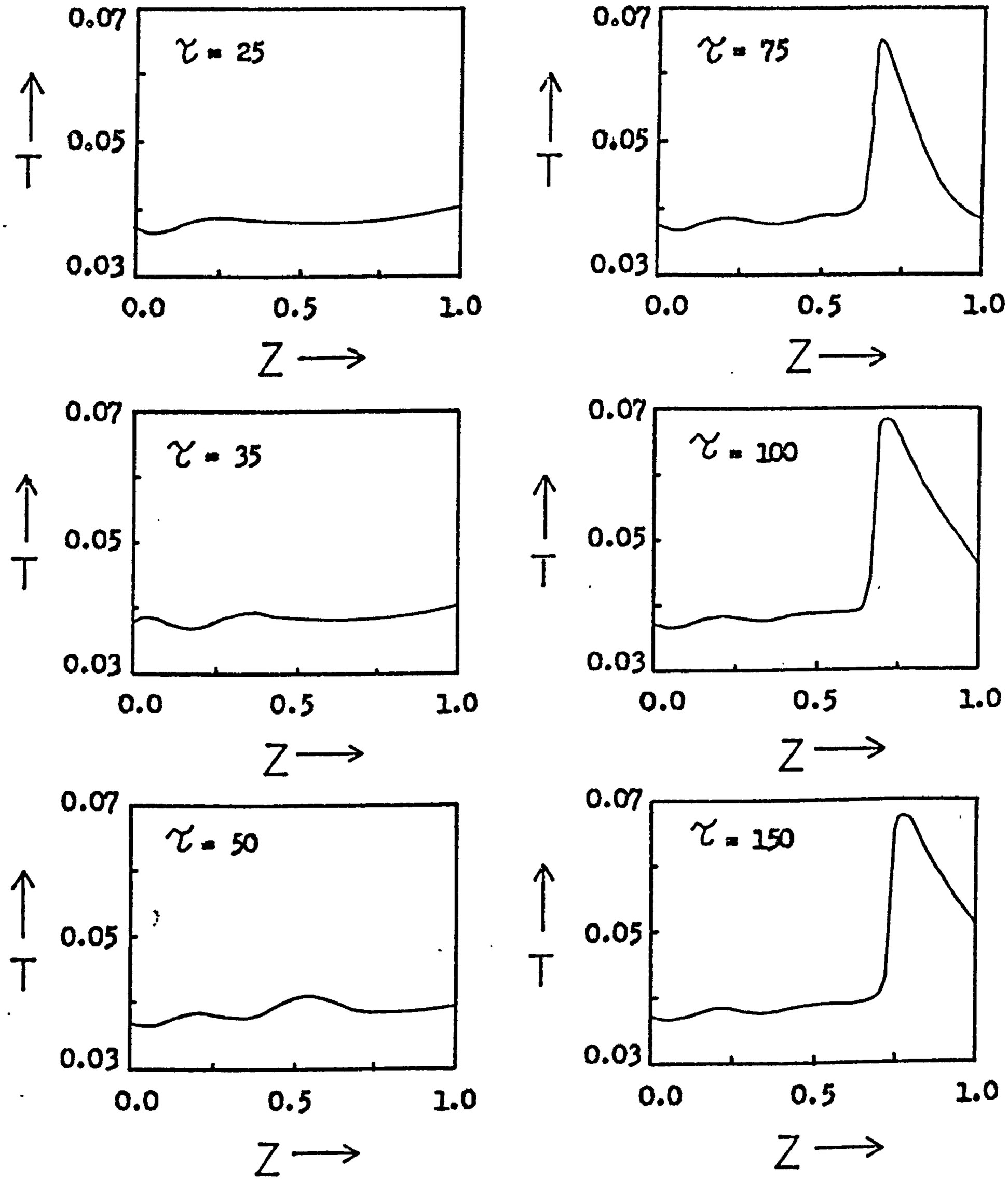

Figure 6.9 Axial profiles of radial mean temperature during the response of the reactor to a dimensionless inlet temperature perturbation of the form : $T_o = 0.03733 + 0.00112 \sin(2\pi \times 0.04 \times \tau)$. (Data as given in Table 5.1)

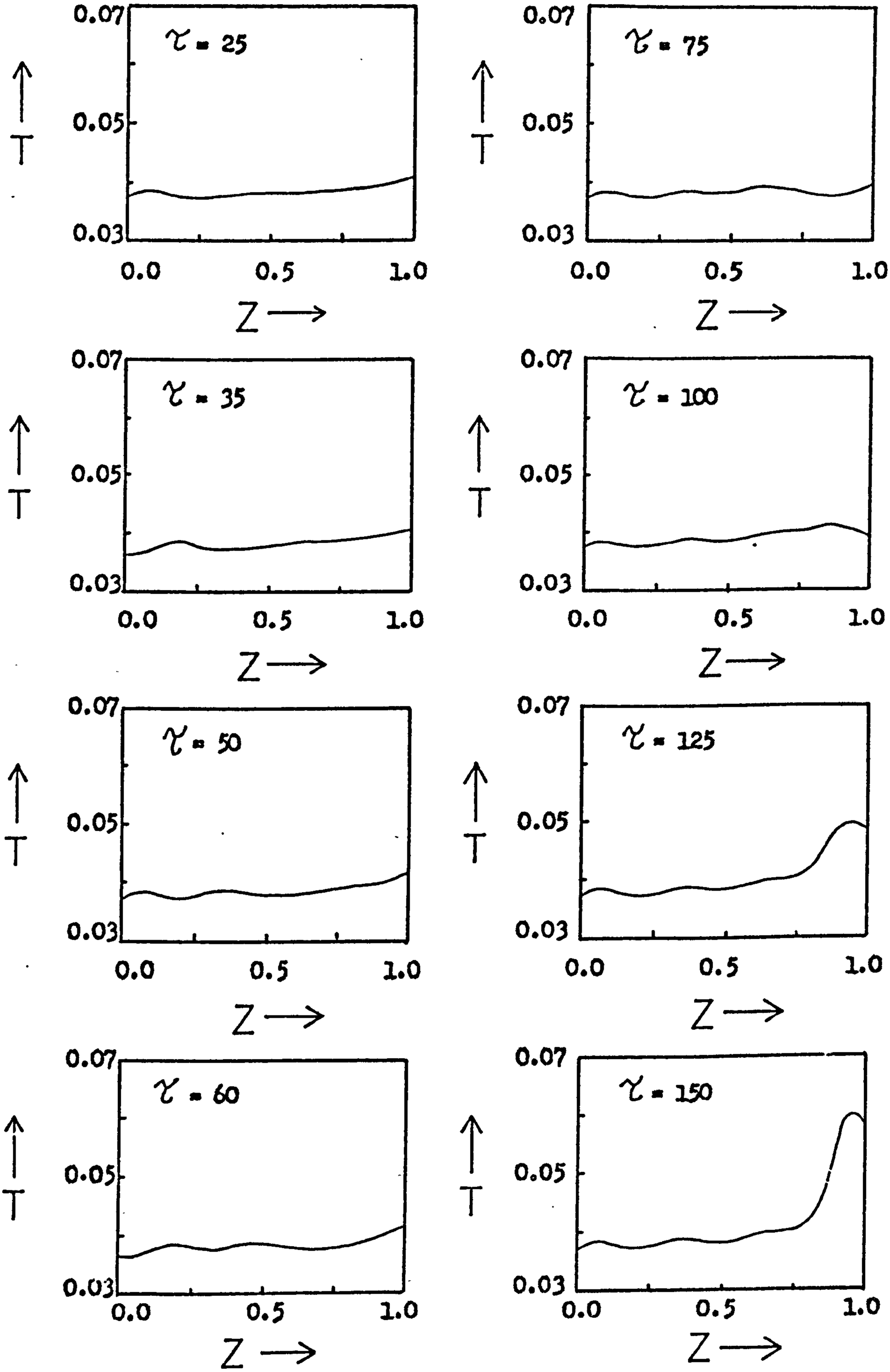

Figure 6.10 Axial profiles of radial mean temperature during the response of the reactor to a dimensionless inlet temperature perturbation of the form : $T_o = 0.03733 \pm 0.00112 \sin(2\pi \times 0.04 \times \gamma)$. (Data as given in Table 5.1)

6.2.2 The Non-Unique Region

When the initial steady state of the reactor lies inside the region of multiple solutions, its response to sinusoidal perturbations of the inlet conditions is different from that when the initial state lies in the region of unique solutions.

In the multiple solution region temperature runaway occurs when all, or part, of the phase trajectory crosses the upper bound of the non-unique region.[12] McGreavy and Thornton[83] have demonstrated that, at least for a single pellet, small excursions across the upper bound of the non-unique region will not always result in temperature runaway if the time spent there is short. Nevertheless, when temperature runaway has occurred in this manner, the lower temperature state can only be regained when the phase trajectory of that part of the reactor which has runaway subsequently crosses the lower bound of the non-unique region.

Thus, when the inlet temperature of a reactor is perturbed sinusoidally from a steady state lying within the non-unique region, if temperature runaway occurs during the initial transient, a necessary, but not sufficient, condition for the subsequent quasi-steady state to be in the low temperature region, is that at the steady state which would occur at the minimum value of the oscillation, that part of the reactor trajectory which is in the runaway state must cross the lower bound of the non-unique region. Unless this condition is fulfilled, then the temperature runaway which occurs in the initial transient will persist in the quasi-steady state. It is this requirement which makes the overall response of the reactor in the region of multiple solutions different from that which occurs in the unique solution region.

To illustrate this consider the following example. Figure 6.11 shows both the axial profiles of radial mean temperature and the phase trajectories for an initial steady state lying in the non-unique region and the steady states which would occur at the maximum and minimum values of an inlet temperature perturbation of 0.00056. The initial state and that at the minimum of the oscillation are clearly within the low temperature region, both of them being entirely in the non-unique region with neither trajectory crossing the lower bound of this region.

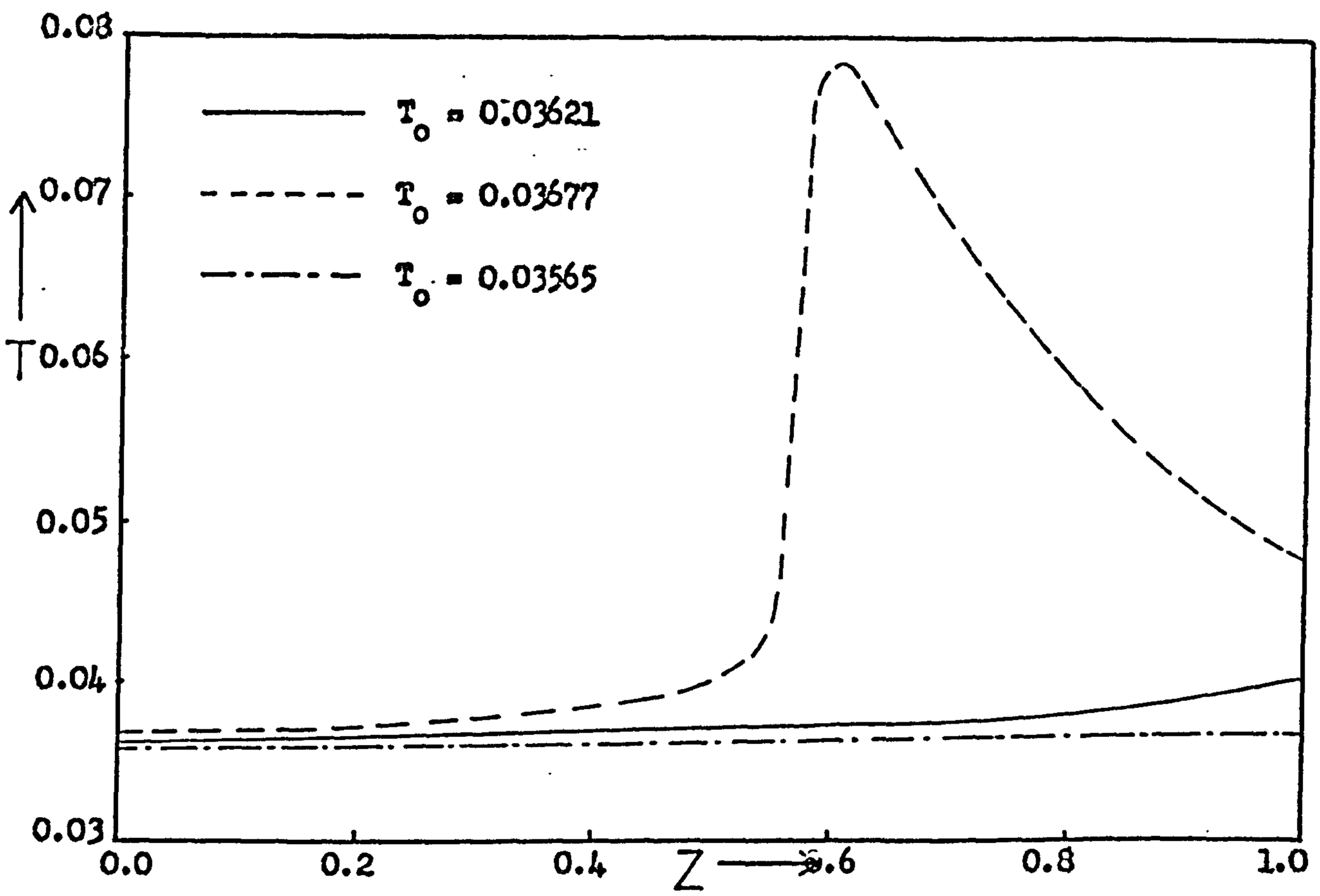

Figure 6.11(a) Steady state axial profiles of radial mean temperature at the mean, maximum and minimum values of a sinusoidal perturbation of dimensionless inlet temperature of amplitude 0.00056 in the non - unique region. (Data as given in Table 5.1)

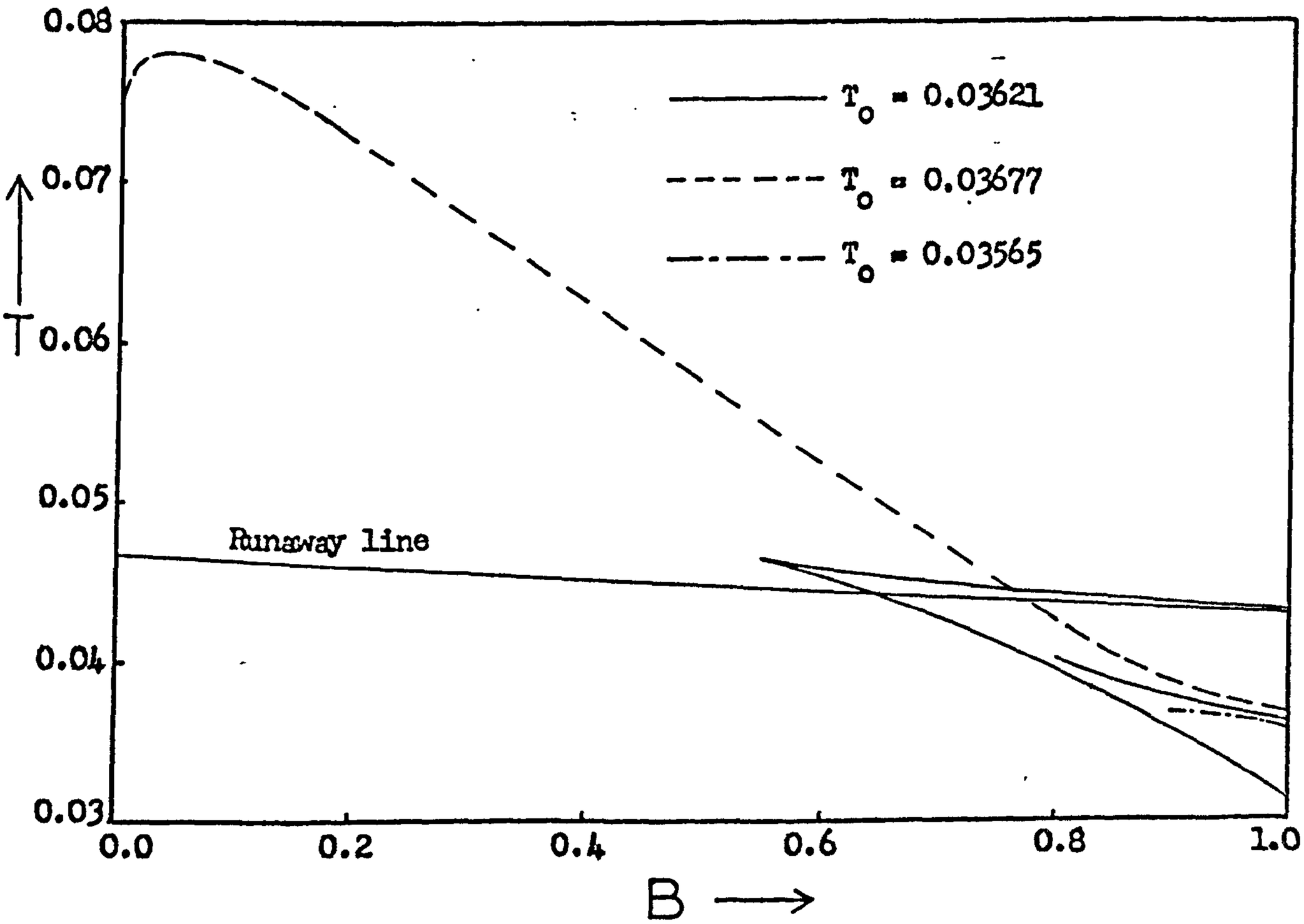

Figure 6.11(b) Steady state reactor trajectories at the mean, maximum and minimum values of a sinusoidal perturbation of dimensionless inlet temperature of amplitude 0.00056 in the non - unique region. (Data as given in Table 5.1)

The steady state at the maximum value of this oscillation is in the runaway state. With this magnitude of oscillation, therefore, once temperature runaway occurs in the initial transient, it persists in the quasi-steady state since the runaway portion of the trajectory cannot be forced below the lower bound of the non-unique region. With a positive sine wave of inlet temperature, of amplitude 0.00056, so that the inlet temperature initially increases, permanent temperature runaway occurs at all frequencies below approximately 0.1 Hz. At frequencies above this, temperature runaway does not occur at all. With a negative sine wave of the same amplitude, the inlet temperature is initially decreasing and temperature runaway occurs at all frequencies below 0.04 Hz, but is not evident above this value. The difference between this behaviour and that observed in the region of unique solutions, namely that here no transient temperature runaway occurs, illustrates quite clearly the effect of the multiple solution region. In the range of frequencies of approximately 0.04 Hz to 0.1 Hz temperature runaway occurs with a positive sine wave because of the effect of the initial transient caused by the first temperature crest to enter the bed, in the same way that transient temperature runaway occurs in the unique solution region. Because the subsequent response of the bed is such that the runaway portion of the bed cannot fall below the lower bound of the non-unique region, the high temperatures of the runaway state are maintained in the quasi-stationary state. At frequencies below approximately 0.04 Hz temperature runaway occurs in the quasi-stationary state due to the length of time which various points in the bed spend at conditions of high temperature and concentration. This is exactly analogous to the occurrence of permanent temperature runaway in the non-unique region.

Increasing the amplitude of the inlet temperature oscillation to 0.00112 causes temperature runaway to occur at higher frequencies; below 0.25 Hz for a positive sine wave and below 0.05 Hz for a negative sine wave.

With the initial steady state used in this study and the parameters given in Table 5.1, a realistic inlet temperature amplitude which would cause the phase trajectory of the steady state at its minimum value to cross the lower bound of the non-unique region, and that at the maximum value of the oscillation

to cross the upper bound of the non-unique region, could not be found. For this reason, transient temperature runaway with temperature forcing in the non-unique region was not observed. In the case of concentration oscillations at the inlet, however, because of the shape of the non-unique region on the phase diagram, the reactor trajectories are more mobile for oscillations of moderate amplitude. This is described in section 6.3.2 of this chapter.

6.2.3 The Quasi-Stationary State

The quasi-stationary state oscillations in both the unique and non-unique regions are similar. Figure 6.12 shows the quasi-stationary state fluid temperature oscillations at various points along the bed for a positive sine wave of amplitude 0.00056 and frequency 0.04 Hz, in the unique region of solutions. This behaviour is typical of all quasi-stationary states in which temperature runaway does not occur. The oscillations are attenuated as they progress down the bed until a region near the exit ($z = 1.0$) is reached where they show a slight increase in amplitude. The reason for this is that in most of the bed, the temperature and, therefore, the reaction rate is low and so heat removal through the reactor wall, by the coolant, tends to predominate. The exit region of the bed, in this quasi-stationary state, is the hottest part and so the reaction rate is greater there causing the larger amplitude. Because the excursions about the mean are very small at all points in the bed, the phase difference of the oscillations along the bed is not very great. Also since the reaction rate is very low throughout the bed there is no distortion of the wave form.

Figures 6.13 and 6.14 show radial mean fluid temperature oscillations at various points along the bed for a typical quasi-stationary state exhibiting temperature runaway. Here, the oscillations increase in amplitude down the bed until the region of temperature runaway (at $z = 0.8$ in this example). In this region and subsequent parts of the bed the oscillations tend to decrease in amplitude. The oscillations tend to increase along the bed as it gets hotter and so the heat generation rate becomes greater than the heat removal rate. At the runaway region, the amplitude decreases because less reactant is reaching this part of the bed, and also because at very high temperatures the reaction rate is less sensitive to concent-

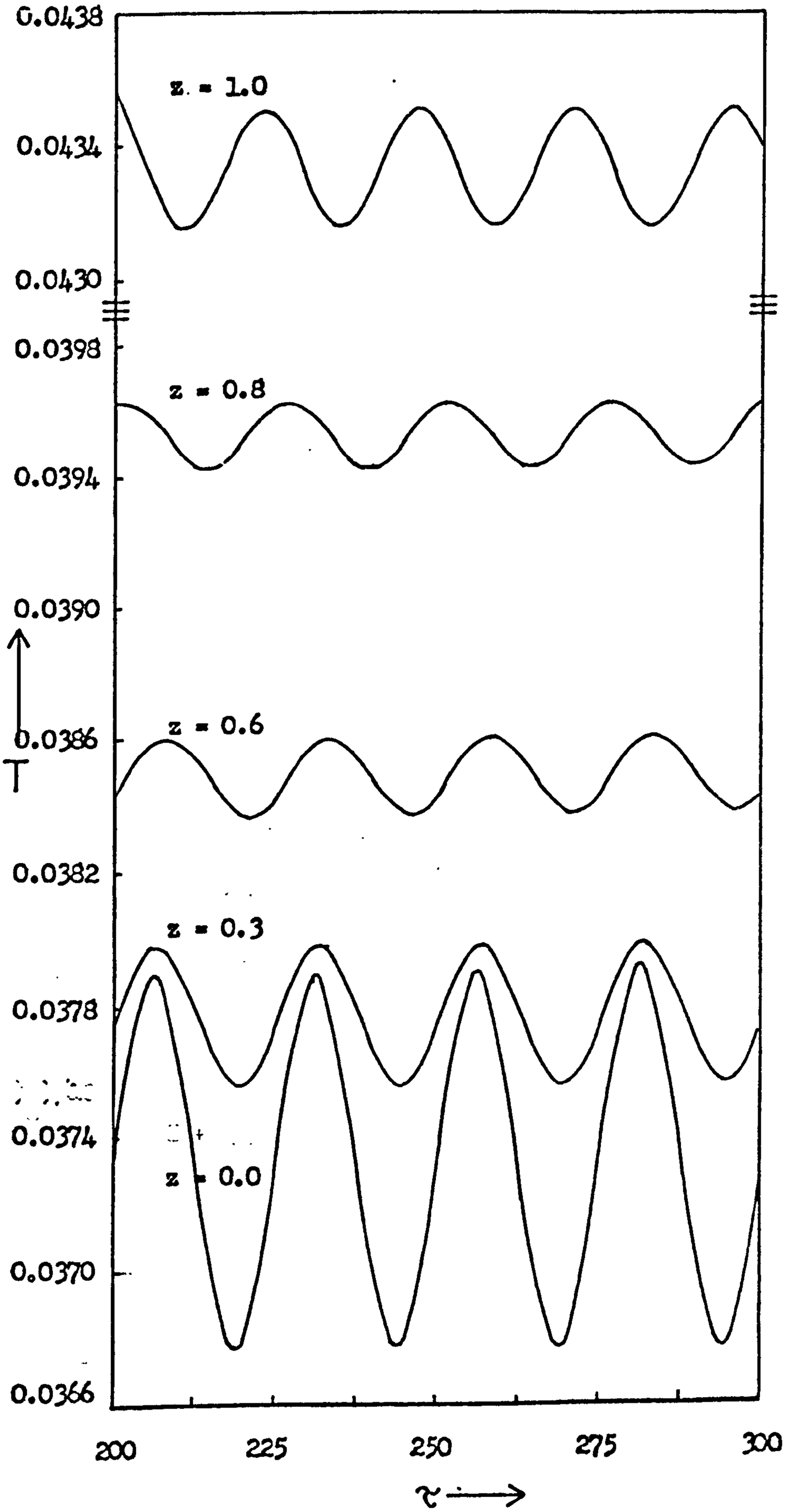

Figure 6.12 Radial mean fluid temperature oscillations at various axial positions during the quasi - stationary state due to a dimensionless inlet temperature perturbation of the form : $T_o = 0.03733 + 0.00056 \times \mathrm{Sin}(2\pi \times 0.04 \times \tau)$. (Data as given in Table 5.1)

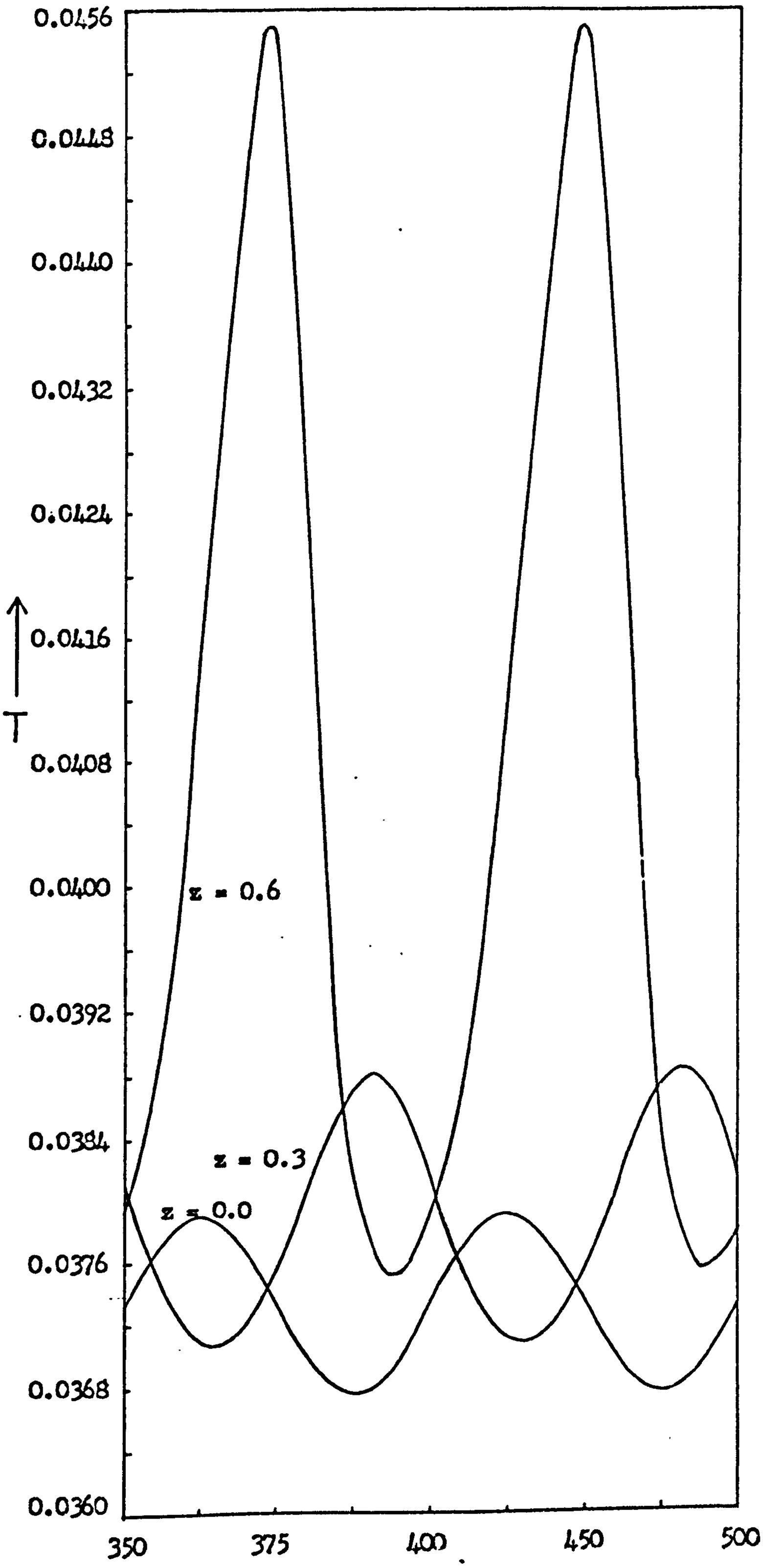

Figure 6.13 Radial mean fluid temperature oscillations at various axial positions during the quasi - stationary state due to a dimensionless inlet temperature perturbation of the form : $T_o = 0.03733 + 0.00056 \sin(2\pi \times 0.02 \times \tau)$. (Data as given in Table 5.1)

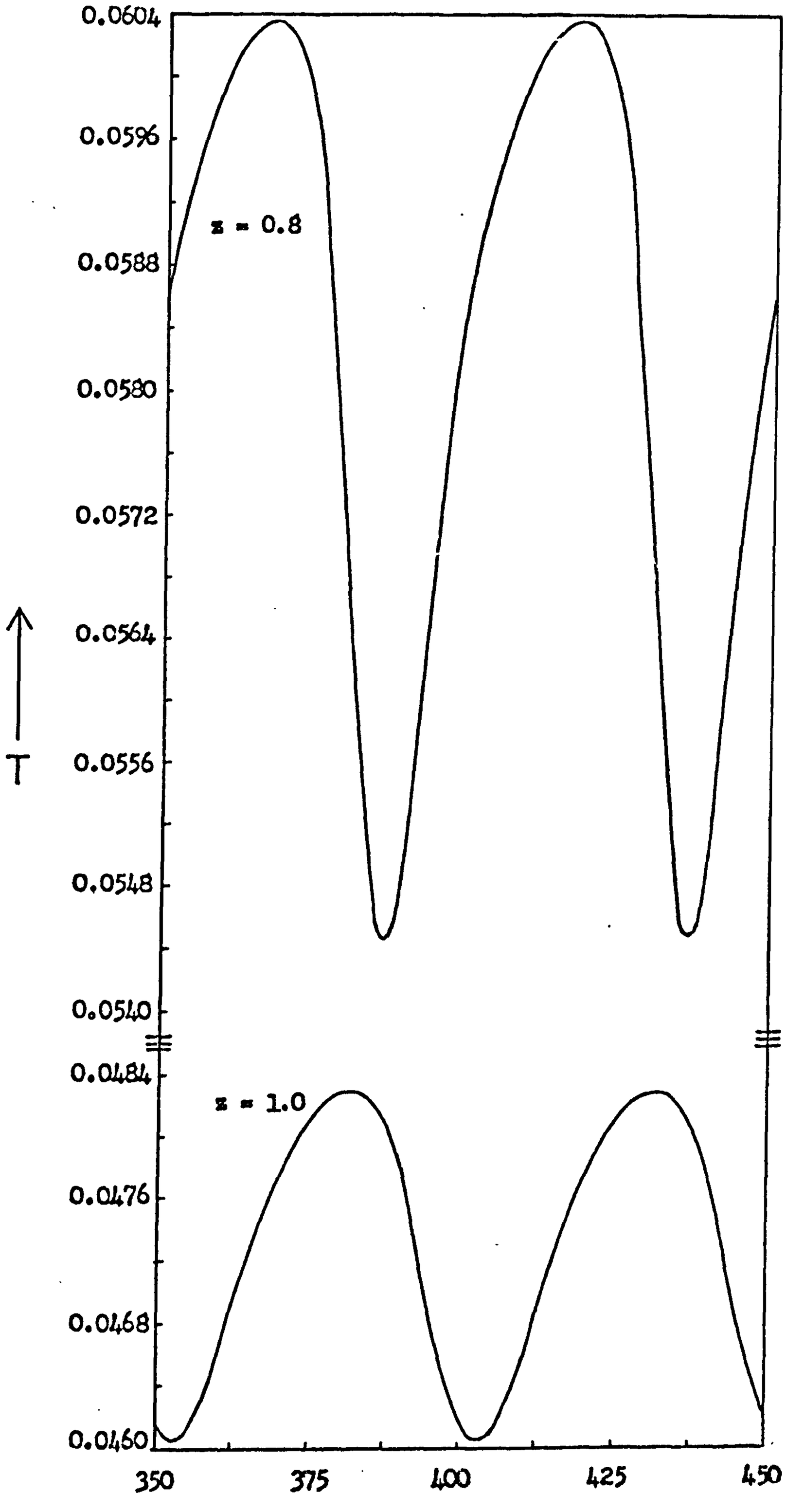

Figure 6.14 Radial mean fluid temperature oscillations at various axial positions during the quasi - stationary state due to a dimensionless inlet temperature perturbation of the form : $T_o = 0.03733 + 0.00056\ \mathrm{Sin}(2\pi \times 0.02 \times \tau)$. (Data as given in Table 5.1)

ration fluctuations. Near the exit of the bed, after the hot spot, there is virtually no reaction at all since most of the reactant is consumed before this point is reached. Consequently, here, the bed is acting primarily as a heat exchanger and the amplitude of the oscillations decreases. The very large temperature fluctuations just before temperature runaway occurs ($z = 0.6$) are due to this part of the bed passing into a region of parametric sensitivity near the runaway line. This is also the reason for the distortion of the temperature waveform at this point. At the low temperatures at the troughs of the waves, very little reaction takes place and so the troughs are flattened. As the temperature rises, the reaction rate increases and so more heat is generated which tends to increase the gradient of the temperature wave and force this part of the bed into a region of parametric sensitivity close to the runaway line. This causes greater sensitivity of the reaction rate to both concentration and temperature and so the crests of the wave are very sharp. Such reasoning is confirmed by the reversal of the shape of the wave distortion which occurs in the runaway region ($z = 0.8$). Here the troughs of the waves approach the parametrically sensitive region close to the runaway line and so they are sharpened. This quasi-stationary state behaviour is in very good agreement with that observed experimentally by Hoiberg, Lyche and Foss.[64] They studied the behaviour of a fixed bed reactor, supporting an exothermic gaseous reaction, towards sinusoidal perturbations of inlet temperature. At high frequencies they found that the temperature wave decreased in amplitude throughout the bed, and at low frequencies the non linear effects were more apparent. Of particular interest is their observation of the sharpening of the temperature crests and flattening of the troughs in the region of the bed before the hot spot occurs and the reversal of this distortion at the hot spot. Clearly, this experimentally determined behaviour is in exact agreement with that predicted by the reactor model used here. Although Hoiberg, Lyche and Foss[64] were unable to determine the reasons for this behaviour, the analysis presented above suggests that it is due to the influence of a region of parametric sensitivity around the runaway line. Hoiberg, Lyche and Foss[64] found that a one dimensional reactor model, very similar in structure to the one used in the work described here, gave excellent agreement with

their experimental results, although they only attempted model fitting at high frequencies and in the quasi-stationary state.

Only when the quasi-stationary state passes through the non-unique region of solutions does the initial direction of the sine wave cause a difference in the two quasi-stationary states. When the initial steady state and the subsequent quasi-stationary states are in the unique region of solutions the effect of the direction of the sine wave is merely to create a phase difference of half a cycle between the quasi-stationary states obtained with positive and negative sine waves, at a given frequency, even after temperature runaway has occurred during the initial transient with a positive sine wave. This is as would be expected purely from the equations; if the quasi-stationary state is unique then only one state can be reached after a disturbance from a given state no matter which path is taken to get there.

When the initial steady state and the quasi-stationary state are in the region of non-unique solutions, then quite clearly, different quasi-stationary states may be obtained with forcing oscillations differing only in sign. The actual quasi-stationary state obtained depends on the path taken. This is clearly shown by the fact that over a range of frequencies of the inlet temperature oscillation temperature runaway occurs in the quasi-stationary state with a positive sine wave whilst with a negative one no temperature runaway occurs. As explained previously, this is because the portion of the bed which crossed the upper bound of the non-unique region, and therefore runaway, does not experience changes in fluid conditions sufficient to subsequently force it to cross the lower bound of the non-unique region. What is, perhaps, not quite so obvious is that even when temperature runaway occurs in the quasi-stationary state with both a positive and negative sine wave of inlet temperature, the two quasi-stationary states will usually differ in more than just the phase angle. This is illustrated by figure 6.15 where radial mean fluid temperature is plotted against time for one cycle of inlet temperature at three points in the bed during the quasi-stationary state which occurs in the non-unique region at an amplitude of 0.00056 and frequency of 0.02 Hz. In the relatively cool portion of the bed (e.g. at $z = 0.6$) the two oscillations differ only in phase angle;

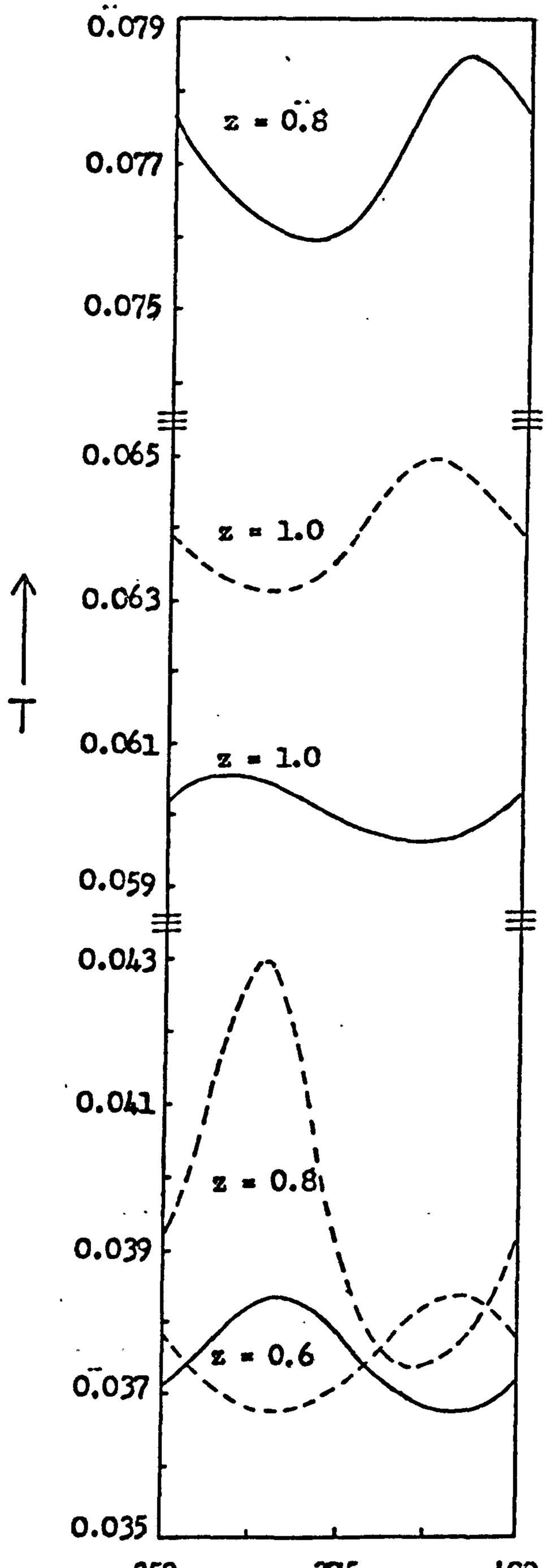

Figure 6.15 Comparison of quasi - stationary state fluid temperature oscillations at various axial positions due to positive (solid line) and negative (broken line) sinusoidal inlet temperature perturbations of the form : $T_o = 0.03621 \pm 0.00056 \sin(2\pi \times 0.02 \times \tau)$. (Data as given in Table 5.1)

this part of the bed was not forced across the upper bound at either amplitude. A great difference in the two oscillations occurs at z = 0.8; with a positive sine wave this point is clearly in the temperature runaway region, but not with a negative one. This is because during the initial transient this point in the bed is forced above the upper bound of the non-unique region, with a positive wave, and is not able to return, due to the amplification of the first temperature crest to enter the bed. This behaviour is a further illustration of the action of the region of non-unique solutions in that the final state reached is dependent upon the path taken to get there and, therefore, upon the initial direction of the perturbation.

6.3 Concentration Forcing

6.3.1 The Unique Region

In order to investigate the effect of oscillating inlet concentration the same initial steady states as those used for temperature oscillations have been employed. Figure 6.16 shows axial profiles of radial mean temperature and phase trajectories of the initial steady state in the unique region of solutions. Also shown are the steady states which would occur at the maximum and minimum values of a concentration oscillation of amplitude 0.1 (i.e. 10% of the inlet value).

The general effects of sinusoidally perturbed inlet concentration are similar to those observed for sinusoidal inlet temperature perturbations. In the unique region of solutions the phenomenon of transient temperature runaway occurs with a positive forcing sine wave. For an inlet concentration amplitude of 0.1, temperature runaway occurs in the quasi-stationary state at frequencies below 0.02 Hz. In the frequency range of 0.02 Hz to approximately 0.036 Hz temperature runaway occurs during the initial transient, but not in the subsequent, quasi-stationary state, and above 0.04 Hz temperature runaway does not occur at all. With a negative sine wave of the same amplitude the quasi-stationary state exhibits temperature runaway only at frequencies below approximately 0.018 Hz.

It is instructive to examine in some detail the initial transient response of the reactor to oscillating inlet concentration since this differs somewhat from that which occurs with oscillating inlet temperature, although the ultimate effect is

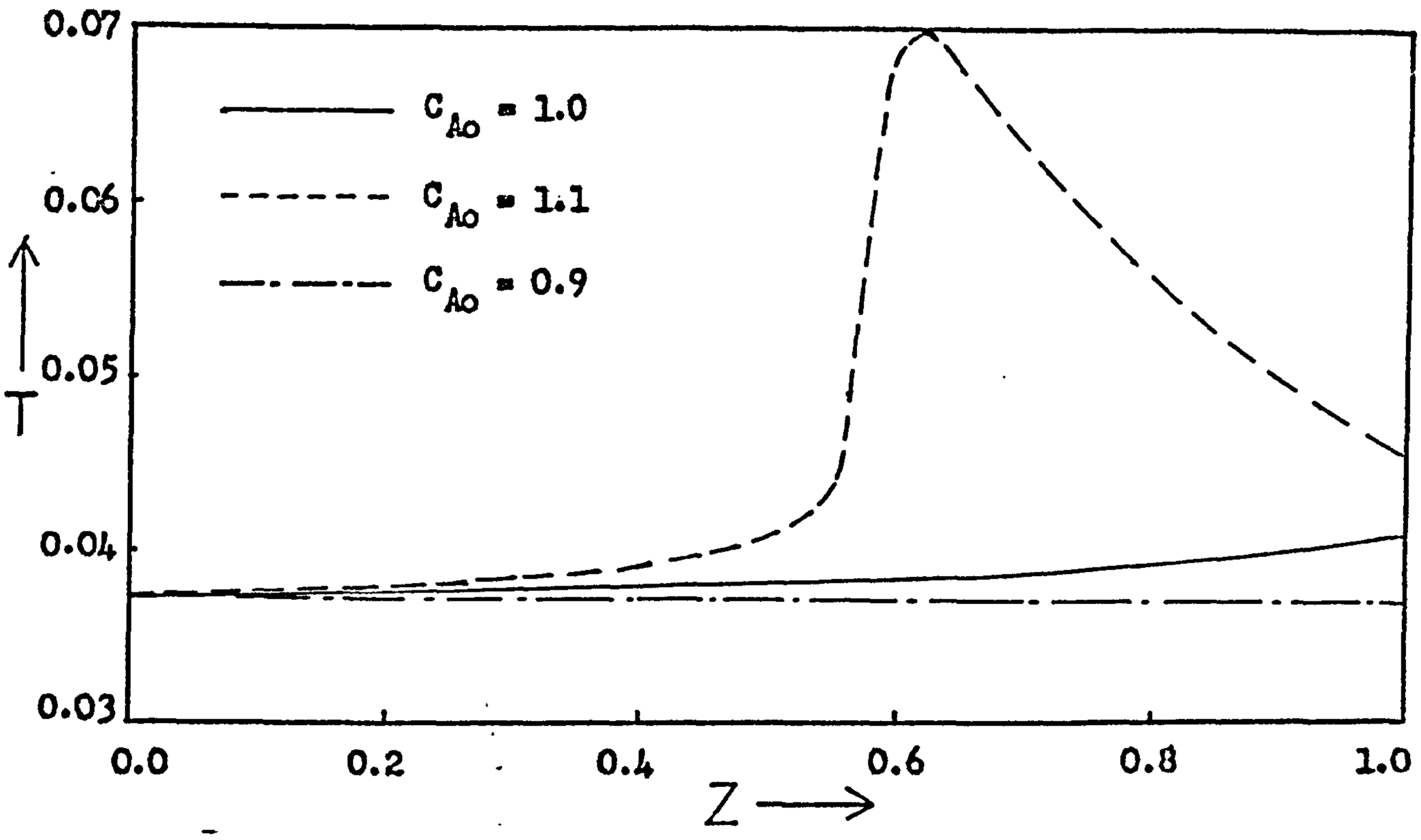

Figure 6.16(a) Steady state axial profiles of radial mean temperature at the mean, maximum and minimum values of a sinusoidal perturbation of dimensionless inlet concentration of amplitude 0.1. (Data as given in Table 5.1)

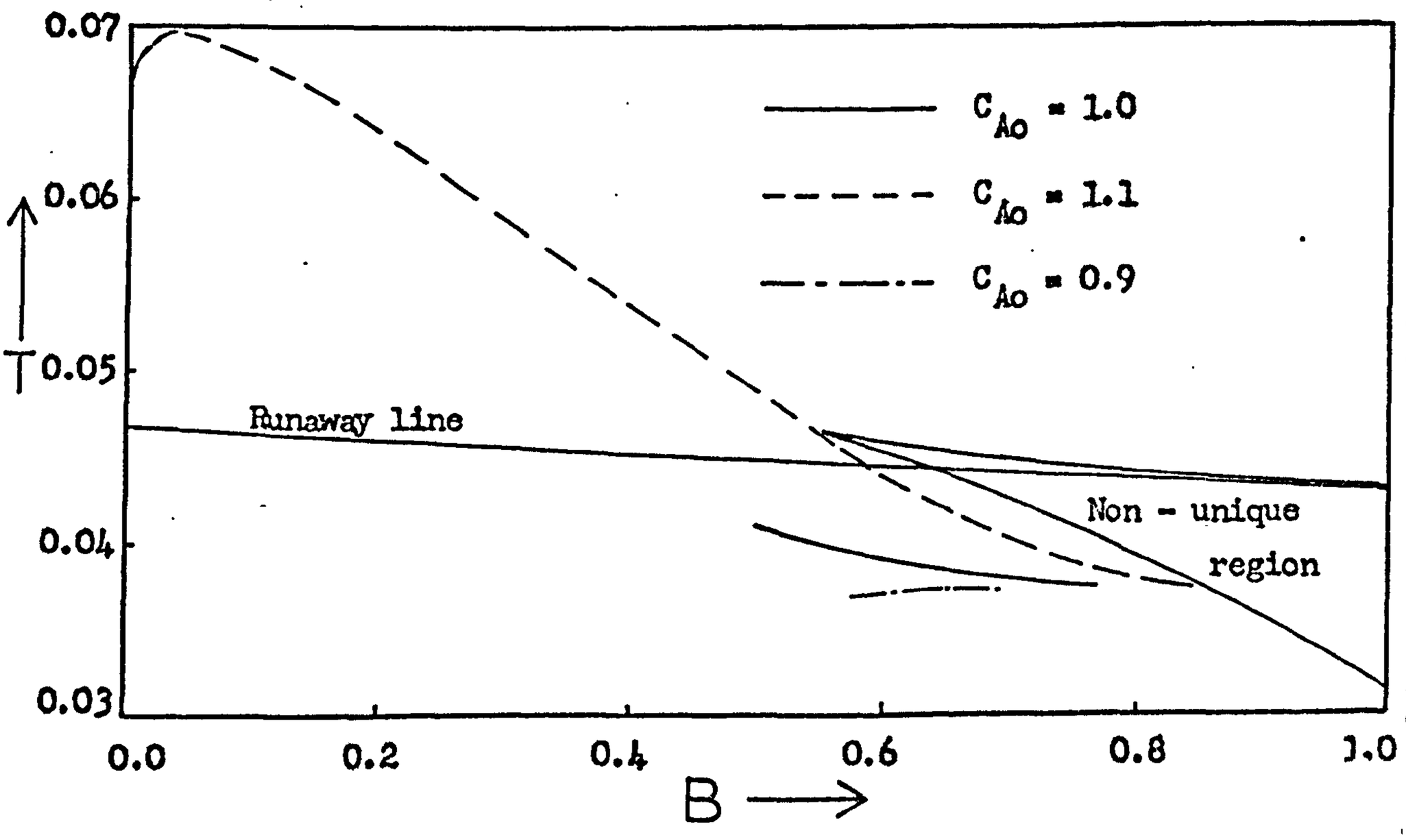

Figure 6.16(b) Steady state reactor trajectories at the mean, maximum and minimum values of a sinusoidal perturbation of dimensionless inlet concentration of amplitude 0.1. (Data as given in Table 5.1)

the same. Figure 6.17 shows axial profiles of the magnitudes of deviations of the radial mean concentration and temperature from the initial steady state, shown in figure 6.16, at various times during a positive concentration oscillation of amplitude 0.1 and frequency 0.02 Hz.

Since the sine wave is positive the concentration first rises above its mean value causing an immediate concentration increase throughout the bed (figures 6.17a and 6.17b). This, of course, causes an increase in reaction rate and so the temperature also rises throughout the bed. The largest temperature rise occurs near the end of the bed since the temperature there was initially highest. Note that the phenomenon of the 'wrong-way' transient response does not occur, for obvious reasons. During the second half-cycle the inlet concentration falls below its steady state value and induces a temperature trough near the entrance of the bed, the temperature near the exit of the bed, however, does not fall very much and remains well above its steady state value. This is because near the entrance of the bed the reaction rate is very low because the temperature there is low and so it is more sensitive to concentration changes. In the hotter exit region of the bed the thermal capacitance of the pellets prevents them from cooling so much, and so the rate of reaction is not reduced so much. Thus, when the inlet concentration rises during the second cycle rapid reaction takes place immediately near the end of the bed, the temperature and concentration there being much higher than the steady state values, and so the temperature there becomes higher and this part of the bed is forced into the runaway region. This effect is exacerbated by the induced temperature troughs which have entered the bed causing more reactant to reach the hot region. These effects are repeated during subsequent cycles and temperature runaway occurs near the exit. It is the thermal capacitance of the catalyst pellets, coupled with the non-linear dependence of the reaction rate on temperature, which causes runaway to develop. The thermal capacitance of the pellets acts, of course, both at high and low temperatures. However, the rate of heat generation at low temperatures is less sensitive to temperature and more sensitive to concentration than at high temperatures. At high temperatures the bed cools more slowly when the concentration decreases, and therefore remains hot so

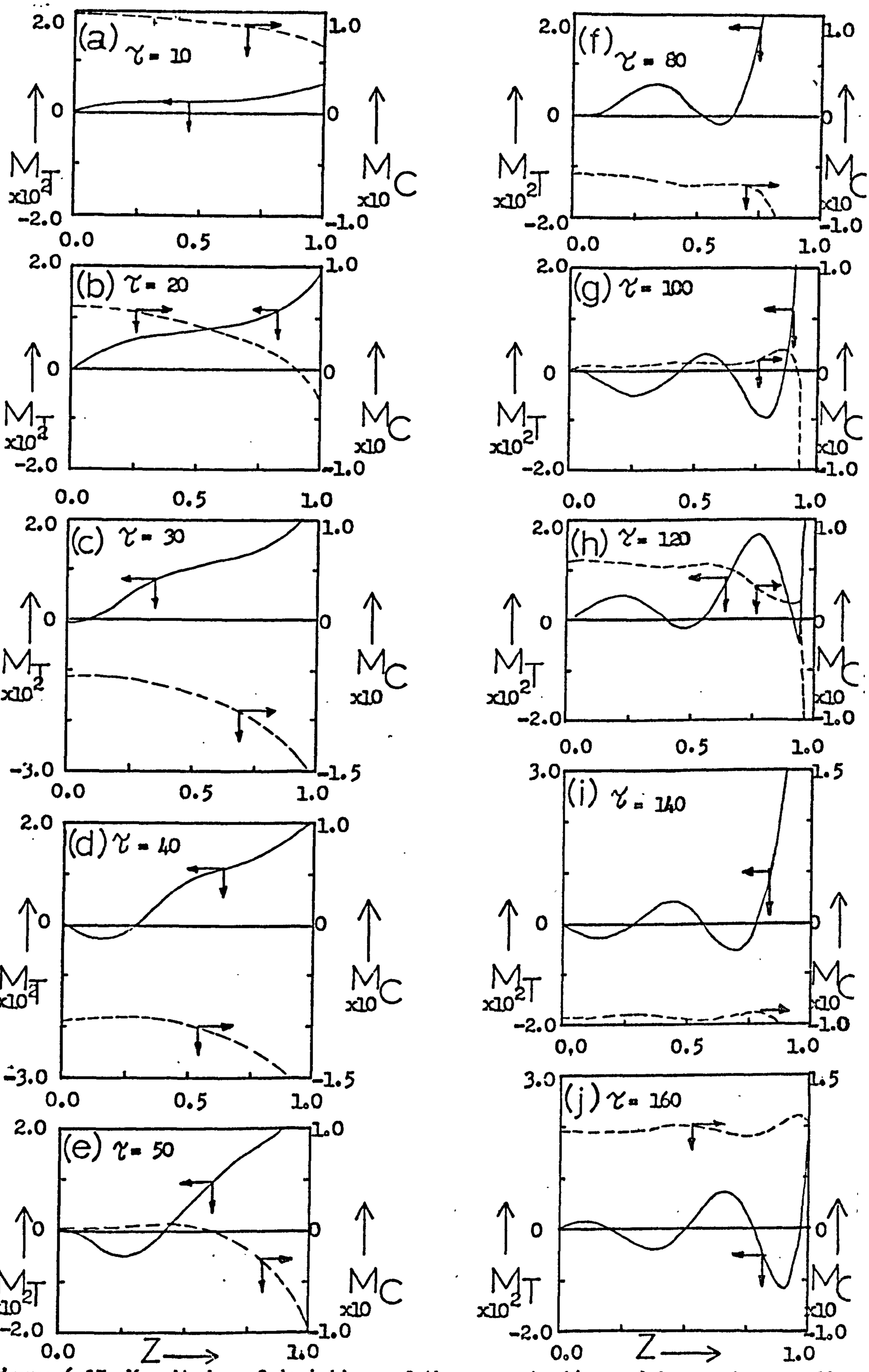

Figure 6.17 Magnitudes of deviations of the concentration and temperature profiles from the initial steady state during the response to a dimensionless inlet concentration perturbation of the form : $C_{Ao} = 1.0 + 0.1 \sin(2\pi \times 0.02 \times \tau)$. (Data as given in Table 5.1)

that when the concentration increases rapid reaction ensues. By this process, repeated during oscillations of concentration, the temperature of the hotter regions is raised further.

Temperature runaway does not occur during the quasi-stationary state because the region of the bed which ran away initially is cooled by the induced temperature troughs. Thus, when the concentration rises again this region of the bed has to be heated from a temperature lower than the initial steady state and the thermal capacitance of the catalyst pellet acts in the opposite direction. That is to say, it causes the pellets to remain longer at the lower temperature. This quasi-staticnary state behaviour is exactly the same as that described previously for inlet temperature oscillations.

When the inlet concentration sine wave is negative, the concentration throughout the bed initially decreases causing the rate of reaction and, therefore, the temperature everywhere to decrease. This is shown by figure 6.18 where axial profiles of the magnitudes of deviations of the radial mean concentration and temperature from the initial steady state are plotted at various times during the response of the bed to a negative sine wave of inlet concentration of amplitude 0.1 and frequency 0.02 Hz. When the rate of reaction begins to fall near the end of the bed, heat removal by the coolant tends to become greater than heat generation by the reaction and so the temperature falls even further. When the inlet concentration rises, the thermal capacitance of the pellets slows down the temperature rise so that when the concentration falls again the temperature falls even further. Thus, temperature runaway does not develop at this frequency with a negative amplitude, because of the initial cooling of the bed. Eventually the greatly cooled exit region of the bed is heated up by the induced temperature crests. Temperature runaway is prevented from occurring because of the combined effects of the forcing frequency of the inlet concentration and the thermal capacitance of the pellets, as described previously.

At lower frequencies temperature runaway occurs during the quasi-stationary state for both positive and negative sine waves for reasons similar to those described previously. In the case of positive sine waves the concentration increase exists long enough to cause the induced temperature crests to be

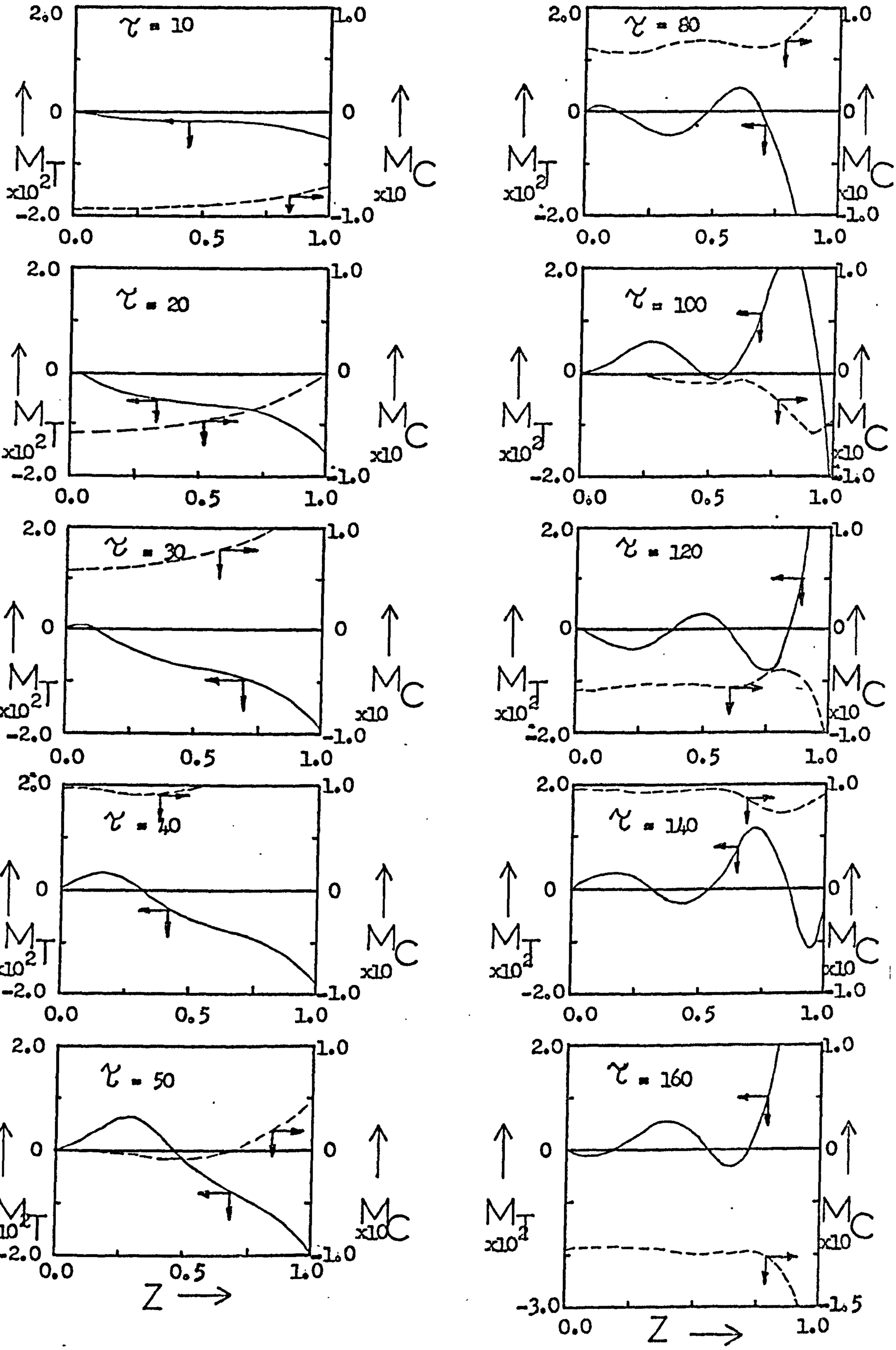

Figure 6.18 Magnitudes of deviations of the concentration and temperature profiles from the initial steady state during the response to a dimensionless inlet concentration perturbation of the form : $C_{Ao} = 1.0 - 0.1 \sin(2\pi \times 0.02 \times \tau)$. (Data as given in Table 5.1)

amplified into the non-unique region. With negative sine waves, the low frequencies cause a similar amplification of the induced temperature crests and so the much cooled exit region of the bed is heated up to runaway temperatures.

At high frequencies, temperature runaway does not occur with a positive sine wave because the exit, or hot, region of the bed is not able to remain at a high concentration long enough to run away.

6.3.2 The Non-Unique Region

The response of the bed to oscillating inlet concentration in the region of multiple solutions is exactly analogous to that for oscillating inlet temperature.

Figure 6.19 shows the initial steady state used in this study, and those which would occur at the maximum and minimum values of an inlet oscillation of amplitude 0.1. With a positive sine wave of this amplitude temperature runaway does not occur at frequencies above approximately 0.018 Hz. Below this value, however, the quasi-stationary state exhibits runaway. When the wave is negative, at this amplitude runaway occurs at frequencies below 0.0111 Hz.

It is interesting that transient temperature runaway does not occur at this amplitude despite the fact that the trajectory of the steady state which would occur at the minimum of the oscillation crosses the lower bound of the non-unique region, as shown in figure 6.19b. Even with an inlet concentration amplitude of 0.143 which has a steady state at the minimum of the oscillation entirely outside the non-unique region, below the lower bound, transient temperature runaway does not occur.

It would appear that once runaway has occurred due to the reactor trajectory crossing the upper bound of the non-unique region, the temperatures reached in the runaway portion of the bed are so high that the thermal capacitance of the pellets helps prevent them cooling sufficiently, during a decrease in concentration, to bring this region of the bed below the lower bound of the non-unique region.

The way in which temperature runaway develops at low frequencies is exactly the same as that described in the previous section, as is the way it is prevented at high frequencies.

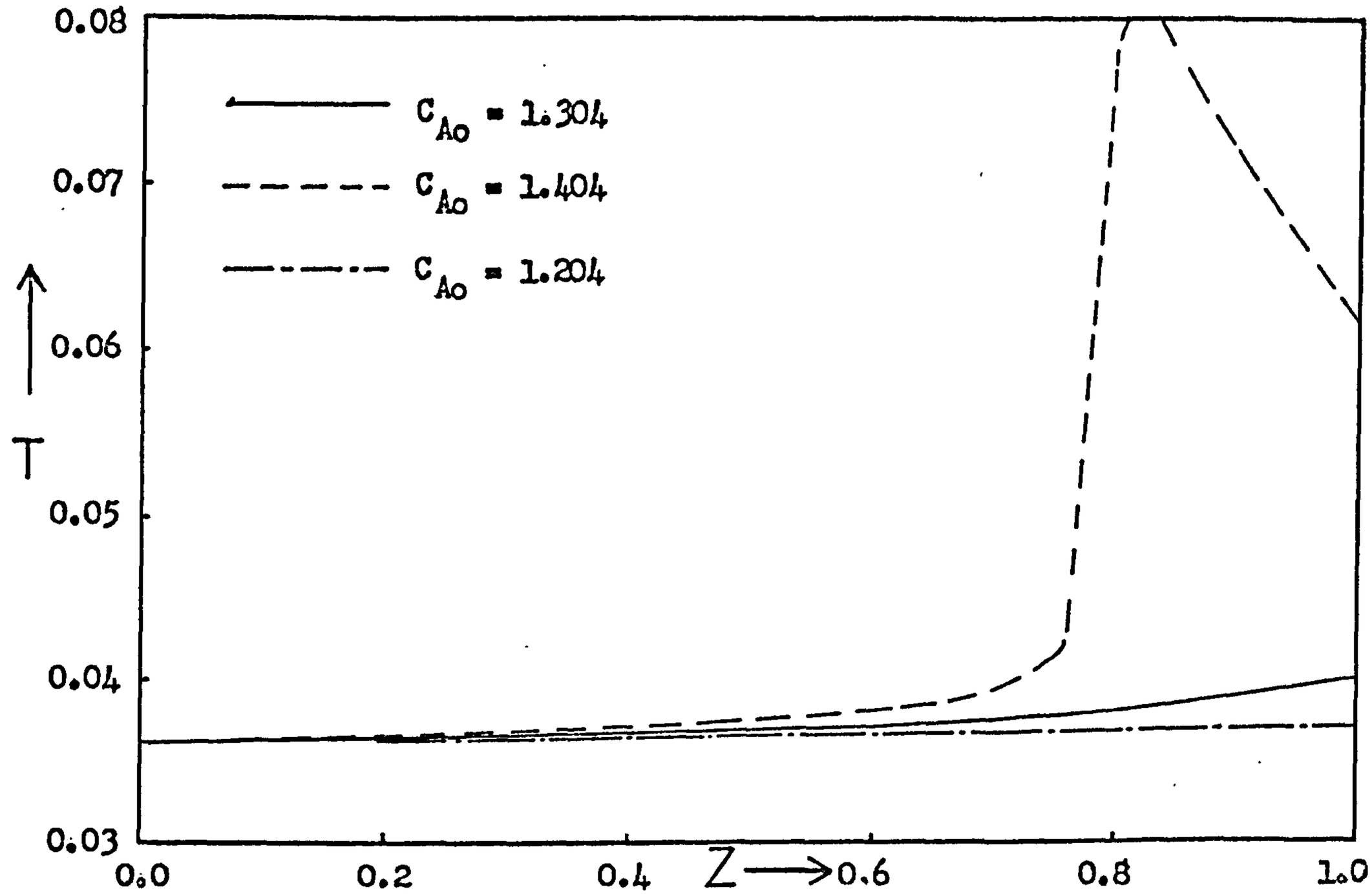

Figure 6.19(a) Steady state axial profiles of radial mean temperature at the mean, maximum and minimum values of a sinusoidal perturbation of dimensionless inlet concentration of amplitude 0.1 in the non - unique region. (Data as given in Table 5.1)

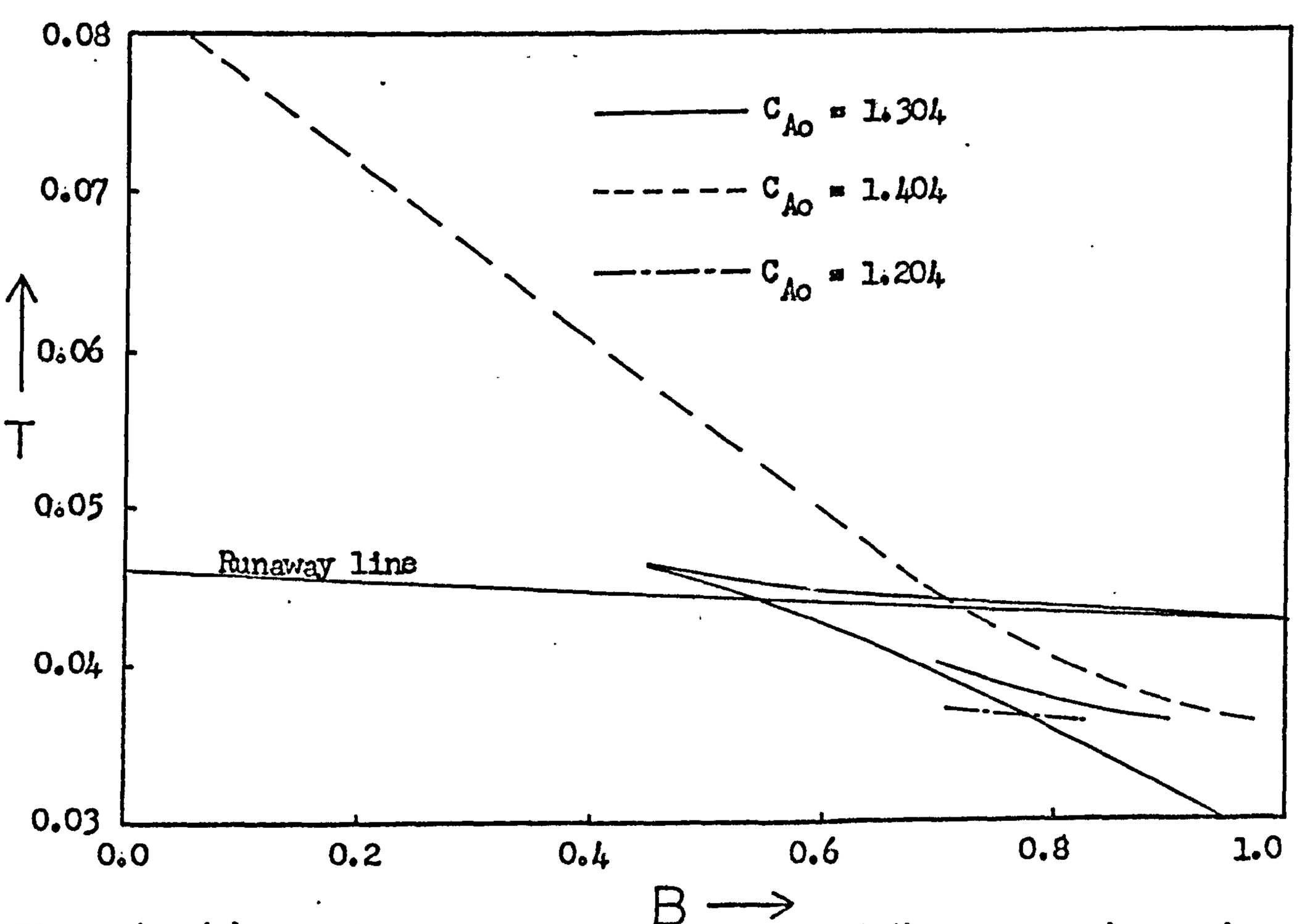

Figure 6.19(b) Steady state reactor trajectories at the mean, maximum and minimum values of a sinusoidal perturbation of dimensionless inlet concentration of amplitude 0.1 in the non - unique region. (Data as given in Table 5.1)

6.3.3 The Quasi-Stationary State

The quasi-stationary state behaviour of the reactor with concentration forcing is very similar to that described in section 6.2.3 for temperature forcing. For this reason it is only dealt with briefly here.

The main difference is the greater amplitude of the temperature oscillations, at all points in the bed, due to the greater concentration disturbances experienced. This feature allowed the observation of some points in the bed oscillating across the runaway line, between high and low temperature states, when the quasi-stationary state was entirely the unique region of solutions. When this occurs, subsequent points in the bed remain entirely in the runaway region. With the parameter values used in the work reported here, similar behaviour is not observed in the non-unique region, although McGreavy and Adderley[113] have reported results showing parts of a bed oscillating through the cusp of the non-unique region, between high and low temperature states, with subsequent regions of the bed remaining entirely in the runaway state. These observations suggest that once temperature runaway occurs in the quasi-stationary state, provided that it occurs before the bed exit, the runaway state will persist, unless the forcing amplitude is extremely large. The reason for this is probably the relative insensitivity of the reaction rate to concentration at high temperatures.

6.4 Concluding Remarks

This study of disturbance propagation has revealed one aspect of dynamical behaviour which appears to have been ignored by previous investigations. This is the importance of the initial transient response of the reactor, and therefore, the initial direction of the perturbation, before quasi-stationary state oscillation occurs.

In the non-unique region of solutions, over a range of frequencies the action of the initial transient determines whether temperature runaway occurs in the quasi-stationary state. In the unique region of solutions, although the quasi-stationary state is unaffected by the initial transient, temperature runaway may occur before a safe quasi-stationary state is achieved. Clearly, this behaviour is of importance in the design of a

control system.

The occurrence of such phenomena depends upon several factors besides the amplitude and frequency of the inlet oscillation. The role of the thermal capacitance of the catalyst pellets has been clearly demonstrated. This is to slow down the propagation of the temperature disturbance through the bed, and thereby either promote or prevent temperature runaway. This is accomplished on the one hand, by causing the pellet temperature to remain at a high value during a decrease in reactant concentration so that rapid reaction ensues when the concentration rises again, and on the other, by preventing the temperature from rising too high during an increase in concentration. The relative importance and domination? of these two effects depends on the spatial variation of the competing effects of heat generation by reaction, and heat removal by the coolant. This, in turn, is a function of the temperature level at any point in the bed and, therefore, depends on the initial steady state. Although only two initial states have been used in this study each amply demonstrates the general features of the reactor behaviour in unique and non-unique regions of operation.

The effect of sinusoidally varying the reactor inlet conditions has been shown to be generally similar to the results of previous single pellet studies,[85,12] although in these, one of the fluid state variables was assumed to be held constant whilst the other was perturbed. This is not, of course, how the disturbances would appear for pellets in the reactor. Here both fluid variables are continually changing at each point and the disturbances experienced at each point depend on the behaviour of the previous pellets in the bed. Because of this, global stability of the reactor is related to local stability and the general features described here indicate how these factors are related.

The ability of the reactor model used here to predict quasi-stationary state behaviour of similar general form and also showing the same unusual features as that observed experimentally indicates that it correctly identifies and describes the important physical processes in the system. Moreover, its usefulness in the interpretation of unusual experimental results has also been demonstrated.

Clearly, further investigation is required using a more detailed two dimensional model of the reactor, such as that developed in chapter 5. This would enable the determination of the important factors in the radial variations of concentration and temperature within the bed.

It would also be desirable to obtain a relationship between the forcing amplitude and frequency of the oscillation to enable the a priori prediction of temperature runaway, both transient and permanent. Such a relationship has been determined for a single pellet.[85] However, the results described here clearly demonstrate the highly non-linear nature of the reactor, and the complexity of the interactions between the important phenomena. It seems likely that this may preclude a general approach to the determination of critical parameters if an accurate description of the system is to be preserved.

CHAPTER 7

THE EFFECT OF THE COOLANT

7.1 Introduction

The results of steady state studies of heterogeneous fixed bed reactors supporting highly exothermic reactions[12,15,117] suggest that perturbations in the coolant conditions may be a source of potential operating difficulties caused, for example, by parametric sensitivity. Whilst heat transfer between the coolant and reactor tube has received considerable attention, surprisingly little work has been reported on the effects of coolant heating and flow direction in the steady state, and on the effects of perturbations arising in the coolant on the transient response of the reactor. The somewhat extensive studies of reactor performance and stability have been almost totally confined to adiabatic reactor operation or the use of a constant temperature coolant, such as a boiling liquid, surrounding the reactor tube. Although such modes of operation are widely used in industrial plants, many processes are encountered where it is not possible, and even not desirable, to operate reactors in this manner.[114,118]

Paris and Stevens[119] have shown that by appropriate cooling jacket design the hot spot in the reactor may be controlled. Banchero and Smith[118] have attempted to optimise the product yield in a shell and tube reactor containing a liquid homogeneous reaction by appropriate choice of the coolant flow rate and inlet temperature. The behaviour of autothermal ammonia synthesis converters, in which the feed gases are preheated by flowing countercurrently along the outside of the reactor tubes, has been examined by Van Heerden[124] using a very simple quasi-homogeneous reactor model. Luss and Medellin[117] have investigated steady state multiplicity in an unpacked liquid reactor with a countercurrent coolant flow. In each of these studies attention was confined to the steady state, probably because of both experimental and computational difficulties encountered with the unsteady state.

There appears to be no information on either the steady state performance or the dynamics of gaseous fixed bed heterogeneous reactors associated with coolant flow or temperature

distribution. That such a study is necessary is indicated by the results of previous investigators.[12,118,119] Also the information obtained could be used in the development of mathematical models of multitubular reactors as discussed in the next chapter. The work reported here is intended to identify the main features of reactor behaviour associated with a flowing coolant.

The models used are of a single, catalyst packed tubular reactor surrounded by an annular jacket through which the coolant flows cocurrently or countercurrently to the reacting gases. A few assumptions are necessary to facilitate the mathematical description of the system. Firstly, it is assumed that the reactor tube wall offers no resistance to heat flow and has a negligible thermal capacitance. This, of course, does not affect the steady state description of the system but greatly simplifies the dynamic model. Also, the assumption of negligible thermal capacitance of the tube wall is justified by the results presented in chapter 5. (It is interesting to note that these results suggest that a dynamic model of an autothermal system would need to take account of the tube wall since the heat transfer coefficients on each side of it are of comparable magnitude in such a system). Axial conduction of heat in both the tube walls and the coolant has been neglected and the coolant is assumed to be in plug flow. One further assumption is that there are no heat losses from the outside of the annular cooling jacket.

The reaction considered is the simple, first order, irreversible, gaseous A⟶B scheme with Arrhenius kinetics. The reactor model is the one dimensional formulation with an assumed parabolic radial temperature profile described in Appendix (2), and this is coupled with the lumped thermal resistance model of the catalyst pellet.

7.2 The Steady State Cocurrent Model

7.2.1 Formulation and Solution of the Equations

For the system described above with cocurrent coolant flow, a heat balance on the coolant gives:

$$M_c c_{pc} \frac{dT'_c}{dz'} - 2\pi RU(T'|_{y=R} - T'_c) = 0 \qquad (7.1)$$

with the boundary condition:

$$T'_c = T'_{c0} \quad \text{at} \quad z' = 0$$

$T'\big|_{y=R}$ is the temperature of the tubeside gases at the tube wall.

Making equation (7.1) dimensionless and expressing the tubeside gas temperature in terms of its radial mean value gives:

$$\frac{dT_c}{dz} - \frac{2Nu^*_w}{G_{cc}}(\bar{T} - T_c) = 0 \qquad (7.2)$$

with the boundary condition $T_c = T_{c0}$ at $z = 0$

where

$$G_{cc} = M_c c_{pc} / \pi L K_f e$$

and the other symbols are as previously defined.

Equation (7.2) is coupled with the tubeside equations given in Appendix (2), through $\bar{T}$ and T_c, and must, therefore, be solved simultaneously with them. The most convenient method of solution has been found to be the finite difference procedure, used for the tubeside equations, described in Appendix (2) since the existing subroutines could be used. The only difference in the method of solution of the set of equations from that described in Appendix (2) is that at each axial position along the reactor, the value of T_c must be first assumed and then subsequently calculated in the same manner as the reactor state variables, C_A and $\bar{T}$.

7.2.2 Discussion of the Results

The basic set of data used for the simulations is given in Table 5.1. The value of the dimensionless group G_{cc} is proportional to both the mass flow rate of the coolant and its specific heat. The other parameters which consitute G_{cc} appear in dimensionless groups in the tubeside equations. Thus, variations in the size of G_{cc} alone reflect changes in the size of the annular cooling jacket, the velocity of the coolant or its physical properties. Molten inorganic salts are usually used as the cooling medium at the high temperatures of interest here. What little data is available on the heat transfer properties of molten salts[120,121] suggests that the coolant to wall heat transfer coefficient is not a strong function of temperature and varies with $M^{0.8}$ where M is the mass flow rate per unit cross-

sectional area of the tube. (It should be noted that this is for flow inside a cylindrical tube, although it appears that the relationship also holds for flow of the salt through an annulus.[121] In the simulations discussed in this chapter, the value of this heat transfer coefficient is assumed to be constant. For reactors of this type, it is usually arranged that the inside gas to wall heat transfer coefficient is smaller than the outside wall to coolant coefficient by at least an order of magnitude and so variations in the outside value have but little effect on the overall value. This point is discussed in more detail in the next chapter. For this reason no relation between the overall heat transfer coefficient and the coolant flow rate, or value of G_{cc}, need be considered in the models, although for the basic data set a value of G_{cc} (approximately 600) has been computed which is consistent with the overall heat transfer coefficient used, for a ratio of 1:10 between the gas to wall and wall to coolant coefficients.

Figure 7.1 shows axial profiles of both the radial mean tubeside gas temperature and the coolant temperature predicted by the model described above compared with those predicted by the constant coolant temperature model. Clearly, for the data and coolant flow rate which have been used here the difference between the two models is extremely small. The coolant is flowing fast enough to avoid being significantly heated. At lower coolant flow rates much more heating takes place. This effect is demonstrated by figure 7.2 which shows the two temperature profiles at various values of G_{cc}. The effect of G_{cc} on these profiles is non-linear. This is because a lower coolant flow rate causes greater heating of the coolant which, therefore, maintains the latter regions of the bed at a higher temperature. This, in turn, causes a greater rate of reaction and, therefore, heat generation and the rate of reaction is non-linearly dependent on temperature. This causes greater heating of the coolant, and so on. It is apparent from both figures 7.1 and 7.2 that except at very low values of G_{cc} (i.e. low values of coolant flow rate or heat capacity) very little coolant heating occurs.

The effect of the coolant inlet temperature on the axial temperature profiles within the bed at two extreme values of G_{cc} is shown in figure 7.3. As would be expected from previous

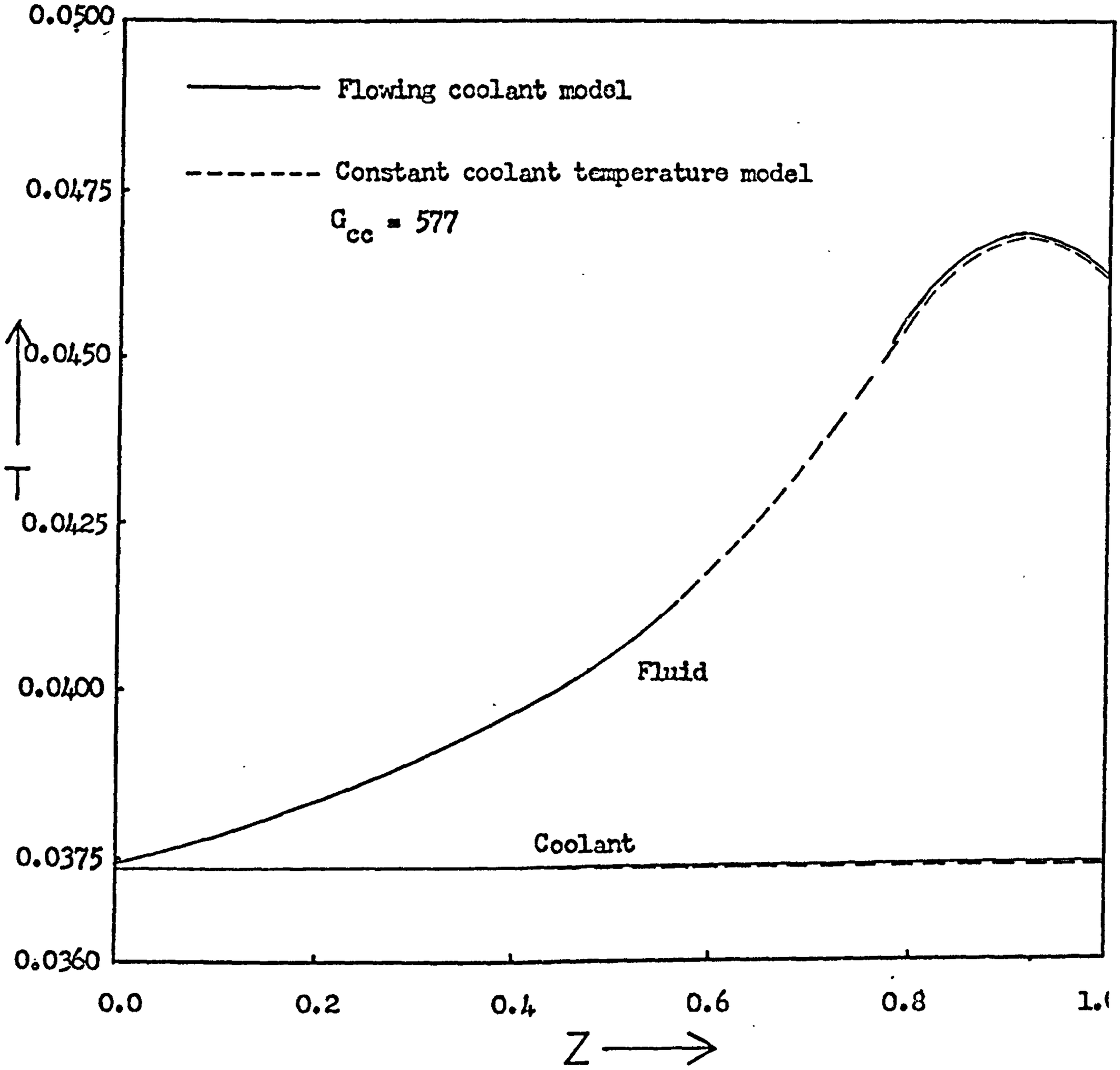

Figure 7.1 Comparison of the steady state axial profiles of radial mean tubeside temperature and coolant temperature predicted by the cocurrent flowing coolant reactor model and the constant coolant temperature model. (Data as given in Table 5.1)

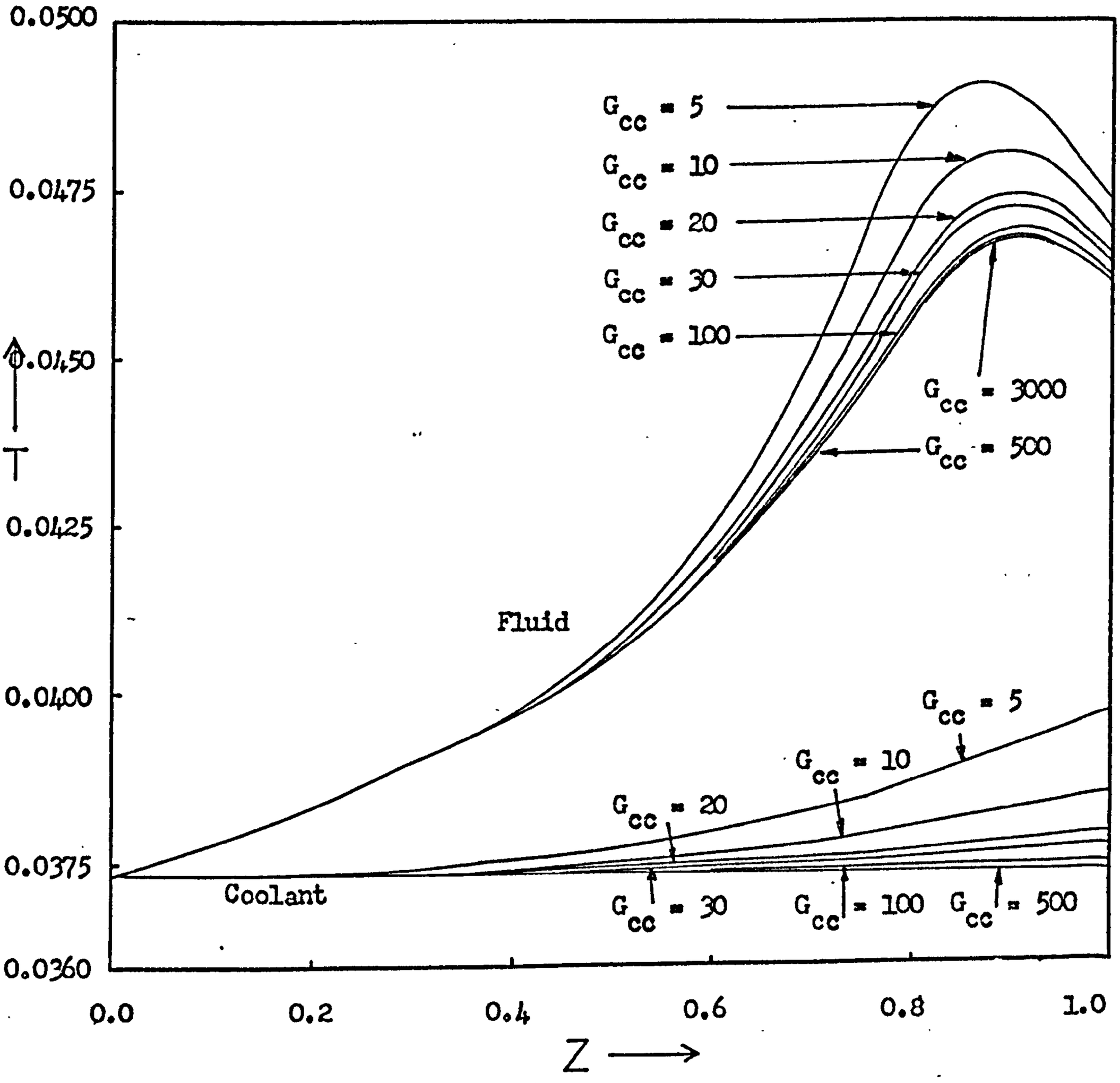

Figure 7.2 The effect of the parameter G_{cc} on the axial profiles of radial mean tubeside temperature and coolant temperature with cocurrent cooling of the reactor tube. (Data as given in Table 5.1)

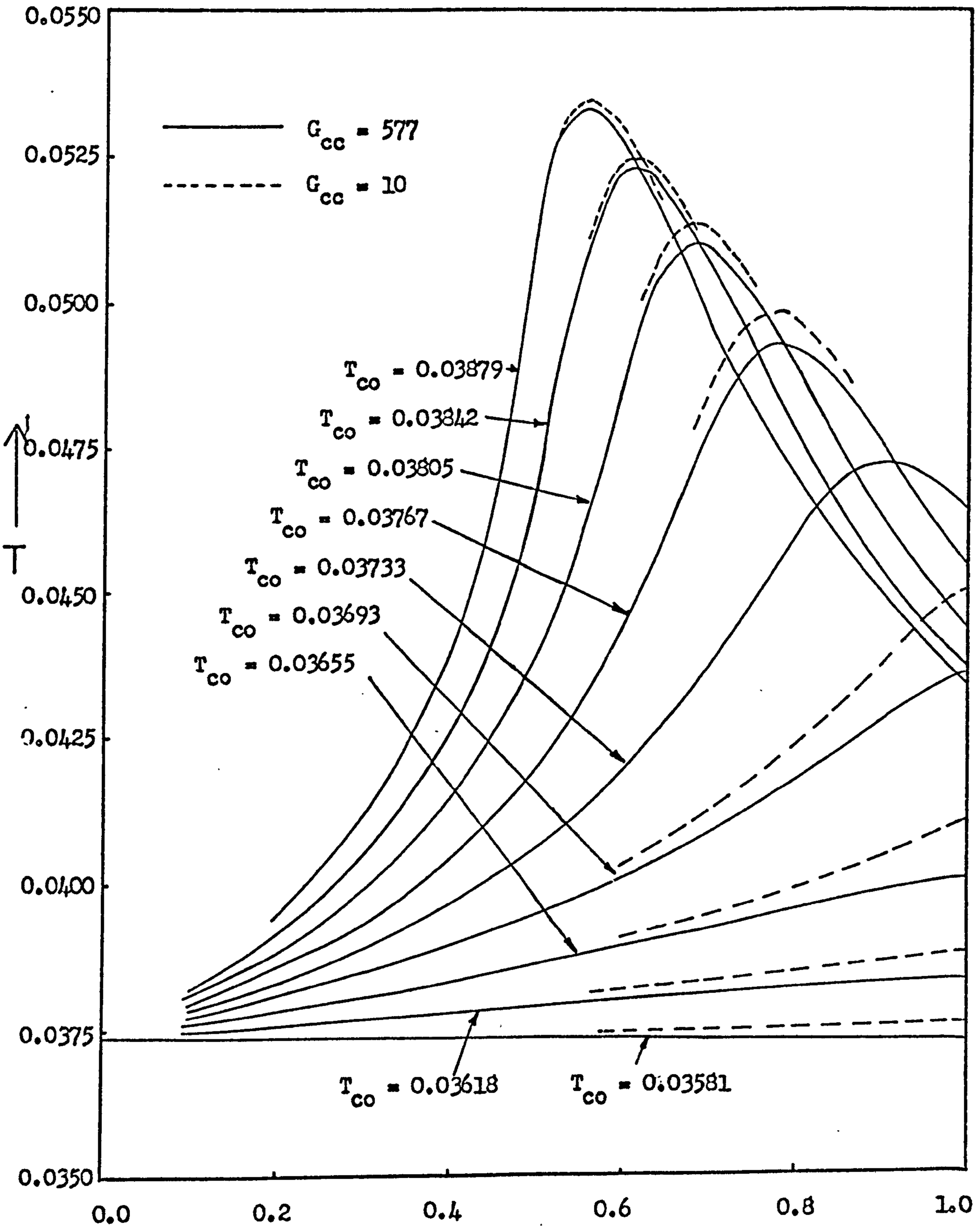

Figure 7.3 The effect of the coolant inlet temperature on the axial profiles of radial mean tubeside temperature at two values of G_{cc} with cocurrent cooling. (Data as given in Table 5.1)

results, the system shows the same sensitivity to inlet coolant temperature as is displayed with constant temperature coolants. This further emphasises the need for an investigation of the effect of coolant perturbations on the reactor.

The steady state performance of the reactor is not significantly affected when the coolant and gas streams flow co-currently; so, at least for the data used here, the assumption of a constant temperature coolant appears to be a reasonable approximation in the steady state. This, of course, means that the steady state stability criteria developed for constant coolant temperature reactors may also be applied in the case of a co-currently flowing coolant. However, since the extra computational effort required by the flowing coolant model is very small it is particularly convenient for defining accurately the initial conditions for the dynamic model which is discussed in section 7.4.2 of this chapter.

7.3 The Steady State Countercurrent Model

7.3.1 Formulation and Solution of the Equations

For coolant flow countercurrent to that of the gases in the system described in section 7.1 a heat balance on the coolant gives, in dimensionless form:

$$\frac{dT_c}{dz} + \frac{2Nu^*_w}{G_{cc}} (T - T_c) = 0 \qquad (7.3)$$

with the boundary condition

$$T_c = T_{c0} \quad \text{at } z = 1$$

Equation (7.3) is, of course, coupled with the tubeside equations given in Appendix (2). The model of the whole system is now a split boundary value problem since the coolant boundary condition is given at $z = 1$ and that of the tubeside fluid at $z = 0$. Solution of the model has been accomplished by the finite difference method as described for the cocurrent model in section 7.2.1. An iteration process is necessary to meet the boundary condition of equation (7.3) at the reactor exit. The method of solution is as follows:

(1) Assume a value for T_c at $z = 0$
(2) Solve the fluid equations simultaneously with equation (7.3) for the whole bed from $z = 0$ to $z = 1$ and so obtain a value of T_c at $z = 1$.

(3) Compare the value of T_c at $z = 1$ from step (2) with the actual (given) value. If convergence to within a prespecified limit is obtained then the solution is complete. If not, adjust the value of T_c at $z = 0$ accordingly and repeat from step (2).

A very simple method of convergence has been used to obtain the correct value of T_c at $z = 0$; if a linear relationship between $T_c|_{z=0}$ and $T_c|_{z=1}$ does not give sufficient accuracy then a quadratic fit is attempted. Failing this a cubic relationship is employed. At high values of G_{cc} the linear relationship usually proves adequate and so convergence occurs after only three iterations. As the value of G_{cc} decreases a parabolic or cubic fit becomes necessary depending on the accuracy of the first guess. Even with G_{cc} as low as 10.0, the cubic fit gives sufficient accuracy and so only five iterations are required. Since each iteration requires only approximately fifteen seconds computation when programmed in Fortran on an IBM 1130 computer, this rather crude method of obtaining convergence of the solution is quite tolerable.

7.3.2 Discussion of the Results

Figure 7.4 shows axial profiles of the tubeside gas temperature and coolant temperature at two quite different values of G_{cc} and with the coolant inlet temperature for both cocurrent and countercurrent cooling equal to the gas inlet temperature in each case. At the higher value of G_{cc} the countercurrently cooled bed is heated to a slightly higher temperature but there is very little difference between the two profiles. At the lower value of G_{cc}, however, countercurrent cooling produces a much greater temperature rise in the bed with the hot spot nearer the inlet of the reactor than in the cocurrently cooled case. This difference in the tubeside gas temperature profiles is also reflected by the coolant temperature profiles. Clearly, the reactor is much more sensitive to the coolant flow rate (or the value of G_{cc}) with countercurrent cooling.

Figure 7.5 shows plots of coolant inlet temperature ($T_c|_{z=1}$) versus coolant outlet temperature ($T_c|_{z=0}$) at various values of G_{cc}. Where a hump occurs in these curves, multiple solutions exist over a range of coolant temperatures.

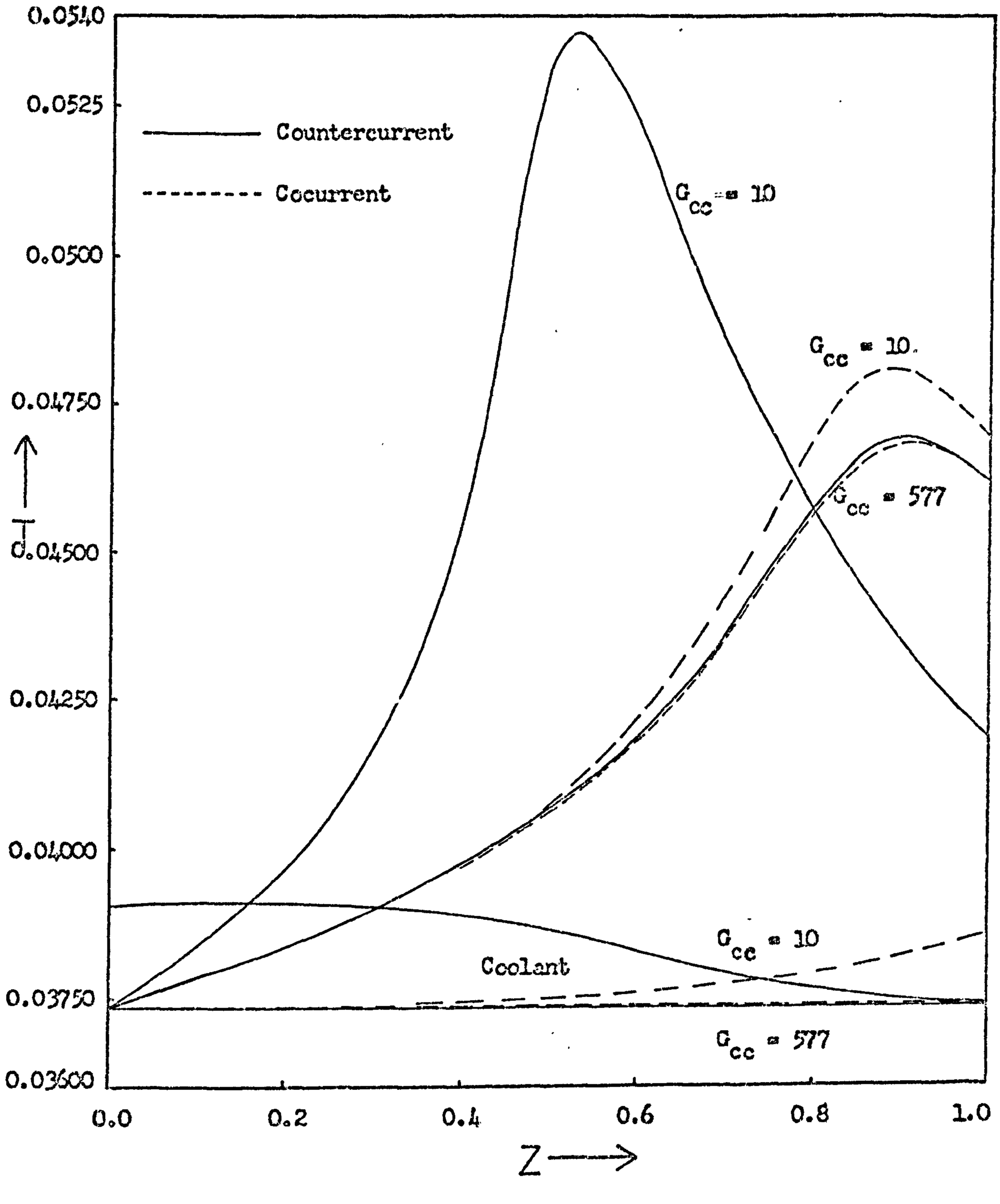

Figure 7.4 Comparison of the effects of cocurrent and countercurrent cooling on the axial profiles of radial mean tubeside temperature and coolant temperature at two values of G_{cc}. (Data as given in Table 5.1)

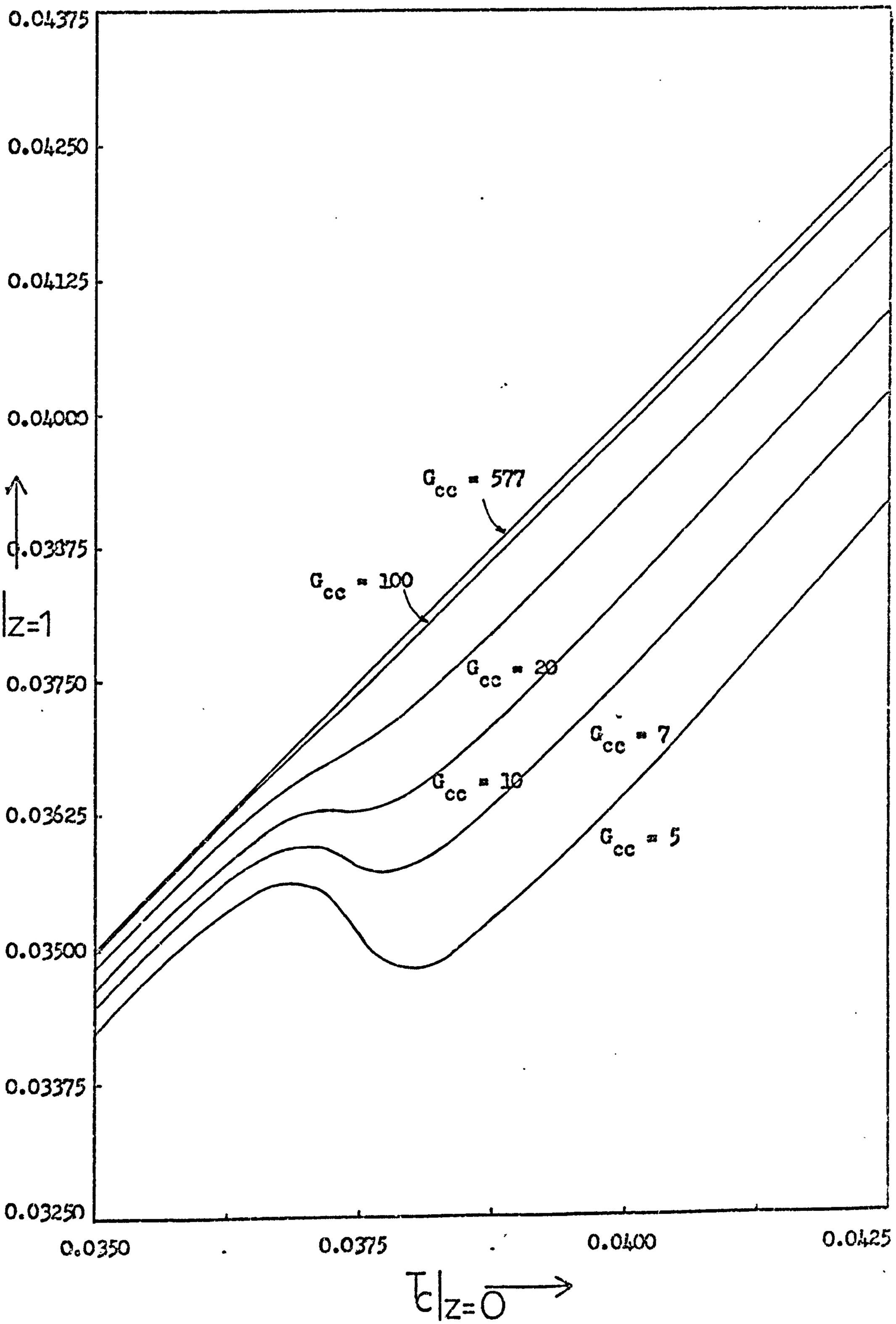

Figure 7.5 The effect of the parameter G_{cc} on plots of coolant inlet temperature versus coolant outlet temperature with counter - current cooling. (Data as given in Table 5.1)

It should be noted that this multiplicity is not due to multiplicity of the catalyst pellet solutions since the inlet value of the thermal load factor, B_0, lies well to the left of the cusp of the pellet non-unique region on the T vs. B phase diagram, and so the reactor trajectories cannot pass through this non-unique region.

Similar behaviour to that shown here has been observed experimentally by Luss and Medellin[117] with an unpacked liquid reactor and also in countercurrent liquid-liquid extraction.[122,123] It can be seen from figure 7.5 that these multiple states only occur at low values of G_{cc}, that is at low values of coolant flow rate or heat capacity. For the data used here, G_{cc}= 10.0 represents the critical value below which multiple states occur. When the heat of reaction is increased then the critical value of G_{cc} also increases; for example with $(-\Delta H)$ = 400 kcal/gmole the critical value of G_{cc} is 20.0 for the system considered here. Increasing the heat of reaction also lowers the coolant inlet temperature below which the multiple states occur for a given value of G_{cc}. This shows that the multiple states arise because of the amount of coolant heating and, therefore, the amount of heat feedback which can take place.

Figure 7.6 shows the three steady states predicted for a value of G_{cc} of 5.0 and a coolant inlet temperature of 0.0355. In the high temperature steady state temperature runaway occurs and the latter half of the reactor acts merely as a coolant preheater. The hot coolant reaching the first half of the bed causes a high rate of reaction there and so the heat generation is sufficient to cause temperature runaway. At the low temperature steady state, heat removal by the coolant is greater than heat generation by reaction in the second half of the bed and so this region is cooled. However, the coolant reaching the first half of the bed is not hot enough to heat the incoming gases and so it removes most of the heat generated there. Thus, heat removal by the coolant dominates the heat generated by reaction throughout the bed. The intermediate steady state arises as a balance of these two effects; heat generation competes with heat removal at an even rate throughout the bed.

Which steady state is attained in any given situation will clearly depend on the past history of the system, or, for example, the way the reactor is started up or shut down.

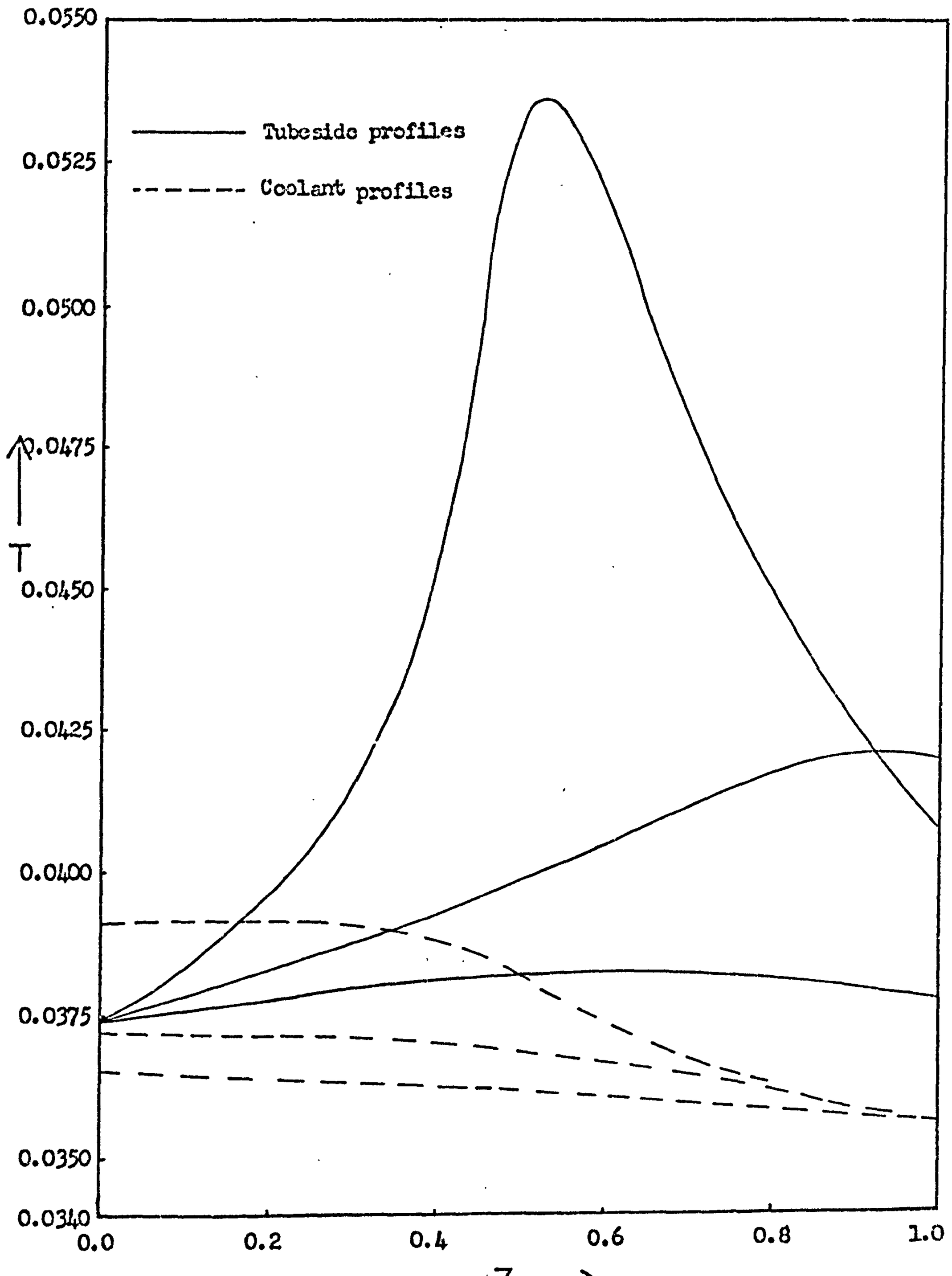

Figure 7.6 Axial profiles of radial mean tubeside temperature and coolant temperature in the three simultaneous steady states obtained $G_{cc} = .5$ and $T_c|_{z=1} = 0.0355$. (Data as given in Table 5.1)

Referring to the schematic diagram of coolant inlet temperature versus outlet temperature shown in figure 7.7, it can be seen that for a given value of G_{cc} with which multiple states are possible, the region of multiple states is bounded by an upper and a lower value of coolant inlet temperature. Multiple states do not occur at coolant inlet temperatures below T_{cl} because here the inlet coolant temperature is so low that no significant heating of the coolant can occur; the coolant inlet temperature is so far below the reactor inlet temperature that heat removal by the coolant dominates throughout the bed and prevents any reaction taking place. At coolant inlet temperatures above T_{ch}, the maximum amount of heat generation always takes place because the coolant temperature is so much greater than the inlet gas temperature and so only one steady state is possible. It can also be seen from figure 7.7 that a hysteresis effect is caused by this multiple states region. If the coolant inlet temperature is slowly raised from some point below the multiple states region for a fixed value of G_{cc}, say point A in figure 7.7, then the coolant outlet temperature will also increase and follow the curve AB. Raising the coolant inlet temperature from T_{ch} will then cause the outlet value to jump from T_{c02} to T_{c04} and with subsequent increase of outlet temperature the system will follow the curve CF. Slowly lowering the inlet temperature from, say, point F of figure 7.7 will cause the outlet coolant temperature to fall following the curve FD. Then decreasing the inlet temperature from T_{cl} will cause the outlet temperature to jump from T_{c03} to T_{c01} and then follow the curve EA. This shows why it is undesirable to operate the system in the region of multiple solutions, since severe changes in the system performance can occur if perturbations arise in the coolant inlet temperature, due to this hysteresis effect.

It is worth noting that for the data used here, the critical value of G_{cc} corresponds to an extremely low value of the coolant flow rate. However, several points must be borne in mind. Numerical simulations have shown that the critical value of G_{cc} increases with the length of the reactor, the overall coolant to fluid heat transfer coefficient and the thermal load factor at the reactor inlet, B. Luss and Medellin[117] found that in their system the occurrence of multiple states was fairly sensitive to the reactor length. Clearly, the reason for this is that the longer the reactor the more the coolant can be heated;

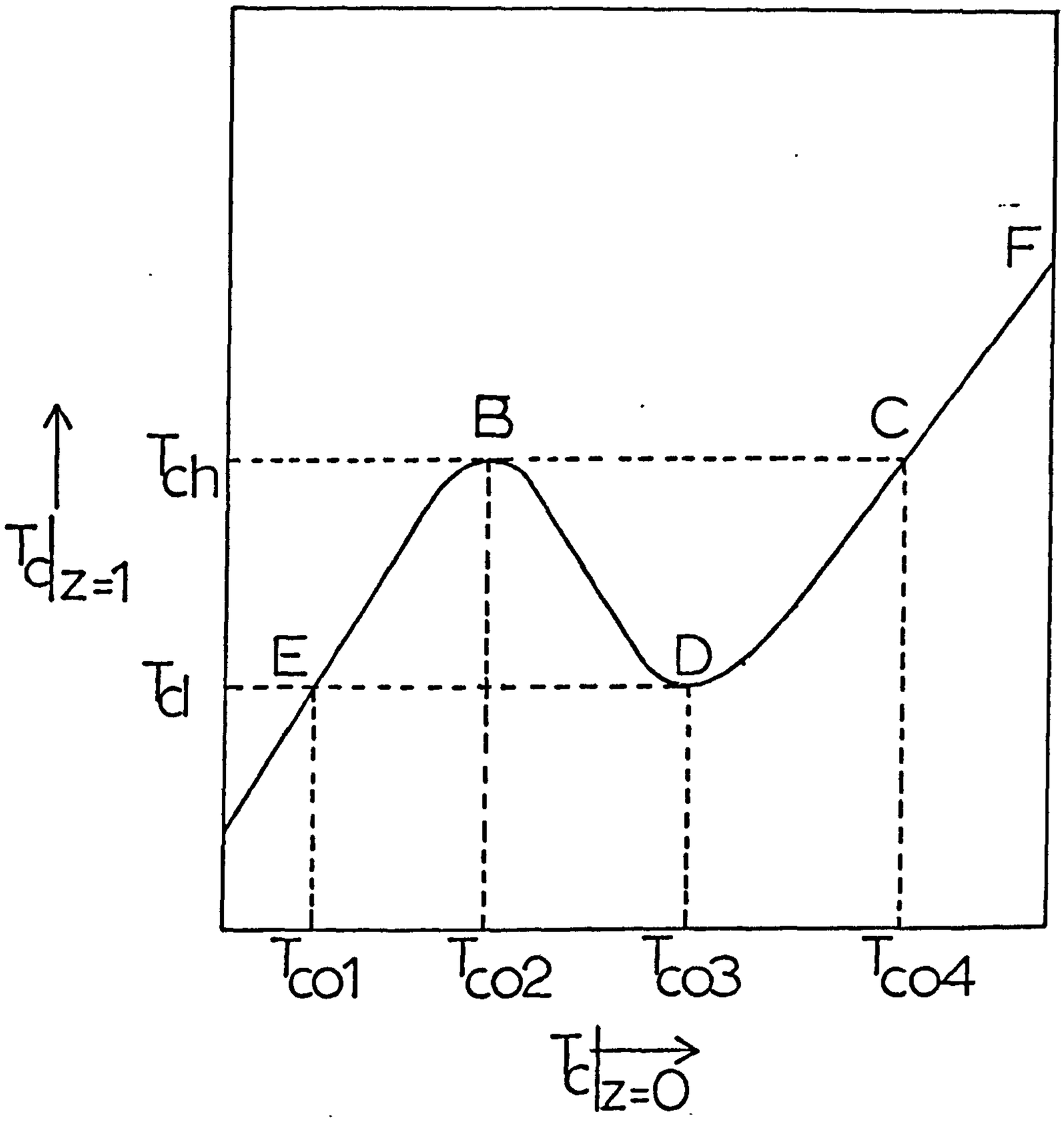

Figure 7.7 Schematic diagram of coolant outlet temperature plotted against coolant inlet temperature illustrating the multiple steady states.

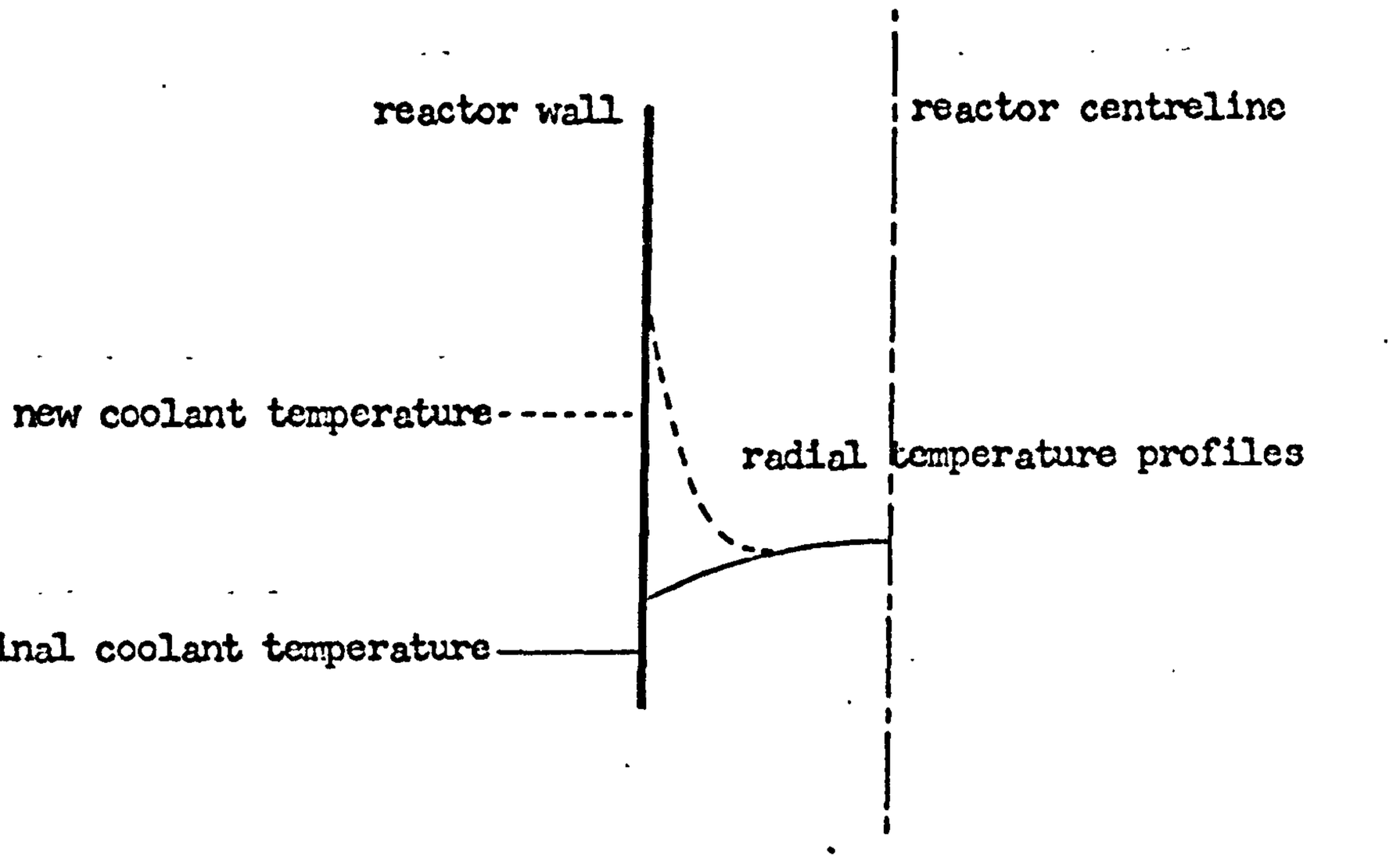

Figure 7.8 Diagram showing temporary inversion of the radial temperature profile due to a large increase in the coolant temperature.

lengthening the reactor is, in this respect, equivalent to decreasing the coolant flow rate. Since the inlet value of the thermal load factor, B_0, is a function of both the inlet reactant concentration and the heat of reaction, in some reaction systems the critical value of G_{cc} may become quite large. Also because the existence of multiple solutions has been identified with the occurrence of significant coolant heating, it provides a useful insight into the possible behaviour of large multitubular reactors where considerable coolant heating can occur. In the next chapter, a model of a countercurrently cooled multitubular reactor is developed which predicts the occurrence of similar multiplicity due to heating of the backward flowing coolant at moderate coolant flow rates.

A final point which must be considered is the effect of the rate limiting processes due to the transport resistances associated with the catalyst pellets. In the system considered here a heterogeneous model of the reactor has been used and so these reaction rate limiting processes have been taken into account. If a quasi-homogeneous reactor model had been used then it would have predicted this type of multiplicity at much higher values of G_{cc} for the same inlet conditions. This is because the quasi-homogeneous model does not take into account the reaction rate limitations associated with the catalyst pellets and, therefore, predicts a greater rate of reaction and heat generation for the same conditions. Clearly, then, any operating conditions determined by a quasi-homogeneous reactor model to avoid this type of multiplicity would tend to be rather conservative and this is a further illustration of the need to use a heterogeneous model for heterogeneous systems.

7.4 Dynamic Models

7.4.1 Introduction

To investigate the response of the reactor to perturbations arising in the coolant, as with the study of any dynamical system, it is desirable to use a model which can be rapidly solved and yet is reasonably accurate. This is especially so in the case of a reactor with countercurrent cooling where an iterative type of solution is necessary because of the split boundary conditions. The one dimensional model is, therefore, immediately more attractive than the two dimensional description for the reasons given in chapter 5. However, perturbations in

coolant temperature may affect the shape of the radial temperature profiles to such an extent that the one dimensional model, which gives radial mean temperatures based on the assumption of retention of the parabolic form of these profiles, does not give an adequate description of the dynamic characteristics of the reactor. For example, a sudden increase in coolant temperature above that of the gas near the tube wall will tend to invert the radial temperature profile in the bed in the manner shown schematically in figure 7.8.

Such distortions might occur transiently due to the non-linear dependence of the reaction rate on temperature. The one dimensional model will not be able to describe this behaviour which could, of course, affect the performance of the rest of the bed.

However, because the one dimensional model is so much more computationally attractive, several factors must be considered, including the use to which it is put. Firstly, in reactors supporting highly exothermic reactions, it is unlikely that the coolant would be used at a temperature very much, if at all, higher than the gas and so the heat of reaction would tend to keep the gas temperature much higher than the coolant, and therefore, lessen the possibility of such behaviour. Secondly, the steady state simulations indicate that only at extremely low coolant flow rates is there any significant increase in coolant temperature, and even then the gases within the tube are at a much higher temperature than the coolant in the region where heating occurs. Thirdly, the relatively large thermal capacitance of the coolant suggests that it would tend to slow down the temperature change of the coolant and so enable the whole radial temperature profile and, therefore, the mean value to follow it more closely.

In order to gauge some of the inherent shortcomings of the one dimensional model, it has been compared with the two dimensional description under what may be regarded as the most severe form of coolant perturbation. Using the constant coolant temperature models, described in chapter 5, the steady state axial profiles of radial mean temperature predicted by both models have been made to agree as closely as possible by appropriate adjustment of the overall effective wall Nusselt number, Nu_w^*, as shown in that chapter. The transient response predicted

by both models was then computed for a step increase in coolant temperature along the whole length of the reactor. Figure 7.9 shows axial profiles of radial mean temperature predicted by both models during this response. As can be seen, the agreement between the two models is good and certainly no worse than that obtained during perturbations of the bed inlet conditions (see chapter 5). The two dimensional model does, in fact, show some inversion of the radial temperature profiles near the entrance to the bed since the coolant temperature is higher than the gas inlet temperature. Since the gas temperature, and therefore the rate of reaction, is relatively low in this region the radial profiles are comparatively flat and so the radial mean temperatures predicted by both models are almost identical. Such behaviour occurs in the steady state when the coolant temperature is higher than the gas inlet temperature and Turner [71] has suggested a method of obtaining greater accuracy with a one dimensional model in such cases. In the greater part of the bed the gas temperature is so much higher than that of the coolant that the radial profiles tend to retain their parabolic shape.

Thus, the one dimensional model of the reactor would appear to be as useful for investigating the transient response of the reactor to coolant perturbations as it is for perturbations of the inlet gas concentration and temperature. This is especially so since it requires only one fifteenth of the computation time of the two dimensional model. As was emphasised in chapter 5, however, the usefulness of the one dimensional model is in obtaining an understanding of the general dynamic characteristics of the reactor and in identifying the important qualitative rather than quantitative features of behaviour.

7.4.2 Cocurrent Cooling; Formulation and Solution of the Equations

The results presented in chapter 5 show that the thermal capacitance of the tube wall has no significant effect on the dynamic response of industrial reactors; for this reason the effect of the tube wall is neglected in the formulation of the dynamic equations for a flowing coolant, and the concept of an overall heat transfer coefficient between the coolant and the tubeside gases is employed.

For cocurrent cooling, a heat balance on the coolant gives:

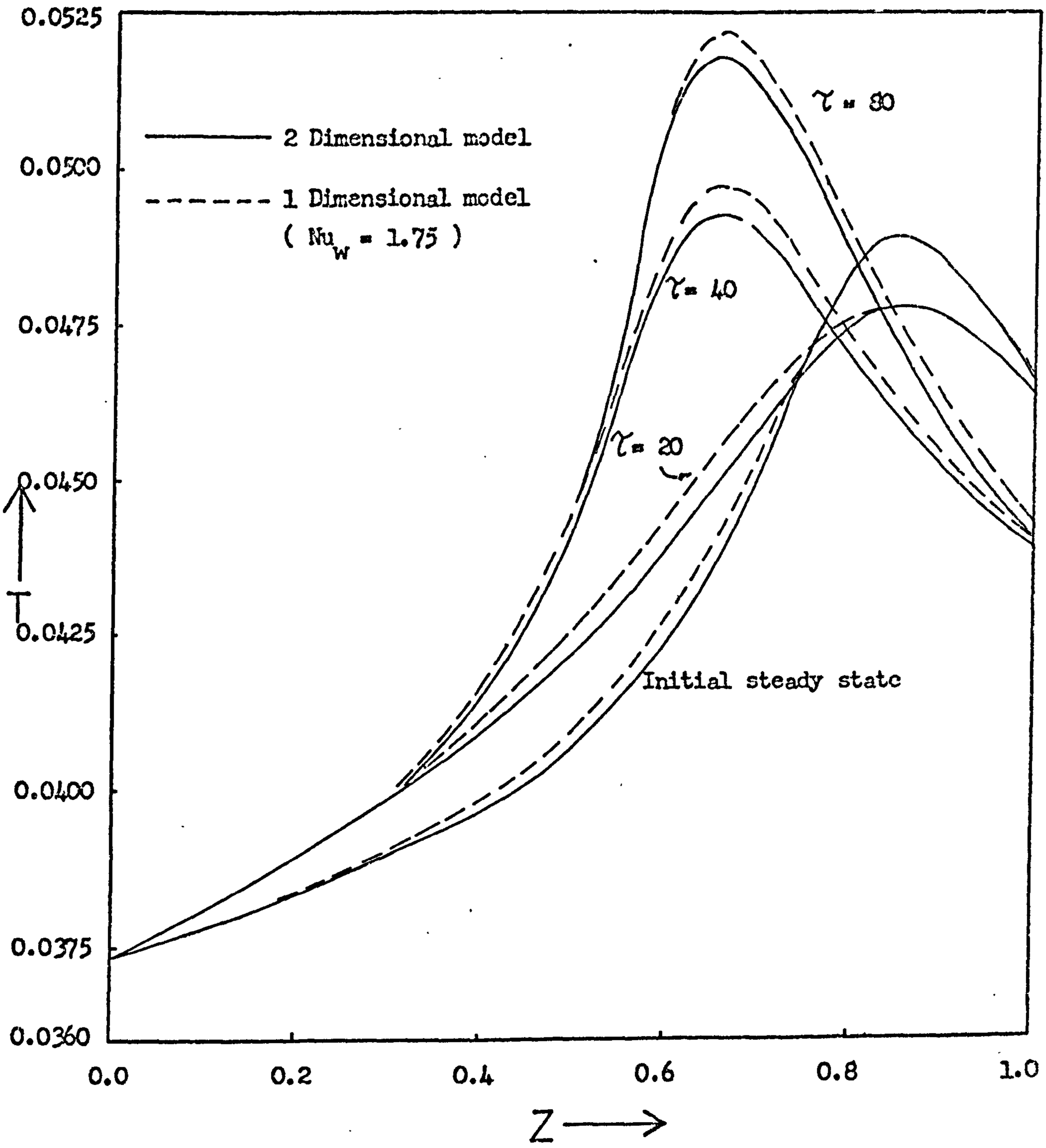

Figure 7.9 Comparison of axial profiles of radial mean temperature predicted by the one and two dimensional constant coolant temperature models following a step increase of 0.00075 in the dimensionless coolant temperature. (Data as given in Table 5.1)

$$\frac{\partial T_c}{\partial z} + \frac{2Nu^*_w}{G_{cc}}(T_c - T) + K_c \frac{\partial T_c}{\partial \tau} = 0 \qquad (7.4)$$

with boundary conditions:

$$T_c = T_{c0}(\tau) \quad \text{at } z = 0 , \tau \geq 0$$

$$T_c = T_{c0}(z) \quad \text{at } \tau = 0 , z \geq 0$$

where $K_c = L/u'_c$ and the other symbols are as previously defined.

Equation (7.4) is coupled, through the dependent variable T_c, with the dynamic reactor equations given in Appendix (2), and must be solved simultaneously with them.

Numerical studies have indicated that when equation (7.4) is solved using an implicit finite difference scheme, a very small time step of the order of 0.01 seconds is necessary to obtain a converged solution when step changes occur in the inlet coolant temperature. However, using the method of lines to solve equation (7.4), time steps of 0.1 to 0.5 seconds have been found to be adequate. This further emphasises the importance of the one dimensional model; at this size of time step use of the two dimensional model proposed in chapter 5 would be impractical.

Appendix (6) shows the application of the method of lines to equation (7.4). The method of solution of the model is similar to that described for the reactor with a constant temperature coolant in Appendix (2) except that at each axial position equation (7.4) must be solved, together with the bed equations.

7.4.3 Cocurrent Cooling; Discussion of the Results

It is not possible to investigate the response of the reactor to all possible perturbations of the coolant temperature. A more practical approach is study the kind of response for particular forms of disturbance and so try to find some pattern or general features which will characterise the system and must be taken into account when designing a reactor or its associated control system.

The dangers inherent in attempting to control the reactor by manipulation of the coolant temperature alone are well demonstrated by figure 7.10 which shows the response of the reactor following a step decrease in the inlet coolant temperature.

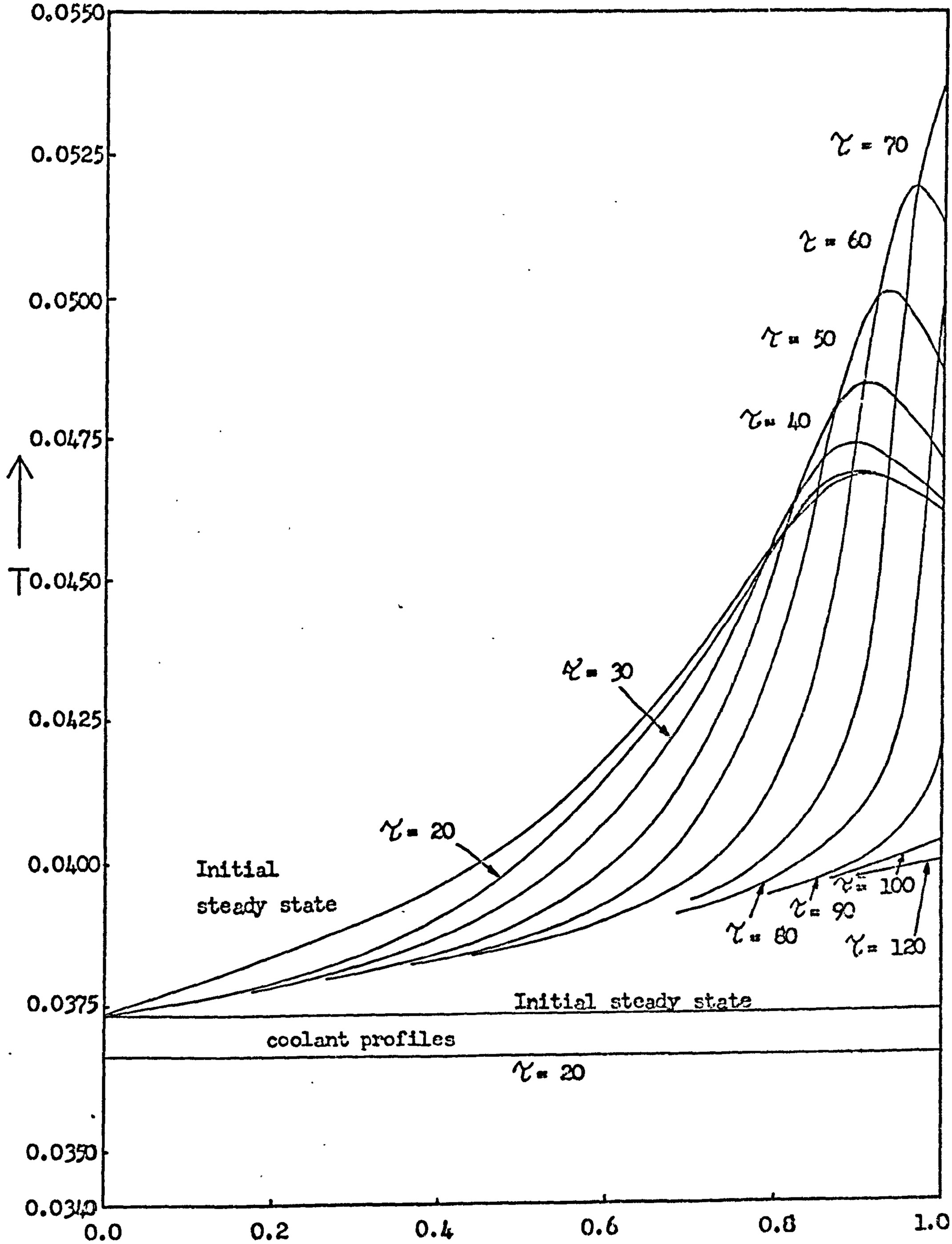

Figure 7.10 Axial profiles of radial mean tubeside temperature and coolant temperature following a step decrease of 0.00075 in the dimensionless coolant inlet temperature with cocurrent cooling. (Data as given in Table 5.1)

This induces a transient response which is in the opposite direction to the perturbation; i.e. the temperature peak increases in magnitude and runs away before the whole bed is cooled to the new low temperature state. The reasons for this behaviour are somewhat similar to those which cause similar responses when changes occur in the gas inlet temperature. The lower coolant temperature at the reactor entrance cools the gas and thereby lowers the rate of reaction there. This enables more reactant to reach the high temperature region near the end of the bed where rapid reaction ensues raising the temperature. Eventually, the heat removal by the lower temperature coolant is sufficient to force the runaway peak out of the bed and cool the whole bed. The important aspect of this behaviour is that the temperature rise shown by the hot spot is not due to the occurrence of a large temperature gradient in the coolant. At the mass flow rate given in Table 5.1 the coolant takes some 16 seconds to travel the whole length of the reactor. It might, therefore, be expected that the initial increase in reaction rate at the hot spot, caused by cooling at the inlet region, would be rapidly quenched by the lower temperature coolant reaching that part of the reactor. As figure 7.10 shows, this is not the case. This is due to spatial variation in the balance between heat removal and heat generation. Heat removal by the coolant predominates in the low temperature regions of the bed so that when the coolant temperature changes there it fairly rapidly changes the gas temperature. At the hot spot, heat generation is the dominant process and the increase in the rate of reaction caused by a higher concentration of reactant reaching this region causes heat to be generated faster than it can be removed even though the coolant temperature is lowered.

This type of response is an excellent demonstration of the distributed parameter effect and of how an apparently safe action, i.e. reduction of the coolant temperature, may give rise to temperature runaway with its associated undesirable effects.

Figure 7.11 shows the response of the reactor following a step increase in coolant temperature. Again the response is similar to that which occurs after a step increase in the gas inlet temperature. The original steady state peak decays as

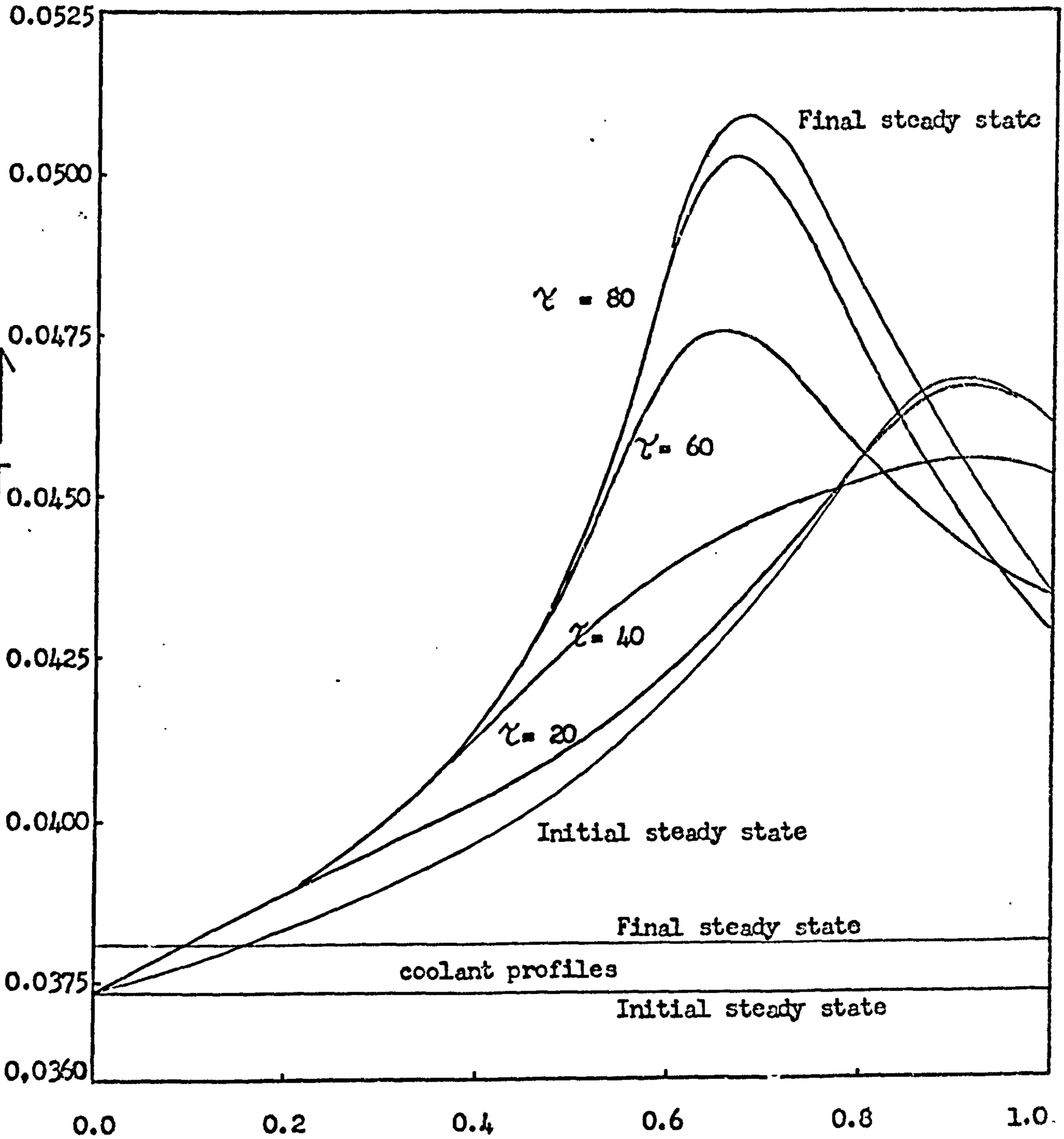

Figure 7.11 Axial profiles of radial mean tubeside temperature and coolant temperature following a step increase of 0.00075 in the dimensionless coolant inlet temperature with cocurrent cooling. (Data as given in Table 5.1)

a new one forms nearer the reactor entrance. In the light of the above comments this is the behaviour which would be expected.

The response of the reactor to ramp changes in the coolant temperature is less severe than that to step changes. Figure 7.12 shows the effect of applying a ramp decrease in the coolant inlet temperature for 40 seconds and then holding it at its final value. A wave of temperature of increasing amplitude passes from the initial steady state hot spot and out of the bed as the rest of the bed cools. The peak temperature does not reach as high a value as in the case of a step change of the same magnitude because the changes are occurring more slowly and the system has effectively more time to settle down after each change. Applying a ramp increase in coolant temperature for a limited period causes a response qualitatively similar to a step increase of the same total magnitude. This is to be expected since most of the response does not occur until after the coolant temperature has reached its final steady state.

These results further demonstrate the dangers of relying on intuitive considerations when planning a control strategy for the reactor. Although the sensitivity of the reactor to coolant temperature shown by the steady state studies indicates the coolant temperature as an attractive control variable, particularly near regions of temperature runaway, because of the distributed parameter effect of the system, considerable care must be used in its manipulation.

7.4.4 Countercurrent Cooling; Formulation and Solution of the Equations

For countercurrent cooling, the heat balance on the coolant, in dimensionless form, becomes:

$$\frac{\partial T_c}{\partial z} - \frac{2Nu^*_w}{G_{cc}}(T_c - T) - K_c \frac{\partial T_c}{\partial \tau} = 0 \qquad (7.5)$$

with boundary conditions:

$$T_c = T_{c0}(\tau) \quad \text{at } z = 1 \,, \tau \geqslant 0$$

$$T_c = T_{c0}(z) \quad \text{at } \tau = 0 \,, z \geqslant 0$$

As in the case of cocurrent cooling, equation (7.5) has been solved by the method of lines simultaneously with the dynamic reactor equations. The method of solution of the whole model is, however, slightly different since an iterative pro-

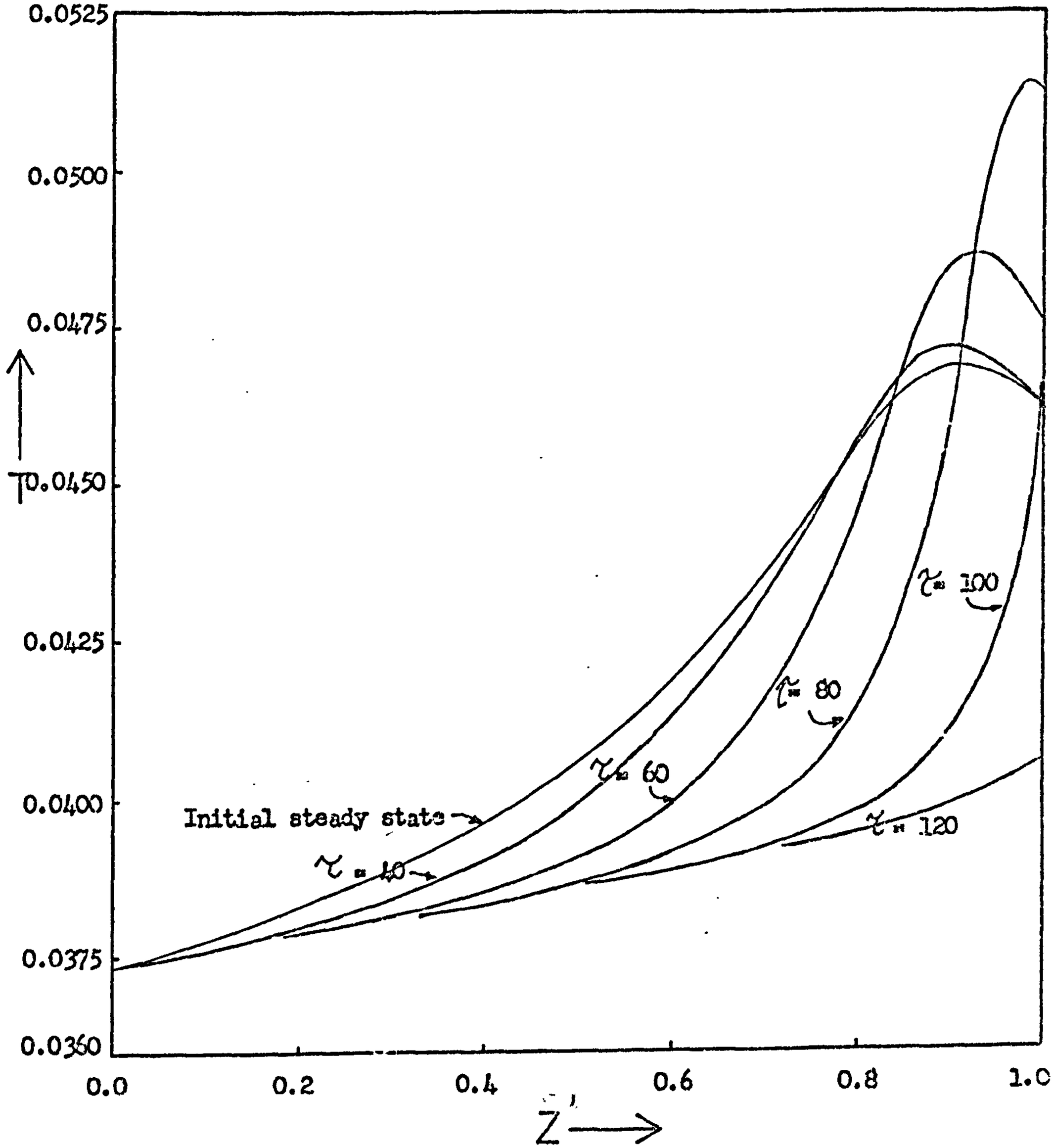

Figure 7.12 Axial profiles of radial mean tubeside temperature caused by a ramp decrease in the dimensionless coolant inlet temperature of 0.187×10^{-4} per second applied for 40 seconds with cocurrent cooling. (Data as given in Table 5.1). For the given E this change represents approximately 0.25 K per sec.

cedure is required at each time step because of the split boundary conditions.

7.4.5 Countercurrent Cooling; Discussion of the Results

It might reasonably be expected that perturbations in coolant temperature during countercurrent cooling cause a somewhat different response than with cocurrent cooling. However, as was demonstrated in the cocurrent case, the form of the response is determined by relative rates of the two main processes occurring within the bed; namely heat generation and heat removal. It is the interaction between these phenomena which makes purely intuitive reasoning unreliable.

Figure 7.13 shows the response of the reactor following a step decrease in coolant inlet temperature. Since the lower temperature coolant takes a finite time to travel backwards along the bed, the initial movement of the hot spot in the opposite direction to the perturbation observed with cocurrent cooling does not, at first, occur. Initially, the hot spot is experiencing a cooler environment than the inlet region of the bed and so the temperature there falls. As the lower temperature coolant moves further down the bed towards the entrance it causes more cooling to take place so that after 20 seconds the whole bed is at a lower temperature than it was in the initial steady state. However, the cooling of the entrance regions of the bed allows more reactant to reach the hot spot and so raise the rate of heat generation there. This increased rate of heat generation gradually overcomes the heat removal rate near the end of the bed and so the temperature rises. Eventually, as the bed cools down the hot spot is forced out of the exit. Thus, after an initial safe response, unsafe behaviour occurs. Since the hot spot experiences a lower coolant temperature before the rest of the bed, heat removal overcomes heat generation and cooling occurs there. The subsequent increase in reactant concentration reaching the hot spot, due to cooling of the entrance regions of the bed increases the rate of reaction sufficiently for heat generation to overcome heat removal. This illustrates the problems which can arise if only the hot spot temperature is monitored; both the direction of the coolant perturbation and the initial response of the reactor are apparently safe and yet unsafe behaviour still occurs.

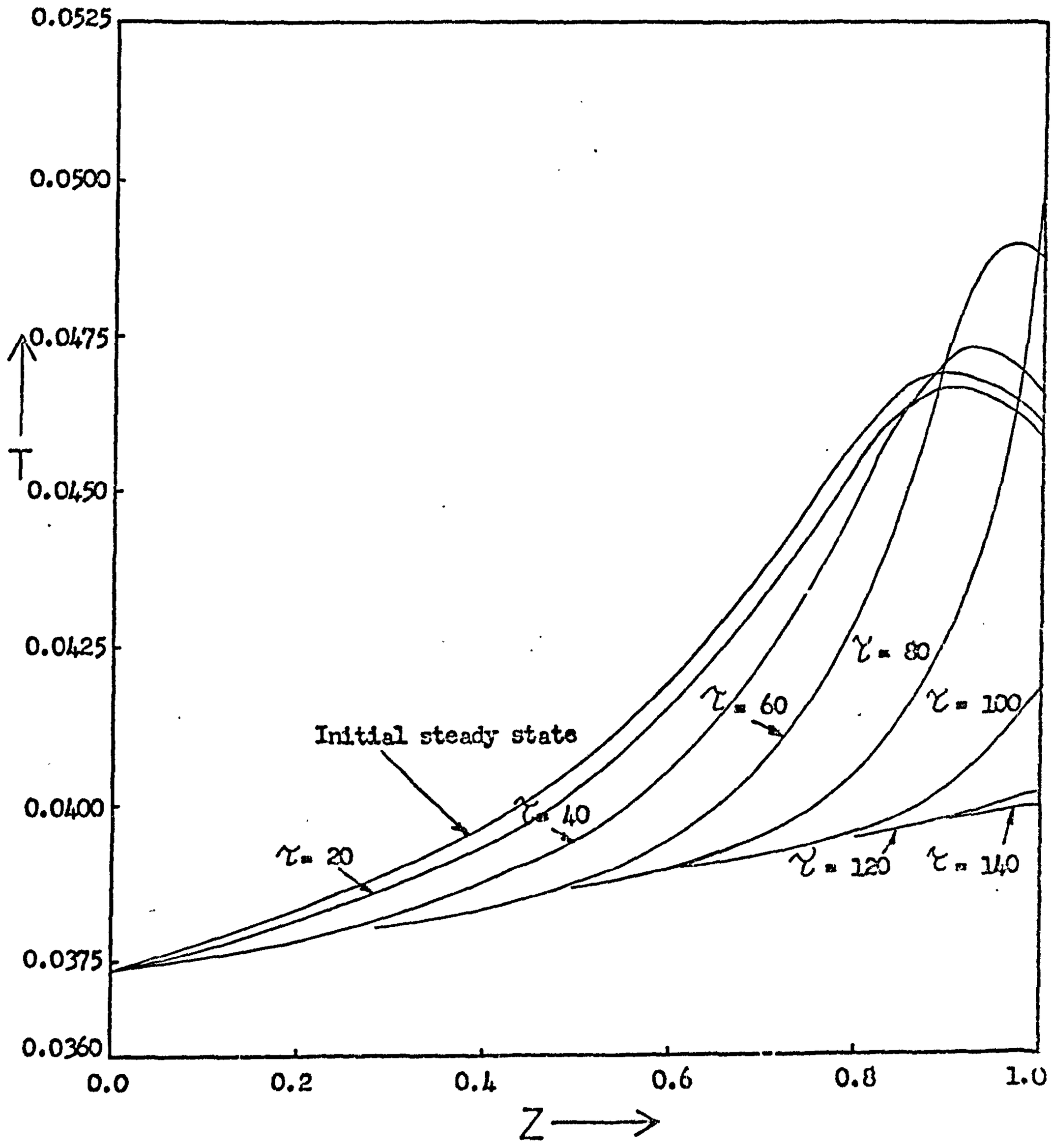

Figure 7.13 Axial profiles of radial mean temperature in the reactor following a step decrease of 0.00075 in the dimensionless coolant inlet temperature with countercurrent cooling. (Data as given in Table 5.1)

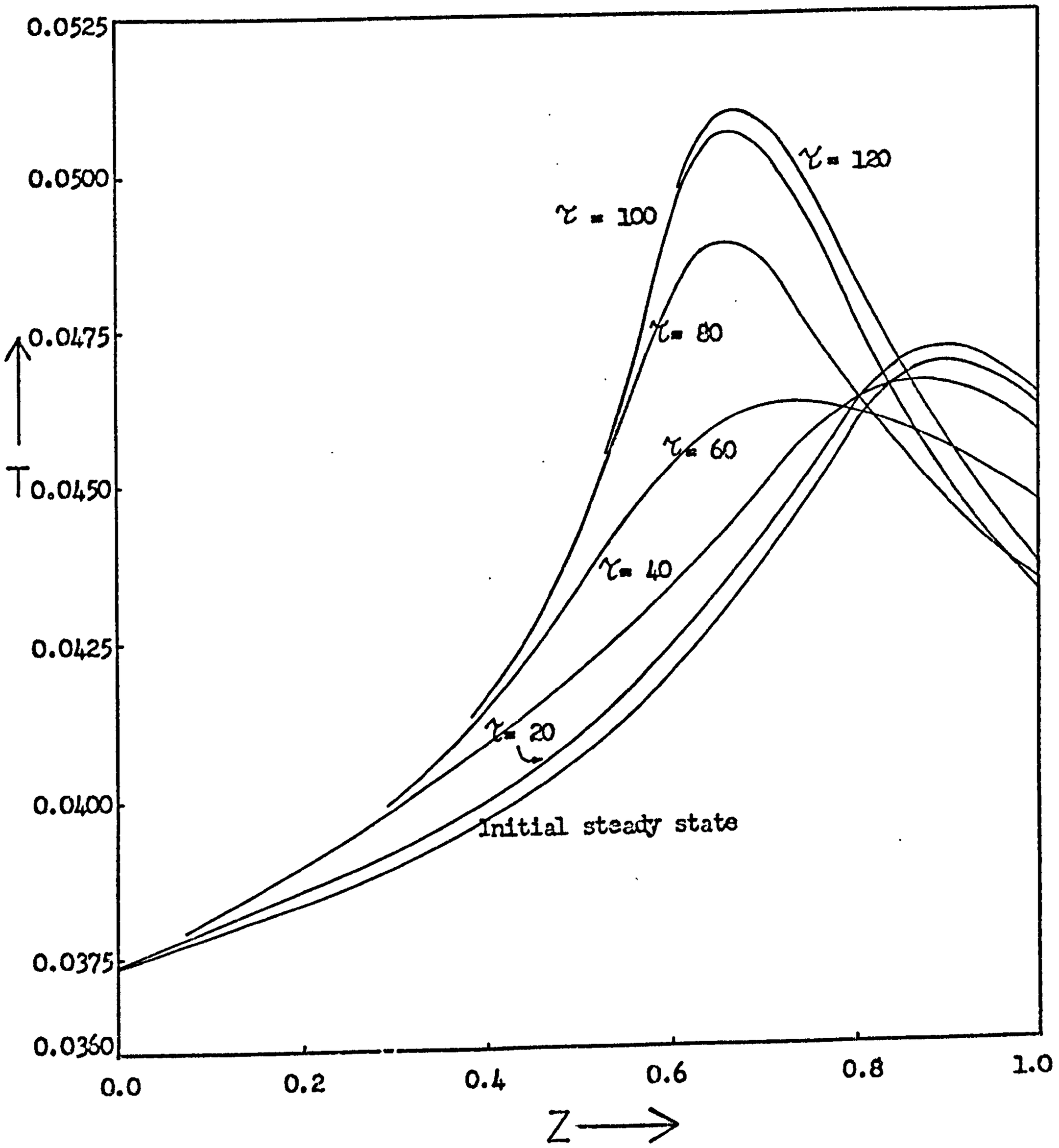

Figure 7.14 Axial profiles of radial mean temperature in the reactor following a step increase of 0.00075 in the dimensionless coolant inlet temperature with countercurrent cooling. (Data as given in Table 5.1)

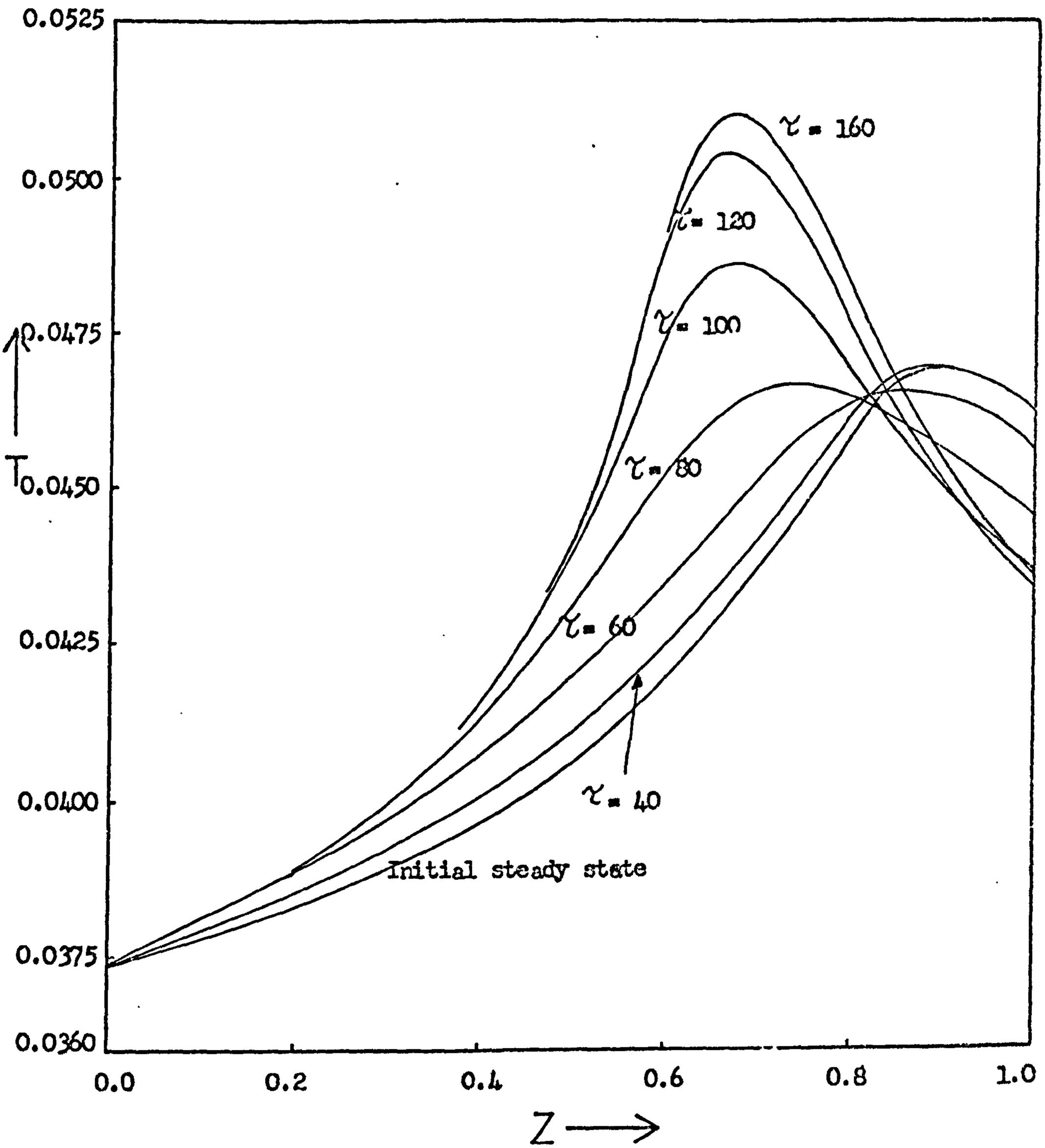

Figure 7.15 Axial profiles of radial mean temperature in the reactor caused by a ramp increase in the dimensionless coolant inlet temperature of 0.187×10^{-4} per second applied for 40 seconds with countercurrent cooling. (Data as given in Table 5.1)

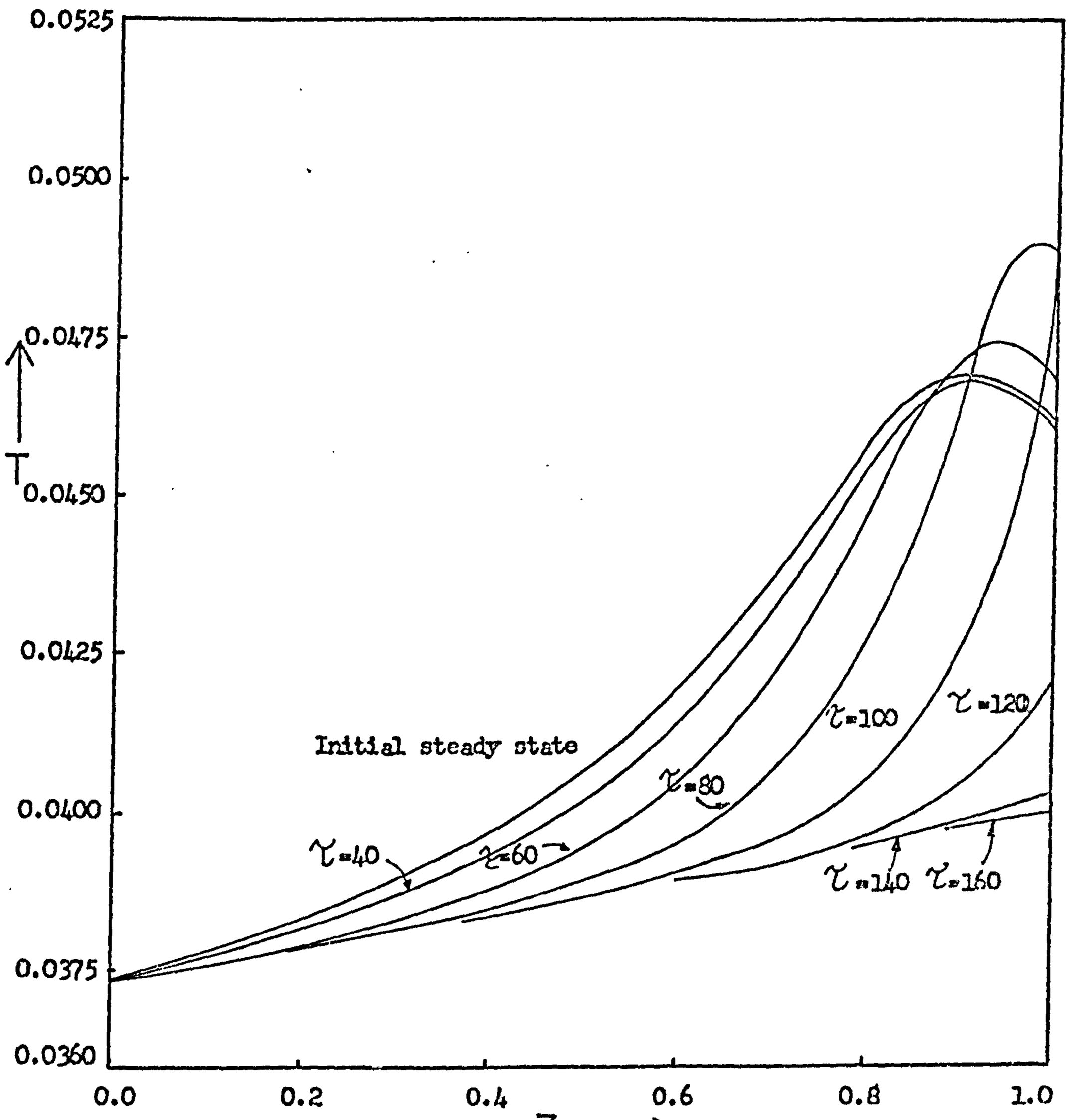

Figure 7.16 Axial profiles of radial mean temperature in the reactor caused by a ramp decrease in the dimensionless coolant inlet temperature of 0.167×10^{-4} per second applied for 40 seconds with countercurrent cooling. (Data as given in Table 5.1)

Similar behaviour is evident following a step increase in the coolant inlet temperature, as shown in figure 7.14. The hot spot region near the bed exit (coolant entrance) initially rises in temperature before it cools, and the response is then very similar to that which occurs following the same perturbation but with cocurrent cooling.

The response to ramp changes in coolant temperature is shown in figures 7.15 and 7.16. Although generally the behaviour is similar to that when step changes in coolant temperature are applied, because the coolant perturbation is far less severe the initial movement of the peak temperature in the same direction as that of the coolant is not so great. Clearly, this depends on both the actual change in the coolant temperature and the coolant flow rate. The faster the movement of the coolant, then the more the response will resemble that occurring with cocurrent cooling.

7.5 Concluding Remarks

The steady state simulations of both cocurrent and countercurrent cooling applied to the single tube reactor show that in the practical range of coolant flow rates little heating of the coolant occurs and so the behaviour in each case is very much the same. However, the amount of heating experienced by the coolant obviously depends on other factors besides the coolant flow rate; the specific heat of the coolant, the heat of reaction and the overall heat transfer coefficient between the tubeside gases and the coolant are also important parameters, and so generalisation in this respect may be inappropriate.

When coolant heating does occur along the outside of the reactor tube then the differences in reactor behaviour caused by the coolant flow direction become more apparent. In order to retain a consistent set of reactor data for purposes of comparison, heating of the coolant has been simulated by decreasing its flow rate. This has shown that at low coolant flow rates multiple steady states may occur during countercurrent cooling. This phenomenon is due to the feedback of heat by the coolant along the reactor tube. Thus, it is symptomatic of coolant heating of which a low flow rate is just one possible cause. Indeed, other workers[117] have observed similar behaviour as a function of tube length. Clearly, in a large industrial system, such as a multitubular reactor considerable

coolant heating may occur at even moderate coolant flow rates, and this point is investigated in the next chapter.

The results from the dynamic simulations clearly indicate the dangers which may arise by attempting to control the reactor by manipulation of the coolant temperature. Since the behaviour of the reactor is regulated by a balance between the competing effects of heat removal and heat generation, which can vary with time and position in the bed, the response to coolant perturbations cannot easily be predicted without simulation. This brief study has identified the important and unusual features to be expected.

The need for a more extensive study of the effect of coolant perturbations is clearly indicated and this should include a two dimensional description of the bed so that radial effects may be examined. It is hoped that improved numerical techniques currently under development[15] will make this possible.

CHAPTER 8

MULTITUBULAR REACTORS

8.1 Introduction

8.1.1 General Comments

There has been virtually no published work on the modelling of multitubular fixed bed catalytic reactors. Wanka and Gütlhuber [114] have given an excellent general account of the design factors of such reactors. Banchero and Smith [118] and Norton and Smith [125] have also described mathematical models of 'multitubular' reactors, although they have not considered the tube bundle in detail, but rather as a single tube with increased heating of the coolant.

The important features of the tubeside behaviour are now fairly well established for a single reactor tube. Since in a multitubular reactor each tube experiences a different environment which may also vary along the length of the tube, the interactions between individual tubes and how these affect the behaviour of the tube bundle as a whole need to be examined. The non-linear nature of the behaviour of a single tube suggests that these interactive effects are not purely additive, so that it may not be valid to predict the performance of a tube bundle solely by extrapolation of the behaviour shown by a single tube. Nevertheless, since a model of the tube bundle must necessarily contain a description of a single tube, it is essential to know how the single unit will behave under various conditions and this is why information from single tube studies is required. The work described here is intended as a preliminary study of the type of model which might be used in the design of multitubular reactors and an examination of the behaviour and problems associated with them.

It is appropriate to start with a description of the main types of multitubular reactors and their relative advantages and disadvantages.

Basically, a multitubular reactor is the parallel arrangement of many individual reaction units or tubes. Wank and Gütlhuber [114] have reported the construction of reactors consisting of up to 30,000 tubes. Cooling of the tubes, in the

case of an exothermic reaction, is effected externally by a flowing coolant. In the case of extremely exothermic reactions at, or, above 500C a molten salt is usually used as the cooling medium. Referring to the flow direction of the coolant around the tubes, the reactors may be divided into two broad classes; parallel flow and crossflow reactors. There are also other variations on these two main types; for example the radial flow reactor, but these will not be dealt with here.

8.1.2 Parallel Flow Reactors

Figure 8.1 shows schematically the coolant flow direction in this type of unit. The coolant flows through the tube bundle parallel to the tubes, either cocurrently or countercurrently to the direction of flow of the gases within the tubes. The advantage of this construction lies mainly in an extremely uniform temperature distribution in the horizontal plane of the coolant, across the tube bundle. Also, coolant pumping costs are reduced since the pressure drop in the coolant, as it flows through the bundle, is relatively low. The disadvantage of this type of reactor, however, is that the achievable heat transfer coefficient between the tubes and the coolant is small compared with other types of reactor, and this can be a problem in extremely exothermic reactions where there is a high heat load.

As in the case of crossflow reactors, heat losses from the shell are minimised by insulation. Thus, if the reactant concentrations and temperature at the inlet of all the tubes is uniform, as is usually the case, and the coolant enters the tube bundle at a uniform temperature, there will be virtually no radial temperature gradients in the coolant. Some heating of the coolant will occur, but this will be almost solely in the axial direction and can be controlled fairly easily.[114] The effects of axial heating of the coolant have been studied in the previous chapter. Thus, the behaviour of each tube in the bundle will be very similar in the steady state. A preliminary continuum-type model of this type of reactor has confirmed that this is indeed the case, even with the maximum realisable heat transfer coefficient at the tube wall. For this reason, this type of reactor will not be considered any further here.

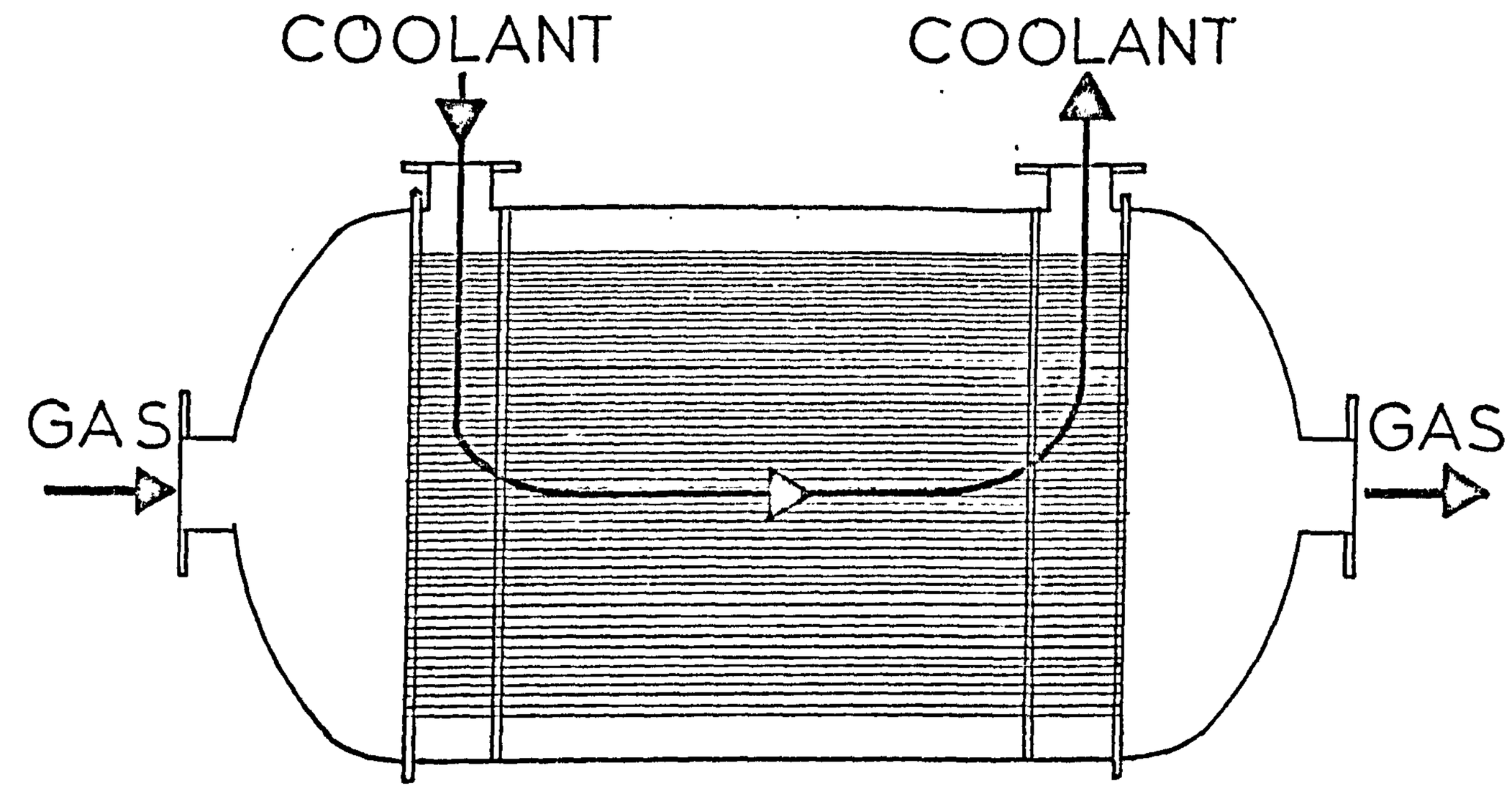

Figure 8.1 Schematic diagram of a parallel flow multitubular reactor.

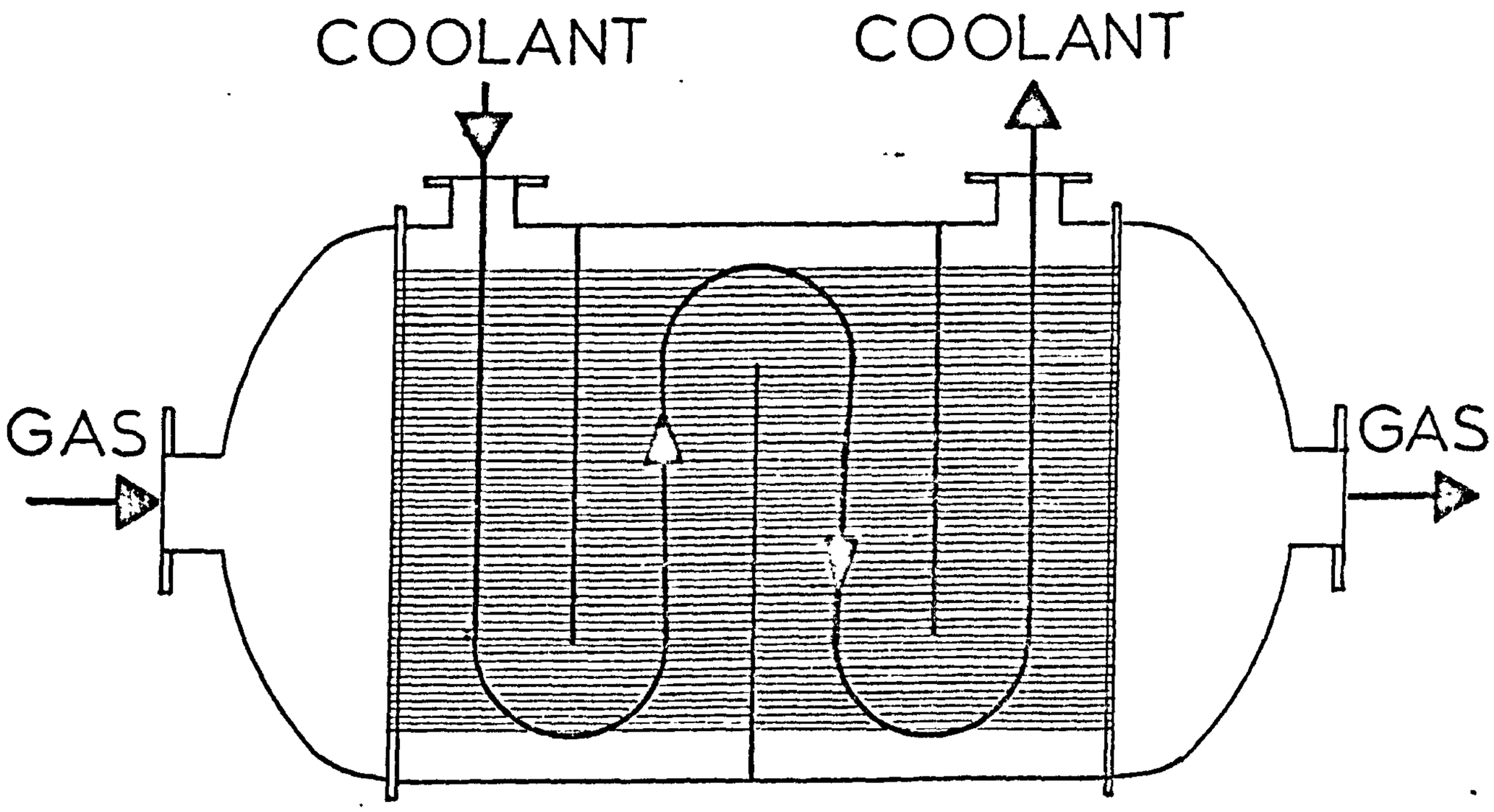

Figure 8.2 Schematic diagram of a cross flow multitubular reactor.

8.1.3 Crossflow Reactors

This type of reactor, shown schematically in figure 8.2, is separated into several sections by means of baffle plates which are installed crosswise throughout the tube bundle and which have openings at alternate sides. The coolant, therefore, travels in several passes through the tube bundle. The overall direction of the coolant may be either cocurrent or countercurrent to the direction of flow of the reactant gases.

The advantage of this type of reactor lies in the high rate of heat transfer which may be achieved between the coolant and the tubes. However, there are several disadvantages, namely a large pressure drop in the coolant and heating up of the coolant as it flows across the tube bundle. This latter factor means that a uniform temperature gradient in the horizontal plane of the tube bundle cannot be guaranteed and so tubes on opposite sides of the bundle may exhibit different behaviour. A further disadvantage of this type of reactor is the coolant leakage which can occur via the gaps between the tubes and the baffle plates. This can lead to "dead-spots," along the tubes, which are not being cooled very effectively. For these reasons, crossflow cooling is usually restricted to small diameter tube bundles.

The method of modelling both the cocurrent and countercurrent crossflow reactor is basically the same, although the performance of each type is somewhat different. For this reason the two types are dealt with separately.

Two conceptual representations of the system present themselves; the continuum model and the discrete mixing cell. The continuum model allows for an easier study of such things as mixing of the coolant, whilst the merits of the mixing cell model lie in its faster numerical solution. For these reasons both types of model of the tube bundle have been considered and compared in the cocurrent case. In the countercurrent coolant flow arrangement only the mixing cell model has been examined because of both the prohibitively large amount of computation time of the continuum model and the results of comparison of the two models in the cocurrent case.

8.2 The Tubeside Model

A reaction of industrial importance and representative of those carried out in multitubular fixed bed catalytic reactors is the partial air-oxidation of benzene to maleic anhydride which has the following reaction scheme:

$$C_6H_6 + 4O_2 \longrightarrow C_4H_2O_3 + CO + CO_2 + 2H_2O$$

$$2C_4H_2O_3 + 5O_2 \longrightarrow 6CO_2 + 2CO + H_2O$$

$$2C_6H_6 + 13O_2 \longrightarrow 8CO_2 + 4CO + 6H_2O$$

These reactions are all highly exothermic and are usually carried out in the presence of a large excess of air. Because of this the rate of each reaction can be treated as a function of the concentration of benzene or maleic anhydride only and the reaction scheme may be regarded as follows:

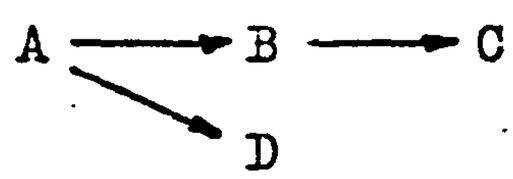

This reaction has been studied experimentally by Dave[126] and McKeon,[107] and Thornton[12] investigated the development of a suitable mathematical model of the system.

The reaction presents some difficult control problems since high conversion to maleic anhydride is desired but over-oxidation of this product, to carbon oxides and water, must be avoided. For the purposes of this study the three reaction steps are considered to be first order, irreversible Arrhenius-type reactions. The preheated air is usually greatly in excess of the benzene and so the oxygen concentration does not appear in the rate expressions.

Because there is so very little heat transfer and hydraulic data available it is sufficient to use a one dimensional model of each reactor tube. This is the model given in Appendix (2) with an assumed parabolic radial temperature profile and coupled with the isothermal catalyst pellet model given in Appendix (1).

8.3 The Crossflow Co-Current Continuum Model

8.3.1 Assumptions

For a complete and accurate description of the crossflow reactor, a momentum balance as well as a heat balance is necessary on the coolant. For design purposes it is desirable

that the velocity and, hence, the pressure drop of the coolant at all points in the tube bundle are known. For this, the amount of coolant leakage across the baffle plates must be known. Without the knowledge of hydrodynamic data, an attempt to produce such a complex model of the tube bundle would serve little purpose. Wanka and Gütlhuber[114] have found that such a model, although sometimes necessary for complete design of the reactor, must be backed up by an experimental study on a pilot reactor in order that all the parameters might be determined. Here, however, such a pilot reactor is not available, indeed the models described in this chapter might serve as a guide as to which experiments would be necessary on a pilot rig, so a simple model is proposed embodying specific assumptions about the coolant flow. By examining the resulting behaviour the important criteria for making assumptions can be determined.

Firstly, it is assumed that the coolant velocity is constant and unidirectional across the tube bundle. Clearly, this will not be the case in practice. The coolant will flow in one general direction across the tube bundle, but it will swirl around the tubes and vary in speed. However, since no data is available at present, this assumption is necessary here. The variations in coolant velocity will affect the heat transfer coefficient between the tubes and the coolant. However, it is the overall heat transfer coefficient, from the coolant to the inside of the tube wall, which is important. The external, tube-coolant, heat transfer coefficient is usually ten to twenty times greater than the inside one [114] and so large variations in the external coefficient tend to be damped down by the internal one in the evaluation of the overall coefficient. This may be illustrated by the following example. For the data given in Table 8.1, a typical value of the internal coefficient is 6×10^{-3} cal cm^{-2} k^{-1} $sec.^{-1}$ Wanka and Gütlhuber[114] give a typical value of the external coefficient as 6×10^{-2} cal cm^{-2} k^{-1} $sec.^{-1}$ Neglecting the heat transfer resistance of the tube wall, the overall coefficient would be 5.45×10^{-3} cal cm^{-2} k^{-1} $sec.^{-1}$ On doubling the external value to 12×10^{-2} cal cm^{-2} k^{-1} $sec.^{-1}$ the overall coefficient becomes 5.7×10^{-3} cal cm^{-2} k^{-1} $sec.^{-1}$ Thus, a change of 100% in the value of the external coefficient has produced only a 5% change

TABLE 8.1 Data used in the multitubular reactor models.

A_{o1}	3.62×10^{9}	sec^{-1}	θ_1	2.09×10^{5}
A_{o2}	7.99×10^{5}	sec^{-1}	θ_2	3.10×10^{3}
A_{o3}	1.60×10^{5}	sec^{-1}	θ_3	1.39×10^{3}
E_1	32.0×10^{3}	cal $gmole^{-1}$	B_o	5.01×10^{-5}
E_2	21.0×10^{3}	cal $gmole^{-1}$	H_2	0.695
E_3	18.0×10^{3}	cal $gmole^{-1}$	H_3	1.695
$(-\Delta H_1)$	367×10^{3}	cal $gmole^{-1}$	Sh_A	500
$(-\Delta H_2)$	255×10^{3}	cal $gmole^{-1}$	Sh_B	500
$(-\Delta H_3)$	622×10^{3}	cal $gmole^{-1}$	Nu	1.0
D_{pA}, D_{pB}	3.66×10^{-3}	$cm^2\ sec^{-1}$	Δ	1.0
k_{gA}, k_{gB}	4.36	cm sec^{-1}	δ	1.0
h	1.2×10^{-3}	cal $cm^{-2}\ sec^{-1}\ K^{-1}$	G_2	0.152
b	0.21	cm	G_3	0.525
L	200	cm	G_4	123.0
K_p	5.04×10^{-4}	cal $cm^{-1}\ sec^{-1}\ K^{-1}$	Nu_w	14.6
u	164	cm sec^{-1}	Nu_w^*	3.14
R	2.1	cm		
U	4.9×10^{-3}	cal $cm^{-2}\ sec^{-1}\ K^{-1}$		
e	0.4			
c_p	0.25	cal $gm^{-1}\ K^{-1}$	C_{Ao}	1.0
C_O	3.05×10^{-7}	gmole cm^{-3}	C_{Bo}	0.0
T_o'	660	K	T_o	0.0408
T_{co}'	660	K	T_{co}	0.0408
ε_c	0.2		A_1	128.0
e_c	0.43		A_2	16.8
K_c'	6.4×10^{-2}	cal $cm^{-1}\ sec^{-1}\ K^{-1}$		
u_c	5.0	cm sec^{-1}	G_c	95.0
m_c	450	gm sec^{-1}		
ρ_c	1.715	gm cm^{-3}		
c_{pc}	0.373	cal $gm^{-1}\ K^{-1}$		

TABLE 8.1 (Continued)

P_D	5.25	cm
l_c	454	cm
l_B	50	cm
l_T	1.05	cm
Number of coolant passes : 4		
Number of tubes across bundle diameter : 50		

in the value of the overall coefficient. This illustrates that it is the internal heat transfer coefficient which is limiting and so fluctuations in the external value may be neglected. The effect of variations in the inside coefficient will obviously be important. Since we are concerned with the structure of the extra-tubular model this effect has not been examined here but some results are available from Naim [15] who has investigated this problem.

An important assumption is that although a coolant temperature profile may develop along the outside of each tube there is no heat or mass transfer across the baffle plates between adjacent coolant paths. Relaxation of the assumption of no coolant leakage across the baffle plates would necessitate a detailed mass balance on the coolant in each baffled section of the tube bundle. Of course, coolant leakage does occur around the tubes as they pass through the baffle plate. The assumption of no heat transfer across the baffle plates is necessary to avoid a very time consuming iterative calculation. The effect of this assumption is discussed later.

The baffle plates are assumed to be of negligible thickness. This assumption is necessary in the light of the previous one of no heat transfer across the baffle plates. Relaxing this assumption would require the calculation of a baffle plate temperature or temperature profile. Since this would add greatly to the amount of computation to be performed, the greater sophistication is not considered worthwhile at this elementary stage.

Because of the type of model used for the tube-side conditions, the coolant temperature around the circumference of each tube is assumed constant. Temperature variations around the tubes will probably occur but they will be small and in any case they could not be measured sufficiently accurately for their inclusion in the model to be meaningful.

One further assumption is that the row of tubes across the diameter of the tube bundle is characteristic of those in other parts of the bundle. This assumption is related to that of constant velocity of the coolant. The coolant velocity will, of course, be greatest at the diameter of the tube bundle and will decrease away from the diameter where the length of the coolant path decreases. To relax this assumption would

mean considering every row of tubes in the bundle, and at this preliminary stage this is not considered to be necessary.

Mixing of the coolant in the direction perpendicular to flow is described in the continuum model presented here, but no allowance is made for mixing of the coolant along the direction of flow.

The geometric configuration considered is that of a tube bundle with the tubes arranged on a triagular pitch with a pitch circle diameter of 1.25 times the tube diameter.

8.3.2 Formulation and Solution of the Equations

Applying the above assumptions, the following differential heat balance on the coolant may be derived for each coolant pass.

$$K'_c e_c \frac{\partial^2 T'_c}{\partial z''^2} - u_c \varrho_c c_{pc} \varepsilon_c \frac{\partial T'_c}{\partial x'} + UA'(T'|_{y=R} - T'_c) = 0 \quad (8.1)$$

with boundary conditions:

$$T'_c = T'_{c0} \qquad \text{at } x' = 0,\ 0 \leqslant z'' \leqslant l_B$$

$$\frac{\partial T'_c}{\partial z''} = 0 \qquad \text{at } z'' = 0,\ 0 \leqslant x' \leqslant l_c$$
$$z'' = l_B$$

where:

K'_c = Thermal conductivity of the coolant in the direction perpendicular to the coolant flow.

e_c = voidage of the tube bundle in the direction perpendicular to the coolant flow.

ε_c = voidage of the tube bundle in the direction of the coolant flow.

A' = surface area of the tubes per unit volume of the tube bundle.

x' = co-ordinate in the direction of the coolant flow.

z'' = co-ordinate perpendicular to the coolant flow.

l_B = distance between the baffle plates.

l_c = diameter of the tube bundle.

The other symbols have the meanings used previously.

Rearrangement of equation (8.1) in dimensionless form gives:

$$\frac{\partial^2 T_c}{\partial z_c^2} - A_1 \frac{\partial T_c}{\partial x} + A_2 Nu_w^* (T - T_c) = 0 \qquad (8.2)$$

with boundary conditions:

$$\begin{aligned} T_c &= T_{c0} && \text{at } x = 0,\ 0 \leqslant z_c \leqslant 1 \\ \frac{\partial T_c}{\partial z_c} &= 0 && \text{at } z_c = 0,\ 0 \leqslant x \leqslant 1 \\ & && \quad z_c = 1 \end{aligned} \qquad (8.3)$$

where:

$$z_c = \frac{z''}{l_B} \qquad x = \frac{x'}{l_c}$$

$$A_1 = \frac{u_c \rho_c c_{pc} \varepsilon_c l_B^2}{K_c' l_c e_c} \qquad A_2 = \frac{A' K_f e l_B^2}{K_c' e_c R}$$

Equation (8.2) coupled with the boundary conditions (8.3) may be expressed in finite difference form as shown in Appendix (7).

Solution of the finite difference equations may be accomplished by marching across the tube bundle from the coolant inlet to the outlet in each coolant pass as follows:

(1) Assume a coolant temperature profile perpendicular to the direction of coolant flow at the first (i.e.inlet) or next position along the direction of flow.

(2) Using this temperature profile solve the tubeside model for the length of tube in the pass under consideration.

(3) Using the tubeside temperature profile from step (2) solve the coolant finite difference equations in the direction perpendicular to coolant flow to obtain a new coolant temperature profile in this direction.

(4) Check whether the coolant temperature profile calculated at step (3) agrees with the assumed one from step (1). If not, using the profile from step (3), repeat the calculation from step (2). If convergence is obtained and $x < 1$ (i.e.the outlet of the

(4) coolant from the pass is not reached)
go on to the next position in the direction of coolant flow and repeat from step (1). If $x = 1$ (i.e. the outlet from the coolant pass is reached), go on to the next coolant pass and repeat from step (1).

At the end of each coolant pass, where the flow reverses direction for the next pass, it is assumed that complete mixing of the coolant occurs so that it enters each pass at a uniform temperature in the direction perpendicular to flow.

Since the coolant temperature gradient in both directions has been found to be relatively small, no problems of convergence with grid size have been encountered. It is convenient to use the same grid spacing in the direction perpendicular to coolant flow, as used in the solution of the tube side model (i.e. 200 increments along the whole length of each tube). To obtain convergence in the direction perpendicular to the coolant flow, approximately 100 increments are required across the tube bundle in each pass. When programmed in Fortran on an I.C.L. 1906A computer, solution time is approximately 12 minutes with these grid sizes and the data given in Table 8.1.

8.3.3 Discussion of the Results

No data is available for the thermal conductivity of the coolant perpendicular to its direction of flow. It has, therefore, been estimated that this value might be two or three orders of magnitude greater than the molecular value of the thermal conductivity of the coolant. Several computations have been carried out using different values of this parameter and it has been found that the coolant and, therefore, the tubeside gas temperature profiles are very insensitive to the size of the coolant conductivity. Figure 8.3 shows coolant temperature profiles at the exit of each pass of a four pass tube bundle with 50 tubes across its diameter for two thermal conductivities; one is the molecular value and the other is 1000 times greater than this. As can be seen the difference between the two profiles is very small. There is also correspondingly little difference between the tubeside temperature profiles although these are not shown here. The reason for this insensitivity to K_c' is that the coolant temperature grad-

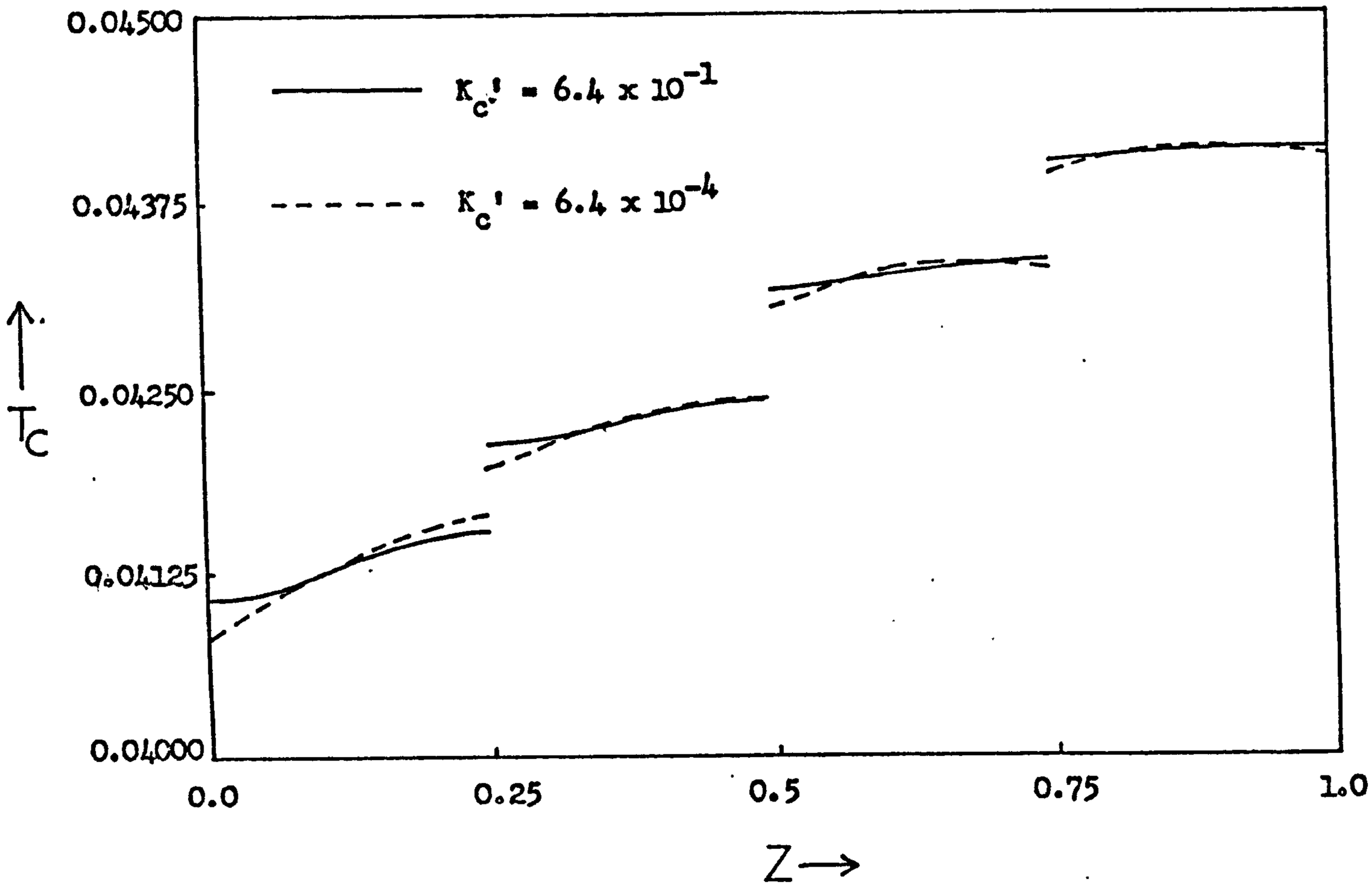

Figure 8.3 Coolant temperature profiles at the exit of each pass predicted by the cocurrent continuum model using two values of the parameter K_c'. (Data as given in Table 8.1)

ients in the direction perpendicular to coolant flow are very small since little heating of the coolant occurs in this direction. These rather flat coolant temperature profiles suggest that it might be reasonable to assume that there is no temperature gradient in the coolant in this direction and, therefore, use a mixing cell type of model for the tube bundle. This is examined in the next section of this chapter.

For purposes of identification, the first tube encountered by the coolant in its first pass across the bundle is referred to as tube 1, and the tube at the exit of the coolant from the first pass is referred to as tube N when there are N tubes across the diameter of the bundle.

Figure 8.4 shows the effect of the coolant velocity, u_c, on the tubeside temperature profiles on opposite sides of the bundle. Clearly, the slower the coolant flows across the bundle, the more it is heated and so the greater the difference between the coolant temperature profiles on opposite sides of the bundle in each pass. This means that the tubes at the coolant inlet and outlet of each pass are experiencing quite different environments and, therefore, show correspondingly different behaviour. The non-linear effect of the coolant flow rate on the tubeside temperature profiles is also evident from figure 8.4. At the higher values of flow rate a 100% change in the flow rate has little effect on the tubeside temperature profiles, whereas at the lower values such a change has a marked effect and causes tubes on opposite sides of the bundle to exhibit quite different behaviour.

Perhaps the most striking feature of the tubeside temperature profiles shown in figure 8.4 is the occurrences of discontinuities in their slopes especially at the lower coolant flow rates. This arises as a consequence of the assumption of no heat transfer across the baffle plates. This assumption causes sharp changes in coolant temperature along the tubes from pass to pass. Paris and Stevens[119] describe similar abrupt changes of slope in tubeside temperature profiles, arising from sudden changes in both coolant temperature and tube wall heat transfer coefficient, in their approach to the design of a special cooling jacket for a single reactor tube. However, they appear to have made no comment on the occurrence or attempt to eliminate it.

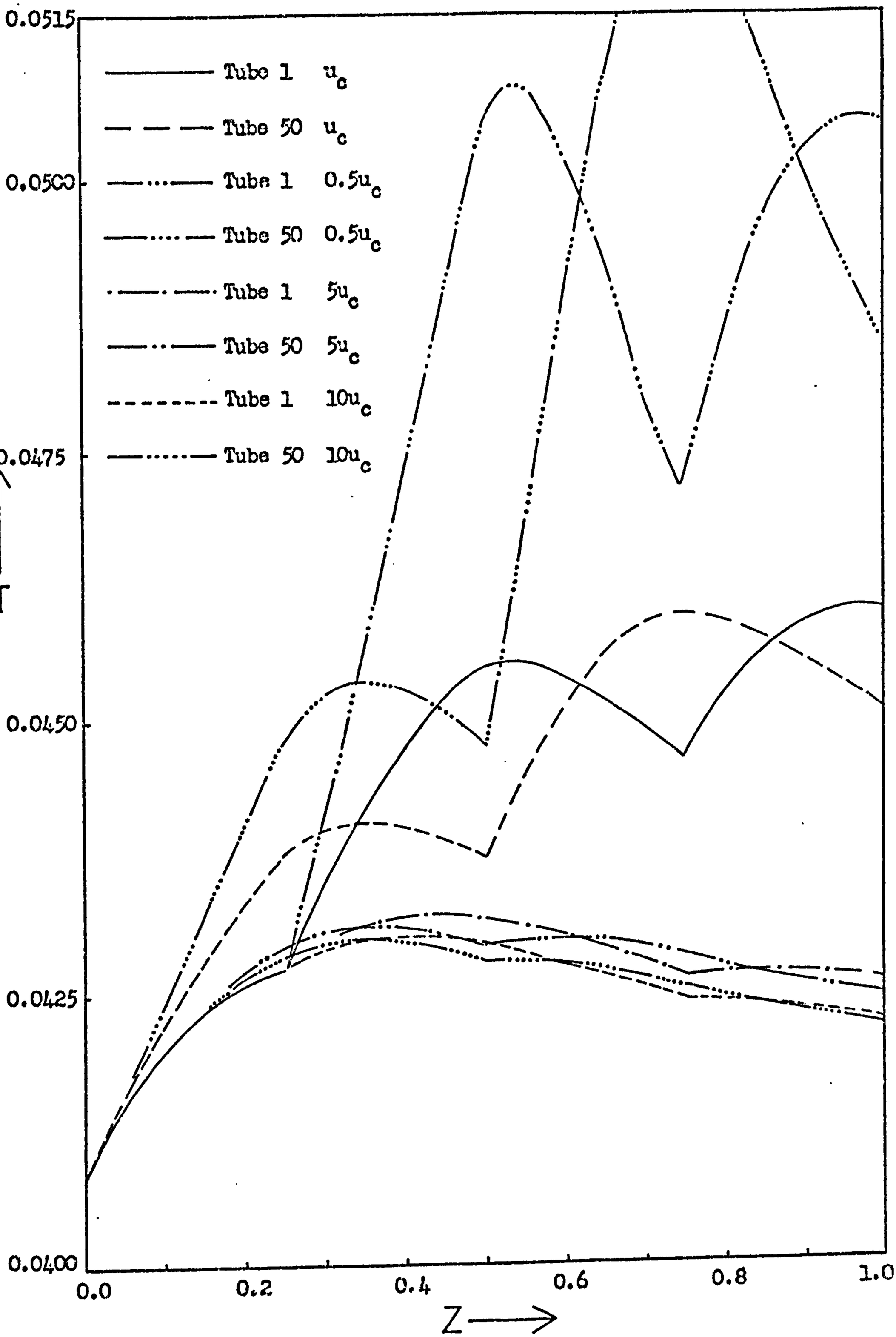

Figure 8.4 The effect of the coolant velocity on the axial profiles of radial mean temperature within tubes on opposite sides of the bundle predicted by the cocurrent coolant continuum model. (Data as given in Table 8.1)

It is highly unlikely that such abrupt changes in the coolant temperature, and therefore, such sharp changes in the slope of the tubeside gas temperature profiles occur in practice since there is transport of both heat and mass between adjacent coolant passes at the baffle plates. The coolant can leak through the gap between the tubes and the baffle plate, and indeed this is sometimes encouraged[114] so that 'dead spots' receiving no coolant are eliminated and also to give a smoother temperature distribution in the coolant. Figure 8.4 shows that the changes in slope of the temperature profiles become less marked and may disappear if the coolant is prevented from heating up too much as it flows across the tube bundle, by keeping the flow rate high. This causes less sudden changes in the coolant temperature at the baffle plates and so reduces the discontinuity of slope in the tubeside profiles. Even though the continuum model allows for a coolant temperature profile along the outside of the tubes in each baffled section, abrupt changes of slope in the tubeside temperature profile still occur.

In examining these discontinuities of slope of the temperature profiles, the distorted scale of the graphs must be borne in mind. The length of the reactor tubes is two metres and a change in dimensionless temperature of 0.001 represents approximately 15 K for the activation energy given in Table 8.1. Thus, at the third baffle plate ($z = 0.75$) in figure 8.4, the change in slope which occurs in tube 1 for the coolant velocity of u_c is actually a drop in temperature of approximately 4 K over 10 cm. (from $z = 0.7$ to 0.75) followed by an increase of 9 K over the next 10 cm. ($z = 0.75$ to 0.8).

In both the continuum model of the tube bundle and the mixing cell model presented in the next section, to allow for heat transfer across the baffle plates would result in an extremely time consuming, nested-iterative calculation. Although this would probably eliminate, or at least reduce, the changes in slope of the tubeside temperature profiles, it is arguable that the accuracy of the models as a whole precludes the need for this calculation at the present stage.

Because of the relatively large amount of computation time necessary for the solution of this continuum model of

the multitubular reactor, it is perhaps of limited use for preliminary design purposes. The relatively flat coolant temperature profiles in the direction perpendicular to coolant flow suggest that no great loss of accuracy will occur if the coolant temperature in this direction is assumed to be uniform. For these reasons a second type of model of the tube bundle which is only slightly simpler than the continuum model, but which can be solved more rapidly, has been investigated and compared with the continuum model. This is described in the next section.

8.4 The Crossflow Cocurrent Mixing Cell Model

8.4.1 Assumptions

The assumptions for the mixing cell model of the tube bundle proposed here are basically the same as those for the continuum model. The main difference is that the coolant temperature is assumed to be constant along the outside of each tube in each baffled section. This allows the tube bundle to be divided up into mixing cells, each cell having a length equal to that of the baffled section. The layout of the cells in each pass is shown in figure 8.5. The coolant is assumed to be perfectly mixed in each cell.

8.4.2 Formulation and Solution of the Equations

Referring to figure 8.5, the coolant flows from cell i to cell i + 1 and so on across the row of tubes. As in the continuum model described previously, flow of the coolant in any direction other than horizontally is not explicitly accounted for. From the point of view of heat generation there are effectively two tubes in each cell. A heat balance on cell i gives:

$$m_c c_{pc} T'_{c(i-1)} + 4\kappa RU \int_{z'_2}^{z'_1} (T'|_{y=R}(T'_{c(i)}, z') - T'_{c(i)}) dz' = m_c c_{pc} T'_{c(i)} \qquad (8.4)$$

where:

$m_c = u_c \varrho_c l_B l_T$

z'_1 and z'_2 are the limits of the length of the baffled section

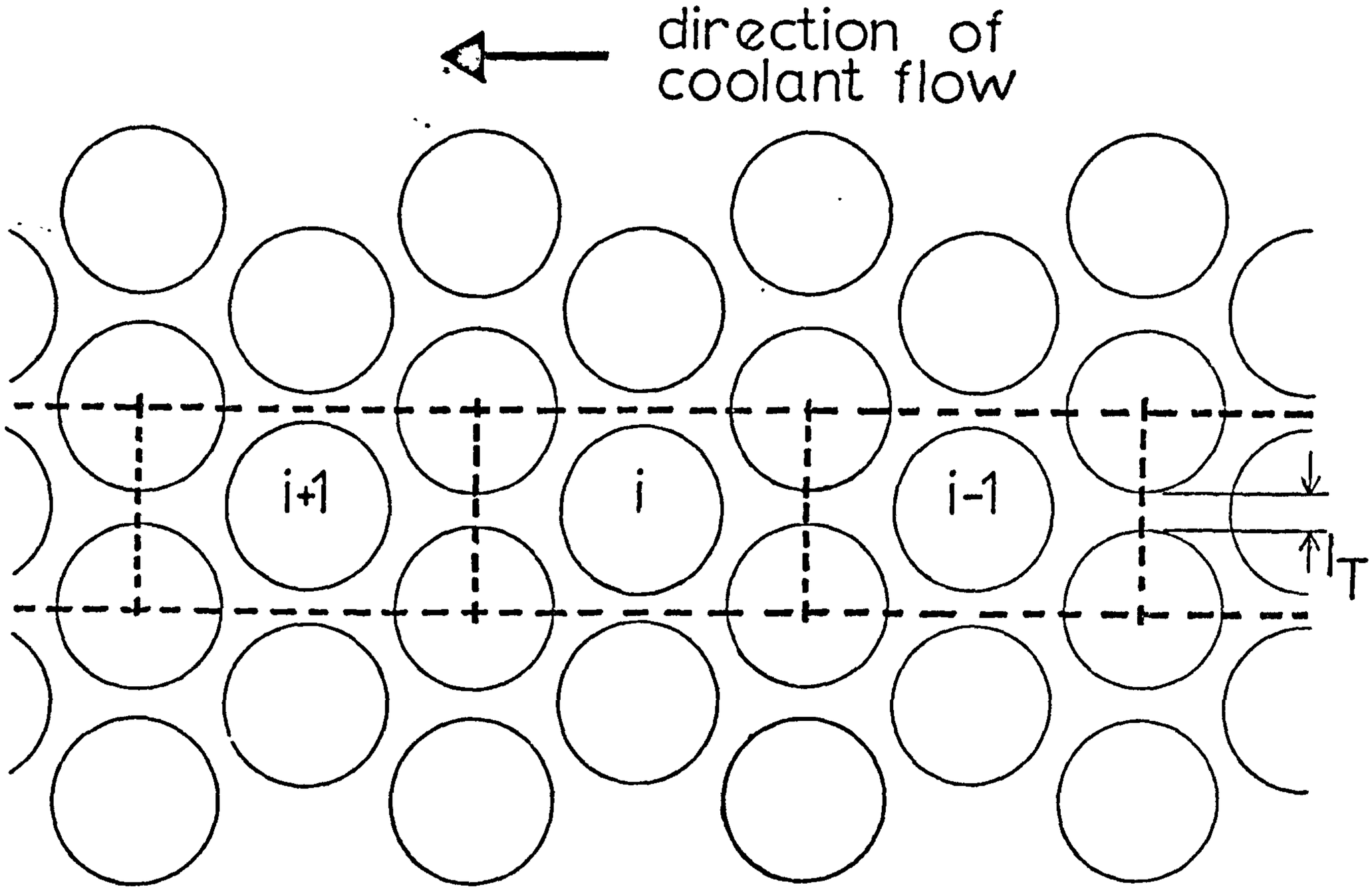

Figure 8.5 Schematic diagram of the tube bundle cross - section showing the arrangement of the mixing cells in the cocurrent crossflow model.

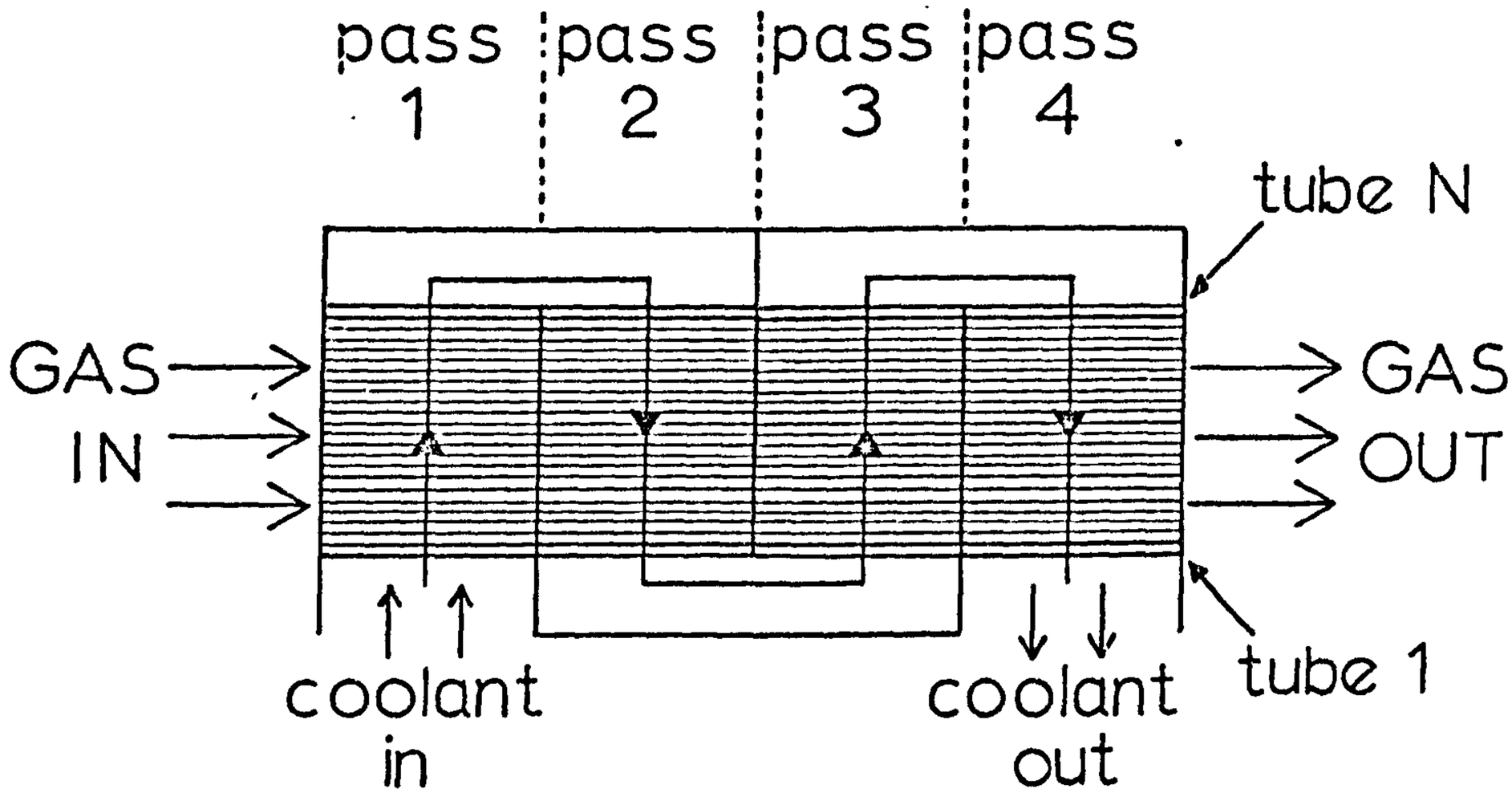

Figure 8.6 Tube and coolant pass labelling system used in the cocurrent crossflow model.

$$l_B = z_2' - z_1'$$

l_T is the minimum distance between adjacent tubes (see figure 8.5) = $P_D - 2b$

Rearrangement and making equation (8.4) dimensionless gives:

$$T_{c(i-1)} + \frac{Nu_w}{G_c}\int_{z_1}^{z_2}(T|_{r=1} - T_{c(i)})dz = T_{c(i)} \qquad (8.5)$$

where: $G_c = \frac{m_c c_{pc}}{4\pi K_f e l}$

The tubeside model used here gives directly the radial mean tubeside temperature making use of the effective wall Nusselt number, Nu_w^*. Therefore, equation (8.5) may be rewritten:

$$T_{c(i)} = T_{c(i-1)} + \frac{Nu_w^*}{G_c}\int_{z_1}^{z_2}(T - T_{c(i)})dz \qquad (8.6)$$

It should be noted that in equation (8.6), T is a function of $T_{c(i)}$.

Thus, for a bundle with N tubes across the diameter there are N equations of the form of equation (8.6) coupled with the tubeside equations (Appendix (2)) for each coolant pass. The coolant flow across the tube bundle is shown schematically in figure 8.6.

The method of solution of the model is as follows:

(1) Assume a value of T_c at the first or next cell.

(2) Solve the tubeside equations for the length of the cell using this value of T_c.

(3) Using the tubeside temperature profile from step (2) evaluate the integral term in equation (8.6).

(4) Solve equation (8.6) using the value obtained from step (3) to give a new value of T_c.

(5) Compare the value of T_c from step (4) with that assumed at step (1). If the two values are converged to within predetermined limits move on to the next cell and repeat from step (1). If the values are not converged use the value of T_c from step (4) and repeat from step (2).

This procedure is repeated in each pass until the exit cell is reached, when solution is complete.

8.4.3 Simplification of the Model

For a reactor of 49 cells (i.e. 50 tubes) across its diameter and four equal length coolant passes, solution of the model for the data given in Table 8.1, when programmed in Fortran on an I.C.L. 1906A computer, takes approximately six minutes. Although at first sight this may not seem an excessive time, two points must be borne in mind; firstly the I.C.L. 1906A computer is a very powerful machine and secondly, if larger tube bundles are considered the computation time will increase proportionately. Preliminary calculations have shown that provided that the coolant flow rate is not too small, a very effective simplifying assumption can be made; namely that the heat gained by the coolant in each cell is approximately constant over a certain number of cells. This is best illustrated by the following equations. From equation (8.6):

$$T_{c(i)} = T_{c(i-1)} + \frac{Nu^*_w}{G_c} F_{(i)} \qquad (8.7)$$

where:

$$F_{(i)} = \int_{z_1}^{z_2} (T - T_{c(i)})dz$$

Similarly, for cell (i+1):

$$T_{c(i+1)} = T_{c(i)} + \frac{Nu^*_w}{G_c} F_{(i+1)} \qquad (8.8)$$

Substituting for $T_{c(i)}$ in equation (8.8) from equation (8.7) gives:

$$T_{c(i+1)} = T_{c(i-1)} + \frac{Nu^*_w}{G_c} (F_{(i)} + F_{(i+1)})$$

Thus for cell (i + n):

$$T_{c(i+n)} = T_{c(i-1)} + \frac{Nu_w^*}{G_c} \sum_{k=0}^{n} F_{(i+k)} \qquad (8.9)$$

Now, if $F_{(i)} \doteqdot F_{(i+1)} \doteqdot F_{(i+2)} \doteqdot \cdots\cdots \doteqdot F_{(i+n)}$

then equation (8.9) becomes:

$$T_{c(i+n)} = T_{c(i-1)} + \frac{Nu_w^*}{G_c} (n + 1)F_{(i)} \qquad (8.10)$$

Table 8.2 shows values of $F_{(i)}$ for each mixing cell in a 49 cell diameter bundle with four equal coolant passes. As can be seen, if n is not too large then the approximation will be valid and so equation (8.10) will hold.

Figures 8.7, 8.8 and 8.9 show the effect of this approximation with n = 24 on the temperature and concentration profiles of tubes on opposite sides of a 50 tube diameter bundle. As may be seen, the differences between the detailed and the simplified mixing cell models are not very large. The largest discrepancies occur in the hottest part of the bundle since at higher temperatures the tubeside gas temperature is more sensitive to the coolant temperature. The reduction in computing time is very great for this small sacrifice in accuracy with n = 24. When programmed in Fortran solution of the simplified model requires only approximately 24 seconds compared with the previously quoted figure of 6 minutes for the detailed model. In other words a reduction by a factor of about 15. If more accuracy is required, for example at lower values of coolant flow rate, then a smaller value of n may be used. It is interesting to note that the simplified model predicts higher temperatures than the detailed model. It may, therefore, be regarded as a safe approximation since any operating conditions decided on the basis of predictions of the simplified model would tend to be conservative.

It seems, therefore, that this simplification is satisfactory for preliminary studies provided that the value of n is chosen with some care.

Cell No.		1	2	3	4	5	6	7	8	9	10
1st Pass	1	0.0621	0.0621	0.0621	0.0622	0.0622	0.0622	0.0622	0.0622	0.0623	0.0623
	2	0.0623	0.0623	0.0624	0.0624	0.0624	0.0625	0.0625	0.0625	0.0626	0.0626
	3	0.0626	0.0626	0.0627	0.0627	0.0628	0.0628	0.0628	0.0629	0.0629	0.0629
	4	0.0630	0.0630	0.0631	0.0631	0.0631	0.0632	0.0633	0.0633	0.0633	0.0634
	5	0.0634	0.0635	0.0635	0.0636	0.0636	0.0637	0.0637	0.0638	0.0638	
2nd Pass	1	0.1255	0.1251	0.1247	0.1242	0.1238	0.1234	0.1229	0.1225	0.1221	0.1217
	2	0.1213	0.1209	0.1205	0.1202	0.1197	0.1194	0.1189	0.1186	0.1182	0.1179
	3	0.1174	0.1171	0.1167	0.1164	0.1160	0.1156	0.1153	0.1149	0.1146	0.1142
	4	0.1138	0.1135	0.1132	0.1128	0.1125	0.1122	0.1118	0.1114	0.1111	0.1108
	5	0.1105	0.1101	0.1098	0.1095	0.1092	0.1089	0.1086	0.1083	0.1079	
3rd Pass	1	0.1394	0.1385	0.1376	0.1367	0.1359	0.1349	0.1341	0.1331	0.1323	0.1314
	2	0.1305	0.1296	0.1288	0.1279	0.1269	0.1261	0.1252	0.1243	0.1235	0.1226
	3	0.1217	0.1208	0.1199	0.1191	0.1182	0.1173	0.1164	0.1156	0.1147	0.1138
	4	0.1129	0.1121	0.1112	0.1103	0.1094	0.1086	0.1077	0.1068	0.1059	0.1051
	5	0.1042	0.1033	0.1024	0.1015	0.1006	0.0997	0.0989	0.0980	0.0971	
4th Pass	1	0.1102	0.1096	0.1090	0.1084	0.1078	0.1072	0.1066	0.1059	0.1053	0.1047
	2	0.1040	0.1034	0.1028	0.1021	0.1015	0.1008	0.1002	0.0995	0.0988	0.0982
	3	0.0975	0.0968	0.0961	0.0954	0.0947	0.0940	0.0933	0.0926	0.0919	0.0912
	4	0.0904	0.0897	0.0890	0.0883	0.0875	0.0868	0.0861	0.0853	0.0846	0.0838
	5	0.0830	0.0823	0.0815	0.0807	0.0799	0.0792	0.0784	0.0776	0.0768	

TABLE 8.2 Values of F_i from the cocurrent coolant mixing cell model. Data as given in Table 8.1.

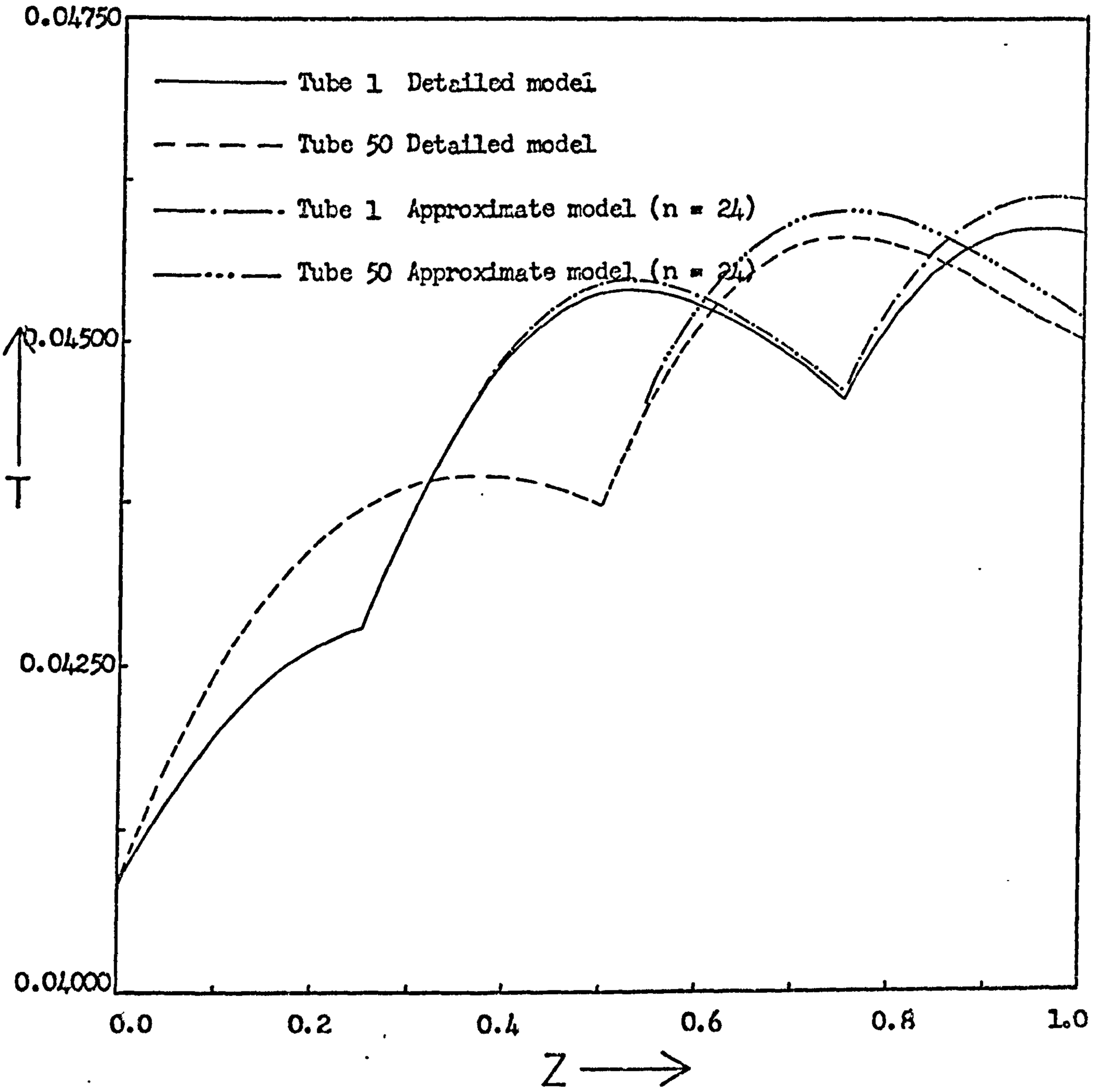

Figure 8.7 Comparison of axial profiles of radial mean temperature in tubes on opposite sides of the bundle predicted by the detailed and the simplified cocurrent coolant mixing cell models. (Data as given in Table 5.1)

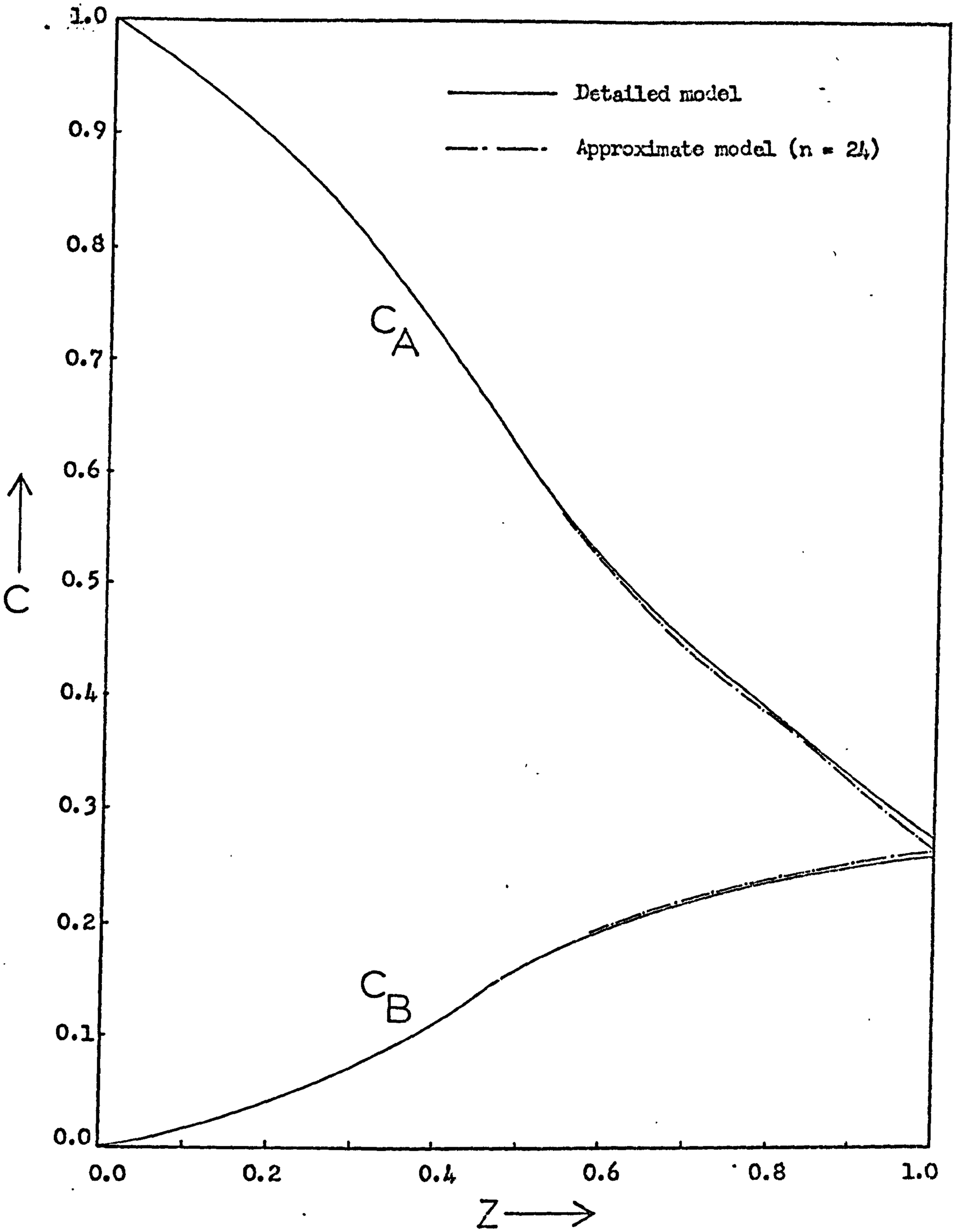

Figure 8.8 Comparison of axial profiles of radial mean concentration within tube 1 predicted by the detailed and the simplified cocurrent coolant mixing cell models. (Data as given in Table 8.1)

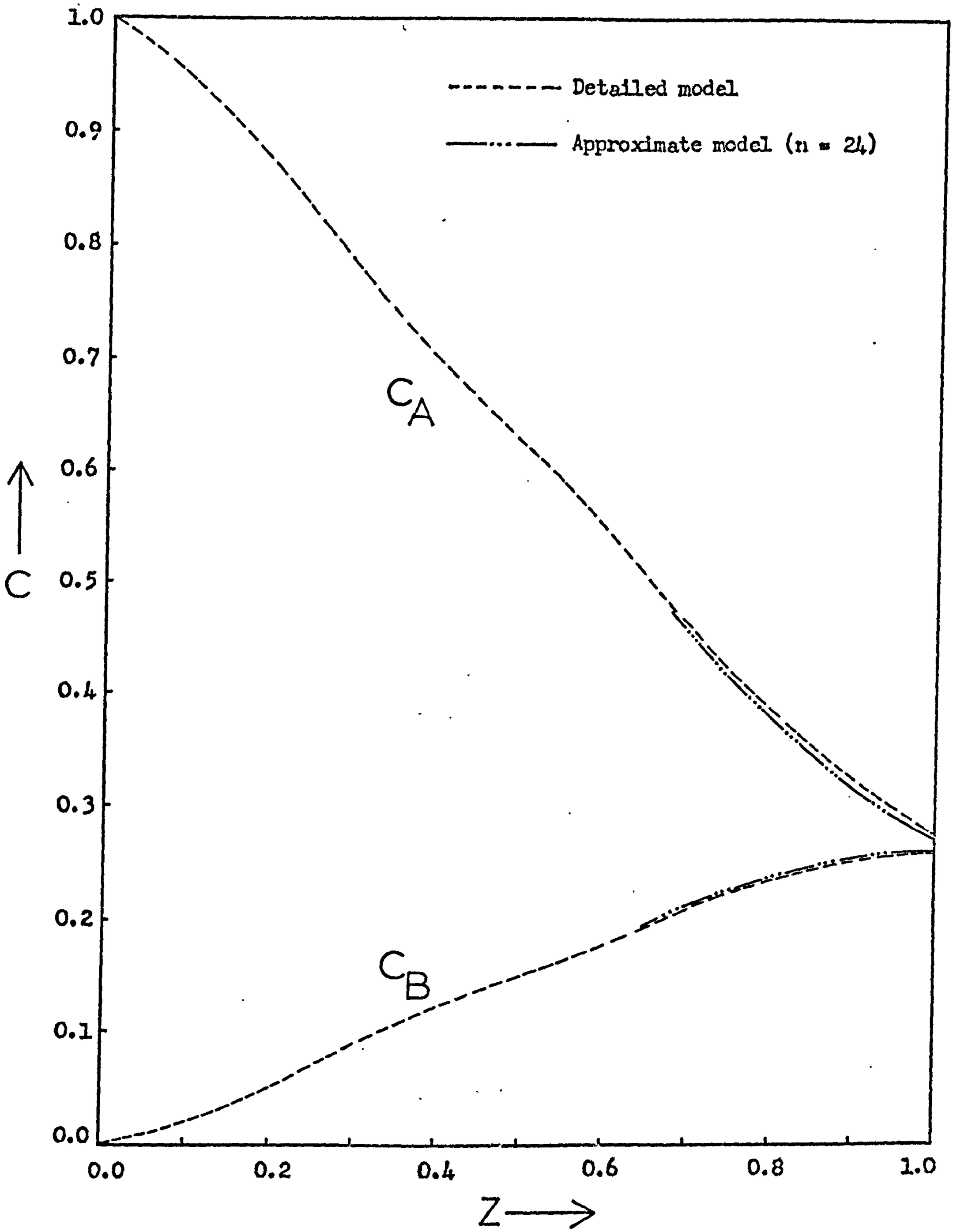

Figure 8.9 Comparison of axial profiles of radial mean concentration within tube 50 predicted by the detailed and the simplified cocurrent coolant mixing cell models. (Data as given in Table 8.1)

8.4.4 Comparison with the Continuum Model

Figure 8.10 shows the comparison of the radial mean tubesidetemperature profiles in tubes on opposite sides of the tube bundle predicted by the continuum and the mixing cell model. As can be seen, the agreement between the two models is very good. The slight differences which do occur are due to small coolant temperature gradients perpendicular to the coolant flow, predicted by the continuum model. Similar agreement is obtained between the concentration profiles predicted by the two models, although these are not shown here. At higher coolant flow rates the agreement between the two models is even better since much less heating of the coolant occurs. At the lower flow rates the discrepancies between the two models become slightly greater since significant coolant heating occurs and so the coolant temperature gradients become more pronounced. Even so, the agreement has still been found to be very good.

The mixing cell model, in its simplified form, requires much less computation (a factor of 30 less) and yet agrees very well with the continuum model, as figure 8.10 shows. It, therefore, appears very suitable for a preliminary examination of the behaviour of multitubular reactors especially in the absence of more reliable data or a pilot plant.

8.4.5 The Influence of the Model Parameters

From equation (8.6) it can be seen that a change in the value of the group Nu_w^*/G_c may be interpreted as a change in the coolant flow rate with the accompanying change in the value of Nu_w^*. But note that the value of Nu_w^* is required explicitly for the solution of the tubeside model. For this reason, in the absence of any reliably accurate heat transfer data giving the dependence of the coolant-side wall heat transfer coefficient on coolant flow rate, the effect of both the coolant flow rate and the wall heat transfer coefficient has been simulated by varying G_c at constant Nu_w^* and Nu_w^* at constant G_c.

In studying the effect of some of the parameters of the model, only temperature and concentration profiles within tubes on opposite sides of the bundle have been presented, since these represent two extremes within the bundle. The other

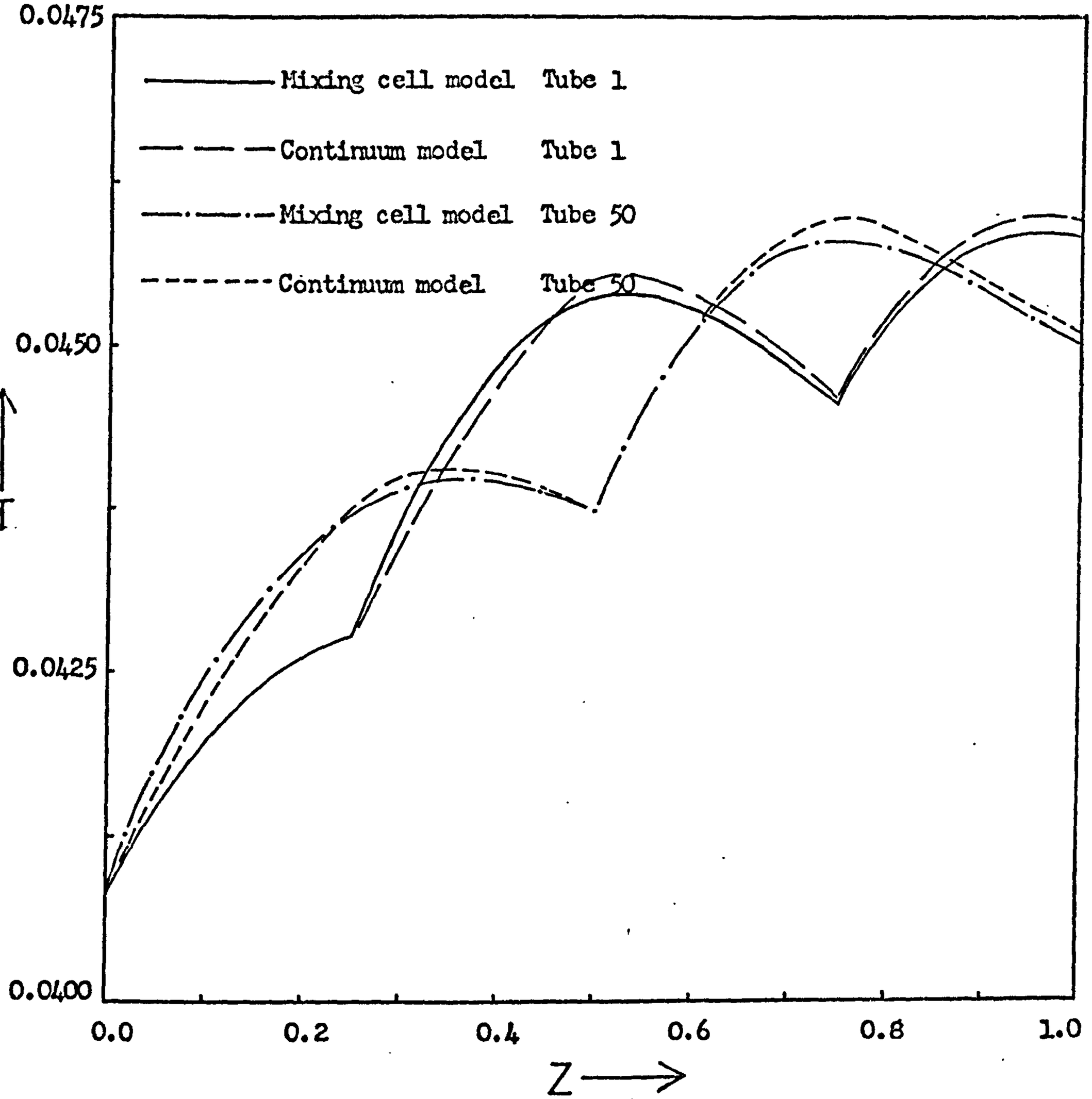

Figure 8.10 Comparison of axial profiles of radial mean temperature within tubes on opposite sides of the bundle predicted by the cocurrent coolant continuum and mixing cell models. (Data as given in Table 8.1)

tubes in the bundle exhibit a gradual change in profiles between these two extremes on passing across the bundle in the direction of the coolant in each baffled section.

Figures 8.11, 8.12 and 8.13 show the effect of coolant flow-rate at constant Nu_w^* on the temperature and concentration profiles in a tube bundle with 49 cells across its diameter and with four equal coolant passes. At the high coolant flow rates (high values of G_c) there is very little difference between tubes on opposite sides of the bundle. Although the fairly high wall Nusselt number causes a large amount of heat to be removed from the tubes, the coolant does not heat up very much because of its high flow rate. Consequently, tubes on opposite sides of the tube bundle are receiving coolant at similar temperatures in each pass, and therefore, exhibit similar behaviour.

As a consequence of the coolant remaining relatively cool near the gas inlet, at these high coolant flow rates, the reaction gases are prevented from becoming hot and thereby generating more heat to further increase the reaction rate. Although this may be desirable in the case of a very temperature sensitive catalyst, it causes a low conversion of the reactant. Figures 8.12 and 8.13 show that at the high coolant flow rates used to produce the profiles labelled (1) and (2), approximately half of the reactant (species A) remains unconsumed at the reactor exit. Operation under conditions similar to these would, therefore, necessitate a large recycle of the reactor exit gases, with accompanying separation plant, as well as high pumping power requirements for the pumping of the coolant through the reactor. An alternative to the recycle would be a much longer reactor. This would further increase the coolant pumping costs and also increase the capital cost of the reactor.

At low coolant flow rates the coolant heats up much more rapidly as it flows across the tube bundle, and so tubes on opposite sides of the bundle experience coolant at quite different temperatures. This produces large differences in the temperature and concentration profiles within them (see profiles labelled (3) and (4) in figures 8.11, 8.12 and 8.13).

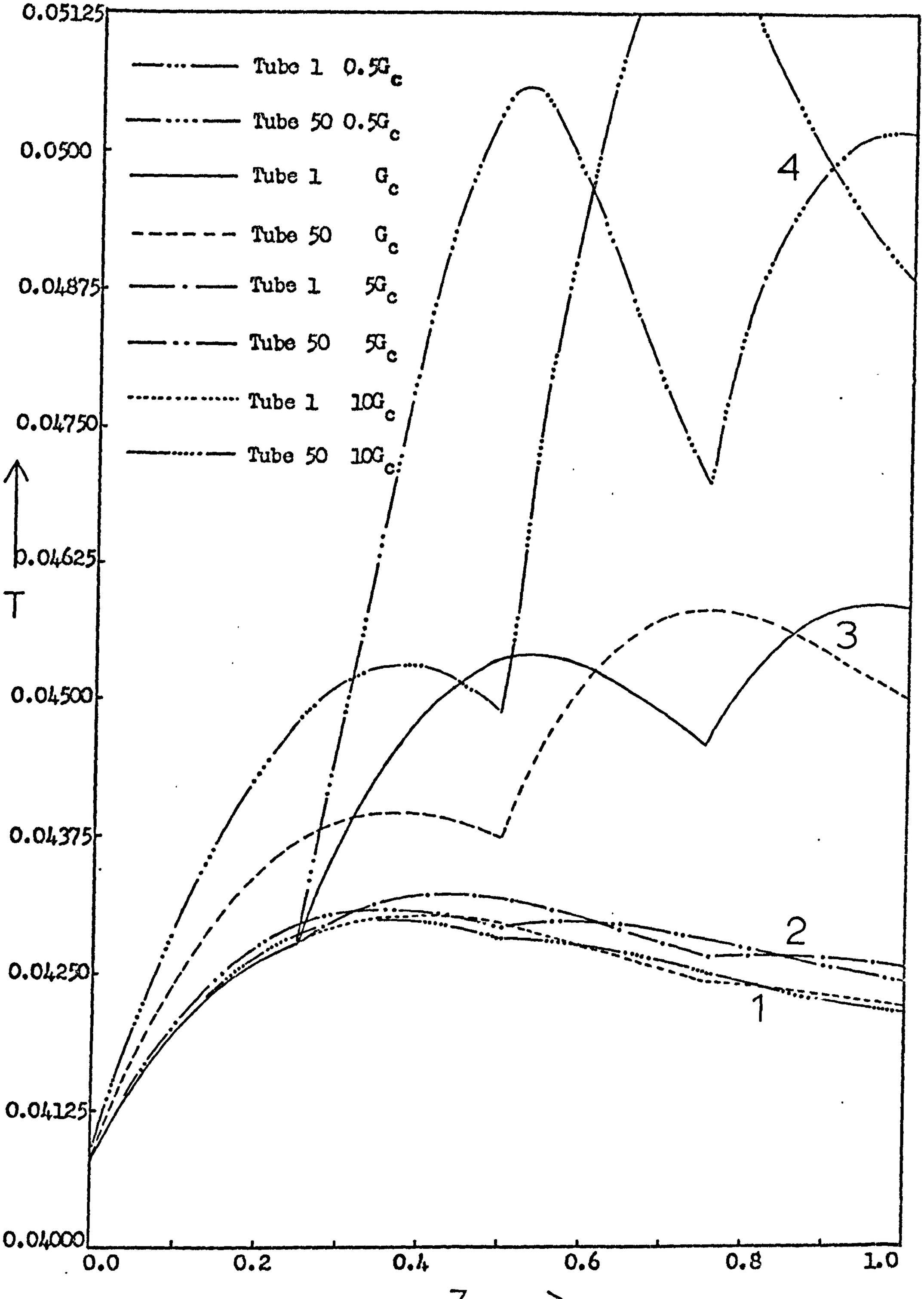

Figure 8.11 The effect of the coolant flowrate on the axial profiles of radial mean temperature within tubes on opposite sides of the bundle predicted by the cocurrent coolant mixing cell model. (Data as given in Table 8.1)

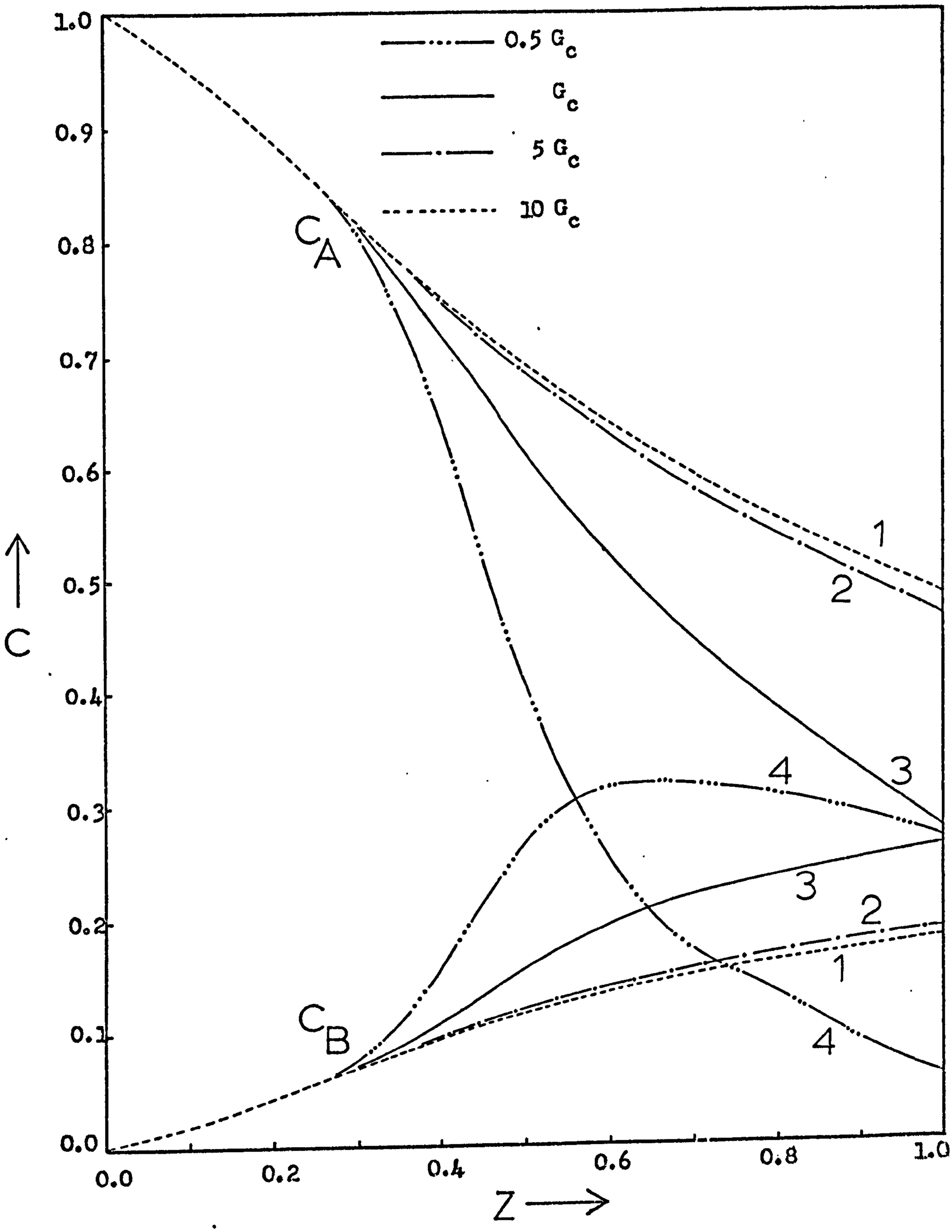

Figure 8.12 The effect of the coolant flowrate on the axial profiles of radial mean concentration within tube 1 predicted by the cocurrent coolant mixing cell model. (Data as given in Table 8.1)

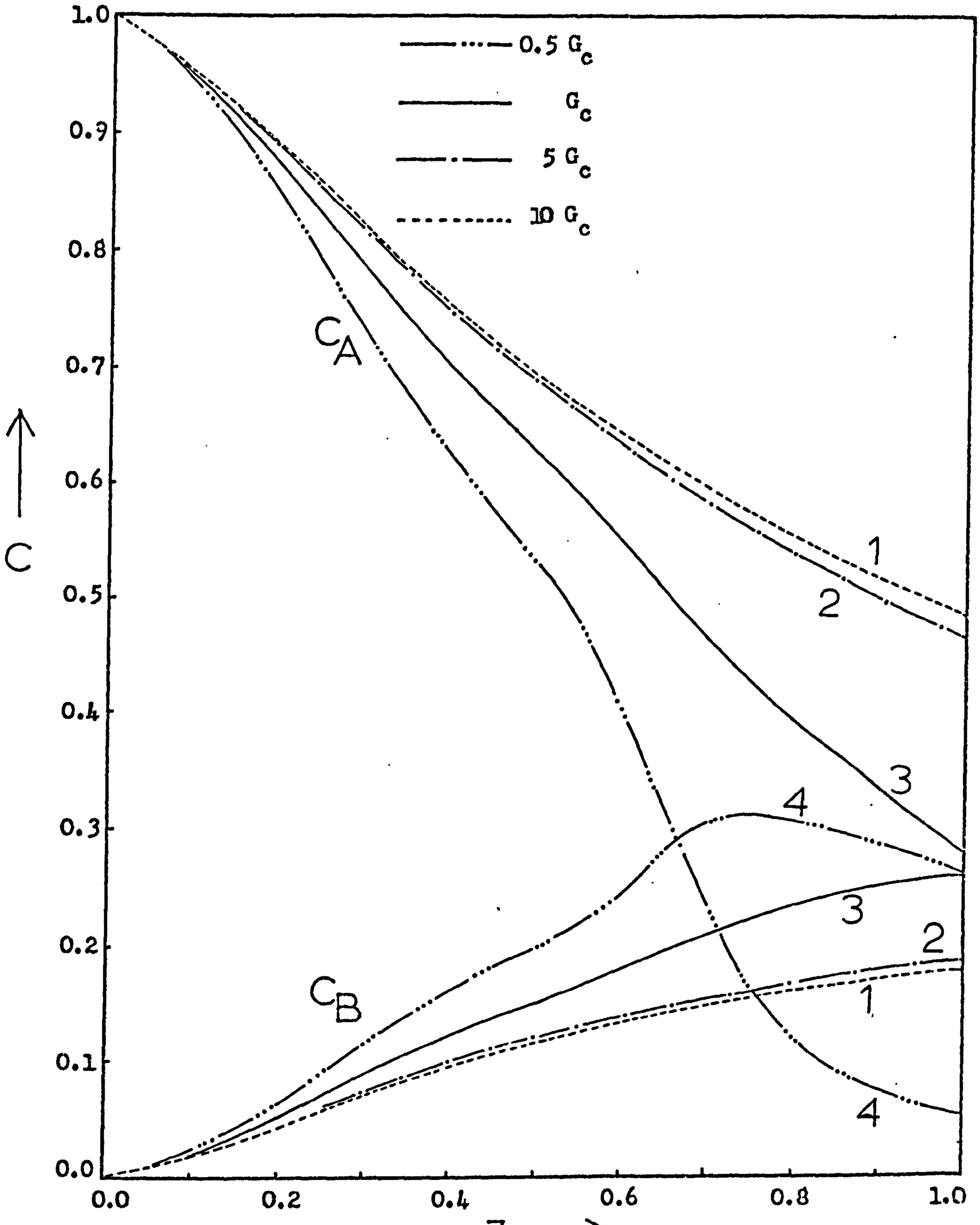

Figure 8.13 The effect of the coolant flowrate on the axial profiles of radial mean concentration within tube 50 predicted by the cocurrent coolant mixing cell model. (Data as given in Table 5.1)

The non-linear effect of the coolant flow rate on the shapes of the tubeside temperature profiles is also evident. The tubeside profiles are much more sensitive to the coolant flow rate at the low flow rates than at the high ones as has been demonstrated with the continuum model. This is due to the way in which heat is generated and dissipated within the tube bundle; the lower the coolant flow rate, then the more rapidly the coolant heats up. However, the higher coolant temperatures allow greater reaction rates, within the tubes, and therefore greater heat generation causing even more heating of the coolant. This effect is propagated throughout the tube bundle. The undesirability of a low coolant flow rate is shown by the profiles labelled (4) in figures 8.11, 8.12 and 8.13. Here the very low flow rate enables the coolant to heat up by quite a large amount in each pass and this leads to quite different conditions within tubes on opposite sides of the bundle, at all points along the tubes. It is also evident that a high temperature peak and even temperature runaway might occur twice within the same tube. In figures 8.12 and 8.13 the consequences of allowing the coolant temperature to become too high are evident from the fall off in concentration of product B near the reactor exit. This is because species B is being consumed faster than it is formed from A.

Another reason for preventing the coolant temperature from becoming too high is that the coolant might decompose or exacerbate corrosion of the shell and tubes at high temperatures. In the case of molten salts, charring as well as decomposition of the salt can occur at high temperatures and this can cause fouling of the coolant flow paths and a fall-off in the coolant-side wall heat transfer coefficient.

Figures 8.14 and 8.15 show the effect of varying the wall Nusselt number at a constant coolant flow rate. (Note. Only the concentration profiles in tube 1 are shown in figure 8.15 for clarity. The effect of Nu_w on the concentration profiles in tube 50 is very similar). A high wall Nusselt number causes good heat transfer between the tubes and the coolant and provided that the coolant flow rate is not too high, preventing the coolant from heating up, this appears to lead to a fairly even temperature profile within the tubes and moderate conversions of reactant. Too low a wall Nusselt

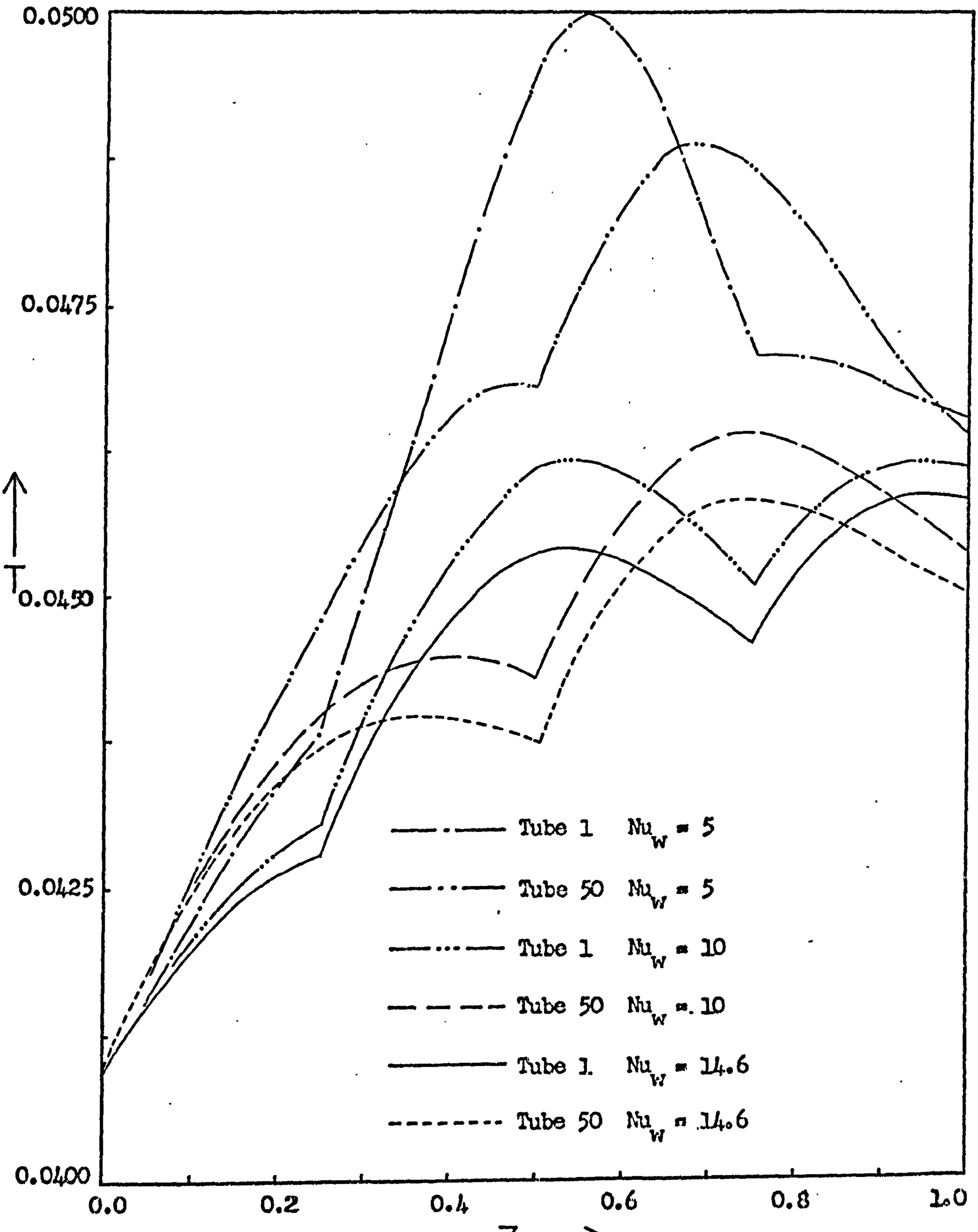

Figure 8.14 The effect of the wall Nusselt number on the axial profiles of radial mean temperature within tubes on opposite sides of the bundle with cocurrent cooling. (Data as given in Table 8.1)

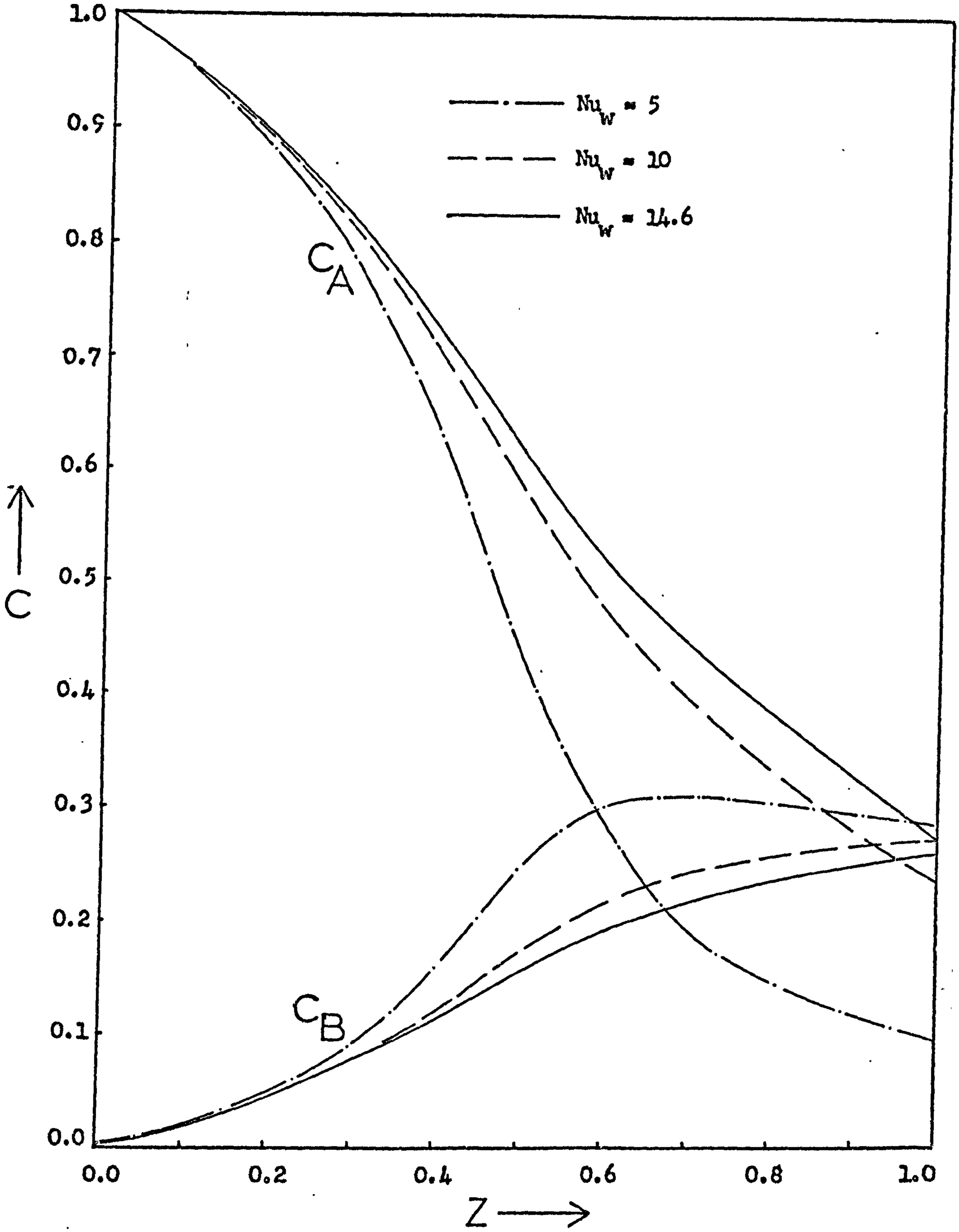

Figure 8.15 The effect of the wall Nusselt number on the axial profiles of radial mean concentration within tube 1 with cocurrent cooling. (Data as given in Table 8.1)

number means that bad heat transfer occurs between the tubes and the coolant and so the tubeside gas temperature becomes high. This may lead to poor selectivity if uncontrolled and so as shown in figure 8.15 the concentration of product B decreases near the exit. A low wall Nusselt number also gives rise to a lack of sensitivity to the coolant temperature.

As mentioned previously, the wall Nusselt number is usually controlled by the tubeside heat transfer coefficient and can, therefore, be held more or less constant or at least prevented from varying over a very wide range.

The effect of changing the number of coolant passes across the tube bundle is shown in figures 8.16 to 8.19. In these figures the effect of four, five and six coolant passes at a constant coolant velocity is shown. It should be noted that although the coolant velocity is constant, since the length of the baffled sections changes with the number of coolant passes, the coolant mass flow rate across the tube bundle also changes and this is reflected in the value of G_c.

Increasing the number of coolant passes by decreasing the length of each baffled section might, at first, be thought to lead to lower and more even tubeside gas temperature profiles. As figures 8.16 to 8.19 show, this is not always the case. Increasing the number of coolant passes, whilst keeping the coolant velocity constant, in fact causes an increase in the tubeside temperature in the latter half of the reactor for the data used here. The reason for this is the way the heat is generated and passed to the coolant throughout the reactor. Consider, for example, a change from four to five coolant passes across the same tube bundle. The increase in the number of passes results in a decrease in the length of each baffled section. In the first coolant pass the tubeside gases heat up as the reaction gets going, leaving this pass at a higher temperature than when they entered. Thus, more heat is transferred from the tubes to the coolant near the exit of the tubes from this pass than near the reactor entrance. Therefore, on shortening the length of the tubes in this pass by increasing the number of passes, the amount of heat which can be transferred to the coolant decreases and so the coolant does not heat up so much as it flows across the bundle. This is despite the decrease in mass flow rate of the coolant across

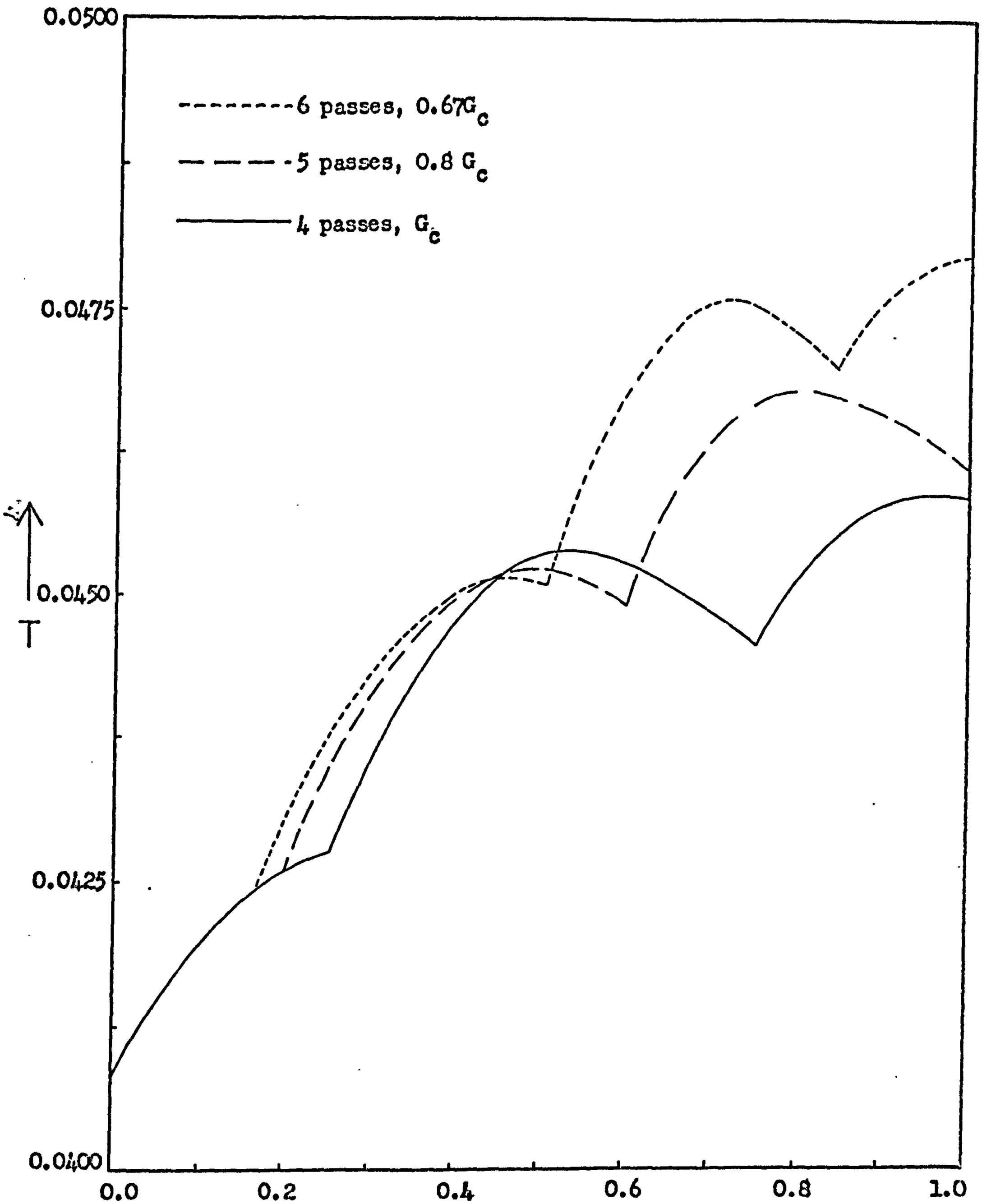

Figure 8.16 The effect of the number of coolant passes (at constant coolant velocity) on the axial profiles of radial mean temperature within tube 1, with cocurrent cooling. (Data as given in Table 8.1)

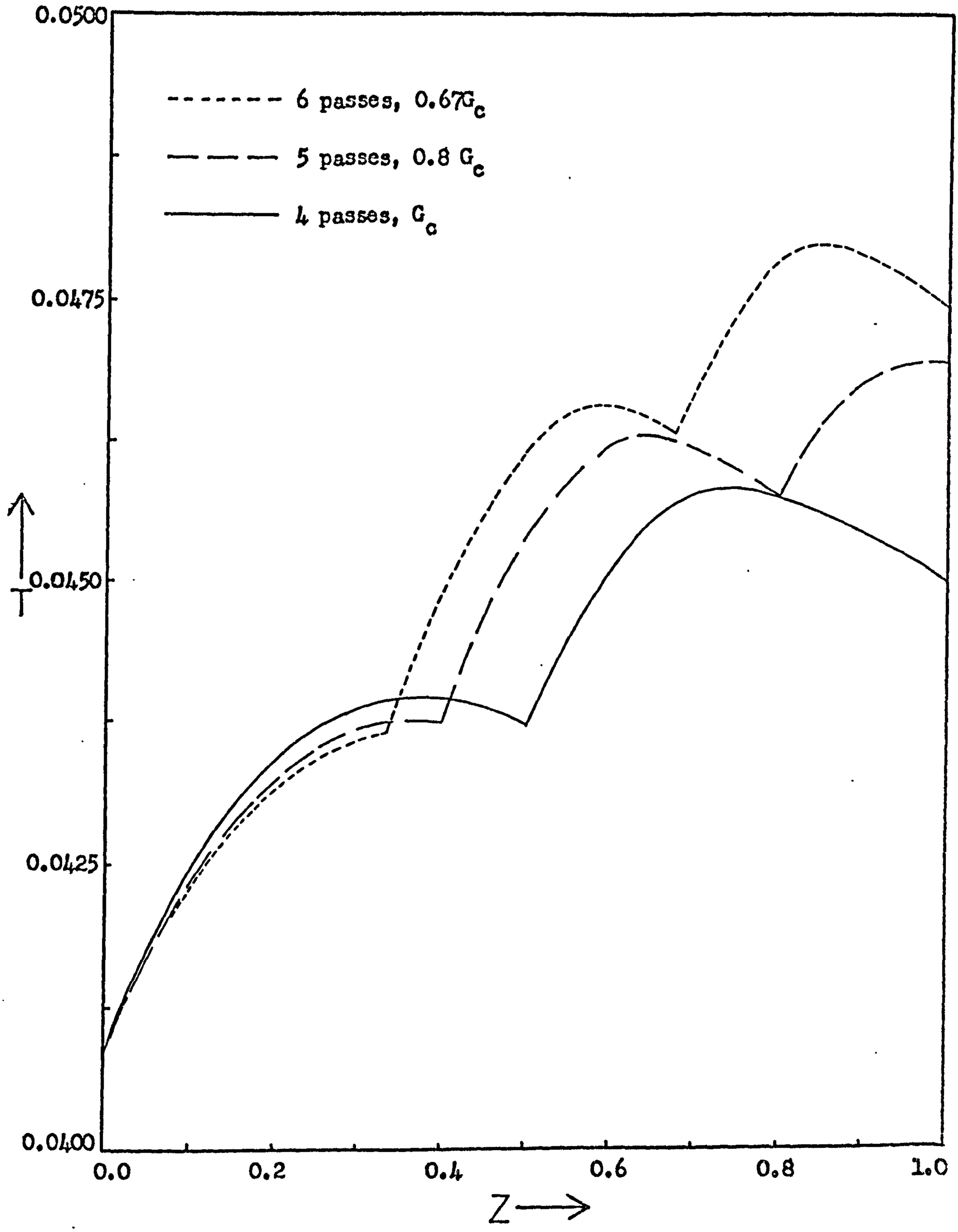

Figure 8.17 The effect of the number of coolant passes (at constant coolant velocity) on the axial profiles of radial mean temperature within tube 50, with cocurrent cooling. (Data as given in Table 8.1)

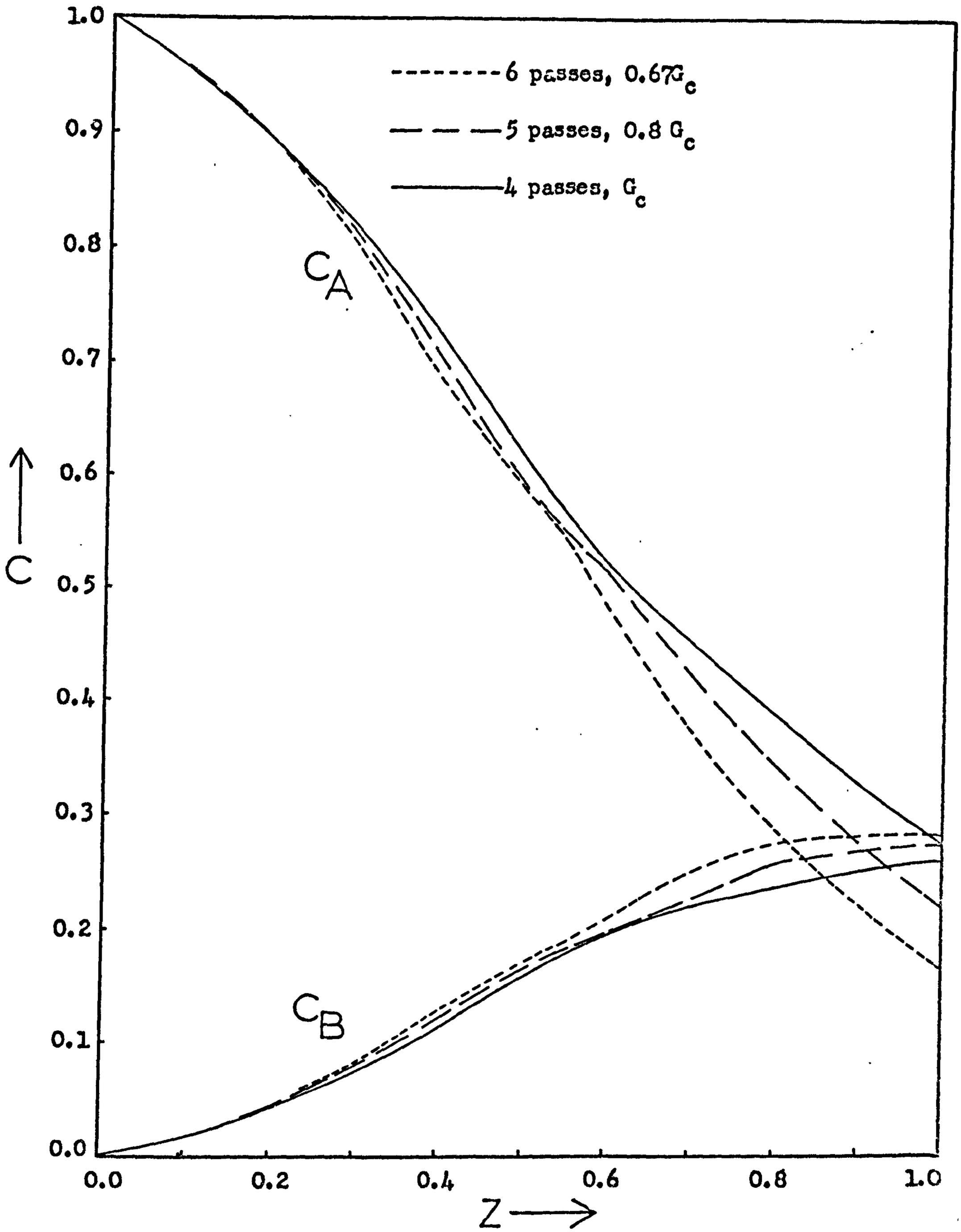

Figure 8.18 The effect of the number of coolant passes (at constant coolant velocity) on the axial profiles of radial mean concentration within tube 1, with cocuurent cooling. (Data as given in Table 8.1)

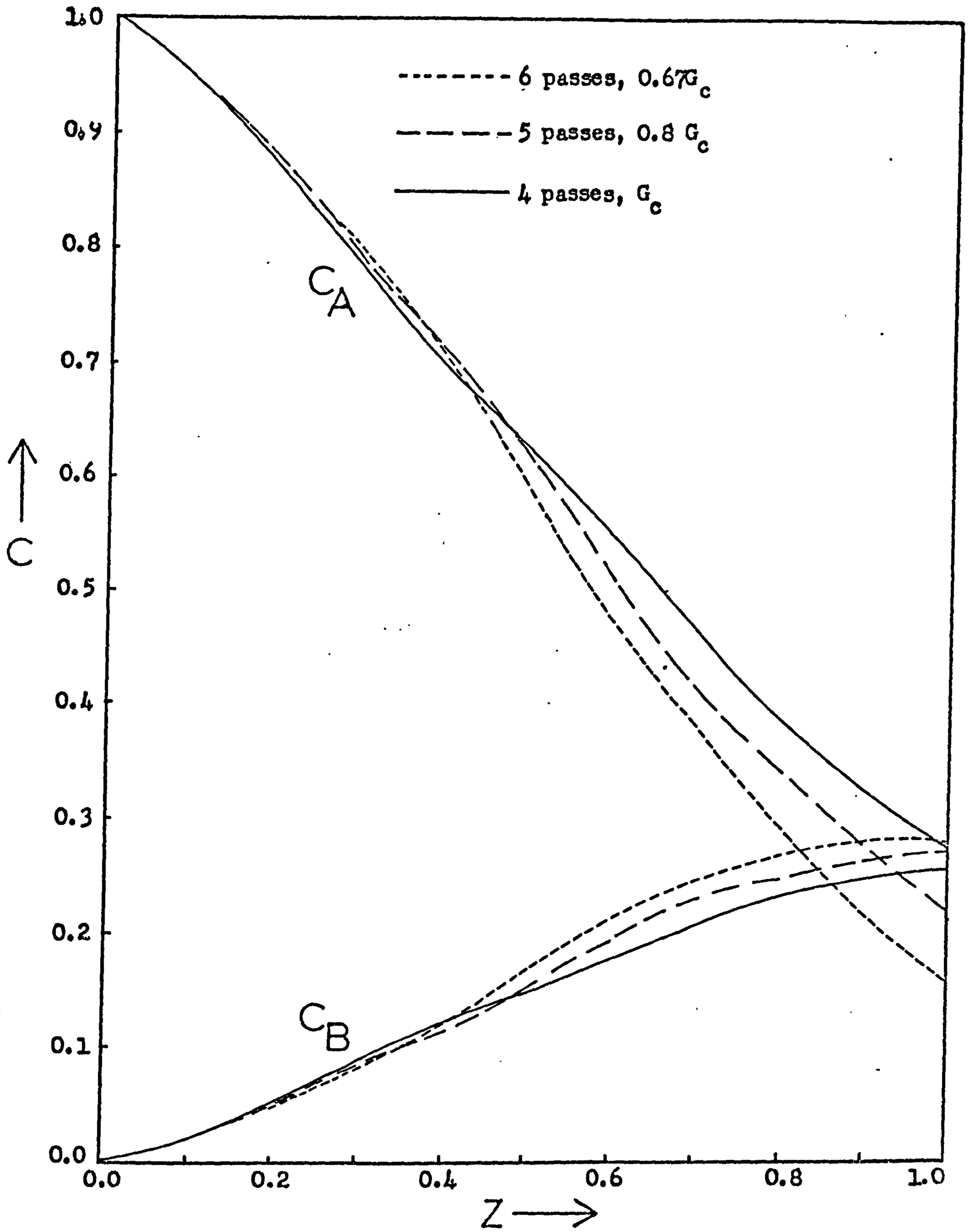

Figure 8.19 The effect of the number of coolant passes (at constant coolant velocity) on the axial profiles of radial mean concentration within tube 50, with cocurrent cooling. (Data as given in Table 8.1)

this pass. Consequently, the tubeside gases do not become so hot, in the first pass, with five passes as with four. In the second and subsequent passes more reaction takes place in the case of five passes, since less reactant has been consumed in the first pass. This causes greater heat generation and, therefore, greater heating of the coolant. The hotter coolant experienced by the tubes in turn causes more reaction to take place causing even more heat generation. The process is somewhat exacerbated by the lower mass flow rates caused by shortening the baffled sections at constant coolant velocity.

More than six coolant passes are not usually used in multitubular reactors because of the increase in pressure drop of the coolant and consequently increased pumping costs.

8.5 The Crossflow Countercurrent Mixing Cell Model

8.5.1 Assumptions

The assumptions upon which this model is based are identical to those employed in the cocurrent mixing cell model described in section 8.4. The only difference is the direction of flow of the coolant relative to the direction of flow of the gases. This is shown schematically in figure 8.21, together with the tube labelling system.

8.5.2 Formulation and Solution of the Equations

Figure 8.20 shows the mixing cell arrangement. Using the same nomenclature as in section 8.4, a heat balance on cell i gives:

$$T_{c(i+1)} = T_{c(i)} - \frac{Nu_w^*}{G_c} \int_{z_1}^{z_2} (T - T_{c(i)}) dz \qquad (8.11)$$

Note that T is a function of $T_{c(i)}$ in equation (8.11).

For a tube bundle of N tubes across the diameter there will be N equations of the form of equation (8.11), coupled with the tubeside equations, for each coolant pass across the tube bundle.

Figure 8.21 shows that the coolant enters the tube bundle at the baffled section from which the reaction gases leave. The tubeside equations must be solved from the point where the gases enter the tubes and because usually only the coolant

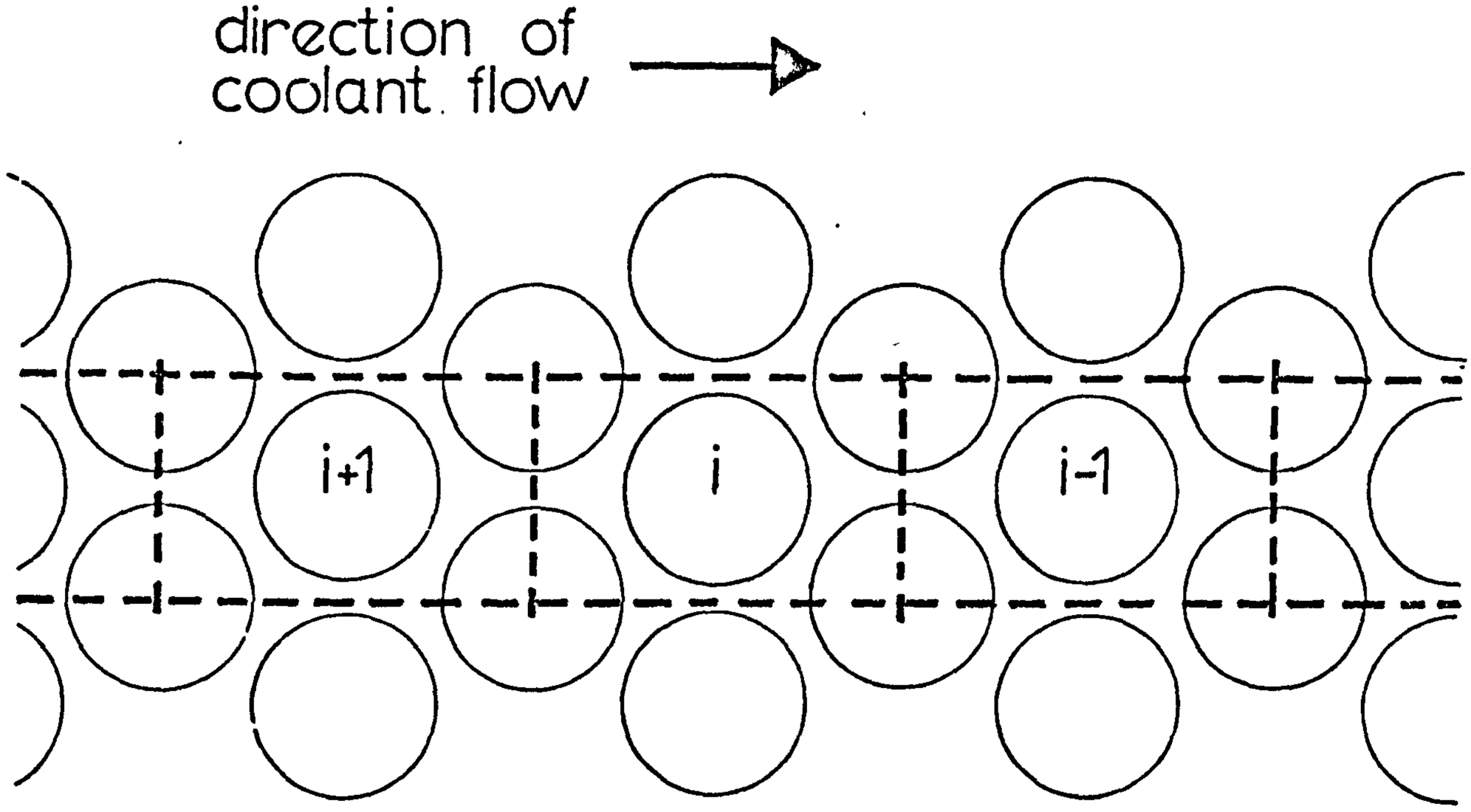

Figure 8.20 Schematic diagram of the tube bundle cross - section showing the arrangement of the mixing cells in the countercurrent crossflow model.

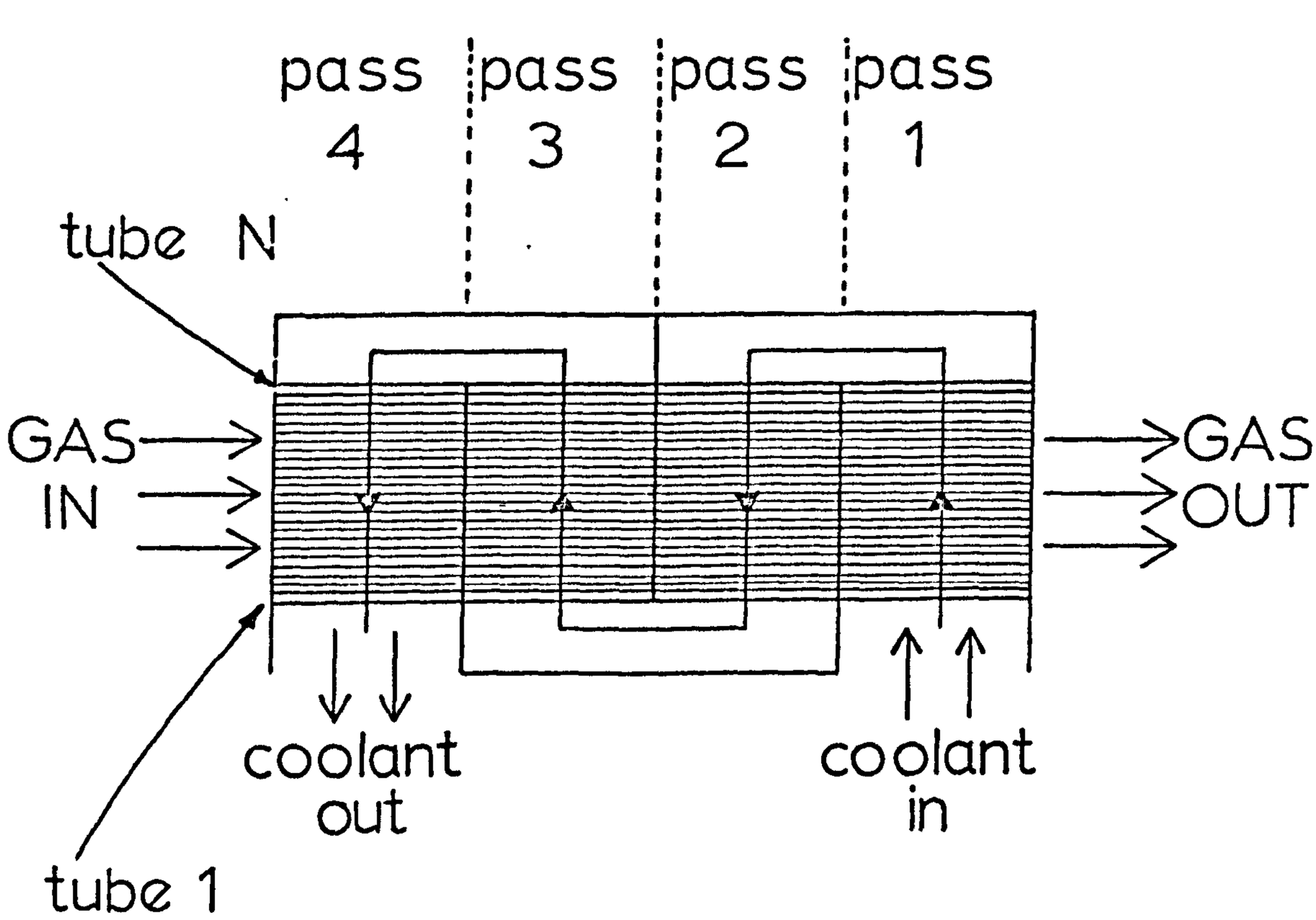

Figure 8.21 Tube and coolant pass labelling system used in the countercurrent crossflow model.

inlet temperature is specified, its value at this point is not known. This necessitates an iterative solution on the coolant. The coolant exit temperature is assumed and the equations are solved marching across the tube bundle in the direction opposite that of the coolant flow to calculate the coolant inlet temperature. This may then be compared with the actual inlet temperature. If the two values do not agree, a new coolant exit temperature is assumed and the calculation is repeated.

From equation (8.11) it can be seen that since T is a function of $T_{c(i)}$ and not $T_{c(i+1)}$ the latter may be computed directly without the need for iteration on the individual cell equations. The method of solution is as follows:

(1) Assume a value for T_c at the cell at the coolant exit from the bundle.

(2) Solve the tubeside equations using this value.

(3) Compute the value of T_c in the next cell across the bundle from equation (8.11).

(4) Check whether the last cell in the bundle (i.e. at the coolant entrance) has been reached. If not, repeat from step (2) using the value of T_c from step (3). If the last cell has been reached go on to step (5).

(5) Compare the computed value of the coolant inlet temperature from step (3) with the actual value. If the values are the same, then the solution is complete. If not, repeat from step (1).

A quadratic convergence technique appears to be sufficient in most cases to obtain convergence of the coolant inlet temperature with four iterations. More iterations are usually required in the region of multiple solutions discussed in section 8.5.4.

8.5.3 Simplification of the Model

For a tube bundle with 50 tubes across the diameter and with the data given in Table 8.1, one iteration on the tube

bundle requires approximately 3 minutes computation when programmed in Fortran on an I.C.L. 1906 A computer. This is faster than the cocurrent model because no iteration is needed on the individual cell equations. If three or four iterations on the bundle are needed to obtain convergence of the inlet coolant temperature, then the computation time becomes prohibitive for a detailed investigation of the reactor.

For this reason, the approximation described in section 8.4.3 of this chapter has been tested on this model, namely that the heat gained by the coolant in each cell is approximately the same over a number of cells.

Putting: $$F_{(i)} = \int_{z_1}^{z_2} (T - T_{c(i)})dz$$

then from equation (8.11):

$$T_{c(i+1)} = T_{c(i)} - \frac{Nu_w^*}{G_c} F_{(i)} \qquad (8.12)$$

Similarly:

$$T_{c(i+2)} = T_{c(i+1)} - \frac{Nu_w^*}{G_c} F_{(i+1)}$$

Therefore from equation (8.12):

$$T_{c(i+2)} = T_{c(i)} - \frac{Nu_w^*}{G_c} (F_{(i)} + F_{(i+1)})$$

Thus

$$T_{c(i+n)} = T_{c(i)} - \frac{Nu_w^*}{G_c} \sum_{k=0}^{n-1} F_{(i+k)} \qquad (8.13)$$

Now, if $F_{(i)} \doteq F_{(i+1)} \doteq F_{(i+2)} \doteq \cdots\cdots \doteq F_{(i+n-1)}$

then equation (8.13) becomes:

$$T_{c(i+n)} = T_{c(i)} - \frac{Nu_w^*}{G_c} nF_{(i)} \qquad (8.14)$$

Figure 8.22 shows the effect of this approximation on the temperature profiles within tubes on opposite sides of a 49 cell diameter bundle with four equal coolant passes and $n = 6$. As might be anticipated from the results of the cocurrent mixing cell model, the difference between the detailed and the simplified models increases with temperature. Because of the higher coolant temperatures near the reactor entrance,

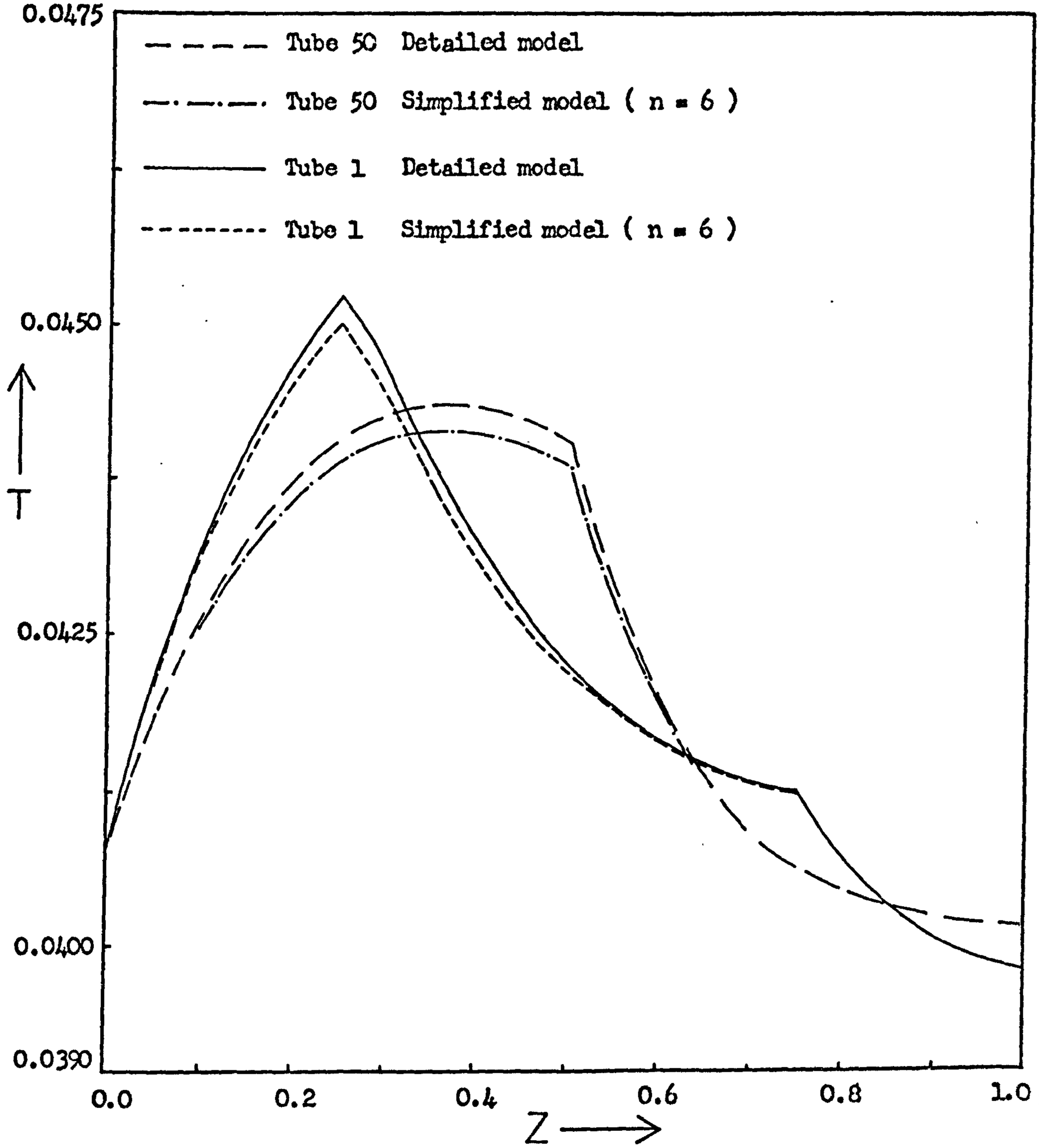

Figure 8.22 Comparison of the axial profiles of radial mean temperature within tubes on opposite sides of the bundle predicted by the detailed and simplified countercurrent coolant mixing cell models. (T_{co} = 0.03920, other data as given in Table 8.1)

more heat is generated there in the countercurrent than in the cocurrent case with the data used here. Consequently, a smaller value of n is necessary to obtain good agreement between the simplified and the detailed models. Even so, the reduction in computing time makes the approximation worthwhile. To construct figure 8.22 with n = 6 one iteration on the tube bundle requires approximately 35 seconds computing time on the I.C.L. 1906A computer. Because of this saving in computation time, the simplified model can probably be useful especially when the other assumptions inherent in the model are considered. In critical cases a smaller value of n may be used to obtain greater accuracy.

Abrupt changes in the slopes of the temperature profiles similar to those predicted by the cocurrent model are also evident in the countercurrent case. They appear less severe than those discussed previously since they involve mostly a change in only the magnitude of the temperature gradients and not the sign.

8.5.4 Multiple Steady States

In chapter 7 the existence of multiple steady states in a countercurrently cooled single tube reactor was discussed. It was found that multiple solutions could occur when the coolant was able to heat up appreciably - either at low coolant flow rates or in long tubes. Since the coolant in a multitubular reactor can be heated considerably even at moderate coolant flow rates, it seems reasonable to expect multiple solutions to occur in countercurrent flow. This, indeed, can be demonstrated using the mixing cell model. Figure 8.23 shows coolant inlet temperature plotted against coolant outlet temperature at various values of the parameter G_c for a four pass, 50 tube diameter bundle with the data given in Table 8.1. As the value of G_c is decreased a region develops where the coolant outlet temperature becomes very sensitive to the inlet value. A further decrease of G_c leads to the occurrence of multiple steady states. For a given coolant, decreasing G_c represents a decrease in the coolant mass flow rate or velocity across the tube bundle. Although for the data used here, the multiple steady states occur at apparently low values of coolant flow rate, with larger tube bundles much more heating of the coolant will occur and so higher values of

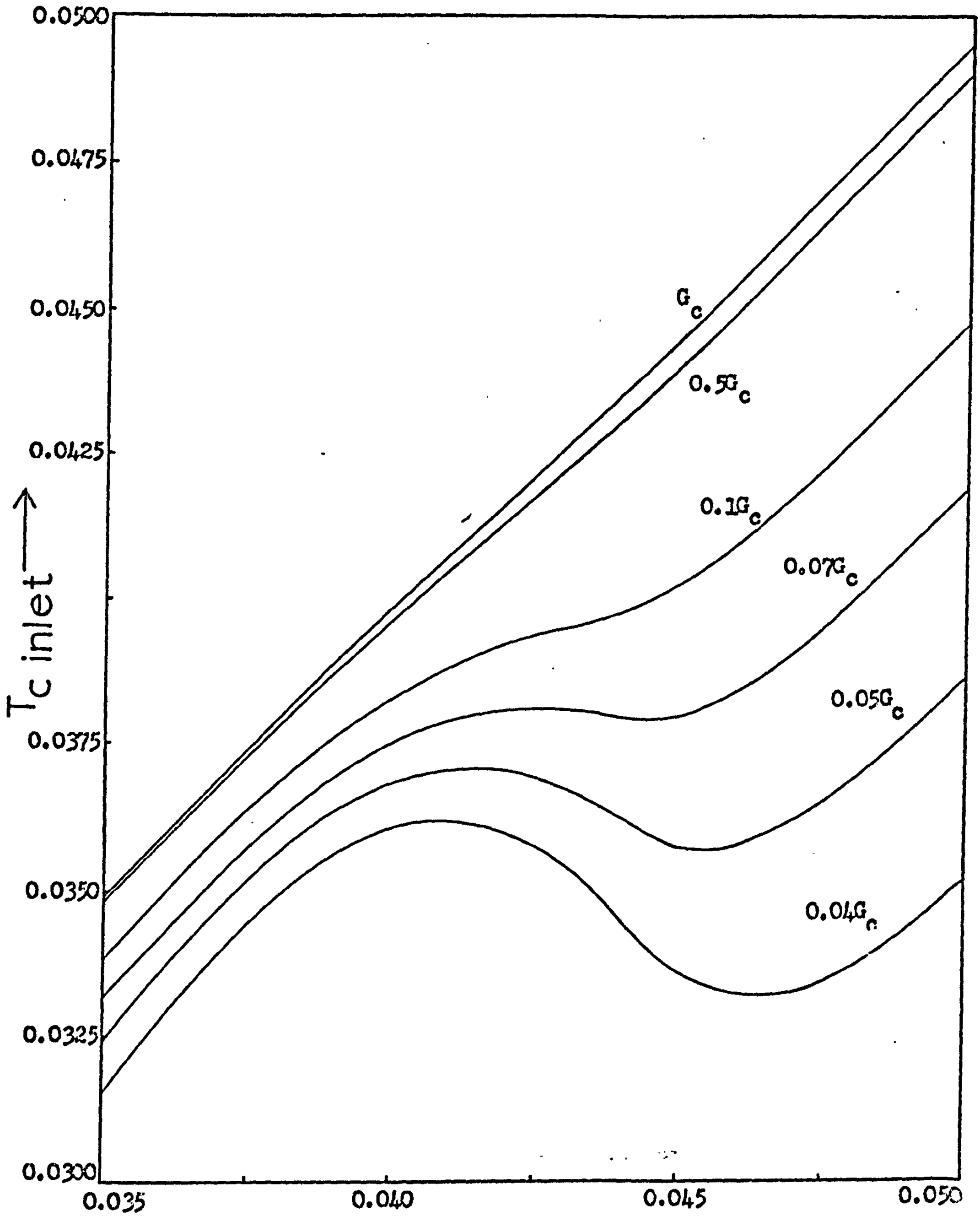

Figure 8.23 The effect of the parameter G_c on plots of coolant inlet temperature versus coolant outlet temperature with counter-current cooling. (Data as given in Table 8.1)

the flow rate will be necessary to avoid this phenomenon.

Figure 8.24 shows temperature profiles within tubes on opposite sides of the bundle for the three steady states which can occur with G_c = 63.1 and the coolant inlet temperature of 0.03790. There exists a high temperature steady state (HTSS), a moderate temperature steady state (MTSS) and a low temperature steady state (LTSS). For this value of G_c the HTSS and MTSS are close together. However, as figure 8.23 shows, a further decrease in G_c leads to greater separation of these two. In examining what is occurring in these three steady states and explaining their existence, it is perhaps easiest to start at the coolant exit (reactor entrance, coolant pass four). Nevertheless, what is happening to the coolant further along the reactor must also be borne in mind in each case. To this end, figure 8.25 has been constructed, which shows the coolant temperature at equispaced intervals in each of the steady states.

In the fourth coolant pass, where the coolant meets tube 50 first, as it flows across the tube bundle, the temperature changes by different amounts in each of the steady states. It enters this pass at the highest temperature in the HTSS and at the lowest temperature in the LTSS. In the HTSS, since the coolant is very hot it causes a large amount of reaction to take place, generating a lot of heat and thereby becoming hotter itself. As it flows across the tube bundle it, therefore, tends to generate even more heat within the tubes. Near the exit from this pass, the much greater rate of reaction causes very high tubeside temperatures and, therefore, a large amount of reactant consumption. This process is similar in the LTSS, but since the coolant enters this pass at a much lower temperature than in the HTSS, less reaction takes place, generating less heat and so neither the tubeside temperatures nor the coolant temperature become so high as in the HTSS. Also, of course, less reactant is consumed. The behaviour in the MTSS in this pass lies between that of the HTSS and the LTSS.

In the third coolant pass (second from the reactor entrance) the coolant flow direction is reversed. It flows from tube one across the bundle to leave at tube 50. In this pass the coolant entrance temperature in the MTSS is greatest,

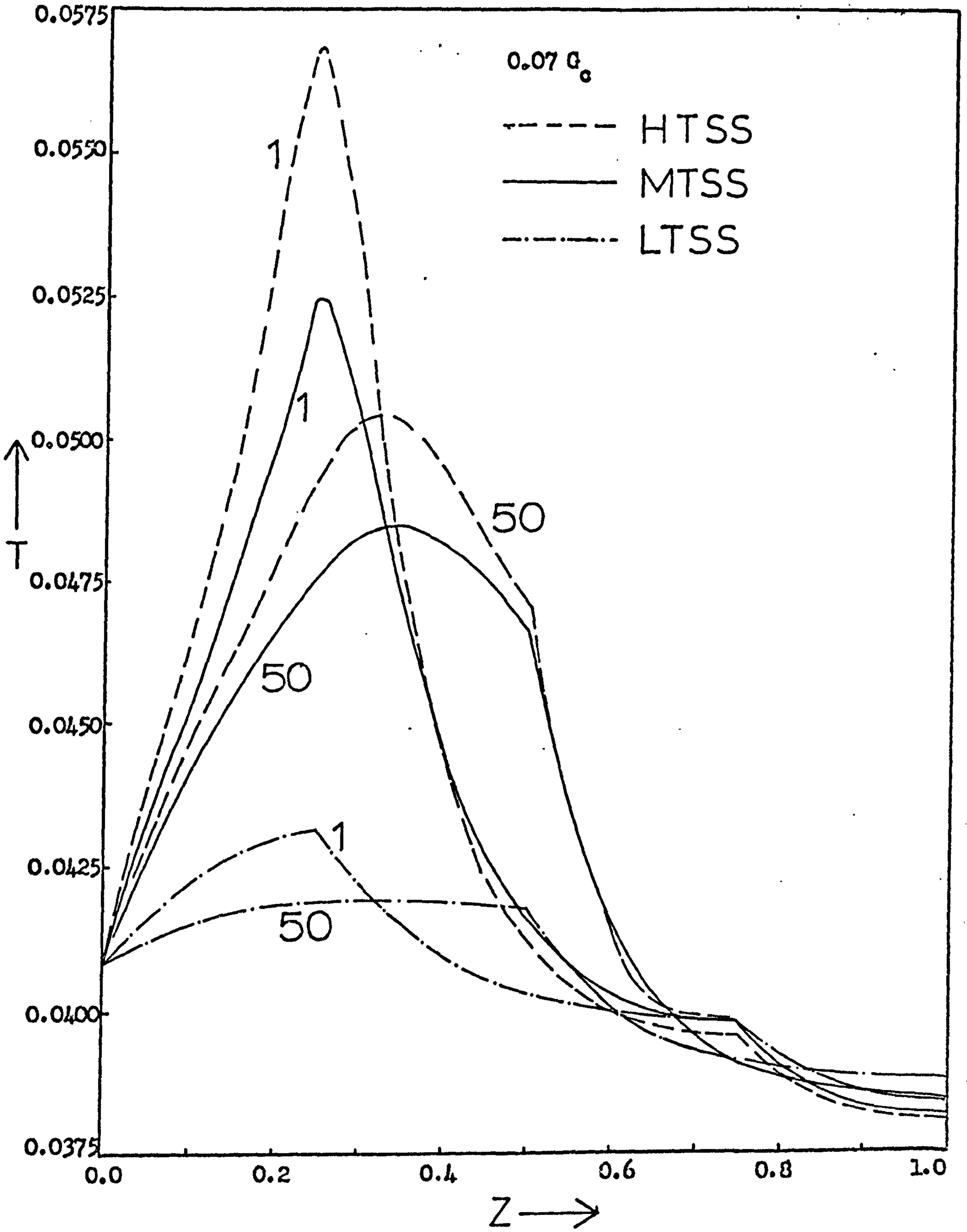

Figure 8.24 Axial profiles of radial mean temperature within tubes on opposite sides of the bundle for the three simultaneous steady states occurring with $G_c = 63.1$ and $T_{co} = 0.03790$ in the countercurrently cooled reactor. (Data as given in Table 8.1)

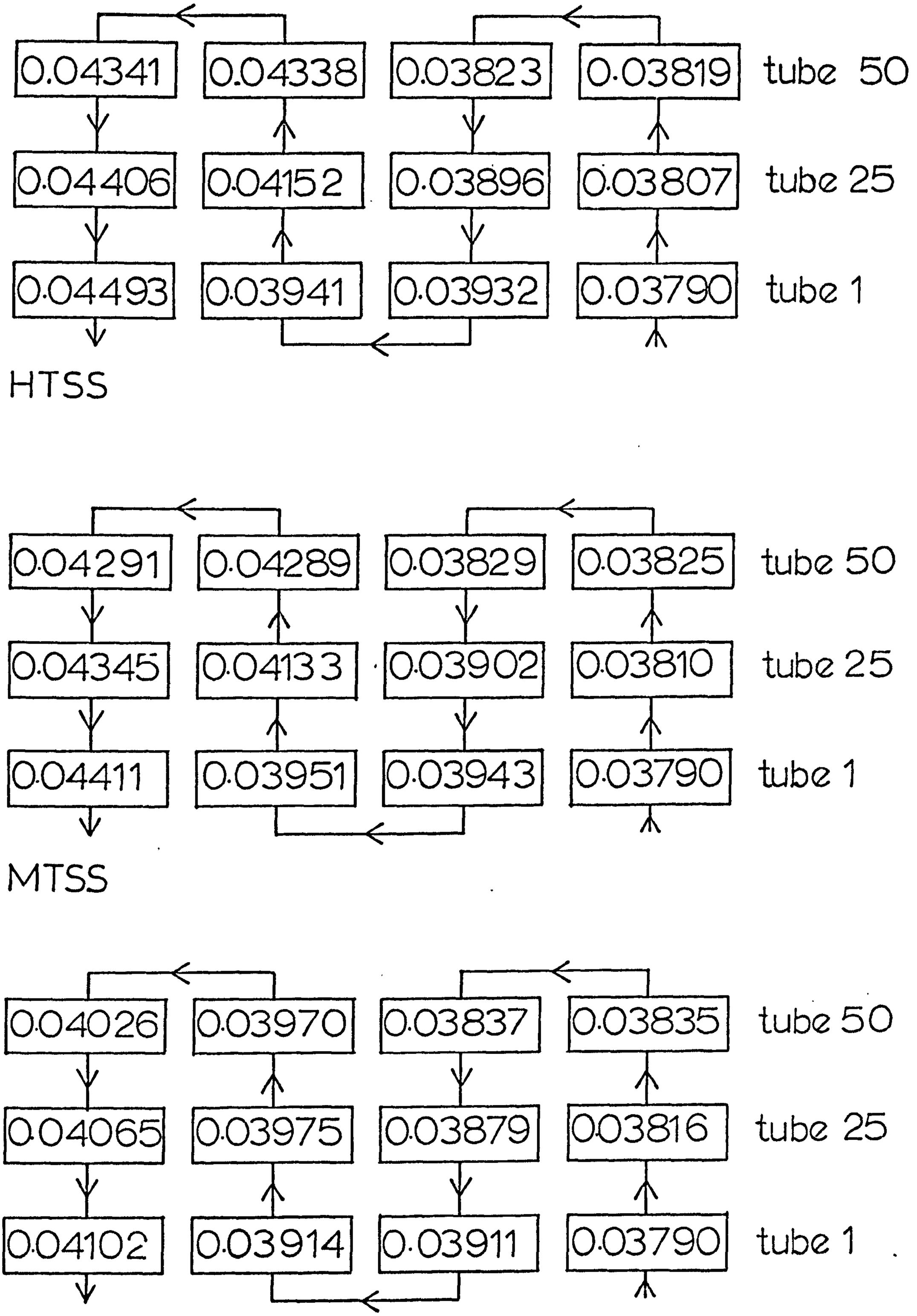

Figure 8.25 Coolant temperatures in the three steady states occurring with G_c = 63.1. The tubeside temperature profiles are shown in figure 8.24. (Other data as given in Table 8.1)

and least in the LTSS. But as described above on leaving this pass to enter the fourth pass it is greatest in the HTSS and least in the LTSS. In the HTSS the tubeside gases entering this pass are hottest and leanest in reactant near the coolant entrance (tube 1). This is also true of the LTSS and the MTSS, but for the reasons explained above in the fourth pass, the levels of temperature and reactant concentration are greatest in HTSS in this pass. In the HTSS the heat removed by the coolant in the first half of this pass is mainly the excess heat of the tubeside gases, since the temperature difference between tube and coolant is very large here. Consequently, relatively little reaction takes place in the first half of this pass. Also it must be remembered that here the tubeside gases are very lean in reactant because of consumption in the fourth pass and so any reaction which takes place reduces the reactant concentration to a very low value. In the second half of this pass in the HTSS the situation is somewhat different. A hotter coolant is reaching cooler tubes with greater reactant concentration than in the first half of the pass. This causes more reaction to take place generating more heat. This heat cannot be removed so easily since the coolant is becoming hotter and so the gases leaving this half of the pass are at a higher temperature than those leaving the first half. The reactant concentration is also higher here than in the first half of the pass.

At the coolant entrance to the third pass in the LTSS the entering tubeside gases are much cooler and richer in reactant than in the HTSS (tube 1) and they are experiencing on lower temperature coolant than in the HTSS. In the first part of the pass, the entering gas temperature is high enough to cause a fair amount of reaction to take place despite the low coolant temperature. Because of the low coolant temperature the reaction heat is easily removed by the coolant, which, therefore, becomes hotter as it flows across the tube bundle. In the last part of the pass the gases entering the tubes are at a lower temperature than in the first part, and the increased temperature of the coolant in this part is sufficient to maintain the reaction rate, but still low enough to remove the generated heat. Consequently, the gases leaving this coolant pass increase in temperature in the direction of coolant flow,

but contain approximately the same amount of reactant through out the pass. Because of the lower tubeside temperatures and reaction rates in this pass in the LTSS the coolant is not heated so much as in the HTSS.

The situation in the MTSS in this pass is very similar to that in the HTSS, but because the tubeside temperatures are lower, not so much heating of the coolant occurs as in the HTSS.

At the second coolant pass (third from the reactor entrance) the coolant entering in the LTSS is at the highest temperature and that of the HTSS is lowest. At the coolant exit from this pass, however, the MTSS coolant temperature is highest and that of the LTSS is lowest. In this pass the coolant flows across the bundle from tube 50 to tube 1. In the HTSS, the tubeside gases entering this pass are hottest and richest in reactant at the coolant entrance (tube 50) but cool and very lean in reactant near the coolant exit (tube 1). Thus, in the first part of this pass the coolant heats up by removing the excess heat of the gases since it is much cooler and so prevents much reaction taking place. Less heating of the coolant occurs in the second part of this pass in the HTSS since the gases here are much cooler than in the first part. Also since the tubeside gases are much leaner in reactant near the coolant exit from this pass, less reaction takes place than in the first part despite the higher coolant temperature. In the HTSS in this pass, the coolant is heated mainly by the excess heat of the gases rather than by removal of generated reaction heat.

In the LTSS the heat removed by the coolant is mostly generated reaction heat since the tubeside gases are fairly cool. Although the amount of heat generated is much greater than in the HTSS the coolant does not become as hot as in the HTSS because of the very large amount of excess heat removed in the HTSS.

In the MTSS the situation is similar to the HTSS in this pass. However, since the gases are richer in reactant than in the HTSS, more reaction takes place and so the coolant becomes hotter than both the HTSS and the LTSS.

The coolant enters the fourth pass at the same temperature in each steady state. In the LTSS the gases are richer in

reactant than the HTSS and so more reaction takes place, thereby heating the coolant more than in the HTSS. In the HTSS very little reaction occurs in the first part of this pass since the gases are very lean in reactant. In the second part of this pass, however, more reaction takes place but the entering tubeside gases are cooler. Again, the behaviour of the MTSS is similar to that of the HTSS, but being richer in reactant than the HTSS, more reaction takes place and so the coolant becomes slightly hotter.

It can be seen that the existence of the multiple states is due to the feed-back of heat through the tube bundle by the coolant. Clearly, if the coolant is prevented from heating up very much by, for example, operating the reactor at high coolant flow rate then the feed-back of heat cannot occur and the possibility of multiple states is avoided. The necessary coolant flow rate depends on several factors including the heat of reaction, the number of tubes in the bundle and the overall heat transfer coefficient between the gases and the coolant. Too high a coolant flow rate may cause quenching of the reaction, but this can be avoided by using a higher coolant inlet temperature. Sometimes the situation may arise when cross-flow cooling is essential to achieve the correct amount of heat transfer, but only low flow rates are possible because of pumping costs. In which case cooling of the coolant between passes by, for example, using it to raise steam may be necessary if the possibility of multiple states is to be avoided.

8.5.5 The Influence of the Model Parameters

Figures 8.26 and 8.27 show the effect of coolant flow-rate, in terms of G_c, on the tubeside temperature and concentration profiles outside the region of multiple solutions (Note. Only the concentration profiles in tube 1 are shown since those in tube 50 are similar). The effect is similar to that found in the cocurrent case; increasing the coolant flow rate leads to lower tubeside temperatures due to the smaller amount of heating experienced by the coolant. The countercurrent reactor shows greater sensitivity to G_c than the cocurrent one (c.f. figure 8.11) even at high values. This is because the entrance regions of the tubes, which are the parts richest in reactant, experience higher coolant temperatures in the countercurrent case, and so more reaction takes place there. For

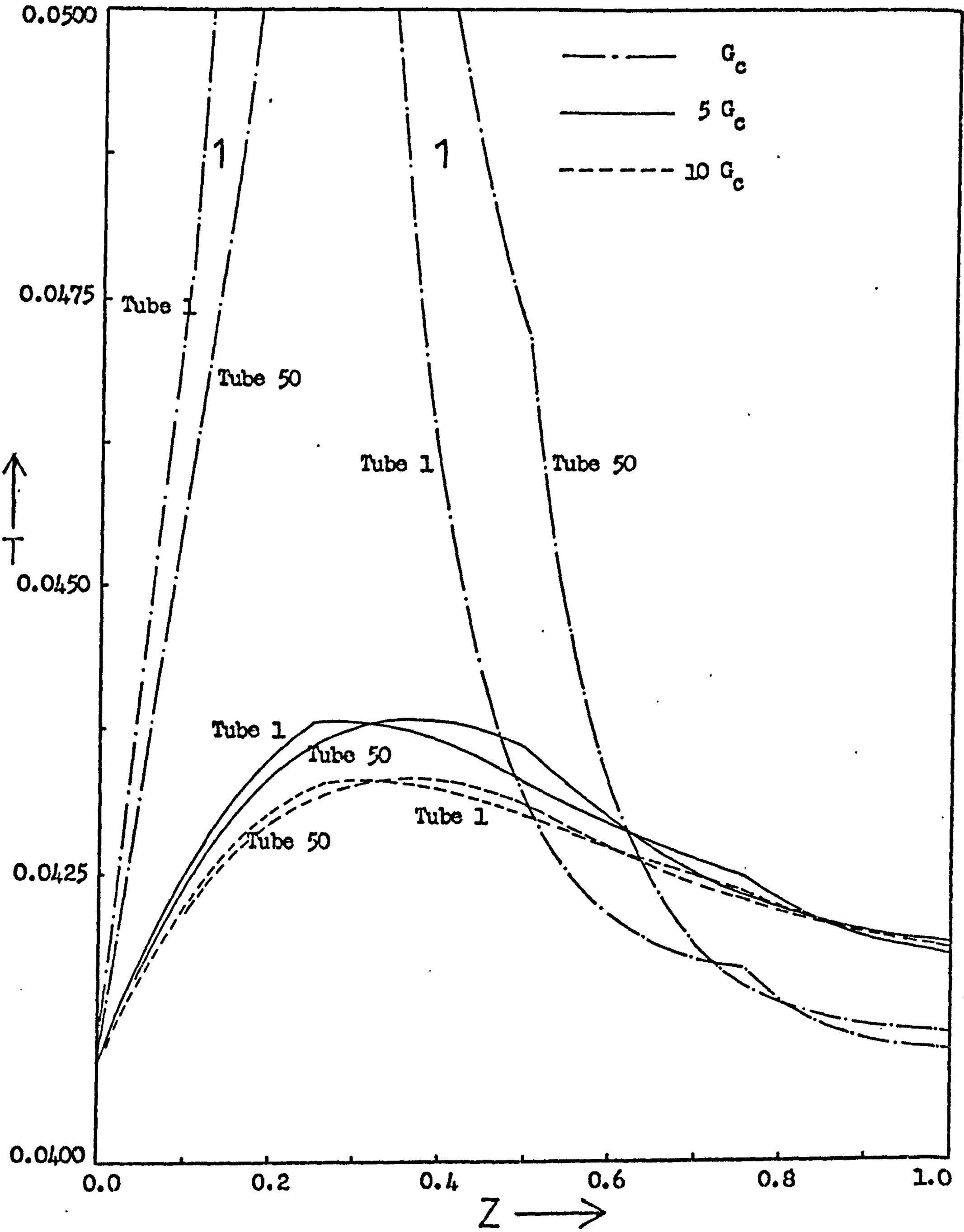

Figure 8.26 The effect of the coolant flowrate on the axial profiles of radial mean temperature within tubes on opposite sides of the bundle in the countercurrently cooled reactor. (Data as given in Table 8.1)

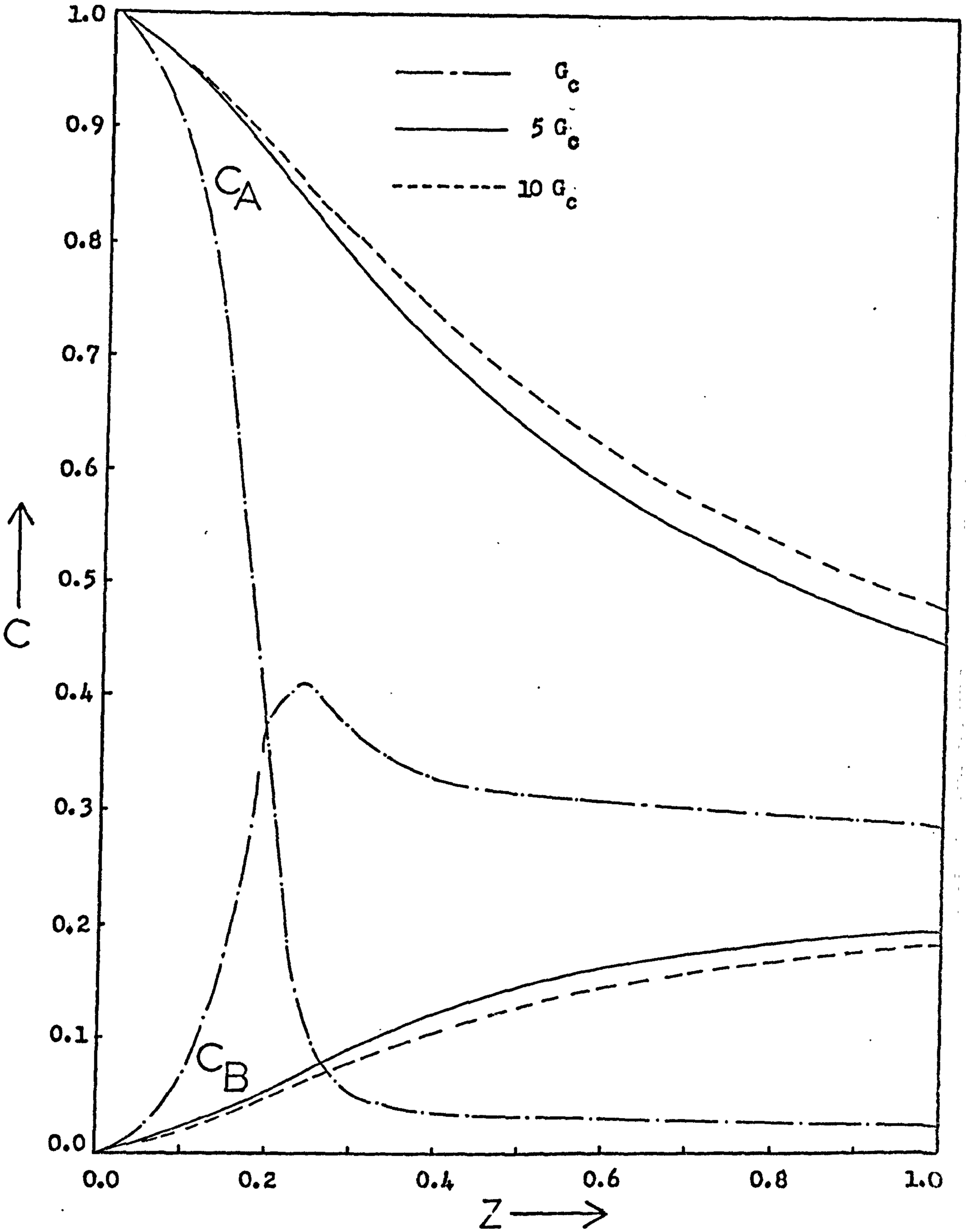

Figure 8.27 The effect of the coolant flowrate on the axial profiles of radial mean concentration within tube 1 in the countercurrently cooled reactor. (Data as given in Table 8.1)

the data used here, temperature runaway occurs at a much lower value of G_c in the countercurrent reactor than in the cocurrent. From figure 8.27, it appears that the last 60% to 70% of the reactor length serves only to preheat the coolant for the first part of the reactor, most of reactant A having been consumed before the last section is reached and mainly product B being consumed there. Clearly, this behaviour is undesirable.

It appears that the countercurrent reactor must be operated at higher coolant flow rates than the cocurrent.

The effect of increasing the number of coolant passes at a constant total coolant mass flow rate (i.e. constant G_c) is shown in figures 8.28 and 8.29. Increasing the number of coolant passes from four to six whilst keeping the mass flow rate constant has little effect on either the tubeside temperature profiles, or the coolant outlet temperature. Indeed, if graphs similar to figure 8.23, where the coolant inlet temperature is plotted against its outlet value, are constructed for the case of five and six coolant passes, then in the region of multiple solutions the differences between them are extremely small.

For a given coolant flow rate it is possible to divide the coolant inlet and outlet temperatures into two regions. Referring to figure 8.23 these two regions are roughly a low outlet temperature region from 0.035 to 0.40 where the coolant inlet temperature is correspondingly low, and a high outlet temperature region from 0.040 onwards. With this division, the insensitivity of the reactor to the number of coolant passes is more easily examined.

In the low coolant outlet temperature zone, the coolant temperature throughout the tube bundle is very low. Consequently, at all points in the reactor the rate of reaction and, therefore, the rate of heat generation is very small. This means that the amount of heat to be removed by the coolant is so small that changing the number of coolant passes has no effect. In the higher coolant outlet temperature zone, the situation is somewhat different. Because the coolant outlet temperatures are high in the first part of the tube bundle, a large amount of reaction takes place consuming most of the reactant. In

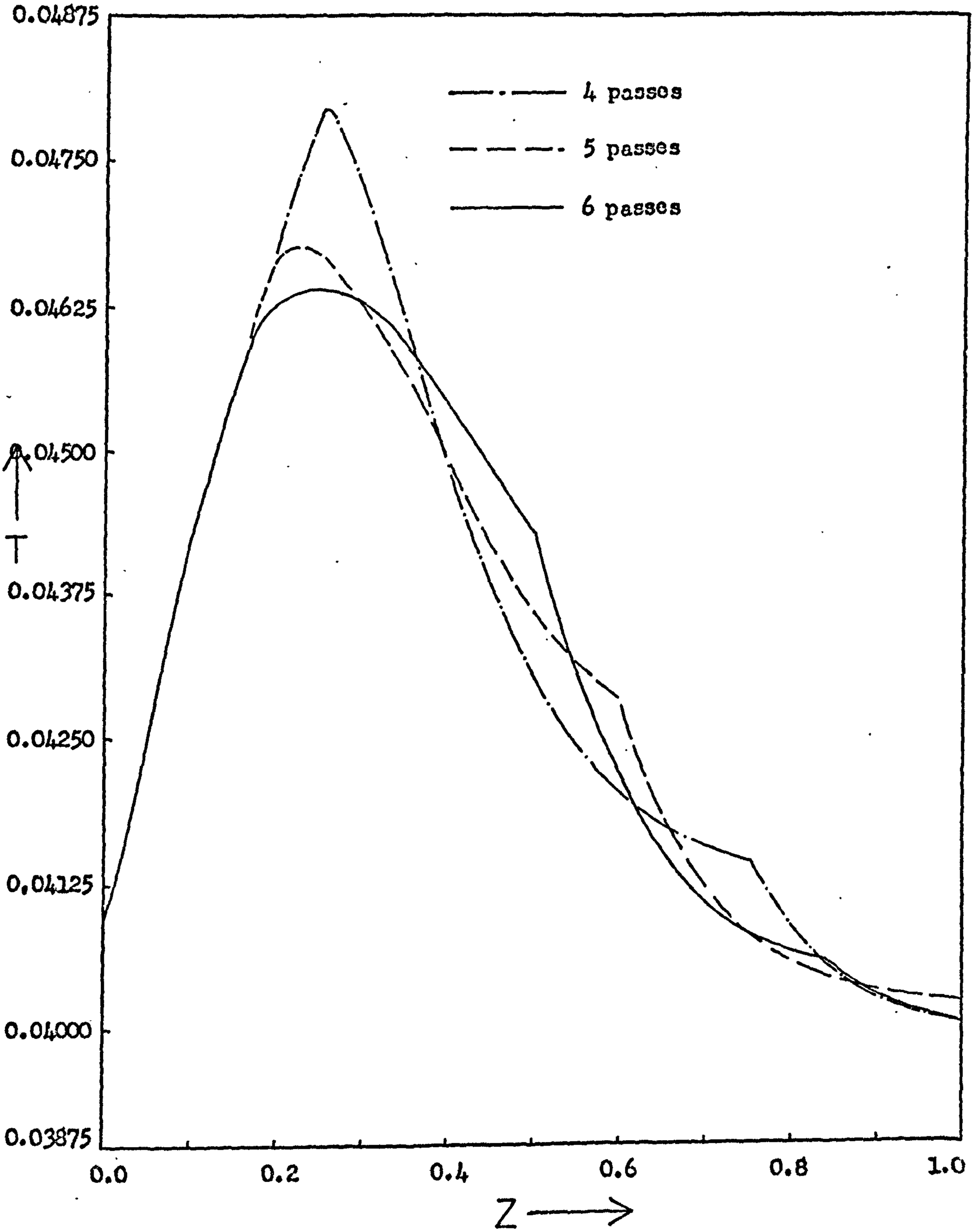

Figure 8.28 The effect of the number of coolant passes (at a constant coolant mass flowrate) on the axial profiles of radial mean temperature within tube 1 in the countercurrently cooled reactor. (Data as given in Table 8.1)

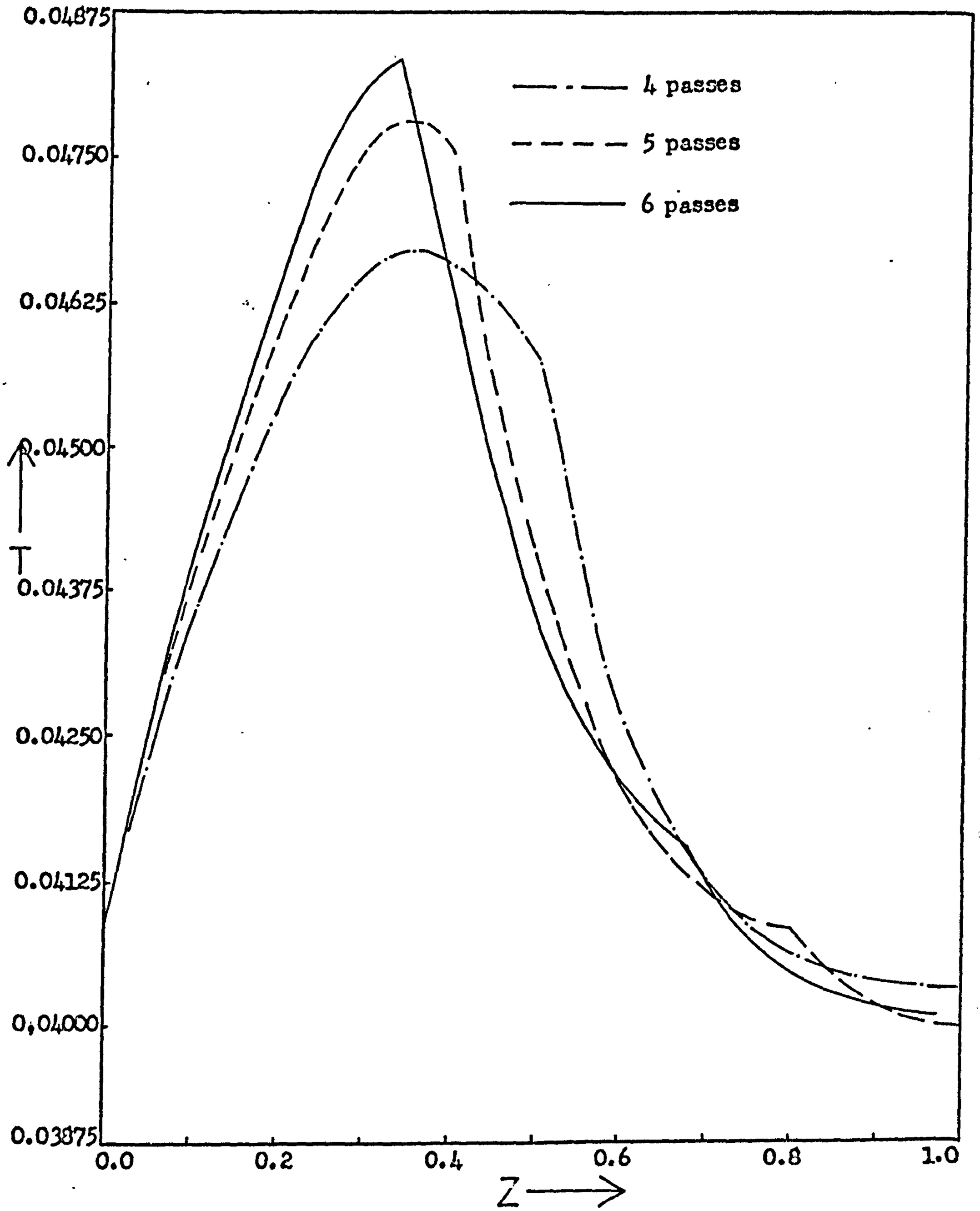

Figure 8.29 The effect of the number of coolant passes (at a constant coolant mass flowrate) on the axial profiles of radial mean temperature within tube 50 in the countercurrently cooled reactor. (Data as given in Table 8.1)

this part of the reactor the heat generation within the tubes is the dominant process. In the second part of the reactor, near the coolant inlet, very little reaction takes place and heat transfer from the tubes to the coolant is the dominant process. This can be for two reasons. It is either that so much reactant has been consumed in the first part of the tubes that there is insufficient to cause much reaction in the second part, or that the coolant temperatures in this part of the reactor (near the inlet) are low enough to quench the reaction. Consequently, this part of the reactor is acting essentially as a heat exchanger, and since the gases entering it are at approximately the same temperature whether the number of passes is four, five or six, and the coolant mass flow rate is the same in each case, they are cooled by similar amounts and the coolant is heated by similar amounts. In the first half of the reactor, heat is being generated much faster than it can be removed and so the tubeside temperatures tend to be similar whatever the number of coolant passes. Thus, there is a similar amount of heat available to the coolant in each case so that although the amount of coolant heating in each pass varies with the length of the tubes, the total coolant heating in this part of the reactor is similar in each case and it therefore leaves the reactor at very similar temperatures.

From this it may be concluded that, at least for the data used here, increasing the number of coolant passes beyond four gains no specific advantage.

8.6 Comparison of Reactor Performance with Single Tube Predictions

The usefulness of the simple multitubular models may be demonstrated by comparing their predictions with those of a single tube model. The single tube model used for this purpose is that described in chapter 7, with the coolant flowing parallel to the tube axis. The two models are not strictly comparable because of differences of achievable coolant to tube heat transfer coefficient in the crossflow and parallel flow case. For this reason two cases of the single tube model have been considered. All parameters, including the coolant mass flow rate, are the same as used in the multitubular model in each case with the exception of the overall tube-coolant

heat transfer coefficient. In one case the same value as that used with the multitubular model has been used, and in the other a lower value computed from Chechetkin's[121] data for parallel flow has been used. For the coolant mass flow rate used this gives a value of 9.0 for the wall Nusselt number.

Figure 8.30 shows the axial profiles of radial mean temperature predicted by both models for cocurrent coolant flow. Obviously, the predictions of the single tube model are quite different from those of the multitubular model. Neither of the single tube predictions appear typical of the multitubular behaviour. This is to be expected since the coolant in the multitubular case is heated by other tubes in the bundle, and there is no allowance for this in the single tube model. A multitubular reactor designed on the basis of the single tube predictions would obviously not function in the manner intended.

This is further emphasised by the countercurrent coolant models. The temperature profiles labelled (1) in figure 8.31 were predicted by the single tube model with countercurrent cooling at the same parameter values and coolant inlet temperature as the profiles labelled (1) in figure 8.26 which were obtained with the multitubular model. This suggests that an apparently safe design based on the single tube model would, in fact, give rise to temperature runaway. The profiles labelled (2) in figure 8.31 are comparable with the multitubular prediction shown in figure 8.22. Again both models predict quite different behaviour.

8.7 Concluding Remarks

Two very simple models of a multitubular reactor have been formulated and used for a preliminary study of the performance of these systems. Both consist essentially of a heat balance on the coolant within the tube bundle, a momentum balance being precluded by several simplifying assumptiors.

The continuum model which, as its name implies, describes the tube bundle as a continuum in a manner analogous to the single tube reactor models, has shown that the temperature gradients in the coolant perpendicular to the coolant flow are relatively small. This model has been compared with another in which the tube bundle is divided into a series of connected

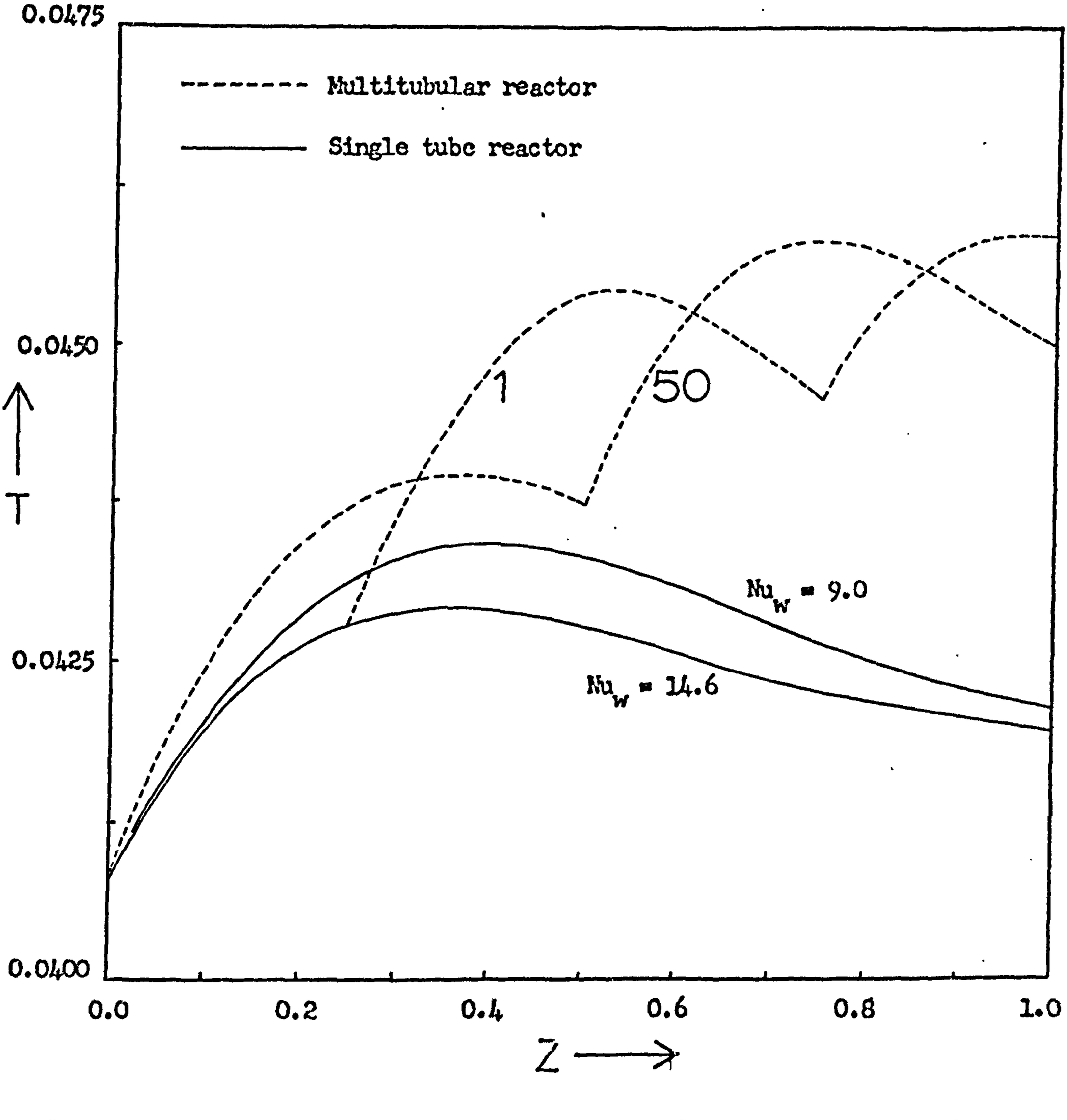

Figure 8.30 Comparison of the axial profiles of radial mean temperature predicted by the multitubular and single tube reactor models with cocurrent cooling. (Data as given in Table 8.1)

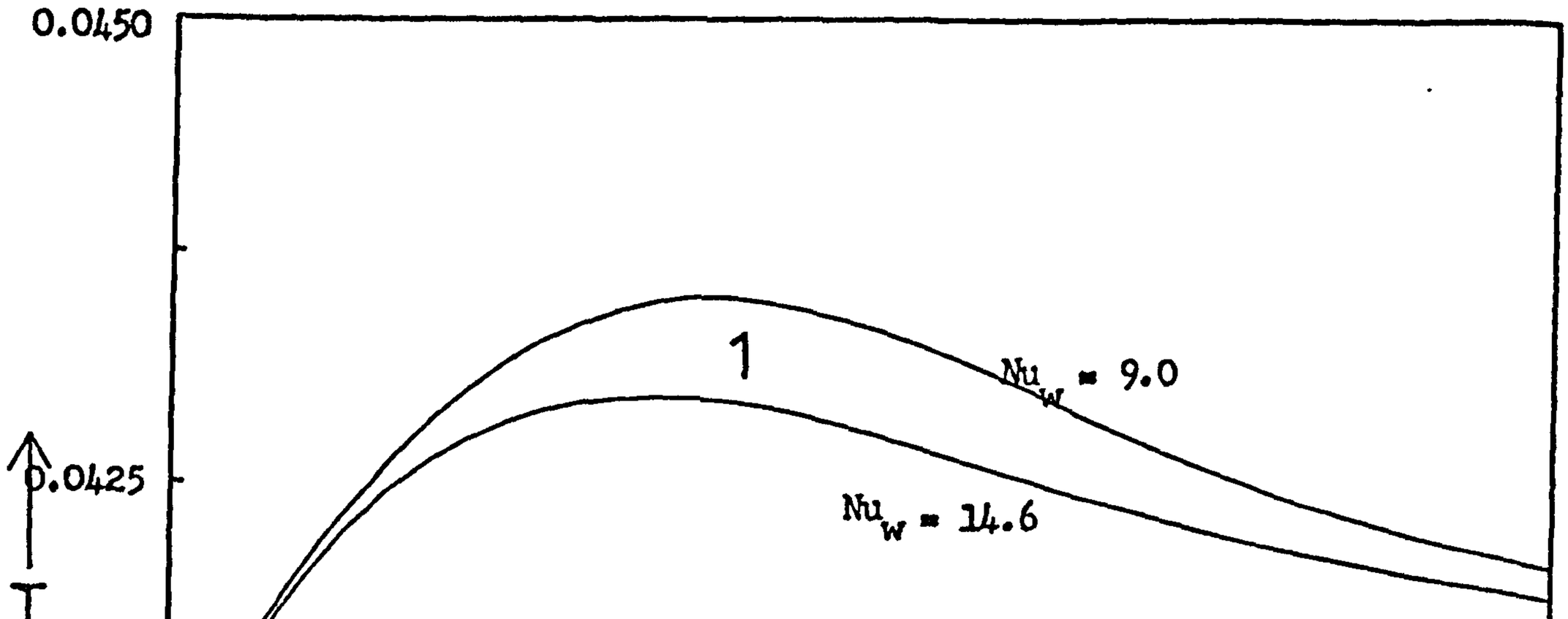

Figure 8.31 Axial profiles of radial mean temperature predicted by the single tube reactor model, with countercurrent cooling, at two values of coolant inlet temperature and wall Nusselt number. Curves 1 correspond with curves 1 of figure 8.26 and curves 2 with the multitubular reactor profiles shown in figure 8.22. (Data as given in Table 8.1)

mixing cells with the coolant temperature assumed uniform, in the direction perpendicular to flow, in each cell. Both models show very good agreement as might be expected from the results of the continuum study. However, the advantage of the mixing cell model is its much faster computation time. It has been shown that provided that the coolant is not heated too rapidly as it flows across the bundle, the mixing cell model can be further simplified so that it requires approximately one thirtieth of the computation time of the continuum model.

It seems probable that because of the assumptions embodied in both models, they tend to predict higher coolant temperatures than actually occur, at all but the highest flow rates. This problem might be overcome by the inclusion of a more detailed heat and mass balance on the coolant, although this would seriously affect the computation time. Despite this shortcoming, the mixing cell model appears to be particularly useful for determining a suitable experimental research programme on tube bundles and in indicating the important aspects in multitubular reactor design.

Using the mixing cell model, both cocurrent and countercurrent reactor configurations have been simulated. It has been shown that even at moderate coolant flow rates, tubes in different parts of the bundle can show significantly different behaviour. This means that with highly exothermic reactions such as those considered here it is necessary to monitor several tubes in the bundle. However, it must be emphasised that this does not imply that the information obtained from the study of single tube reactors is of little use in the design of multitubular systems. Since the single tube models form the building blocks of a multitubular model, a knowledge of their behaviour as individual units is required. Pilot plant studies for gaining data, especially about the tubeside behaviour of the system, are more conveniently carried out using a single tube. Although the non-linear effect of the environment, in multitubular reactors, on individual tubes prevents a single tube from being totally representative of the whole bundle, the general features of behaviour are the same whether the tube is in a bundle or on its own. Moreover, in parallel flow reactors radial coolant temperature gradients are small and so a single tube is representative of the bundle.

In countercurrently cooled reactors, the possibility of the occurrence of multiple steady states has been demonstrated, together with the existence of regions of great sensitivity to the coolant inlet temperature. Such regions of operation may be avoided by using a high enough coolant flow rate or some form of inter-pass heat exchange of the coolant.

For the data used in this study, it appears that a co-currently cooled reactor is preferable to countercurrent cooling since greater conversions of the reactant at high coolant flow rates are obtained in this case. If the coolant must be prevented from becoming too hot, the cocurrent configuration is still more attractive since for a given tubeside temperature rise, and reactant conversion, a lower coolant flow rate is acceptable, which, therefore, means that pumping costs are reduced. However, since for the data given in Table 8.1, at most coolant flow rates the second half of the countercurrently cooled reactor acts essentially as a coolant preheater, a shorter reactor could be used with a separate heat exchanger. This would probably give great savings in the capital cost of the reactor.

Further work is necessary to formulate a more detailed model of a multitubular reactor taking into account the fluid dynamics of the coolant as well as heat and mass transfer between adjacent coolant passes. This should, preferably, be done in conjunction with experimentation on a suitable reactor in order to establish the validity of the model structure and to investigate the possibility of obtaining reliable values of the parameters.

CHAPTER 9

FINAL COMMENTS

9.1 Summary of the Present Work

Consideration has been given to various aspects of the dynamic behaviour of fixed bed reactors supporting highly exothermic reactions and to the development of a mathematical model suitable for describing the steady state behaviour of a multitubular reactor. A method has been proposed for predicting the onset of parametric sensitivity and its application in the design and control of a heterogeneous fixed bed reactor has been discussed. This work has clearly identified the important features of behaviour of these systems.

In order to establish the structure of a two dimensional model of the reactor, two methods of describing radial heat transfer in fixed bed reactors have been compared and the significance of the various mechanisms contributing to the radial heat flux has been discussed. Under most conditions the radial heat flux due to the presence of the catalyst pellets is likely to be small compared with that caused by lateral mixing of the gas. Even when it is significant, it can be automatically accounted for in a single phase heat transfer model, which refers radial heat transport to the gas phase, by appropriate estimation of its effect on the pellet to gas surface heat transfer coefficient and a method has been proposed for this. Furthermore, the single phase heat transfer model is a more appropriate formulation since it allows the very important reaction rate limiting effects due to mass transport resistances within the catalyst pellet to be determined as the calculation of the reactor behaviour proceeds. This is not possible in the two phase heat transfer model for conceptual reasons and so the effectiveness factor must somehow be estimated a priori.

The single phase heat transfer model has been used in the formulation of a two dimensional dynamic model of the heterogeneous fixed bed reactor which has been used to evaluate a simpler one dimensional model incorporating the assumption of a parabolic radial temperature profile. Although the simpler formulation can be made to give good agreement with the two

dimensional model in terms of the radial mean state variables, it tends to underestimate the centre line temperature in the reactor. Nevertheless, it is very suitable for a qualitative study of the dynamic behaviour and has, therefore, been used extensively in this thesis. The computational effort demanded by the two dimensional model precludes its use in a comprehensive study of reactor dynamics. It must, however, be used in those circumstances where the simpler model is unsuitable; for example where the axial rather than the radial mean temperature must be accurately predicted and where serious distortion of the radial temperature profiles is likely to occur.

The effect of the tube wall on the transient response of the reactor has been examined and found to be negligible when the heat transfer resistance between the wall and the coolant is much less than that on the inside of the tube. Since in most industrial reactors this is usually the case the tube wall does not appear to be a significant dynamic element and, therefore, need not be included in a dynamic model of these systems.

When the reactor is controlled by manipulation of the inlet conditions some oscillation of these variables is likely to occur. For this reason the behaviour of the reactor towards sinusoidally varying inlet temperature and concentration has been examined. The response of the reactor to this type of perturbation may be divided into two distinct stages; an initial transient period during which the greatest disturbances occur and a subsequent quasi-stationary state in which regular oscillation of the whole bed is established. As might be anticipated, outside of the region of multiple states of the catalyst pellets the amplitude and frequency of the forcing oscillation determine whether or not the quasi-stationary state exhibits temperature runaway. Depending on the initial direction of the perturbation, temperature runaway may occur during the initial transient period even though the subsequent quasi-stationary state is safe. The reasons for this behaviour have been examined in detail and it appears to be due to the relative speeds of propagation of temperature and concentration waves within the bed coupled with the effect of parametric sensitivity. The thermal capacitance of the

catalyst pellets slows down the initial temperature wave so that at certain amplitudes and frequencies of the forcing oscillation it may interact constructively with the crests of the fast moving induced concentration waves. This causes high temperatures to develop which remain until the initial temperature wave leaves the bed.

This behaviour has not been observed when the reactor trajectories lie in the non-unique region of solutions. In this case once temperature runaway occurs during the initial transient period it is sustained in the quasi-stationary state unless the amplitude of the forcing oscillation is sufficient to regain the lower temperature state.

In both the unique and non-unique regions of operation, a safe quasi-stationary state may occur even though the amplitude of the inlet perturbation is sufficient to cause temperature runaway under non-oscillating conditions. Similar behaviour has been observed in previous single pellet studies[85] and is determined by the frequency of the oscillation.

This behaviour of the reactor towards oscillating inlet conditions has important implications on the control strategies which may be adopted. It also serves to illustrate the complex way in which the various physical and chemical processes within the system can interact to give quite unexpected behaviour making an intuitive analysis unreliable.

The nature and importance of the effect of a flowing coolant on the behaviour of a single tube reactor has been examined for both cocurrent and countercurrent flow. An analysis of the cause of multiple states during countercurrent operation has shown that although this phenomenon will probably not cause difficulties with single tube reactors it may be a problem in multitubular systems. The dynamic studies of the effect of perturbations of the coolant temperature, although somewhat limited, have clearly shown that control of the reactor by manipulation of this variable may be as difficult as with the inlet temperature of the reaction gases. Indeed, the response of the reactor to changes in the coolant temperature shows exactly the same features as that to changes in the gas inlet temperature; namely a rise in the hot spot temperature before the bed cools when the coolant temperature

is reduced and a fall in the hot spot temperature before a new peak develops when the coolant temperature is raised. This behaviour, which is due to the distributed nature of the system, occurs with both cocurrent and countercurrent cooling although in the latter case the temperature profiles within the bed do show some initial tendency to move in the same direction as the disturbance so that the subsequent response is slower and less severe.

The effect of the cooling environment has been further studied by the formulation of a steady state model of a multitubular reactor. Although the proposed model represents the minimum level of detail which may be adopted in tne mathematical description of these complex systems, it has nevertheless amply demonstrated some of the problems which may arise in their operation. In particular, there is considerable interaction not only between different tubes in the bundle but also between different parts of the same tube due to the transport of heat through the bundle by the coolant. In countercurrently cooled crossflow reactors the backward movement of heat in the coolant may cause multiple states to develop at low coolant flow rates. This undesirable phenomenon is more likely to occur in multitubular than in single tube systems because of the larger amounts of heat which are generated and the limitations which may be imposed on the coolant flow rate by pumping costs. The problems associated with heat removal in multitubular reactors are very great. Too high a coolant flow rate can cause too much cooling and, therefore, poor reactant conversion whereas too high a value leads to severe coolant heating and very high tubeside temperatures which may also cause bad selectivity of the desired product. Even at moderate coolant flow rates the nature of heat dissipation is such that tubes in different parts of the same bundle may exhibit quite different behaviour so that no single tube is representative of the whole. This means that design and control based on only a single tube could be inappropriate and the use of even a simple multitubular model for these purposes is essential.

The stability problem associated with parametric sensitivity in heterogeneous reactors has been examined and a method for predicting parametric sensitivity has been proposed. This method, which is based on the inherent properties of heterogeneous

systems rather than arbitrarily defined temperature levels or gradients, enables regions of parametric sensitivity to be plotted on a simple phase diagram for any set of system parameters. Reactor trajectories may be plotted on the same diagram so that potential operating difficulties due to temperature runaway are immediately apparent. The use of this parametric sensitivity criterion in the design and control of heterogeneous reactors has been discussed and it has been shown that simple charts may be prepared which show the relationship between local and global stability of the reactor. The analysis has further emphasised the importance of considering all of the essential transport resistances within the catalyst pellet. This form of parametric sensitivity arises due to the heterogeneity of the system and is, therefore, quite distinct from that observed in quasi-homogeneous systems which is only a manifestation of the non-linear dependence of the reaction rate on temperature. This makes sensitivity and stability criteria derived for quasi-homogeneous systems inappropriate for application to heterogeneous reactors.

9.2 Suggestions for Further Work

Much remains to be done. Since this work has been concerned mainly with establishing a qualitative picture of reactor behaviour, further investigation in quantitative terms is necessary using a more detailed reactor model. In particular, since for control purposes the centre-line temperature in the reactor is the most critical it must be more accurately studied. The results of a parallel study[15] have already shown that the computational load of the two dimensional model can be greatly reduced by the use of a more efficient method of solution and a one dimensional dynamic model which more accurately describes the radial temperature profiles is now available.[15] Both of these should be used to re-examine the important features of reactor behaviour which have been revealed in this work.

It is necessary to establish the relationship between amplitude and frequency of the inlet oscillations which produce temperature runaway in both the initial transient response and the quasi-stationary state. The results of a similar study on a single catalyst pellet[85] suggest that this will require a semi-empirical rather than wholly analytical approach.

The effect of both pulsed and noisy inlet disturbances on the reactor behaviour must also be examined since these may have similar effects to the oscillatory disturbance.

The study of the effects due to the coolant is by no means complete. No attempt has been made to investigate either oscillating coolant inlet temperatures or changing coolant flow rates. For this work a two dimensional model of the reactor will be essential because of the distortion of the radial temperature profiles which is likely to occur. It may be possible to take advantage of the distributed nature of the system and control the reactor by sequential or parallel manipulation of both the coolant temperature and one of the inlet variables so that the effects of one disturbance are used to oppose those of the other. Clearly, there are a whole range of such combinations but it should be possible to establish some general rules suitable for use in the design of a control system. This study could be combined with further investigation of the stability problem. Although the work reported here has shown that it is possible to predict the change necessary in each of the inlet variables when the other is disturbed if safe operation is to be maintained, no information has been obtained on how these changes should be made. This is particularly important since temperature runaway must be avoided in the transient period as well as the steady state.

The problems investigated with multitubular reactors merit much more study. A more detailed model must be formulated to include more tubes and a momentum balance on the coolant. This would then enable the study of the effects of the variation of the coolant velocity across the bundle and also facilitate a more judicious investigation of suitable coolant flow rates. The results obtained in the present work leave little doubt that the dynamic behaviour of multitubular reactors requires study. It seems probable, however, that the computational effort required in such an investigation might preclude more than a limited study. It may be possible to obtain some indication of the dynamic behaviour of these systems using a quasi-homogeneous model for the reactor tubes since this will greatly reduce the computational burden. However, the results obtained would obviously not be applicable in a heterogeneous situation and should, therefore, be treated with caution.

Finally, experimental work with both single tube and multitubular reactors is necessary. The theoretical studies have shown what information is required and the pitfalls to be avoided in obtaining it. Experimentation should be directed at checking out some of the assumptions embodied in the models as well as obtaining more physical data for specific systems. In this way the mathematical models may be more widely applied so that the advantages of improved reactor design and control through their use may be realised.

APPENDIX 1

THE CATALYST PELIET MODELS

A1.1 The Fully Distributed Catalyst Pellet Model

A1.1.1 The Steady State

For a spherical catalyst pellet in which the n th order A⟶B reaction with Arrhenius kinetics occurs, a mass balance on species A gives:

$$\frac{1}{S^2}D_{pA}\frac{d}{dS}\left[S^2\frac{dC'_{pA}}{dS}\right] - A_0\exp(-E/R_gT_p)C'^{n}_{pA} = 0 \qquad (A1.1)$$

Similarly, a heat balance gives:

$$\frac{1}{S^2}K_p\frac{d}{dS}\left[S^2\frac{dT_p}{dS}\right] + (-\Delta H)A_0\exp(-E/R_gT_p)C'^{n}_{pA} = 0 \qquad (A1.2)$$

Equations (A1.1) and (A1.2) are subject to the boundary conditions:

$$\frac{dC'_{pA}}{dS} = \frac{dT_p}{dS} \qquad \text{at } S = 0 \qquad (A1.3)$$

$$\left.\begin{aligned} D_{pA}\frac{dC'_{pA}}{dS} &= k_{gA}(C'_{fA} - C'_{pA}) \\ K_p\frac{dT_p}{dS} &= h(T - T_p) \end{aligned}\right\} \quad \text{at } S = b \qquad (A1.4)$$

These equations may be written in dimensionless form as:

$$\frac{d^2C_{pA}}{dy^2} - \frac{2}{(1-y)dy}\frac{dC_{pA}}{dy} - \theta^2\exp(-1/t)C^n_{pA} = 0 \qquad (A1.5)$$

$$\frac{d^2t}{dy^2} - \frac{2}{(1-y)dy}\frac{dt}{dy} + B_0Nu\,\theta^2\exp(-1/t)C^n_{pA} = 0 \qquad (A1.6)$$

with boundary conditions:

$$\frac{dC_{pA}}{dy} = \frac{dt}{dy} = 0 \qquad \text{at } y = 1 \qquad (A1.7)$$

$$\frac{dC_{pA}}{dy} = \frac{Sh}{2}_A(C_{pA} - C_A)$$

$$\frac{dt}{dy} = \frac{Nu}{2}(t - T) \qquad \text{at } y = 0 \qquad (A1.8)$$

where:

$$C_{pA} = \frac{C'_{pA}}{C_O} \qquad C_A = \frac{C'_{fA}}{C_O} \qquad t = \frac{R_g T_p}{E} \qquad T = \frac{R_g T}{E}$$

$$y = 1 - S/b$$

$$\theta^2 = \frac{b^2 A_O}{D_{pA}} \qquad B_O = \frac{(-\Delta H) D_{pA} C_O R_g}{2bhE}$$

$$Sh_A = \frac{2bk_{gA}}{D_{pA}} \qquad Nu = \frac{2bh}{K_p}$$

Equations (A1.5) and (A1.6) may be solved numerically to give the temperature and concentration profiles in the pellet. The effectiveness factor, η, is given by:

$$\eta = \frac{4\pi b^2 k_{gA}(C'_{fA} - C'_{pA}|_{s=b})}{\frac{4}{3}\pi b^3 A_O \exp(-E/R_g T) C'^{n}_{fA}}$$

which in dimensionless form becomes:

$$\eta = \frac{1.5 Sh_A (C_A - C_{pA}|_{y=0})}{\theta^2 \exp(-1/T) C_A^n} \qquad (A1.9)$$

A1.1.2 The Unsteady State

The unsteady state mass balance on the pellet gives:

$$\frac{D_{pA}}{b^2 \varepsilon^*}\left[\frac{\partial^2 C_{pA}}{\partial y^2} - \frac{2}{(1-y)}\frac{\partial C_{pA}}{\partial y}\right] - \frac{A_O}{\varepsilon^*}\exp(-1/t) C^n_{pA} = \frac{\partial C_{pA}}{\partial \tau} \qquad (A1.10)$$

Similarly the unsteady state heat balance gives:

$$\frac{K_p}{\rho^* c_p b^2}\left[\frac{\partial^2 t}{\partial y^2} - \frac{2}{(1-y)}\frac{\partial t}{\partial y}\right] + \frac{(-\Delta H) A_O R_g}{\rho^* c_p E}\exp(-1/t) C^n_{pA} = \frac{\partial t}{\partial \tau} \qquad (A1.11)$$

with boundary conditions

$$\frac{\partial C_{pA}}{\partial y} = \frac{\partial t}{\partial y} = 0 \qquad \text{at } y = 1, \ \tau > 0$$

$$\left.\begin{aligned} \frac{\partial C}{\partial y}_p &= \frac{bk}{D_{pA}}{}_{gA}\,(C_p - C) \\ \frac{\partial t}{\partial y} &= \frac{bh}{K_p}\,(t - T) \end{aligned}\right\} \quad \text{at } y = 0,\ \tau \geqslant 0$$

$$t = t\,\big|_{\tau=0}$$

$$C_{pA} = C_{pA}\,\big|_{\tau=0} \qquad \text{at } \tau = 0,\ 0 \geqslant y \geqslant 1$$

Rearranging equations (A1.10) and (A1.11) and using dimensionless groups, they become:

$$\frac{\partial^2 C}{\partial y^2}_{pA} - \frac{2}{(1-y)\partial y}\frac{\partial C}{\partial y}_{pA} - \theta^2 \exp(-1/t) C_{pA}^n = K_{cc}\frac{\partial C}{\partial \tau}_{pA} \qquad \text{(A1.12)}$$

$$\frac{\partial^2 t}{\partial y^2} - \frac{2}{(1-y)\partial y}\frac{\partial t}{\partial y} + B_0 Nu\,\theta^2 \exp(-1/t) C_{pA}^n = K_T\frac{\partial t}{\partial \tau} \qquad \text{(A1.13)}$$

with the boundary conditions:

$$\frac{\partial C}{\partial y}_{pA} = \frac{\partial t}{\partial y} = 0 \qquad \text{at } y = 0,\ \tau \geqslant 0$$

$$\left.\begin{aligned} \frac{\partial C}{\partial y}_{pA} &= \frac{Sh}{2}{}_A\,(C_{pA} - C_A) \\ \frac{\partial t}{\partial y} &= \frac{Nu}{2}\,(t - T) \end{aligned}\right\} \quad \text{at } y = 1,\ \tau \geqslant 0$$

$$t = t_0$$

$$C_{pA} = C_{pA0} \qquad \text{at } \tau = 0,\ 0 \geqslant y \geqslant 1$$

where:

$$K_{cc} = \frac{b^2 e^*}{D_{pA}} \qquad K_T = \frac{\rho^* c_p^* b^2}{K_p}$$

Since $K_{cc} \ll K_T$ equation (A1.12) may usually be replaced by its steady state form, (A1.5)

? not true.

A1.2 The Lumped Thermal Resistance Model of the Catalyst Pellet

A1.2.1 The Steady State

(a) The A⟶B Reaction Scheme

In this model the resistance to heat transfer within the catalyst pellet is assumed to be negligible and the pellet is, therefore, isothermal. Thus, the temperature, t, is constant throughout the pellet. The mass balance on the pellet is identical with that for the fully distributed model. However, since t is not a function of y, equation (A1.5) may be solved analytically for first order reactions (n = 1) to give the concentration profile in the pellet. For non-first order reactions a pseudo first order form of the rate expression may be used,[12] and the parameter θ is then redefined by:

$$\theta^2 = \frac{b^2 A_0 C_{pA}^{n-1}}{D_{pA}}$$

Thus equation (A1.5) becomes:

$$\frac{d^2C_{pA}}{dy^2} - \frac{2}{(1-y)}\frac{dC_{pA}}{dy} - \theta^2 \exp(-1/t) C_{pA} = 0 \qquad (A1.14)$$

with boundary conditions:

$$\frac{dC_{pA}}{dy} = 0 \qquad \text{at } y = 1$$

$$\frac{dC_{pA}}{dy} = \frac{Sh_A}{2}(C_{pA} - C_A) \qquad \text{at } y = 0$$

Solution of equation (A1.14) gives:

$$C_{pA} = \frac{0.5Sh_A \sinh(r(1-y))C_A}{(r\coth(r) + s)(1-y)\sinh(r)} \qquad (A1.15)$$

where:

$$r = \theta \exp(-1/2t) \qquad s = 0.5Sh_A - 1$$

A heat balance on the isothermal catalyst pellet gives, in dimensionless form:

$$B_0 Sh_A (C_A - C_{pA}|_{y=0}) - t + T = 0 \qquad (A1.16)$$

$C_{pA}|_{y=0}$ may be obtained from equation (A1.15) as:

$$C_{pA}\Big|_{y=0} = \frac{0.5Sh_A C_A}{(r\ \coth(r) + s)} \qquad (A1.17)$$

Using (A1.17) in equation (A1.16) and rearranging gives:

$$t = T + \frac{BSh_A(r - g)}{(sg + r)} \qquad (A1.18)$$

where $B = B_0 C_A$ and $g = \tanh(r)$.

Equation (A1.18), therefore, gives the pellet temperature directly and may be solved by any of the normal root finding techniques e.g. Newton-Raphson.

Using equations (A1.17) and (A1.18) in the expression for the effectiveness factor, (A1.9) enables η to be expressed in terms of only t, C_A and T. Thus:

$$\eta = \frac{1.5(t - T)}{B_0\, \theta^2 \exp(-1/\tfrac{t}{T})C_A} \qquad (A1.19)$$

(b) <u>The A ⟶ B ⟶ C, A ⟶ D Reaction Scheme</u>

For this complex reaction scheme, used in Chapter 8 an additional mass balance within the catalyst pellet is required for species B. Also, the reaction rate expressions must take account of the A ⟶ D step. Therefore, assuming first order or pseudo-first order reaction rates, the differential mass balances on species A and B become:

$$\frac{d^2C_{pA}}{dy^2} - \frac{2}{(1 - y)dy}\frac{dC_{pA}}{dy} - (k_1^* + k_3^*)C_{pA} = 0 \qquad (A1.20)$$

$$\frac{d^2C_{pB}}{dy^2} - \frac{2}{(1 - y)dy}\frac{dC_{pB}}{dy} + \delta k_1^* C_{pA} - \delta k_2^* C_{pB} = 0 \qquad (A1.21)$$

subject to the boundary conditions:

$$\frac{dC_{pA}}{dy} = \frac{dC_{pB}}{dy} = 0 \qquad \text{at } y = 1$$

$$\left.\begin{aligned} \frac{dC_{pA}}{dy} &= \frac{Sh_A}{2}(C_{pA} - C_A) \\ \frac{dC_{pB}}{dy} &= \frac{Sh_B}{2}(C_{pB} - C_B) \end{aligned}\right\} \qquad \text{at } y = 0$$

where:

$$k_i^* = \theta_i^2 \exp(-E_i/E_1 t) \qquad i = 1,2,3$$

$$Sh_A = \frac{2bk_{gA}}{D_{pA}} \qquad Sh_B = \frac{2bk_{gB}}{D_{pB}}$$

Subscripts A and B refer to species A and B respectively. Subscript 1 refers to the reaction step A $\longrightarrow$ B.

Subscript 2 refers to the reaction step B $\longrightarrow$ C.

Subscript 3 refers to the reaction step A $\longrightarrow$ D.

Since the pellet is assumed isothermal, equations (A1.20) and (A1.21) may be solved analytically. The solution gives the two concentration profiles within the pellet in terms of the unknown temperature t, which must be obtained by choosing a value to satisfy the heat balance on the pellet:

$$B\,\frac{Sh_A(C_A - C_{pAs})}{C_A(k_1^* + k_3^*)}(k_1^*(1 + H_2) + k_3^* H_3) - \frac{Sh_B}{\delta C_A}(C_{pBs} - C_B)H_2$$

$$- t + T = 0 \qquad \text{(A1.22)}$$

where $C_{pAs} = C_{pA}\big|_{y=0}$ and $C_{pBs} = C_{pB}\big|_{y=0}$.

From the analytic solution cf equations (A1.20) and (A1.21) C_{pAs} and C_{pBs} may be obtained as:

$$C_{pAs} = \frac{0.5Sh_A C_A}{0.5Sh_A - 1 + \sqrt{k_1^* + k_3^*}\coth(\sqrt{k_1^* + k_3^*})} \qquad \text{(A1.23)}$$

$$C_{pBs} = P_2 - P_1 \qquad \text{(A1.24)}$$

where

$$P_1 = \frac{k_1^* C_{pAs}}{k_1^* + k_3^* - \delta k_2^*}$$

$$P_2 = \frac{0.5Sh_B C_B + P_1((0.5Sh_B - 1) + \sqrt{k_1^* + k_3^*}\coth(\sqrt{k_1^* + k_3^*})}{(0.5Sh_B - 1) + \sqrt{\delta k_2^*}\coth\sqrt{\delta k_2^*}}$$

when $\delta k_2^* \neq k_1^* + k_3^*$

and $C_{pBs} = P_4 - P_3$

$$\text{and} \quad P_3 = \frac{k_1^* C_{pAs}}{2\sqrt{k_1^* + k_3^*}\ \tanh(\sqrt{k_1^* + k_3^*})}$$

$$P_4 = \frac{0.5Sh_B C_B + P_3(0.5Sh_B + \sqrt{k_1^* + k_3^*}\ \tanh(\sqrt{k_1^* + k_3^*})}{(0.5Sh_B - 1) + \sqrt{k_1^* + k_3^*}\ \coth(\sqrt{k_1^* + k_3^*})}$$

when $\delta k_2^* = k_1^* + k_3^*$.

These expressions for C_{pAs} and C_{pBs} may be substituted into equation (A1.22) which can then be solved for t by any of the usual root-finding techniques as indicated above.

A1.2.2 The Unsteady State

As in the fully distributed dynamic model of the catalyst pellet, the concentration profiles may be assumed to be at a series of pseudo-steady states[12] since the thermal capacitance of the catalyst pellet is much greater than the mass capacitance. Therefore, for the simple A⟶B reaction scheme, the instantaneous concentration profile of species A is given by equation (A1.15). An unsteady state heat balance on the isothermal catalyst pellet gives:

$$\frac{2}{3}\frac{K_T}{Nu}\frac{dt}{d\tau} = T - t + B_0 Sh_A(C_A - C_{pA}\big|_{y=0}) \qquad (A1.25)$$

where $C_{pA}\big|_{y=0}$ is given by equation (A1.17).

Equation (A1.25) may be conveniently solved using the Runge-Kutta-Merson algorithm.

APPENDIX 2

THE ONE DIMENSIONAL REACTOR MODEL

A2.1 The Steady State Model

For the A⟶B reaction scheme, differential heat and mass balances on the reactor give in dimensionless form:

$$\frac{dC_A}{dz} + G_2 \zeta \theta^2 \exp(-1/T) C_A^n = 0 \qquad (A2.1)$$

$$\frac{dT}{dz} - G_4(t - T) + \frac{2Nu_w^*}{G_3}(T - T_c) = 0 \qquad (A2.2)$$

with the boundary conditions:

$$T = T\big|_{z=0}, \quad C_A = C_A\big|_{z=0}$$

where:

$$G_2 = \frac{(1 - e)LD_{pA}}{b^2 ue} \qquad G_3 = \frac{R^2 u \varrho c_p}{K_f L}$$

$$G_4 = \frac{3(1 - e)hL}{b \varrho u e c_p}$$

$$Nu_w^* = \frac{4Nu_w}{(4 + Nu_w)} \qquad Nu_w = \frac{RU}{K_f e}$$

The axial coordinate in the reactor, z, is dimensionless so that z = 0 at the inlet and z = 1 at the outlet.

It should be noted that the state variables occurring in equations (A2.1) and (A2.2) are all <u>radial mean</u> values. The reaction rate expressions should also be radial mean values, however this causes problems of evaluation since the radial mean reaction rate is less than the rate at the radial mean conditions. This is discussed in detail in chapter 5.

The radial temperature profile which is assumed to be parabolic is given by:

$$T = T_m + 0.25Nu_w^*(T_m - T_c) - 0.5Nu_w^*(T_m - T_c)r^2 \qquad (A2.3)$$

where T_m is the radial mean temperature obtained from equation (A2.2), and r is the dimensionless radial coordinate in the reactor such that r = 0 at the tube centre and r = 1 at the wall.

The overall effective Nusselt number, Nu_w^*, is defined by:

$$Nu_w^*(T_m - T_c) = Nu_w(T\big|_{r=1} - T_c) \qquad (A2.4)$$

Using this definition and assuming a parabolic temperature profile it may be shown that:

$$Nu_w^* = \frac{4Nu_w}{(4 + Nu_w)}$$

The pellet temperature t and the effectiveness factor, η, are obtained from the catalyst pellet model described in Appendix 1.

In the case of the complex reaction scheme:

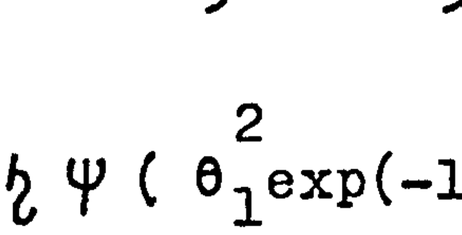

the mass balance equation (A2.1) must be altered to take account of the additional reaction rates and a mass balance on species B must be included. The heat balance equation remains unchanged. The mass balances are:

$$\frac{dC_A}{dz} + G_2\eta\left(\theta_1^2\exp(-1/T)C_A^{n_1} + \theta_3^2\exp(-E_3/E_1T)C_A^{n_3}\right) = 0 \qquad (A2.5)$$

$$\frac{dC_B}{dz} - G_2\eta\psi\left(\theta_1^2\exp(-1/T)C_A^{n_1} + \theta_3^2\exp(-E_3/E_1T)C_A^{n_3}\right) = 0 \qquad (A2.6)$$

with boundary conditions:

$$C_A = C_A\big|_{z=0} \quad \text{and} \quad C_B = C_B\big|_{z=0}.$$

where:

$$\eta = \frac{1.5Sh_A(C_A - C_{pA}\big|_{y=0})}{(\theta_1^2 C_A^{n_1} + \theta_3^2 C_A^{n_2})\exp(-1/T)}$$

$$\psi = \frac{Sh_B(C_{pB}|_{y=0} - C_B)}{Sh_A(C_A - C_A|_{y=0})}$$

Note that the dimensionless temperatures t, T and T_c are expressed in terms of the activation energy of reaction 1. $C_{pA}|_{y=0}$, $C_{pB}|_{y=0}$ and the pellet temperature t are obtained from the catalyst pellet model for the complex reaction scheme which is given in Appendix 1. For the simple reaction scheme equations (A2.1) and (2.2) must be solved simultaneously with the catalyst pellet equations. Similarly, for the complex reaction scheme equations (A2.2), (A2.5) and (A2.6) must be solved simultaneously. The simplest method of solution is by finite differences and this is outlined below.

In the case of non-first order reactions ($n \neq 1$) θ, θ_1, and θ_3 may be redefined to give a <u>local</u> pseudo first order form.[12,3] The general form of equations (A2.1), (A2.2), (A2.5) and (A2.6) then becomes:

$$\frac{df}{dz} + R'f + R'' = 0 \qquad (A2.7)$$

where f, R' and R'' are given in the following table:

Equation	f	R'	R''
A2.1	C_A	$G_2\zeta\theta^2\exp(-1/T)$	0
A2.2	T	$G_4 + 2Nu_w^*/G_3$	$-G_4t - 2Nu_w^*T_c/G_3$
A2.3	C_A	$G_2(\theta_1^2 + \theta_3^2)\exp(-1/T)$	0
A2.4	C_B	0	$-G_2\zeta\psi(\theta_1^2 + \theta_3^2)\exp(-\frac{1}{T})C_A$

In finite difference form equation (A2.7) becomes:

$$\frac{f - xf}{j} + (1 - Q)xR'.xf + (1 - Q)xR'' + QR'f + QR'' = 0 \qquad (A2.8)$$

where Q is a constant such that $0 \leqslant Q \leqslant 1$ and the prefix 'x' denotes the value of a variable at its previous axial position, i.e. it is known. j is the step length in the finite difference grid.

In equation (A2.7) the unknowns are f, r' and R". Solution is accomplished by working from the reactor inlet to the outlet as follows:

(1) Assume values for f (i.e. C_A T for the simple reaction scheme, C_A, C_B and T for the complex scheme) at the first or next axial position where they are unknown.

(2) Use these values to solve the appropriate catalyst pellet model to obtain t and η (and also ψ for the complex reaction scheme) and hence evaluate R' and R".

(3) Calculate new values of f using equation (A2.8).

(4) Test against the assumed values (from step (1)) for satisfactory convergence. If unsatisfactory repear from step (2).

(5) If satisfactory and $z \leqslant 1$ repear from step (1).

The initial assumed values for f used at step (1) may be obtained by extrapolation from the previous axial position. (Note: the same method of solution may be applied to equations (7.2) and (7.3)).

A2.2 The Unsteady State Model

For the A ⟶ B reaction scheme the unsteady state fluid field equations for the reactor are in dimensionless form:

$$\frac{\partial C_A}{\partial z} + G_2 \eta \theta^2 \exp(-1/T) C_A^n + \frac{G_5}{G_1} \frac{\partial C_A}{\partial \tau} = 0 \qquad \text{(A2.9)}$$

$$\frac{\partial T}{\partial z} + \frac{2Nu^*_w}{G_3}(T - T_c) - G_4(t - T) + \frac{G_6}{G_{13}} \frac{\partial T}{\partial \tau} = 0 \qquad \text{(A2.10)}$$

with the initial conditions:

$$C_A = C_A(\tau), \quad T = T(\tau) \quad \text{at} \quad z = 0, \quad \tau > 0$$

$$C_A = C_A(z), \quad T = T(z) \quad \text{at} \quad \tau = 0, \quad z \geqslant 0$$

Equations (A2.9) and A2.10) are coupled with the dynamic model of the catalyst pellet, equation (A1.2). Thornton[12] has shown that the transient response of the reactor predicted

by these equations is slow compared with the residence time so that the fluid equations may be solved as if they were at a pseudo-steady state. Thus, in equations (A2.9) and (A2.10) $G_5 = G_6 = 0$ and the steady state equations ((A2.1 and (A2.2)) result. Solution may then be accomplished in a similar manner to the steady state equations (section A2.1). The essential differences are the when the bed exit ($z = 1$) is reached the time is updated and the procedure must be repeated from step (1). Also, in step (2) the dynamic model of the catalyst pellet must be solved (equation A1.25) to obtain t at the current time. This may be accomplished by the Runge-Kulta-Merson algorithm in which case the values of C and T must be supplied over the time interval. Since the time interval is small, it may be assumed that these vary linearly over the interval.

APPENDIX 3

THE FINITE DIFFERENCE FORM OF THE TWO DIMENSIONAL REACTOR MODELS

A3.1 The Steady State

The heat and mass balance equations for the two dimensional steady state reactor models described in Chapters 3 and 5 have the general form:

$$\frac{\partial^2 f}{\partial r^2} + \frac{1}{r}\frac{\partial f}{\partial r} + K'\frac{\partial f}{\partial z} + R'f + R'' = 0 \qquad \text{(A3.1)}$$

subject to the boundary conditions:

$$\frac{\partial f}{\partial r} = 0 \qquad \text{at } r = 0,\ z > 0 \qquad \text{(A3.2)}$$

$$\frac{\partial f}{\partial r} + Kf + KK^o = 0 \qquad \text{at } r = 1,\ z > 0 \qquad \text{(A3.3)}$$

and the initial condition:

$$f = f(r) \quad \text{at } z = 0 \text{ for } 0 \leqslant r \leqslant 1.$$

Equation (A3.1), together with its boundary conditions, may be solved by a finite difference method. In the method described here the radial derivatives are replaced by their central difference approximations and the axial derivatives by a backward difference approximation. Thus the terms in equation (A3.1) may be written as follows:

$$\frac{\partial^2 f}{\partial r^2} = \frac{1}{h^2}(Q(f_{i+1} - 2f_i + f_{i-1}) + (1 - Q)(xf_{i+1} - 2xf_i + xf_{i-1}))$$

$$\frac{1}{r}\frac{\partial f}{\partial r} = \frac{1}{2hr}(Q(f_{i+1} - f_{i-1}) + (1 - Q)(xf_{i+1} - xf_{i-1})$$

$$K'\frac{\partial f}{\partial z} = \frac{K'}{k}(f_i - xf_i)$$

$$R'f = QR'_i f_i + (1 - Q)xR'_i xf_i$$

$$R'' = QR''_i + (1 - Q)\overset{x}{R}''_i$$

The prefix 'x' indicates the value of a variable at the previous axial position. This is a known value since the equations are initial valued in the axial direction. Q is a constant such that $0 \leqslant Q \leqslant 1$. When Q = 0.5 the equations reduce to the Crank-Nicolson form. The parameters h and k are the step lengths in the radial and axial directions respectively.

Replacing the terms in equation (A3.1) by the expressions given above, and rearranging, gives:

$$m_i f_{i+1} + p_i f_i + n_i f_{i-1} = a_i \qquad \text{(A3.4)}$$

where $m_i = \frac{Q}{h^2} + \frac{Q}{2hr}$

$$p_i = -\frac{2Q}{h^2} + \frac{K'}{k} + QR'_i$$

$$n_i = \frac{Q}{h^2} - \frac{Q}{2hr}$$

$$a_i = -xf_{i+1}\left[\frac{(1-Q)}{h^2} + \frac{(1-Q)}{2hr}\right] - xf_i\left[-\frac{2(1-Q)}{h^2} - \frac{K'}{k} + (1-Q)xR'_i\right] - xf_{i-1}\left[\frac{(1-Q)}{h^2} - \frac{(1-Q)}{2hr}\right] - QR''_i - (1-Q)xR''_i$$

These expressions hold for $1 \leqslant i \leqslant (N-1)$ where N and O are the numbers of the finite difference nodes at the tube wall and centre respectively.

At the tube centre $\frac{\partial f}{\partial r} = 0$ so $\frac{1}{r}\frac{\partial f}{\partial r}$ is indeterminate.

Applying l'Hopital's rule, equation (A3.1) becomes

$$2\frac{\partial^2 f}{\partial r^2} + K'\frac{\partial f}{\partial z} + R'f + R'' = 0$$

and since $f_{-1} = f_1$, $xf_{-1} = xf_1$, etc, the equation in finite difference form becomes:

$$m_0 f_1 + p_0 f_0 = a_0 \qquad \text{(A3.5)}$$

where $m_0 = \frac{4Q}{h^2}$

$$p_0 = -\frac{4Q}{h^2} + \frac{K'}{k} + QR'_0$$

$$a_0 = -xf_1\left[\frac{4(1-Q)}{h^2}\right] - xf_0\left[\frac{-4(1-Q)}{h^2} - \frac{K'}{k} + (1-Q)xR'_0\right] - QR'_0{}' - (1-Q)xR''_0$$

At the wall (r=1, finite difference node N) the boundary condition (A3.3) may be expressed in finite difference form as:

$$\frac{1}{2h}\left[Q(f_{N+1} - f_{N-1}) + (1-Q)(xf_{N+1} - xf_{N-1})\right] + K\left[Qf_N + (1-Q)xf_N\right] + KK^o = 0$$

This equation may be combined with equation (A3.4) expressed at point N to eliminate the hypothetical terms f_{N+1} and xf_{N+1} giving:

$$p_N f_N + n_N f_{N-1} = a_N \qquad \text{(A3.6)}$$

where $p_N = -\frac{2Q}{h^2} + \frac{K'}{k} + QR'_N - 2Kh\left(\frac{Q}{h^2} + \frac{Q}{2h}\right)$

$$n_N = \frac{2Q}{h^2}$$

$$a_N = -xf_N\left[-\frac{2(1-Q)}{h^2} - \frac{K'}{k} + (1-Q)xR'_N - 2Kh\left(\frac{(1-Q)}{h^2} + \frac{(1-Q)}{2h}\right)\right] - xf_{N-1}\left[\frac{2(1-Q)}{h^2}\right] - QR'_N{}'$$

$$- \quad (1 - Q)xR_N'' + \quad KK^o(\frac{2}{h} + 1)$$

Equations (A3.4), (A3.5) and (A3.6) represent a system of simultaneous algebraic equations of the form:

$$\underline{A}\,\underline{f} = \underline{a} \qquad \text{(A3.7)}$$

where the coefficient matrix, $\underline{A}$, is given by:

$$\underline{A} = \begin{bmatrix} p_o & m_o & & & \\ n_i & p_i & m_i & & \\ & \ddots & \ddots & \ddots & \\ & & n_N & p_N & \end{bmatrix}$$

Since $\underline{A}$ is tridiagonal, the equations (A3.7) may be solved by computationally efficient algorithm credited to Thomas and described by Lapidus[127].

The non-linear terms R' and R'' which are involved in the elements of $\underline{A}$ and $\underline{a}$ are unknown and an iterative procedure must be used. This is accomplished as follows: If the solution for $\underline{f}$ is assumed, R' and R'' may be calculated and after using these values to calculate $\underline{A}$ and $\underline{a}$ a new solution for $\underline{f}$ can be obtained. R' and R'' are again evaluated using the new $\underline{f}$, and so on until the solution becomes constant.

A3.2 The Unsteady State

The general form of equations (5.1) and (5.2) is:

$$\frac{\partial^2 f}{\partial r^2} + \frac{1}{r}\frac{\partial f}{\partial r} + K'\frac{\partial f}{\partial z} + R'f + R'' = K''\frac{\partial f}{\partial \tau} \qquad \text{(A3.8)}$$

subject to boundary conditions:

$$\frac{\partial f}{\partial r} = 0 \qquad \text{at } r = 0,\ z > 0,\ \tau > 0$$

$$\frac{\partial f}{\partial r} + Kf + KK^{o} = 0 \qquad \text{at } r = 1,\ z > 0, \tau \geqslant 0$$

and the initial condition:

$$f = f(r, \tau) \qquad \text{at } z = 0,\ 0 \leqslant r \leqslant 1, \tau \geqslant 0$$

The derivatives in equation (A3.8) may be replaced by their finite difference approximations. Thus the terms in equation (A3.8) become:

$$\frac{\partial^2 f}{\partial r^2} + \frac{1}{r}\frac{\partial f}{\partial r} =$$

$$+ \frac{QQ^*}{h^2}(f_{i+1} - 2f_i + f_{i-1}) + \frac{QQ^*}{2hr}(f_{i+1} - f_{i-1})$$

$$+ \frac{(1 - Q)Q^*}{h^2}(xf_{i+1} - 2xf_i + xf_{i-1})$$

$$+ \frac{(1 - Q)Q^*}{2hr}(xf_{i+1} - xf_{i-1})$$

$$+ \frac{(1 - Q^*)Q}{h^2}(of_{i+1} - 2of_i + of_{i-1})$$

$$+ \frac{(1 - Q^*)Q}{2hr}(of_{i+1} - of_{i-1})$$

$$+ \frac{(1 - Q)(1 - Q^*)}{h^2}(oxf_{i+1} - 2oxf_i + oxf_{i-1})$$

$$+ \frac{(1 - Q)(1 - Q^*)}{2hr}(oxf_{i+1} - oxf_{i-1})$$

$$K'\frac{\partial f}{\partial z} = \frac{K'Q^*}{k}(f_i - xf_i) + \frac{K'(1 - Q^*)}{k}(of_i - oxf_i)$$

$$R'f = QQ^*R'_i f_i + Q(1 - Q^*)oR'_i of_i + Q^*(1 - Q)xR'_i xf_i$$

$$+ (1 - Q)(1 - Q^*)oxR'_i oxf_i$$

$$R'' = QQ^*R''_i + Q(1 - Q^*)oR''_i + Q^*(1 - Q)xR''_i$$

$$+ (1 - Q)(1 - Q^*)oxR''_i$$

$$K''\frac{\partial f}{\partial \tau} = \frac{K''Q}{j}(f_i - of_i) + \frac{K''(1 - Q)}{j}(xf_i - oxf_i)$$

where: the prefix 'x' indicates the value of a variable at the previous axial position.

the prefix 'o' indicates the value of a variable at the previous time position.

the prefix 'ox' indicates the value of a variable at the time and axial positions.

j is the step size in the time (τ) direction

k is the step size in the axial (z) direction

h is the step size in the radial (r) direction

Q and Q^* are the weighting factors such that $0 < Q \leqslant 1$, $0 < Q^* \leqslant 1$.

Replacing the terms in equation (A3.8) by the expressions given above, and rearranging, gives:

$$m_i f_{i+1} + p_i f_i + n_i f_{i-1} = a_i \qquad \text{(A3.9)}$$

where:
$$m_i = \frac{QQ^*}{h^2} + \frac{QQ^*}{2hr}$$

$$p_i = \frac{K'Q^*}{k} - \frac{K''Q}{j} + QQ^*R_i' - \frac{2QQ^*}{h}$$

$$n_i = \frac{QQ^*}{h^2} - \frac{QQ^*}{2hr}$$

$$a_i = - xf_{i+1}\left(\frac{(1 - Q)Q^*}{h^2} + \frac{(1 - Q)Q^*}{2hr}\right)$$

$$- xf_i\left(- \frac{K'Q^*}{k} - \frac{K''(1 - Q)}{j} + Q^*(1 - Q)xR_i' - \frac{2(1 - Q)Q^*}{h^2}\right)$$

$$- xf_{i-1}\left(\frac{(1 - Q)Q^*}{h^2} - \frac{(1 - Q)Q^*}{2hr}\right)$$

$$- \; of_{i+1}\left(\frac{Q(1-Q^*)}{h^2} + \frac{Q(1-Q^*)}{2hr}\right)$$

$$- \; of_i\left(\frac{K''Q}{j} + Q(1-Q^*)oR'_i - \frac{2Q(1-Q^*)}{h^2}\right.$$

$$\left. + \frac{K'(1-Q^*)}{k}\right)$$

$$- \; of_{i-1}\left(\frac{Q(1-Q^*)}{h^2} - \frac{Q(1-Q^*)}{2hr}\right)$$

$$- \; oxf_{i+1}\left(\frac{(1-Q)(1-Q^*)}{h^2} + \frac{(1-Q)(1-Q^*)}{2hr}\right)$$

$$- \; oxf_i\left(-\frac{K'}{k}(1-Q^*) + \frac{K''}{j}(1-Q)\right.$$

$$+ (1-Q)(1-Q^*)oxR'_i$$

$$\left. - \frac{2(1-Q)(1-Q^*)}{h^2}\right)$$

$$- \; oxf_{i-1}\left(\frac{(1-Q)(1-Q^*)}{h^2} - \frac{(1-Q)(1-Q^*)}{2hr}\right)$$

$$- \; QQ^*R''_i - Q(1-Q^*)oR''_i$$

$$- \; (1-Q)Q^*xR''_i - (1-Q)(1-Q^*)oxR''_i$$

As in the steady state formulation described in section A3.1 above, these expressions hold for $1 \leqslant i \leqslant (N-1)$ where 0 and N are the numbers of the finite difference nodes at the tube centre and tube wall respectively.

Since $\frac{1}{r}\frac{\partial f}{\partial r}$ is indeterminate at r = 0 (the tube centre) l'Hopital's rule must be applied to equation (A3.8) giving:

$$2\frac{\partial^2 f}{\partial r^2} + K'\frac{\partial f}{\partial z} + R'f + R'' = K''\frac{\partial f}{\partial \tau}$$

Applying the finite difference approximations to this equation and noting that $f_{-1} = f_{+1}$, $xf_{-1} = xf_{+1}$, $of_{-1} = of_{+1}$,

etc. gives:

$$m_0 f_1 + p_0 f_0 = a_0 \qquad \text{(A3.10)}$$

where:

$$m_0 = \frac{4QQ^*}{h^2}$$

$$p_0 = -\frac{4QQ^*}{h^2} + \frac{K'Q^*}{k} + QQ^*R_0' - \frac{K''Q}{j}$$

$$a_0 = -xf_1\left(\frac{4(1-Q)Q^*}{h^2}\right) - xf_0\left(-\frac{4(1-Q)Q^*}{h^2}\right.$$

$$\left. - \frac{K'Q^*}{k} + Q^*(1-Q)xR_0' - \frac{K''(1-Q)}{j}\right)$$

$$- of_1\left(\frac{4Q(1-Q^*)}{h^2}\right) - of_0\left(-\frac{4Q(1-Q^*)}{h^2}\right.$$

$$\left. + \frac{K'(1-Q^*)}{k} + Q(1-Q^*)oR_0' + \frac{K''Q}{j}\right)$$

$$- oxf_1\left(\frac{4(1-Q)(1-Q^*)}{h^2}\right)$$

$$- oxf_0\left(-\frac{4(1-Q)(1-Q^*)}{h^2} - \frac{K'(1-Q^*)}{k}\right.$$

$$\left. + (1-Q)(1-Q^*)oxR_0' + \frac{K''(1-Q)}{j}\right)$$

$$- QQ^*R_0' - Q(1-Q^*)oR_0 - Q^*(1-Q)xR_0'$$

$$- (1-Q)(1-Q^*)oxR_0'$$

Expressing the boundary condition at the tube wall ($r = 1$) in finite difference form and using it together with equation (A3.9) to eliminate the terms at the hypothetical node ($N + 1$) leads to the following expression for the N th node:

$$p_N f_N + n_N f_{N-1} = a_N \qquad \text{(A3.11)}$$

$$\text{where } p_N = \frac{K'Q^*}{k} - \frac{K''Q}{j} + QQ^*R'_N - \frac{2QQ^*}{h^2}$$

$$- 2hK\left(\frac{QQ^*}{h^2} + \frac{QQ^*}{2h}\right)$$

$$n_N = \frac{2QQ^*}{h^2}$$

$$a_N = - xf_N\left(- \frac{K'Q^*}{k} - \frac{K''(1 - Q)}{j} + Q^*(1 - Q)xR'_N\right.$$

$$\left. - \frac{2(1 - Q)Q^*}{h^2} - 2hK\left(\frac{(1 - Q)Q^*}{h^2} + \frac{(1 - Q)Q^*}{2h}\right)\right)$$

$$- of_N\left(\frac{K''Q}{j} + Q(1 - Q^*)oR'_N - \frac{2Q(1 - Q^*)}{h^2}\right.$$

$$+ \frac{K'(1 - Q^*)}{k} - 2hK\left(\frac{Q(1 - Q^*)}{h^2}\right.$$

$$\left.\left. + \frac{Q(1 - Q^*)}{2h}\right)\right)$$

$$- of_{N-1}\left(\frac{2Q(1 - Q^*)}{h^2}\right) -- xf_{N-1}\left(\frac{2(1 - Q)Q^*}{h^2}\right)$$

$$- oxf_N\left(- \frac{K'(1 - Q^*)}{k} + \frac{K''(1 - Q)}{j}\right.$$

$$+ (1 - Q)(1 - Q^*)oxR'_N - \frac{2(1 - Q)(1 - Q^*)}{h^2}$$

$$\left. - 2hK\left(\frac{(1 - Q)(1 - Q^*)}{h^2} + \frac{(1 - Q)(1 - Q^*)}{2h}\right)\right)$$

$$- oxf_{N-1}\left(\frac{2(1 - Q)(1 - Q^*)}{h^2}\right)$$

$$- QQ^*R'_{N'} - Q(1 - Q^*)oR'_{N'} - (1 - Q)Q^*xR'_{N'}$$

$$- (1 - Q)(1 - Q^*)oxR'_{N'} + Q^*KK^o\left(\frac{2}{h} + 1\right)$$

$$+ (1 - Q^*)K_oK^o\left(\frac{2}{h} + 1\right)$$

Equations (A3.9), (A3.10) and (A3.11) again represent a system of simultaneous algebraic equations of the form:

$$\underline{A}\ \underline{f} = \underline{a}$$

The coefficient matrix $\underline{A}$ is tridiagonal and so the equations may be solved using the Thomas[127] method in the same way as the steady state equations described in section A3.1.

In the pseudo-steady state two dimensional model the reactor equations have the same form as the steady state equations. The essential difference is, however, that they are coupled with the dynamic model of the catalyst pellet.

APPENDIX 4

DETERMINATION OF THE RUNAWAY LIMIT FOR A COMPLEX REACTION SCHEME.

In chapter 4 a method was developed for determining the limit of temperature runaway for the simple A ⟶ B reaction scheme. It was shown that for a given reaction this limit is represented by a single line on the T vs B phase diagram. For a more complex reaction scheme such as that represented by

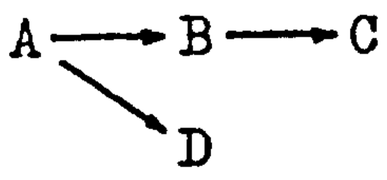

as used in chapter 8, a similar analysis may be applied but the heat balance on the catalyst pellet is more complicated.

As shown in Appendix 1, the heat balance for the complex reaction scheme is given by equation (A1.22). This may be written more simply as:

$$t - T = B(P(1 - f_1)f_2 - Q(f_3 - \frac{C}{C_A}B)) \qquad (A4.1)$$

where: $P = Sh_A$ $\qquad Q = \frac{Sh_B H_2}{\delta}$

$$f_1 = \frac{C_{pAs}}{C_A}$$

$$f_2 = \frac{k_1^*}{k_1^* + k_3^*}(1 + H_2) + \frac{k_3^*}{k_1^* + k_3^*}$$

$$f_3 = \frac{C_{pBs}}{C_A}$$

For a given system, the only variable in the functions f_1 and f_2 is the pellet temperature t. In the function f_3, however, there are two variables: t and $\frac{C}{C_A}B$.

The effect of the ratio of $\frac{C}{C_A}B$ at constant B on the T vs. t curves is shown in figure A4.1.

Differentiating equation (A4.1) with respect to t twice gives:

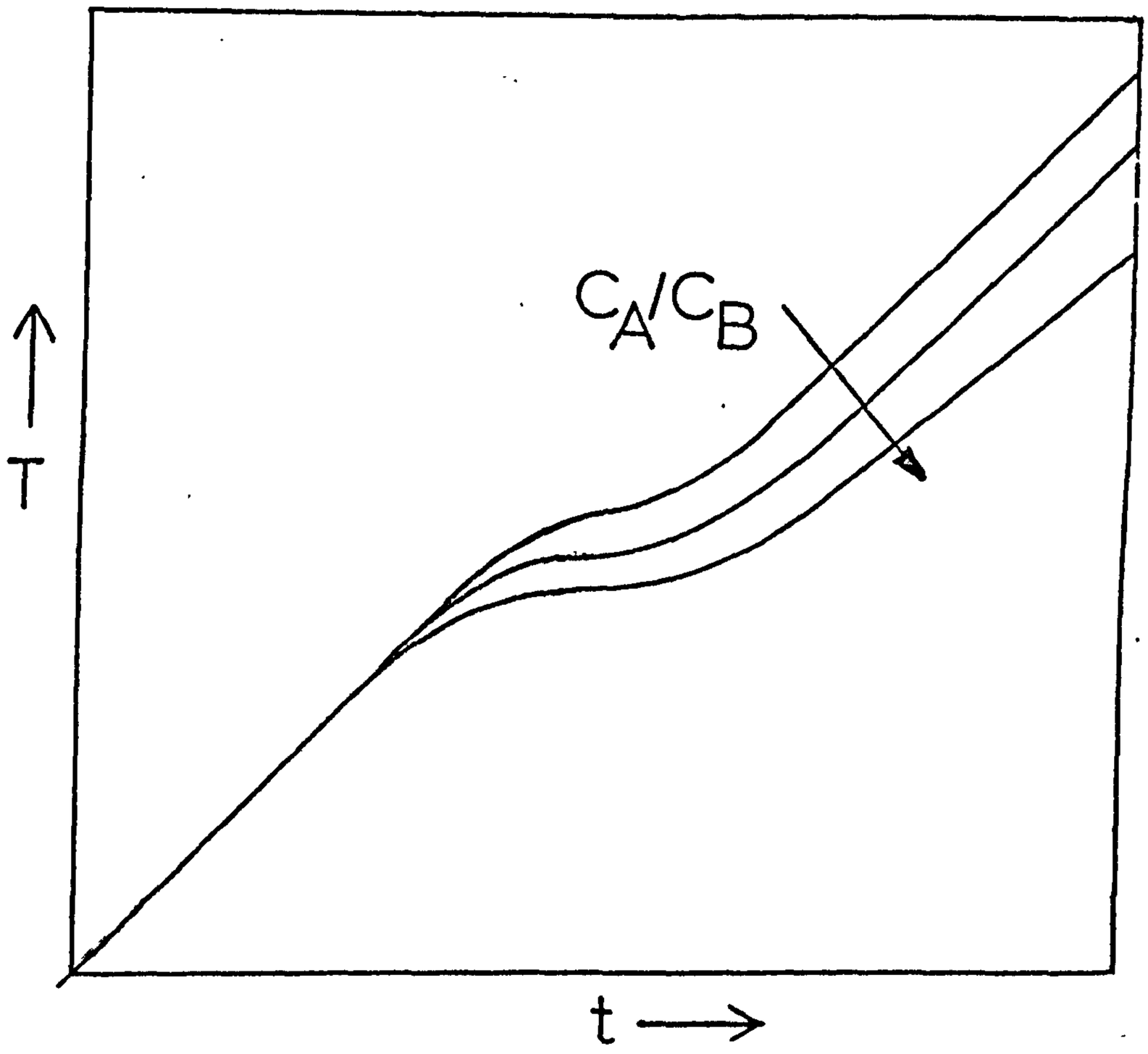

Figure A4.1 Schematic diagram showing the effect of the ratio C_B/C_A on the T vs. t curves at a constant value of B.

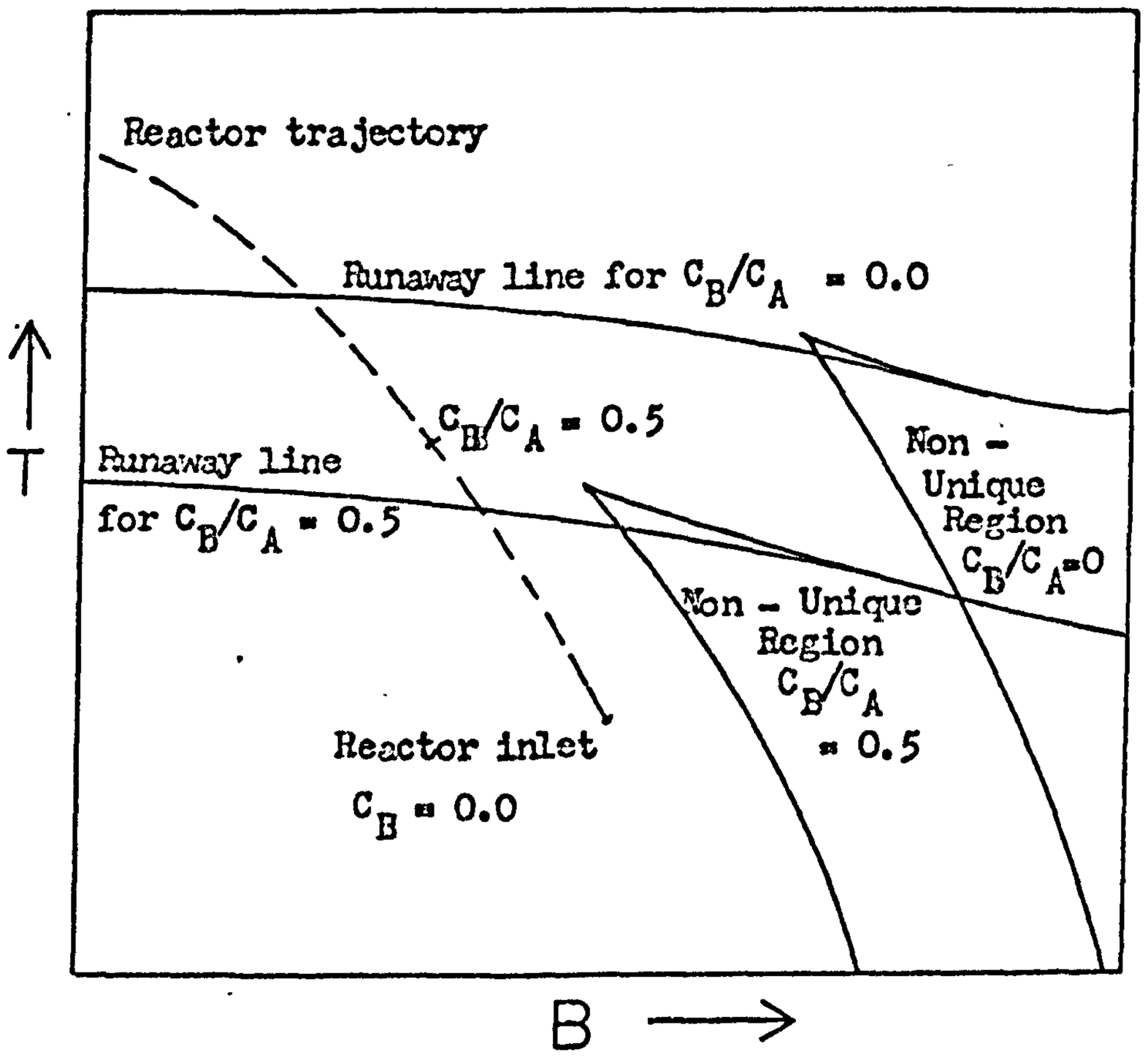

Figure A4.2 Schematic diagram showing how a reactor trajectory may be examined for temperature runaway with a complex reaction scheme.

$$\frac{d(t - T)}{dt} \equiv B(P(1 - f_1)\frac{df_2}{dt} - Pf_2\frac{df_1}{dt} - Q\frac{df_3}{dt}) \qquad (A4.2)$$

$$\frac{d^2(t - T)}{dt^2} = B(P(1 - f_1)\frac{d^2f_2}{dt^2} - 2P\frac{df_1}{dt}\frac{df_2}{dt} - Pf_2\frac{d^2f_1}{dt^2} - Q\frac{d^2f_3}{dt^2}) \qquad (A4.3)$$

It can be seen that for a given system, $\frac{d(t - T)}{dt}$ and $\frac{d^2(t - T)}{dt^2}$ are functions of t and $\frac{C_B}{C_A}$. Thus for a particular value of $\frac{C_B}{C_A}$, t_i, the pellet temperature at the point of inflexion of the (t - T) vs t curve is obtained by setting the right hand side of equation (A4.3) equal to zero. The pellet temperature at which the tangent at the point of inflexion of the (t - T) vs t curve meets the line (t - T) = 0 is given by:

$$t_s = t_i - \frac{(t - T)}{\frac{d(t - T)}{dt}}\Bigg|_{t=t_i} \Bigg|_{t=t_i} \qquad (A4.4)$$

Thus, putting $t = t_i$ in equations (A4.1) and (A4.2) enables t_s to be evaluated from equation (A4.4). It can be seen that t_s is a function of $\frac{C_B}{C_A}$ and, therefore, there is a different value of t_s for each value of $\frac{C_B}{C_A}$. For a given system, at a particular value of $\frac{C_B}{C_A}$ the runaway line on the T vs B phase diagram may be obtained from equation (A4.1) by putting $t = t_s$. Thus a different runaway line is determined for each value of $\frac{C_B}{C_A}$. The bounds on the region of non-unique solutions of the catalyst pellet may also be determined at various values of $\frac{C_B}{C_A}$.

At each point in the reactor it is, therefore, necessary to use the curves at the appropriate $\frac{C_B}{C_A}$ ratio in order to determine whether the temperature runaway region has been entered. This is illustrated in figure A4.2. Although at the reactor inlet where $\frac{C_B}{C_A} = 0$, the trajectory is below the appropriate runaway line, further down the reactor where $\frac{C_B}{C_A} = 0.5$ this point on the trajectory is above the appropriate runaway line and so temperature runaway occurs. It can be seen that an examination of the reactor stability in

this way may be further complicated by the movement of the non-unique region towards the left hand side of the phase diagram as the $\frac{C_B}{C_A}$ ratio increases.

Clearly, the procedure is more laborious than that used for the simple reaction scheme when carried out graphically in this manner. However, once the algebraic expressions for t_i and t_s as functions of $\frac{C_B}{C_A}$ have been determined, examination of each point on the reactor trajectory as it is computed is a simple computational matter.

APPENDIX 5

TEMPERATURE RUNAWAY CRITERIA FOR QUASI-HOMOGENEOUS REACTORS

In a recent paper by Van Welsenaere and Froment[68] some criteria for temperature runaway in quasi-homogeneous reactors are given. One of these criteria appears to have been derived purely by observation of the properties of computed reactor trajectories on the phase diagram. However, it may be shown that the system equations can be used to demonstrate why this criterion is a fundamental property of quasi-homogeneous reactors.

Using a one dimensional reactor model, the trajectories of a quasi-homogeneous system on the T vs B phase diagram are given by:

$$\frac{dT}{dB} = -\frac{2G_4}{3G_2} + \frac{2Nu_w^*(T - T_c)}{G_2G_3\,\theta^2\exp(-\frac{1}{T})B} \qquad (A5.1)$$

Equation (A5.1) may be written more simply as:

$$\frac{dT}{dB} = -P + \frac{Q(T - T_c)}{\exp(-\frac{1}{T})B} \qquad (A5.2)$$

The locus of the maxima of these trajectories, which Van Welsenaere and Froment[68] call "maxima curves" is given by setting the derivative in equation (A5.2) equal to zero. Thus, the maxima curve for a particular coolant temperature, T_c, is given by:

$$P\exp(-\frac{1}{T})B_m - Q(T_m - T_c) = 0 \qquad (A5.3)$$

where B_m and T_m are the thermal load factor and temperature respectively at the maximum on the reactor trajectory. As shown in chapter 4 for the heterogeneous reactor, a family of maxima curves for a particular wall heat transfer coefficient at various values of T_c may be plotted on the T vs B phase diagram. The individual maxima curves also have a maximum, thus there is a value of B_m at which there is only one corresponding value of T_m for any T_c. At values of B_m less than this maximum there are two corresponding values of T_m for each T_c. Van Welsenaere and Froment[68] observed that for quasi-homogeneous systems, reactor trajectories which would have

maxima at values of T_m greater than that at the maximum value of B_m would be subject to parametric sensitivity and temperature runaway. They then derived the equation for the maximum of the maxima curves by setting the derivative $\frac{dB_m}{dT_m}$ from equation (A5.3) equal to zero and called the trajectory through this point the critical one. Thus, their first runaway criterion was given as: "The trajectory going through the maximum of the maxima curve is considered as critical and, therefore, as locus of the critical inlet conditions for B and T corresponding to a given coolant temperature."

For quasi-homogeneous systems this is, indeed, the case. However, it is instructive to examine equation (A5.3) since the reason for the validity of the criterion then becomes apparent.

Equation (A5.3) may be rearranged as:

$$Pexp(-\frac{1}{T})B_m = Q(T_m - T_c)$$

or more simply as:

$$f_1(B_m, T_m) = f_2(T_m, T_c) \qquad (A5.4)$$

The function f_1 is an exponential heat generation function which, it should be noted, will not generally apply in heterogeneous systems at temperature runaway because the reaction rate tends to become limited by internal mass transfer in the catalyst pellet; f_2 is a linear heat removal function. Thus, equation (A5.4) expresses the well known fact that at the maximum of the reactor trajectory the rate of heat removal is equal to the rate of heat generation. f_1 and f_2 may be plotted against T_m for a given value of T_c at various values of B_m. The points at which the two functions intersect then give the points on the maxima curve for that value of B_m. At the maximum value of B_m, equation (A5.4) is only satisfied once, whereas for values of B_m less than this the two functions intersect at least twice (in fact the shape of f_2 is sigmoidal but the third point of intersection is outside the practical range of B_m and T_m). The value of B_m where the two points of intersection are coincident corresponds to the maximum of the maxima curve. If the values of B_m and T_m at this point are B_{mm} and T_{mm} respectively, then for a given value of T_c and $B_m < B_{mm}$ equation (A5.4) is satisfied at two points, once for $T_m < T_{mm}$ and once for $T_m > T_{mm}$. According to the runaway

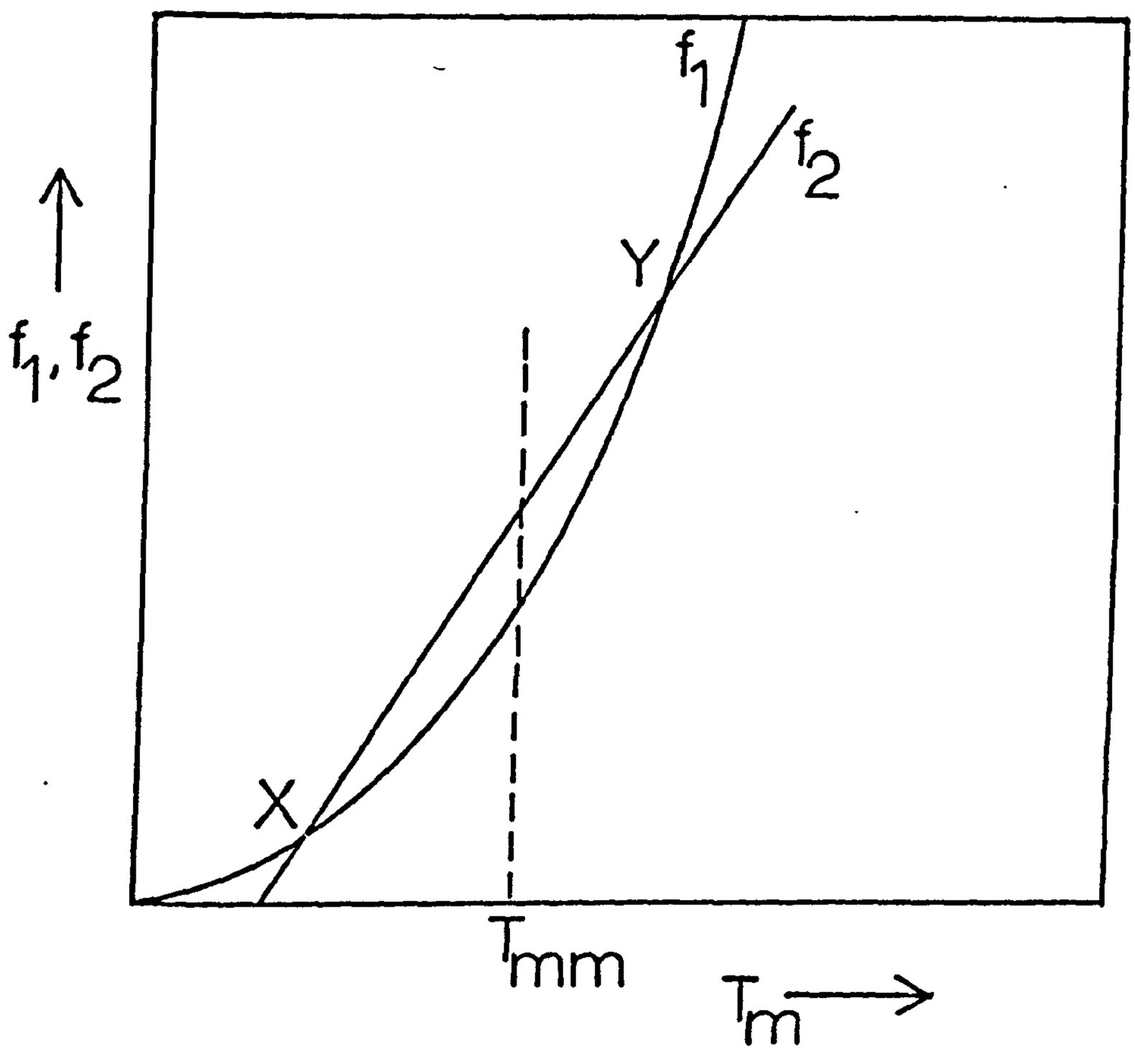

Figure A5.1 Schematic diagram of the heat generation (f_1) and heat removal (f_2) functions plotted against T_m.

criterion, at the points for which $T_m > T_{mm}$ then temperature runaway (or parametric sensitivity) occurs, whereas for $T_m < T_{mm}$ the trajectories are "safe." Reference to figure A5.1, where f_1 and f_2 are plotted against T_m at a given T_c and B_m ($< B_{mm}$), shows why this is so.

The point X in figure A5.1, which corresponds to points on a maxima curve for $T_m < T_{mm}$ (i.e. a "safe" maximum), may be described as "stable" since increasing T_m from this point leads to $f_2 > f_1$ (i.e. heat removal becomes greater than heat generation). The point Y, however, which corresponds to a runaway maximum (i.e. $T_m > T_{mm}$) may be described as "metastable" because increasing T_m from Y causes $f_1 > f_2$ (i.e. heat generation becomes greater than heat removal - and therefore, temperature runaway occurs) and decreasing T_m from Y leads to $f_2 > f_1$ (i.e. heat generation becomes less than heat removal). This, clearly, demonstrates why trajectories with $T_m > T_{mm}$ are "unsafe" for the quasi-homogeneous system. It also gives some insight into how the hot spot of a particular trajectory will behave when the inlet conditions of the reactor are subject to perturbations.

As is shown in chapter 4, the runaway criterion for quasi-homogeneous systems cannot be applied to the heterogeneous case since parametric sensitivity arises for different reasons.

APPENDIX 6

APPLICATION OF THE METHOD OF LINES IN THE SOLUTION OF THE UNSTEADY STATE COOLANT EQUATIONS FOR THE SINGLE TUBE REACTOR MODELS

Equations (7.4) and (7.5) both have the general form:

$$\frac{\partial f}{\partial z} + R'f + R'' = K'\frac{\partial f}{\partial \tau} \qquad \text{(A6.1)}$$

The application of the method of lines to this equation involves replacing one of the derivatives by a finite difference approximation leaving an ordinary differential equation which may be solved by any of the standard integration techniques. Since equations (7.4) and (7.5) must be solved simultaneously with the unsteady state catalyst pellet equation (equation A1.25), it is most convenient to replace the axial derivative by the finite difference approximation so that the remaining ordinary differential equation describing the change of coolant temperature with time may be solved using the same subroutine as used for equation (A1.25)..

In backward difference form, the axial derivative in equation (A6.1) may be written as:

$$\frac{\partial f}{\partial z} = \frac{1}{k}(f_i - xf_i) \qquad \text{(A6.2)}$$

where: k is the step length in the axial direction and prefix 'x' indicates the value of the variable at the previous axial position.

Therefore, substituting for $\frac{\partial f}{\partial z}$ from equation (A6.2) in equation (A6.1) and rearranging gives:

$$\frac{df}{d\tau} = \frac{1}{K'}\left(f_i\left(\frac{1}{k} + R'_i\right) - \frac{xf_i}{k} + R'_i'\right) \qquad \text{(A6.3)}$$

The ordinary differential equation represented by equation (A6.3) may be conveniently solved using the Runge-Kutta-Merson algorithm. For this, it is necessary to be able to specify xf, R' and R" at various points during the integration step other than the initial and final points. This may be done by assuming that they vary linearly over the small time interval as in the solution of the dynamic model of the catalyst pellet.

APPENDIX 7

THE FINITE DIFFERENCE APPROXIMATION OF THE COOLANT EQUATION IN THE CONTINUUM MODEL OF THE MULTITUBULAR REACTOR

Equation (8.2) may be written in general form as:

$$\frac{\partial^2 f}{\partial z^2} + K\frac{\partial f}{\partial x} + R'f + R'' = 0 \qquad \text{(A7.1)}$$

with the boundary conditions:

$$f = f_0 \qquad \text{at } x = 0,\ 0 \leqslant z \leqslant 1$$

$$\frac{\partial f}{\partial z} = 0 \qquad \text{at } \begin{cases} z = 0,\ 0 \leqslant x \leqslant 1 \\ z = 1 \end{cases}$$

In finite difference form, the terms in equation (A7.1) become:

$$\frac{\partial^2 f}{\partial z^2} = \frac{1}{h^2}(Q(f_{i+1} - 2f_i + f_{i-1}) + (1 - Q)(xf_{i+1} - 2xf_i + xf_{i-1}))$$

$$K\frac{\partial f}{\partial x} = \frac{K}{k}(f_i - xf_i)$$

$$R'f = QR'_i f_i + (1 - Q)xR'_i\ xf_i$$

$$R'' = QR''_i + (1 - Q)xR''_i$$

where:

the prefix 'x' indicates the value of a variable at the previous axial (z) position

h is the step length in the axial direction

k is the step length across the tube bundle (x direction)

Q is a constant such that $0 < Q \leqslant 1$. When Q = 0.5 the equations reduce to the Crank-Nicolson form.

Replacing the terms in equation (A7.1) by the expressions given above, and rearranging, gives:

$$m_i f_{i+1} + p_i f_i + n_i f_{i-1} = a_i \qquad \text{(A7.2)}$$

where: $m_i = \frac{Q}{h^2}$

$$p_i = -\frac{2Q}{h^2} + \frac{K}{k} + QR'_i$$

$$n_i = \frac{Q}{h^2}$$

$$a_i = -xf_{i+1}\left(\frac{(1-Q)}{h^2}\right)$$

$$-xf_i\left(-\frac{2(1-Q)}{h^2} - \frac{K}{k} + (1-Q)xR'_i\right)$$

$$-xf_{i-1}\left(\frac{(1-Q)}{h^2}\right)$$

$$-QR''_i - (1-Q)xR''_i$$

These expressions hold for $1 \leqslant i \leqslant (N-1)$ where 0 and N are the numbers of the finite difference nodes at each baffle plate (i.e. at z = 0 and z = 1).

Applying the boundary conditions at z = 0 and z = 1 enables the elimination of the terms at the hypothetical nodes N + 1 and - 1. This leads to the following expressions at the zeroth node:

$$m_0 f_{+1} + p_0 f_0 = a_0 \qquad \text{(A7.3)}$$

where: $m_0 = \frac{2Q}{h^2}$

$$p_0 = -\frac{2Q}{h^2} + \frac{K}{k} + QR'_0$$

$$a_0 = -xf_0\left(-\frac{2(1-Q)}{h^2} - \frac{K}{k} + (1-Q)xR'_0\right)$$

$$-xf_{+1}\left(\frac{2(1-Q)}{h^2}\right) - QR''_0 - (1-Q)xR''_0$$

and at the N th node:

$$p_N f_N + n_N f_{N-1} = a_N \qquad \text{(A7.4)}$$

$$\text{where: } p_N = -\frac{2Q}{h^2} + \frac{K}{k} + QR'_N$$

$$n_N = \frac{2Q}{h^2}$$

$$a_N = -xf_{N-1}\left(\frac{2(1-Q)}{h^2}\right)$$

$$-xf_N\left(-\frac{2(1-Q)}{h^2} - \frac{K}{k} + (1-Q)xR'_N\right)$$

$$-QR'_{N'} - (1-Q)R'_{N'}$$

Equations (A7.2), (A7.3) and (A7.4) represent a system of simultaneous algebraic equations of the form:

$$\underline{A}\,\underline{f} = \underline{a}$$

The coefficient matrix $\underline{A}$ is tridiagonal and so the equations may be solved using the Thomas[127] method in the same way as the two dimensional reactor equations described in Appendix 3.

NOMENCLATURE

a_i	Matrix element in the finite difference formulation of the differential equations
A	Amplitude of sinusoidal perturbations
A'	Surface area of the reactor tubes per unit volume of the tube bundle
A_1, A_2	Parameter groups defined and used in chapter 8
A_0	Arrhenius pre-exponential factor for the simple reaction scheme
A_{0i}	Arrhenius pre-exponential factor for reaction i in the complex reaction scheme
b	Pellet radius
B_0	Dimensionless exothermicity factor $= \frac{(-\Delta H) D_{pA} C_0 R_g}{2bhE}$
B	Thermal load factor = $B_0 \times C_A$
B_i	Value of B at the reactor inlet
B_a	Value of B at the maximum of a maxima curve (defined in chapter 4)
B_{il}	Lower limit on B_i (defined in chapter 4)
B_{iu}	Upper limit on B_i (defined in chapter 4)
B_{cr}	Value of B at the maximum of a critical reactor trajectory (defined in chapter 4)
B_m	Value of B at the maximum value of T on a reactor trajectory (defined in chapter 4)
C_A, C_B	Dimensionless concentration of reactants within the fluid = $\frac{C'_{fA}}{C_0}$ and $\frac{C'_{fB}}{C_0}$, respectively
C_{AO}, C_{BO}	Values of C_A and C_B respectively at the reactor inlet
C_{pA}, C_{pB}	Dimensionless concentration of reactants within the catalyst pellet = $\frac{C'_{pA}}{C_0}$ and $\frac{C'_{pB}}{C_0}$

C_{pAs}, C_{pBs}	Surface values of C_{pA} and C_{pB}
C'_{fA}, C'_{fB}	Reactant concentrations within the fluid
C'_{pA}, C'_{pB}	Reactant concentrations within the catalyst pellet
C_0	Reference concentration of reactant A
$c_p, c_p^*, c_{pc}, c_{pw}$	Specific heats of the fluid, catalyst pellet, coolant and tube wall respectively
d_p	Diameter of the catalyst pellet
D_{fA}, D_{fB}	Effective interstitial radial diffusivities in the fluid
D_{pA}, D_{pB}	Effective radial diffusivities within the catalyst pellet
e, e^*	Porosity of the fixed bed and catalyst pellet, respectively.
e_c	Voidage of the tube bundle in the direction perpendicular to coolant flow
E	Activation energy for the simple reaction scheme
E_i	Activation energy of reaction i in the complex reaction scheme
f	Dependent variable in the general form of the differential equations
f_0	Value of fluid variable, C_A or T, at time γ equals zero during a sinusoidal perturbation
f_{0i}	Inlet value of f_0
$f(\gamma)$	Value of fluid variable, C_A or T, at time γ during a sinusoidal perturbation
$f_i(\gamma)$	Inlet value of $f(\gamma)$
f_1 to f_3	Functions defined in Appendices 4 and 5
F_1 to F_7	Parameter groups defined and used in chapter 3
$F_{(i)}$	Function defined in chapter 8
g	$\tanh(r)$
g_i	$\tanh(r_i)$
g_m	$\tanh(r_m)$

G_1 to G_6	Parameter groups used in the models of the reactor tubes and defined in chapter 5
G_{cc}, G_c	Parameter groups defined and used in chapters 7 and 8 respectively
h	*Step length in a finite difference grid*
h	Effective pellet to fluid surface heat transfer coefficient = $h_c + h_p + h_r$
h_f, h_c	Heat transfer coefficients on the fluid-side and coolant-side, respectively, of the reactor tube
h_c, h_p, h_r	Pellet to fluid surface heat transfer coefficients due to convection, point contact, and radiation respectively
H_2, H_3	Ratios of heats of reaction in the complex reaction scheme = $\frac{(-\Delta H_2)}{(-\Delta H_1)}$ and $\frac{(-\Delta H_3)}{(-\Delta H_1)}$, respectively
i	Reaction number for the complex reaction scheme (1,2 and 3)
i	Number of a node in a finite difference grid
j	Step length in a finite difference grid
k	Step length in a finite difference grid
k_f	Effective radial conductivity of the gas phase in the two phase heat transfer model (referred to superficial area)
k	Dimensionless first order rate constant evaluated at the fluid temperature for the simple reaction scheme = $\theta^2 \exp(-\frac{1}{T})$
k_i^*	Dimensionless first order rate constant evaluated at the pellet temperature for reaction i in the complex reaction scheme = $\theta_i^2 \exp(-\frac{E_i}{E_1 t})$
k_{gA}, k_{gB}	Fluid to pellet mass transfer coefficients
k'_g	Thermal conductivity of the fluid
k_p, k_r	Solid-solid thermal conductivities for point contact and radiation, respectively

k_s	Effective radial thermal conductivity of the solid phase in the two phase heat transfer model (referred to the superficial area)
K, K^o, K', K''	Parameters used in the general formulations of the differential equations
K	Adsorption equilibrium constant (chapter 2 only)
K_c	$\underline{L}$, (used in chapter 7) u_c
K_c'	Effective interstitial thermal conductivity of the coolant in the direction perpendicular to coolant flow
K_{cc}	"Capacitance" of the catalyst pellet to absorb mass = $\frac{b^2 e^*}{D_{pA}}$
K_f	Effective interstitial radial thermal conductivity of the fluid
K_{fs}	Effective superficial radial thermal conductivity of the fluid phase in the two phase heat transfer model = $k_f + k_s$
K_p	Effective thermal conductivity of the catalyst pellet
K_T	"Capacitance" of the catalyst pellet to absorb heat = $\frac{b^2 \rho^* c_p^*}{K_p}$
K_W	Parameter group defined and used in chapter 5
l_B	Distance between baffle plates in the multitubular reactor
l_c	Diameter of the tube bundle in the multitubular reactor
l_T	Minimum distance between adjacent tubes in the multitubular reactor = $P_D - 2b$
L	Reactor tube length
m_c	Total mass flowrate of the coolant across the tube bundle in each coolant pass based on the "interstitial" coolant velocity = $u_c \rho_c l_B l_T$

m_i	Element of the tridiagonal matrix in the finite difference formulation of the differential equations
M_c	Mass flowrate of the coolant along the outside of the reactor tube (used in chapter 7 only)
M_f	Magnitude of deviation of variable f (C_A or T) from the initial steady state during a sinusoidal perturbation = $\frac{f(\tau) - f_0}{f_0}$
n	Number of tubes used in simplified version of the mixing cell models of the coolant in chapter 8
n_i	Element of the tridiagonal matrix in the finite difference formulation of the differential equations
n, n_i	Order of the reaction in the simple reaction scheme and of reaction i in the complex scheme, respectively
N	Number of tubes in the tube bundle of the multitubular reactor
N	Number of radial steps in the finite difference grid
Nu	Modified Nusselt number for heat transfer between the pellet and the fluid = $\frac{2bh}{K_p}$
Nu_w	Nusselt number for heat transfer between the fluid and the coolant = $\frac{RU}{K_{fe}}$ (= $\frac{RU}{K_{fs}}$ in chapter 3)
Nu_w^*	Effective overall Nusselt number for heat transfer between the fluid and the coolant based on the radial mean fluid temperature. Used in the one dimensional model of the reactor tube
Nu_{wf}	Nusselt number for heat transfer between the fluid and the tube wall = $\frac{R_1 h_f}{K_{fe}}$

Nu^{*}_{wf} *Effective overall Nusselt number for heat transfer between the fluid and the tube wall* based on the radial mean fluid temperature. Used in the one dimensional model of the reactor tube in chapter 5.

Nu_{wO} Pseudo-Nusselt number for heat transfer between the tube wall and the coolant = $\frac{R_1 h_c}{K_f e}$. Used in chapter 5

Nu^{f}_{w} Nusselt number for heat transfer between the fluid and the coolant in the two phase heat transfer model = $\frac{RU_f}{k_f}$

Nu^{s}_{w} Nusselt number for heat transfer between the solid and the coolant in the two phase heat transfer model = $\frac{RU_s}{k_s}$

of Value of f at the previous time step (i.e.known)

oxf Value of f at the previous time and axial step (i.e. known)

p_i Element of the tridiagonal matrix in the finite difference formulation of the differential equations

P Emissivity of the catalyst pellets

P_D Pitch circle diameter in multitubular reactor

P_1 to P_4 Functions defined in Appendix 1

Q, Q^* Weighting constants in the finite difference representation of the differential equations such that $0 < Q, Q^* \leq 1$

r Dimensionless radial position in the reactor tube = $\frac{y}{R}$

r $\theta \exp(-\frac{1}{2t})$

r_i $\theta \exp(-\frac{1}{2t_i})$

r_m $\theta \exp(-\frac{1}{2t_m})$

R	Effective radius of the reactor tube
R'	Reaction rate used in chapter 3 = $A_0 \exp(-\frac{1}{t}) C_{pAs}$
R', R''	Non-linear terms in the general forms of the differential equations (Appendices 2,3,6 and 7)
R_g	The gas constant
R_1	Inside radius of the reactor tube
R_2	Outside radius of the reactor tube
s	$\frac{Sh_A}{2} - 1$
S	Distance from the centre of the catalyst pellet
S_1 to S_6	Parameter groups defined and used in chapter 3
Sh_A, Sh_B	Modified Sherwood numbers = $\frac{2bk_{gA}}{D_{pA}}$, $\frac{2bk_{gB}}{D_{pB}}$ respectively
t	Dimensionless pellet temperature = $\frac{R_g T_p}{E}$ for the simple reaction scheme and $\frac{R_g T_p}{E_1}$ in the complex reaction scheme
t_i	Value of t at the point of inflexion of the (t - T) vs t curve
t_m	Value of t at the maximum of a reactor trajectory on the T vs B phase diagram
t_s	Value of t where the tangent at the point of inflexion of the (t - T) vs t curve meets the line (t - T) = 0
t_{s1}	Value of t_s in the non-unique region for $t_s < t_1^*$
t_{s2}	Value of t_s in the non-unique region for $t_s > t_1^*$
t_1^*	Value of t on the upper bound of the non-unique region
t_1, t_2	Temperatures at the surfaces of adjacent catalyst pellets (chapter 3 only)
T	Dimensionless fluid temperature = $\frac{R_g T'}{E}$ for the simple reaction scheme and $\frac{R_g T'}{E_1}$ in the

	complex reaction scheme. In the one dimensional model of the reactor tube, T is the radial mean value of the fluid temperature
T'	Temperature of the fluid
T_0, T_0'	Value of T and T' respectively at the reactor inlet
T_c	Dimensionless coolant temperature = $R_g \underline{T}_c'$ for the simple reaction scheme and $R_g \underline{T}_c'$ E for the complex reaction scheme E_1
T_c'	Temperature of the coolant
T_{c0}, T_{c0}'	Values of T_c and T_c' respectively at the coolant inlet
$T_{c(i)}$	Value of T_c in cell i in the mixing cell models of the multitubular reactor
$T_{c(i)}'$	Value of T_c' in cell i in the mixing cell models of the multitubular reactor
T_{cr}	Value of T at the maximum of the critical trajectory on the T vs B phase diagram
T_m	Value of T at the maximum of a trajectory on the T vs B phase diagram
T_p	Temperature of the catalyst pellet
T_w	Dimensionless tube wall temperature = $R_g \underline{T}_w' / E$
T_w'	Temperature of the tube wall
T_{w0}, T_{w0}'	Values of T_w and T_w' respectively at $\gamma = 0$
u	Interstitial fluid velocity
u_c	Interstitial coolant velocity across the tube bundle in the multitubular reactor model
u_c'	Velocity of the coolant along the outside of the reactor tube (used in chapter 7 only)
u_s	Superficial fluid velocity
U	Fluid to coolant overall heat transfer coefficient
U_f	Fluid to coolant heat transfer coefficient in the two phase heat transfer model

U_s — Solid to coolant heat transfer coefficient in the two phase heat transfer model

x — Dimensionless coordinate across the tube bundle in the direction of coolant flow = $\frac{x'}{l_c}$

x' — Distance across the tube bundle in the direction of coolant flow

xf — The value of f at the previous axial step (i.e. known)

y — Distance from the reactor tube axis

y — Dimensionless pellet coordinate = $1 - \frac{S}{b}$ (Appendix 1)

z — Dimensionless axial coordinate along the reactor tubes = $\frac{z'}{L}$

z' — Axial distance along the reactor tube

z'' — Axial distance along the reactor tubes in each coolant pass, measured between the baffle plates in the continuum model of the multitubular reactor

z_c — Dimensionless coordinate along the reactor tubes in each coolant pass measured between the baffle plates = $\frac{z''}{l_B}$

z_{cr} — Dimensionless axial position at which temperature runaway occurs

z_1', z_2' — Values of z' at the baffle plates in each coolant pass in the multitubular reactor

z_1, z_2 — Values of z at the baffle plates in each coolant pass = $\frac{z_1'}{L}, \frac{z_2'}{L}$

Greek Symbols

ε_2 — Projected fraction of pellet cross-sectional area not in contact with an adjacent pellet

ε_3 — Projected fraction of pellet cross-sectional area

in contact with an adjacent pellet

ε_c — Voidage of the tube bundle in the direction of coolant flow

δ — Ratio of diffusivities within the catalyst pellet = $\frac{D_{pA}}{D_{pB}}$

Δ — Ratio of diffusivities in the fluid = $\frac{D_{fA}}{D_{fB}}$

$(-\Delta H), (-\Delta H_i)$ — Heats of reaction for the simple reaction scheme and reaction i in the complex reaction respectively

η — Effectiveness factor

θ, θ_i — Reaction-diffusion modulus = $b\sqrt{\frac{A_0}{D_{pA}}}$ and $b\sqrt{\frac{A_{0i}}{D_{pA}}}$ respectively. In the case of a non-first order reaction of order n, θ becomes $b\sqrt{\frac{A_0}{D_{pA}}}\ C_A^{(n-1)/2}$

$\rho, \rho^*, \rho_c, \rho_w$ — Densities of the fluid, catalyst pellet, coolant and reactor tube wall respectively

τ — Time (SECONDS)

ϕ — Constant defining the effective gas layer thickness between adjacent catalyst pellets

Ψ — Selectivity for species B in the complex reaction scheme

ω — Frequency of a sinusoidal perturbation

BIBLIOGRAPHY

1. ARIS, R. Introduction to the Analysis of Chemical Reactors, Prentice Hall, N.J. (1965).

2. PETERSEN, E.E., Chemical Reaction Analysis, Prentice Hall, N.J. (1965).

3. LEVENSPIEL, O., Chemical Reaction Engineering, John Wiley, N.Y. (1962).

4. DENBIGH, K. and TURNER, J., Chemical Reactor Theory, C.U.P. (1971).

5. THOMAS, J.M. and THOMAS, W.J., Introduction to the Principles of Heterogeneous Catalysis, Academic Press (1967).

6. COULSON, J.M. and RICHARDSON, J.F., Chemical Engineering, Vol.III, Pergamon Press Ltd., London (1971).

7. PERLMUTTER, D.D., Stability of Chemical Reactors, Prentice Hall, N.J. (1972).

8. FROMENT, G.F., Symposium on Reactor Engineering, University of Leeds, England (1971).

9. FROMENT, G.F., Second International/Fifth European Symposium on Chemical Reaction Engineering, Amsterdam (1972).

10. HLAVACEK, V., Ind. Eng. Chem., 62, 8(1970).

11. RAY, W.H., Fifth European/Second International Symposium on Chemical Reaction Engineering, Amsterdam (1972).

12. THORNTON, J.M., Ph.D. Dissertation, University of Leeds (1970).

13. CRESSWELL, D.L., Ph.D. Dissertation, University of Leeds (1969).

14. HANSEN, K.W., LIVBJERG, H. and VILLADSEN, J., Fifth European/Second International Symposium on Chemical Reaction Engineering, Amsterdam (1972).

15. NAIM, H., Ph.D. Dissertation, University of Leeds (1973).

16. THIELE, E.W., Ind. Eng. Chem., 31 , 916 (1939).

17. ZIELDOWITSCH, J.B., Acta Physicochim U.S.S.R., 10, 583 (1939).

18. WHEELER, A., Adv. in Catalysis, 3, 249 (1951).

19. WEISZ, P.B. and PRATER, C.D., Adv. in Catalysis, 6, 144 (1954).

20. WEISZ, P.B., Z. Physik. Chem., 11, 1 (1957).

21. WEISZ, P.B., Chem. Eng. Prog. Symp. Series, 55 (25), 29 (1959).

22. WHEELER, A., Catalysis, Vol.II, Reinhold, N.Y. (1955).

23. PRATER, C.D., Chem. Eng. Sci., 8, 284 (1958).

24. CARBERRY, J.J., A.I.Ch.E. Jl., 7, 350 (1961).

25. HUTCHINGS, J. and CARBERRY, J.J., A.I.Ch.E. Jl., 12, 20 (1966).

26. FINLAYSON, B.A., Chem. Eng. Sci., 22, 1081 (1971).

27. FERGUSON, N.B. and FINLAYSON, B.A., Chem. Engng. Jl., 1, 327 (1970).

28. OLBRICH, W.E. et al., Trans. I.Ch.E., 44, T207 (1966).

29. BEEK. J., A.I.Ch.E. Jl., 7, 337 (1961).

30. PETERSEN. E. E., Chem. Eng. Sci., 17, 987 (1962).

31. PETERSEN, E. E., Ibid., 20, 587 (1965).

32. GUNN, D. J., Ibid., 21, 383 (1966).

33. PATERSON, W.R. and CRESSWELL, D. L., Ibid, 26, 605 (1971).

34. JOUVEN, V. G. and ARIS, R., A.I.Ch.E. Jl., 18, 402 (1972).

35. McGREAVY, C., ADDERLEY, C. I. and SOLIMAN, M.A., to be published.

36. RESTER, S. and ARIS, R., Chem. Eng. Sci., 27, 347 (1972).

37. RAWLINGS, N., Private Communication.

38. HLAVACEK, V. and KUBICEK, M., Chem. Eng. Sci., 25, 1537 (1970).

39. HLAVACEK, V. and KUBICEK, M., Ibid., 25, 1761 (1970).

40. CUNNINGHAM, R. A. et al., A.I.Ch.E. Jl., 11, 636 (1965).

41. MILLER, F.W. and DEANS, H. A., Ibid, 13, 45 (1967).

42. FULTON, J. W. and CROSSER, O. K., Ibid., 11, 573 (1965).

43. IRVING, J. P. and BUTT, J. B., Chem. Eng. Sci., 22, 1859 (1967).

44. HUGHES, R. and KOH, H. P., Chem. Engng. Jl., 1, 186 (1970).

45. McGUIRE, M. L. and LAPIDUS, L., A.I.Ch.E. Jl., 11, 85 (1965).

46. FEICK, J. and QUON, D., Canad. Jl. Chem. Eng., 48, 205 (1970).

47. HANSEN, K. W., Chem. Eng. Sci., 26, 1555 (1971).

48. KEHOE, J.P.G., and BUTT, J. B., Fifth European/Second International Symposium on Chemical Reaction Engineering, Amsterdam (1972).

49. HORAK, J. and JIRACEK, F., Proceedings of 3rd CHISA Conference, Czechoslovakia (1969).

50. ELNASHAIE, S.S.E.H. and CRESSWELL, D. L., Canad. Jl., Chem. Eng., 51, 201 (1973).

51. DENIS, G.H. and KABEL, R. L., Chem. Eng. Sci., 25, 1057 (1970).

52. NUSSEY, C., Ph.D. Dissertation, University of Leeds (1968).

53. CARBERRY, J. J. and WENDEL, M. M., A.I.Ch.E. Jl., 9, 129 (1963).

54. KARENTH, N. G. and HUGHES, R., Paper presented at Symposium on Heterogeneous Reactors, University of Salford, England (1972).

55. VALSTAR, J. M., A study of the Fixed Bed Reactor with Application to the Synthesis of Vinyl Acetate, Delftsche Uitgevers Maatschappij, N.V., Delft (1969).

56. DEANS, H. A. and LAPIDUS, L., A.I.Ch.E. Jl., 6, 656 (1960).

57. CRIDER, J. E. and FOSS, A.S., Ibid., 12, 514 (1966).

58. FEICK, J., Ph.D. Dissertation, University of Alberta, Edmonton, Alberta (1968).

59. JONES, D. A., Ph.D. Dissertation, University of Leeds (1971).

60. DE WASCH, A. P. and FROMENT, G. F. Chem. Eng. Sci., 26, 629 (1971).

61. CALDERBANK, P.H. et al., Fourth European Symposium on Chemical Reaction Engineering, Brussels (1968).

62. SHADMAN-YAZDI, F. and PETERSEN, E.E., Chem. Eng. Sci., 27, 227 (1972).

63. THIERNEY, J. W. et al., A.I.Ch.E. Jl., 4, 460 (1958).

64. HOIBERG, J. A., LYCHE, B. C. and FOSS, A.S., Ibid., 17, 1434 (1971).

65. STANEK, V. and SZEKELY, J., Canad. Jl. Chem. Eng., 51, 22 (1973).

66. FAN, L.T., CHEN, K.C. and ERICKSON, L.E., Chem. Eng. Sci., 26, 379 (1971).

67. BARKELEW, C. R. Chem. Engng. Symp. Series, 55, (25), 38 (1959).

68. VAN WELSENAERE, R.J. and FROMENT, G. F. Chem. Eng. Sci., 25, 1503 (1970).

69. BILOUS, O. and AMUNDSON, N. R., A.I.Ch.E. Jl., 2, 116 (1956).

70. ERVIN, M. A.and LUSS, D., Ibid., 16, 979 (1970).

71. TURNER, K., Ph.D. Dissertation, University of Leeds (1970).

72. STEWART, W. E. and SØRENSEN, J.P., Fifth European/ Second International Symposium on Chemical Reaction Engineering, Amsterdam (1972).

73. RAYMOND, L. R. and AMUNDSON, N. R., Canad. Jl., Chem. Eng., 42, 173 (1964).

74. HLAVACEK, V. and HOFMANN, H., Chem. Eng. Sci., 25, 173 (1970).

75. HLAVACEK, V. and HOFMANN, H., Ibid., 25, 187 (1970).

76. KAO, Y. K. and BANKOFF, S. G., Ibid., 26, 189 (1971).

77. McGOWIN, C. and PERLMUTTER, D.D., A.I.Ch.E. Jl., 17, 831 (1971).

78. MATSUYAMA, H., Chem. Engng. Jl., Japan, 5, 427 (1972).

79. CARDOSO, M.A.A. and LUSS, D., Chem. Eng. Sci., 25, 1527 (1970).

80. HATFIELD, B. and ARIS, R., Ibid., 24, 1913 (1969).

81. HATFIELD, B. and ARIS, R., Ibid., 24, 1220 (1969).

82. CRESSWELL, D. L., Ibid., 25, 267 (1970).

83. McGREAVY, C. and THORNTON,J.M., Chem. Engng. Jl., 1, 296 (1970).

84. FURUSAWA, T. and KUNII, D., Chem. Engng. Jl., Japan, 4, 274 (1971).

85. McGREAVY, C. and SOLIMAN, M.A., Chem. Engng. Jl., (In Press).

86. BISCHOFF, K. B., Chem. Eng. Sci., 23, 251 (1968).

87. COPELOWITZ, I. and ARIS, R., Ibid., 25, 885 (1970).

88. HLAVACEK, V. and KUBICEK, M., Ibid., 25, 1527 (1970).

89. HORN, F.J. M. et al., Chem. Engng. Jl., 1, 79 (1970).

90. YANG, R.Y.K., et al., Ibid., 2, 218 (1971).

91. JACKSON, R. and HORN, F.J.M., Ibid., 3, 82 (1972).

92. LUSS, D., Ibid., 1, 311 (1970).

93. BRUSSET, H., et al., Chem. Eng. Sci., 27, 1475 (1972).

94. OLBRICH, N.E., Proc. Chemeca '70 Conference, p101, Butterworths (1970).

95. McGREAVY, C. and CRESSWELL, D. L., Canad. Jl.,Chem. Eng., 47, 583 (1969).

96. KUNII, D. and SMITH, J.M., A.I.Ch.E. Jl., 6, 71 (1969).

97. KRUPICZKA, R., Intnl. Chem. Engng., 7, 122 (1967).

98. WAKAO, N. and KATO, K., Chem. Engng. Jl., Japan, 2, 24 (1969).

99. BERNARD, R.A. and WILHELM, R. H., Chem. Eng. Prog., 46, 233 (1950).

100. RAIZ, W. E., Ibid., 48, 247 (1952).

101. SINGER, E. and WILHELM, R. H., Ibid., 46, 343 (1950).

102. ARGO, W. B. and SMITH, J.M., Ibid., 49, 443 (1953).

103. YAGI, S. and KUNII, D., A.I.Ch.E. Jl., 3, 373 (1957).

104. DE WASCH, A.P. and FROMENT, G.F., Chem. Eng. Sci., 27, 567 (1972).

105. McGREAVY, C., Proc. First Pacific Chem. Engng. Congress, Kyoto, Japan (1972).

106. BEEK, J., Adv. in Chem. Engng., 3, (1962).

107. McKEON, T. M., Ph.D. Dissertation, University of Leeds (1970).

108. YAGI, S. and KUNII, D., A.I.Ch.E., Jl., 6, 97 (1960).

109. HANDLEY, D. and HEGGS, P.J., Trans. I.Ch.E., 46, 251 (1968).

110. DAMKOEHLER, G., Der Chemie Ingenieur, Euben Jacob, (Liepzig), 3, 441 (1937).

111. BEVERIDGE, G.S.G. and HAUGHEY, D.P., Intnl. Jl., Heat and Mass Trans., 14, 1093 (1971).

112. McGREAVY, C. and THORNTON, J.M., Canad. Jl.,Chem. Engng., 48, 187 (1970).

113. McGREAVY, C. and ADDERLEY, C.I., I. Chem. E. Symp. Series, No. 35. (1972).

114. WANKA, O. and GUTLHUBER, F., Paper presented at symposium on Heterogeneous Reactors, University of Salford, England, (1972).

115. CRIDER, J.E. and FOSS, A.S., A.I.Ch.E. Jl., 14, 77 (1968).

116. SINAI, J. and FOSS, A.S., Ibid., 16, 658 (1970).

117. LUSS, D. and MEDELLIN, P., Fifth European/Second International Symposium on Chemical Reaction Engineering, Amsterdam (1972).

118. BANCHERO, J.T. and SMITH, T.G., A.I.Ch.E./ASME Heat Transfer Conference, Denver, Colorado (1972).

119. PARIS, J.R., and STEVENS, W.F., Fourth European Symposium on Chemical Reaction Engineering, Brussels (1968).

120. PERRY, J. H., Chemical Engineers Handbook, 4th Edn., McGraw-Hill, Tokyo (1968).

121. CHECHETKIN, A.V., High Temperature Heat Carriers, Pergamon Press, London (1963).

122. GRENS, E. A. and McKEAN, R.A., Chem. Eng. Sci., 18, 291 (1963).

123. LUSS, D. and AMUNDSON, N.R., Ind. Eng. Chem., 6, 436 (1967).

124. VAN HEERDEN, C., Ind. Eng. Chem., 45, 1242 (1953).

125. NORTON, J. P. and SMITH, W., Meas. and Control, 5, 147 (1972).

126. DAVE, K. Ph.D. Dissertation, University of Leeds (1969).

127. LAPIDUS, L., Digital Computation for Chemical Engineers, McGraw-Hill (1962).

128. DENIS, G. H. and KABEL, R. L., A.I.Ch.E. Jl., 16, 972 (1970).

129. HANSEN, K.W., Chem. Eng. Sci., 28, 723 (1973).